2014

Experimental Assessment of Photovoltaic Irrigation System

Khalil Raza

Wright State University

Experimental Assessment of Photovoltaic Irrigation System

A thesis submitted in partial fulfillment
of the requirements for the degree of
Master of Science in Engineering

By

Khalil Raza
B.E., Quaid-e-Awam University, 2011

2014
Wright State University

WRIGHT STATE UNIVERSITY

GRADUATE SCHOOL

September 12, 2014

I HEREBY RECOMMEND THAT THE THESIS PREPARED UNDER MY SUPERVISION BY Khalil Raza ENTITLED Experimental Assessment of Photovoltaic Irrigation System BE ACCEPTED IN PARTIAL FULFILLMENT OF THE REQUIREMENTS FOR THE DEGREE OF Master of Science in Engineering.

____

James Menart, Ph.D.
Thesis Director

____

George Huang, Ph.D.
Chair, Department of Mechanical and Materials Engineering

Committee on
Final Examination

____

James Menart, Ph.D.

____

Rory Roberts, Ph.D.

____

Zifeng Yang, Ph.D.

____

Robert E. W. Fyffe, PhD.
Vice President for Research and
Dean of the Graduate School

Abstract

Raza, Khalil. M.S.Egr., Department of Mechanical and Materials Engineering, Wright State University, 2014. Experimental Assessment of Photovoltaic Irrigation System.

Agriculture is a significant measure of an economy for a number of countries in the world. Currently, the agriculture sector relies heavily on conventional sources of energy for irrigation and other purposes. When, considering factors such as increasing costs of fossil fuels and extending new power lines, especially to remote locations where grid electricity is either inaccessible or expensive, a solar PV (photovoltaic) irrigation system can be an effective choice for irrigating farmland. Solar power eliminates the need to run electrical power lines to remote agriculture locations, which quickly turns the monetary equation in favor of solar irrigation over grid-powered irrigation. In addition, the cost of delivering fossil fuels to remote locations can be expensive. Solar power is ideal for agricultural irrigation, as most irrigation is required when the sun is shining brightly. Consequently, a PV powered irrigation system is a promising technology that could help meet the irrigation needs of remote agricultural.

The two major goals of this research are to get an existing solar PV irrigation system working and to acquire experimental data using this system under various operating conditions. This research work is built upon a series of three senior design projects. These three senior design projects were to design and construct a solar irrigation system, an instrumentation system for this solar irrigation system, and a single axis solar translator. Specifically this thesis work entailed getting the instrumentation system to work properly, writing a LabVIEW program to automatically acquire data from installed sensors, integrating all three of these senior design projects into one PV irrigation system, getting the PV irrigation system installed on the roof of the Russ Engineering Building, and collecting a large amount of data on the system. All have been accomplished successfully.

The PV irrigation system work presented in this thesis use two 224 watt PV modules that are connected in parallel and mounted on a vertical axis solar tracker that follows the sun from east to west to enhance the amount of solar energy collected during the day. Energy developed by these panels is stored in two 100 amp-hour batteries wired in a series arrangement. Energy stored in the batteries is supplied to a direct current water pump that requires 50 watts of power at 24 volts. To harvest maximum energy from the PV modules

and to protect the batteries, a MPPT-charge controller (maximum power point tracker with charge controller) is installed inline between the PV array and batteries. The instrumentation or DAQ (data acquisition) system employed on the PV irrigation system consists of four current sensors, four voltage transducers, four thermocouples, a pyranometer and a flowrate sensor to record associated parameters at various points throughout the PV irrigation system. The DAQ system is structured in such a way that each component's output can be monitored and assessed throughout the system via a LabVIEW program developed as part of this thesis work.

This PV irrigation system has been investigated under four operating configurations. Three of the operating configurations vary the orientation of the PV panels and one operating configuration varies the load on the system. The four configurations tested are:

1. azimuthal solar tracking at an inclination angle of 40° with both the water pump and power dissipating resistors being used to consume the power generated by the PV array,
2. azimuthal solar tracking at an inclination angle of 30° with both the water pump and power dissipating resistors being used to consume the power generated by the PV array,
3. a fixed solar array pointing due south at an inclination angle of 40° with both the water pump and power dissipating resistors being used to consume the power generated by the PV array, and
4. azimuthal solar tracking at an inclination angle of 40° with only the water pump being used to consume the power generated by the PV array, where the water pump is run 24 hours a day.

A large number of measured quantities are presented for each of these configurations for the time period from July 28 to September 1st, 2014 in Dayton, Ohio.

Table of Contents

List of Figures

Acknowledgements

I would like to express my deep gratitude to my supervisor, Dr. James Menart, for all his supervision, motivation and critical evaluation of this research work. Without his guidance and help, this thesis would have not been possible.

I am very thankful to Mr. Dennis Hance for donating most of the equipment used in this PV irrigation system. I would also like to thank Dr. Rory Roberts and Dr. Zifeng Yang for serving on my thesis committee. I would like to offer my special thanks to Stephanie Sasz from Institute of International Education and Fulbright Scholarship Committee for their continuous support, generous funding and extending my grant to finish this research work.

I am grateful to Shashank Nair for his tremendous help in my work, in connecting a number of pieces of this system together and getting it installed on the roof. I would like to thank NEC building construction crew, who facilitated in moving system on to the roof. I am also thankful to personal from physical plant service for their approval and assistance in mounting this system.

Most importantly, none of this would have been possible without the love and support of my parents and immediate family, who have always encouraged and believed in me, in all my endeavors.

Chapter 1

Introduction

In the past few decades the world has witnessed a huge expansion, at a progressive rate, of its population, its industrial output, and its energy use. Energy is one of the fundamental raw materials that have led our world to achieve important advances in our lifestyles [Vanek et al. (2008)]. Due to these facts, there is an ever-growing energy demand. Since conventional energy reserves are limited, it is reasonable to assume that at some time in the future they will be exhausted. While many predictions have been made about when this will happen, many of them have turned out to be wrong. Nevertheless fossil fuels are finite and it behooves our society to look for other supplies of energy. In addition to being limited, fossil fuels also cause environmental damage. These deficiencies of fossil fuels have forced us to look for other energy solutions; ones that are clean, less damaging to environment, and renewable in nature. The result is a growing use of renewable energy technologies such as solar, wind, geothermal, ocean tides, ocean waves etc. It is highly expected that the share of energy generation by renewable technologies will be increased further in the future. Renewable energy technologies are being adopted with existing power systems in various development sectors to harness energy through sustainable means that produce less or zero carbon emissions. Similarly, there lies a potential in the agriculture sector to provide energy through renewable energy sources. Solar photovoltaic electricity generation is a promising technology that could help meet the energy needs of agricultural development.

As a small contribution to this transformation, the work presented in this thesis studies a renewable and clean solar powered irrigation system. The goals of this work are to get a previously designed solar irrigation system working, get the previously designed diagnostics on the solar irrigation system working, and to take measurements on the operating characteristics of the system over a period of time. This work will all be discussed in detail in this thesis, but first I would like to provide some motivation for a societal change in the way our society produces energy and for why a solar powered irrigation system may be beneficial in some agricultural situations. I will start this discussion by providing information on the world's energy situation, then move into a discussion of how solar energy should be a part of the world's energy production mix, and finally talk about why a solar powered irrigation system may be advantageous. This chapter will finish with a discussion of the thesis organization.

1.1. World Energy Scenario

The world's energy scenario is changing rapidly. At the present time fossil fuels such as oil, gas and coal dominate the energy market. However, the increase in demand owing to the world's population growth and an upsurge in the cost of energy from oil and gas make conditions favorable for renewable energy. The World Energy Council estimates that the world's primary energy consumption will increase from 546 EJ (152 PW-h) in 2010 to 879 EJ (193 PW-h) in 2050 [WEC, 2013]. In the future, the demand for all forms of energy will increase; whereas, fossil fuel's share will be reduced from 86% to 76% and energy from renewables will supply 40% of primary energy demand in 2035 [IEA (2013)]. The global energy demand will shift towards the developing countries such as China, India and Middle Eastern Region. China and India are expected to be the largest importer of oil and coal respectively by 2020. The United State could be self-sufficient in meeting its energy needs by 2035 due to adequate measures taken in regards to energy efficiency and progressive production in oil and gas. Nuclear energy is also expected to increase its share in the future energy mix. Though, the calamity in Japan in 2011 has developed serious concerns over the use of nuclear power due to safety issues and secure handling of radioactive waste

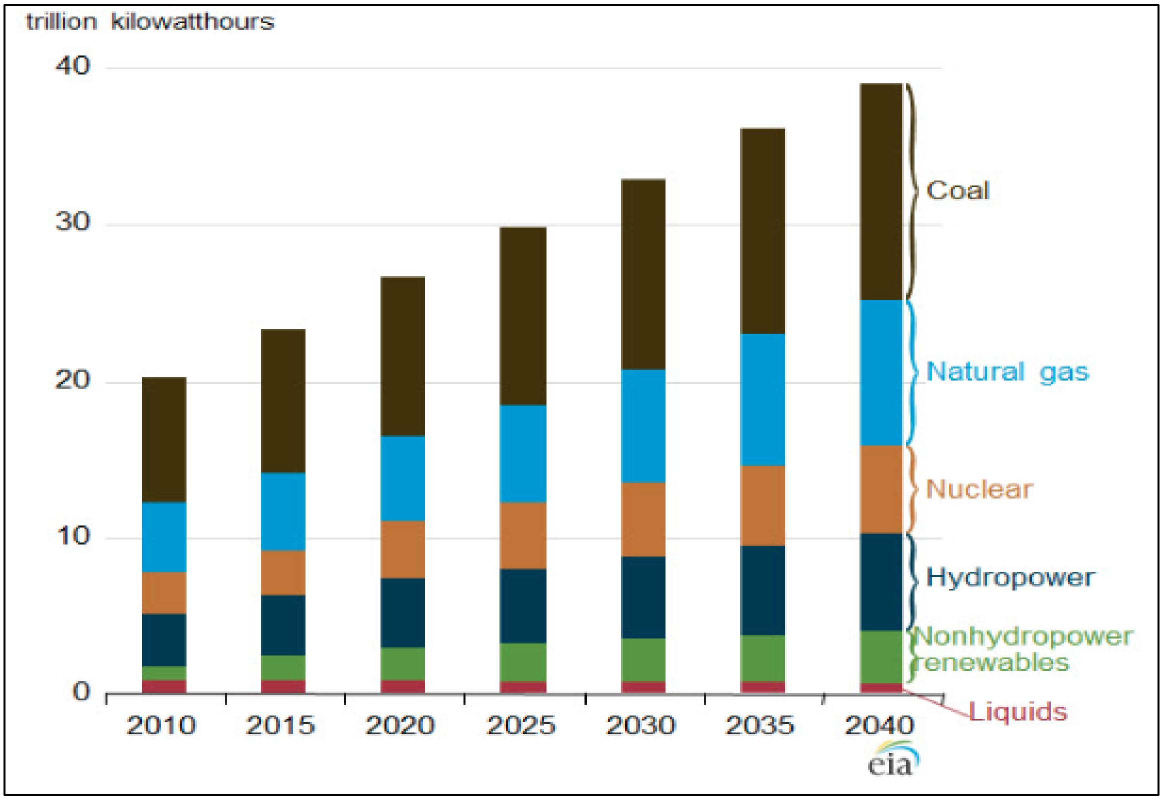

Figure 1.1: Global Electricity Generations by Energy Source [EIA (2013)]

Coal and natural gas are still supplying over half of the world's electrical energy needs in the EIA's future electrical power production scenario shown in Figure 1.1. Whereas, the use of liquid hydrocarbons in supplying electrical energy demand is being reduced. As seen in Figure 1.1 liquid hydrocarbons have never been used extensively to produce electricity because of their high cost compared to coal. Of course, liquid hydrocarbons are predominately used in the transportation sector.

Globally, hydroelectric power generation and energy from wind will supply a large fraction of electrical energy amongst the renewable energy sources. Similarly, solar photovoltaic (PV) and solar thermal have proved to be a promising option in recent years due to drastic reduction in cost in case of solar PV and thermal systems. Renewable Energy Global Futures projected that solar PVs could reach 8,000 GW [REN21, 2013].

1.2 Why Renewable Energy?

The world has seen a massive growth in renewable energy technologies in the past decade. European countries like Germany, Denmark and Spain are producing a substantial fraction of their required energy from renewable energy sources. Investments in renewable power capacity have tripled in the last few years as compared to fossil fuel and nuclear power has grown at much slower pace. This picture shows renewable technologies are capable of meeting the future energy needs sustainably. Policy initiatives to generate more than 50% of electricity using renewable sources is in the near future for some European countries have given a wider space to renewable technologies for progressive growth. In some regions, power generation from solar PV and wind is reaching cost parity with conventional power generation such as coal, oil and natural gas.

Another big advantage of renewable technologies, especially solar and wind is that they can generate electricity in remote locations where it is hard to deliver coal, oil, and gas or supplying grid electricity is considered impractical. The sun shines everywhere and the wind is plentiful in a number of locations. Therefore there can be large cost savings by generating electricity next to the demand without the need of expensive electrical lines or delivering fuel to the location.

The energy potential of solar is limitless. The earth receives more solar power in one hour than the total annual global energy demand [Dahl et al. (2012)]. The cost of solar PV has had remarkable reductions in recent years due to technological advancements. The price of solar PV has been reduced by a factor of 10 from $76/watt in 1977 to $0.76/watt in 2013 [US DOE (2008) and Bloomberg Energy (2013)]. Government incentives for solar PV in several countries, including the United States, further reduce the cost of solar PV. The price of installing solar PV has been reduced as well. Currently, electricity generation in United States from solar PV is estimated at 4 GW nameplate capacity and according to the National Renewable Energy Laboratory it is expected to increase to 170 GW in 2050 [REN21, 2013].

The wind power sector has also grown more than any other form of renewable energy. Wind power at a good site location is highly competitive with conventional power generation in many parts of the world. Newer technological advancements such as light weight materials and aerodynamic efficient blades have made it possible to tap wind power efficiently, while also increasing the life span of wind turbines. Due to this fact, industrial growth of the wind power sector is predicted at much higher rates than other renewable energy sources. In US, wind energy could supply 30 % of its electricity needs by 2030 [US DOE (2013)]. Further developments in the wind power industry may be able to overcome the issues of grid balancing, energy storage and turbine maintenance. Similarly other renewable energy technologies such as tidal, biomass and geothermal have a bright future.

Environmental issues have also played an important role in the development of renewable energy technologies. Currently, a majority of energy generation capacity is fossil fuel based, which is a threat and hazardous for the planet. Combustion of fossil fuel results in the emission of greenhouse gases such as carbon dioxide into the atmosphere. Majority view on these gases is stated to be a main cause of the temperature rise of the earth. Greenhouse gases trap long wavelength thermal radiation in the earth's atmosphere. Due to this increase in earth's temperature, unfavorable weather conditions and atmospheric patterns have been observed in last century. These effects have created serious concern over the use of fossil fuels, which release the greenhouse gas carbon dioxide into the atmosphere. The melting of the artic polar ice cap and water level rise in oceans have indicated the seriousness of these environmental problems, which could result in severe economic loss. With the use of renewable energy technologies, which do not contribute to environmental degradation, the issues of global warming and climate change are avoided.

The current trend of substantial growth of renewable energy technologies and continued reduction in their costs promises a bright future for these energy generation technologies. In addition to this, renewable technologies help alleviating environmental problems; and at the same time help achieve energy security. The conventional sources of electricity generation may be able to meet energy needs but they are limited sources and do not provide long-term solutions.

1.3. Solar Energy Applications in Agriculture

Agriculture is a significant measure of an economy for many countries. Energy plays a fundamental role in agricultural development. A large amount of the agriculture sector uses conventional sources of energy for irrigation and transportation purposes. Renewable energy technologies such as wind and solar can be used cost effectively in agriculture, establishing self-sufficiency and reducing pollution. When, considering factors such as increasing cost of fossil fuels and remote locations where grid electricity is inaccessible or expensive, solar photovoltaic can be a profitable solution.

1.3.1. Solar Photovoltaic Electric Systems

It seems that solar powered irrigation systems may be especially attractive in remote agricultural applications. This is true in third world countries, but it should also be true for agriculture removed from power lines in the United Sates. A need for more irrigation water emerges when the weather is dry and temperatures are hot. Temperatures are usually the hottest when the sun is shining brightly. This makes solar irrigation ideal for agricultural irrigation, as power is required most when the solar insolation is the highest. There seems to be a natural match between power demand and power supply for solar powered irrigation.

Solar PV uses solar panels to convert light energy from the sun into electricity. These systems can be used for variety of agricultural applications such as water pumping, electrification for buildings, field lighting, gate openers, electric fences etc. Water pumping is a basic agricultural need. Solar powered pumping system uses solar photovoltaic panels to generate electricity to pump water from a lake, river, pond, underground source, rainwater collection device, or some storage reservoir. Solar powered systems are higher in capital cost compared to diesel-powered generators. But, they are self-reliant, durable, and last a long time. The major cost associated with such systems is the initial cost but solar panels can be used for 20 years or more. Use of solar photovoltaic power in agriculture can be an especially effective choice for an off-grid agricultural application, rather than investing in new power lines to the remote location. For those times when the sun is not available for required electrical power, a small amount of battery storage will solve this problem. Eliminating the need to run electrical power lines to remote agricultural locations quickly turns the monetary equation in favor of solar power over grid power.

1.3.2. Solar Thermal Heating Systems

Solar thermal energy can be used in various agriculture applications as well; such as water heating, space heating, solar cooking, crop drying and passive greenhouse heating. In some agricultural applications, it is required to maintain a certain temperature level, which is favorable for livestock or a desired water temperature. Solar heating systems usually use flat plat panels or collectors to capture thermal radiation coming from the sun. The heat is absorbed by a working fluid present in the panel's tubing, which heats up the water flowing through the tubes in the panel. The hot water can be circulated to provide hot water or can be used for space heating using heat exchangers at required ventilating locations to preheat the incoming fresh air. Space and water heating takes up significant amount of energy consumption in the farming business [Smil (1992)]. Properly designed solar heaters for buildings and water can cut energy costs drastically. Moreover, solar thermal energy can be used to dry crops and it has been the oldest method used in agriculture. Conventional solar drying of crops has some disadvantages as crops are exposed to open air and could be damaged due to bad weather conditions, rodents and dust. Therefore, non-conventional solar dryers with protective enclosures can be used to protect crops by maintaining their quality and processing them at faster rates.

1.3.3. Feasibility of Solar Powered Irrigation

Small-scale photovoltaic powered irrigation systems have been running cost-effectively at majority of remote locations where the grid electricity is inaccessible [Kelley et al. (2010)]. Feasibility of a photovoltaic irrigation system depends on several factors related to the geographical location of the facility such as the availability of solar insolation, type of crop, weather conditions, type of irrigation methods employed and ground water depth. The power required for pumping is determined by daily flow rate required to irrigate the field and the location from which water is being accessed. The economic feasibility of a solar PV powered irrigation system also depends on the irrigation method used.

Solar array size increases with well depth, locations receiving low solar insolation and higher daily water flow rates required by crops. Such conditions increase the capital cost of photovoltaic system. Locations with low solar insolation have lower rate of return of a solar PV irrigation system and prolong the payback period. In regions with daily solar insolation of 5 kWh/sq.m-day with higher pumping requirements, 2.5% of total field area is required for solar panel array. If the daily insolation were higher at 7 kWh/sq.m-day, the panel array size would require 1.5% area of total field area [Kelley et al. (2010)]. Moreover, drip and center pivot irrigation methods are helpful in reducing the total solar panel array size. Micro or drip irrigation methods use less water for irrigation and are effective in conserving water. Drip irrigation supplies water straight at the roots of crop and can increase the crop yields by 100% and saves water consumption by 40 to 80% depending upon type of the crop [Burney et al. (2010)]

A competitor to remotely located solar PV irrigation systems is remotely located diesel powered irrigation systems. The capital cost of a solar photovoltaic powered pumping system is very high compared to the capital cost of a diesel powered pumping system. However, since the cost of bringing diesel fuel to a remote location can be expensive, the lifecycle cost of a photovoltaic pumping system is less than a diesel-powered system. The running cost of a diesel powered pumping system can be high as 20 times the lifecycle cost of photovoltaic powered systems [Kelley et al. (2010)]. This proposes that solar photovoltaic pumping is economically feasible in remote agricultural locations.

1.4. Objectives of Research

Experimental research is carried out on a 448-watt photovoltaic irrigation system powered by two 224-watt panels to measure the performance of a solar irrigation system. This performance measurement of PV irrigation will be analyzed as a function of weather, time, and orientation at Wright State University in Dayton, OH. The system is comprised of three basic blocks: power production system, irrigation system and diagnostic or Data Acquisition (DAQ) system. The power production system includes the solar photovoltaic panels, solar translator and associated electronic controls. The irrigation system consists of a 100-watt DC pump with tubing to recirculate water supply. This way the same water can be pumped over and over again. The diagnostic part of the system contains the sensors to collect real time data such as temperature, pressure, voltage, current, water flow rate, and solar insolation magnitude.

The goal of this project is to examine the behavior of this system and resulting effects caused by associated parameters such as temperature, solar insolation. The DAQ system is structured in such a way that each component's behavior can be monitored and evaluated. The acquired data will be studied to assess the conditions under which the PV irrigation system performs best. Based on the acquired data of optimum performance of the system results such as tilt angle, temperature effect on power output, and characteristics of voltage and current, the functions of electronics such as the maximum power point tracker (MPPT) and the battery under various load or weather conditions could be accessed. The data can be analyzed at hourly, daily or monthly basis.

Chapter 2

Literature Review

This chapter gives a brief overview on the existing solar photovoltaic powered irrigation systems and their technical and economic viability as documented in the literature. Solar PV irrigation systems are economically and technically feasible in many parts of the world, where the operational cost, electrical distribution and other options are very high. In recent years, use of solar photovoltaic power for irrigation has seen a notable growth. This trend is estimated to grow further as the cost of PV modules continues to decrease. Several small to large-scale solar irrigation projects have been running successfully, mainly in developing countries located in Africa, Asia and other remote locations, where electrical power is inaccessible and solar potential is high.

2.1. General Literature on PV water pumping system

Brian and Clark (2009) present a review on selecting the optimal solar water pumping system. They use comparison analysis methods to evaluate the best renewable energy water pumping methods available at different locations in the United States, i.e. solar water pumping versus wind power pumping. The results showed that irrigation requiring less than 1.5 kW of peak power; solar PV water pumping is a more suitable choice over wind power.

This is due to the nature of solar photovoltaic systems, which are easy to install and require less maintenance for operation.

Cuadros et al. (2004) and Hamidat, et al. (2009) presented a procedure for systematic and optimal sizing of solar PV irrigation systems. Proper sizing of solar PV irrigation system depends on a wide range of considerations such as solar insolation, size of PV array, pumping head, type of crops and whether the pumping system is AC or DC. The optimal sizing of solar PV irrigation significantly increases the power production, efficiency of the system and reduces overall cost.

Kolhe et al. (2002), Odeh et al. (2005) and Purohit (2006) assess the economic and financial evaluation of solar PV pumping and diesel powered pumping of various system sizes. They take the factors of hydraulic demand, irradiance, pumping head, interest rate, PV cost and fuel cost in to account to conclude that solar irrigation is economically suitable to meet the daily energy demand of irrigation up to 15 kWh. The results indicate that interest rates from 0 to 20% for equivalent system sizes of solar PV and diesel pumping, the solar PV demonstrates better economic viability than diesel pumping.

Leah et al. (2010) considers both technical and economic feasibility of solar powered irrigation systems in much more detail and analyze it comparatively with the conventional irrigation methods of diesel powered and grid tied irrigation systems. Major factors considered for technical feasibility in this analysis are location, solar insolation and maximum power required for a solar irrigation pump. Whereas, aspects such as life cycle cost of photovoltaic, diesel and grid irrigation systems, carbon tax and financial incentives for renewable energy are considered for economic feasibility of solar powered irrigation systems. The results concluded that solar powered irrigation systems are technically feasible and there is no technical restraint for using PV pumping as long as enough space is available for mounting the PV panels. Whereas, the factors concerning growing cost of diesel and grid electricity indicate that solar photovoltaic irrigation systems are economically feasible in comparison with conventional irrigation methods.

Keeping in view the massive cost of extending power lines and the high maintenance of conventional irrigation systems**,** solar PV water pumping is a cost effective way to irrigate at remote locations [Kelley et al. (2010)]. Meah et al. (2008), Hamidat et al. (2008) and Mahmoud et al. (2003) evaluate the technical and economic aspects of solar PV pumping systems at remote locations. The results confirm that solar PV pumping is an ideal solution at distant locations where grid electricity is inaccessible. In addition to this, access to water resources can appreciably improve the socio-economic and living conditions of farmers in remote areas.

2.2. Similar Research

PV water pumping systems of various sizes have been studied. Work presented in this section covers PV water pumping systems at different locations used for diverse irrigation applications. Performance measurements in terms of power output, pumping head profile, water delivery and efficiency of PV irrigation systems are discussed in detail in the following sections.

2.2.1. Directly Coupled PV Water Pumping System at Oran, Algeria

A directly coupled solar PV water pumping system was installed in the year 1996 at the campus of the University of Sciences and Technology, Oran, Algeria. Mokeddem et al. (2011) describes this system and performance over 4 months of its operation. This system consisted of PV array with peak power of 1.4 kW, multipurpose centrifugal pump and DC motor. The PV array was comprised of 30 Kyocera LA 361J15 PV modules where each module had a power rating of 51 watts. Two strings of PV modules were connected in parallel and each string had 15 modules connected in series (see Figure 2.1). The DC motor-pump was directly connected to the PV array. This solar PV water pumping system used two equal capacities of storage tanks to store water and did not require batteries for the energy storage. The schematic diagram of the system is shown in Figure 2.2. Directly coupled PV pumps with water storage tanks are analogous to that of PV irrigation systems outfitted with batteries for energy storage. The main advantages of directly coupled PV pumps are that they are simpler in design and low cost, but less efficient than battery-equipped PV irrigation systems. The use of batteries in PV water pumping can increase the efficiency of the motor-pump assembly. This allows the pump and motor to run at their optimal conditions by avoiding reduced load operation at lower irradiance [Wenham et al. (2011)].

Figure 2.1: The 1.4 kW PV array and solar insolation sensor at University of Science and Technology, Oran, Algeria (Mokeddem et al., 2011).

The PV array was fix mounted on the ground facing southwards at a tilt angle of 35°, located at a latitude 35.69° and a longitude of -0.64°. A Leroy Somer permanent magnet DC motor was used to drive a water pump. The DC motor required one horsepower to produce 1750 rpm with a voltage of 180V and drew 4.9 amps of current. An Electropompe CM100 centrifugal pump was used in a DC-motor pump assembly. The pump required 750 watts of power and delivered 80 liters/min of water with a maximum pumping head of 33 meters and at a speed of 2850 rpm. The two water tanks, each with a capacity of 2 m^3, were used and installed at two different static heads, one at a higher head of 11 meters and another at a lower head of 0.60 meters. This particular arrangement of using two different static heads was an attempt to investigate the influence of pumping head on system behavior.

The experimental data was acquired and recorded using an Eprom data acquisition system. Various ranges of sensors were used to acquire the data such as ambient temperature, pressure at water outlet, voltage and current of relevant devices, flowrate and solar insolation. A pyranometer was mounted at the same tilt angles as that of PV modules to measure the insolation incident on the PV array. Although, the PV pumping had been operational for more than 15 years at the time of the experiments, tests were conducted and data was acquired for four months, from December to March. Based on acquired data, I-V curves were obtained for the PV modules and the motor-pump assembly to study the characteristics of the respective devices under two different static head configurations.

The effects of irradiation on the PV array were also studied under various levels of solar insolation. Initially, the effect of temperature on short the circuit current of the PV cells was not taken into account, but later this effect was introduced into the study. Data collected during the experimental period fluctuated between various ranges of solar irradiance, which was particularly based on cloud cover and seasonal change. Solar insolation and ambient temperature were two weather related factors included in the study; the wind speed, however, was not considered during the tests. The results showed that PV pumping required 1 amp of current to activate the pump, which corresponded to 160 W/m^2 of irradiance. The activation or excitation current was the current at which the motor-pump assembly started rotating. Once the pump started running, the activation current continued to decrease while the voltage increased until the operating point was reached.

The operating point fluctuated during the experimental period and was different at various irradiance levels. The relationship between flow rate and pumping input power for static heads of 11 meters and 0.6 meters showed that the pump required a minimum of 288 watts and 56 watts for each of the heads respectively. Moreover, the motor-pump assembly attained maximum efficiencies of 30% and 12% for static heads of 11 m and 0.6 m respectively. At lower static heads, the rotational speed of the motor was within the rated operational range; but at higher static heads the motor operated outside the rated operational speed. The study established that the motor had a larger influence than the pump on the overall efficiency of the motor-pump assembly.

Due to simpler operation of directly coupled PV pumps there are many advantages to such systems. First and foremost the initial cost of the batteries is eliminated. Second, there is a minimum or no requirement for auxiliary electronics. This kind of PV pumping system was proven to be very cost effective and reliable for lower flow rate applications.

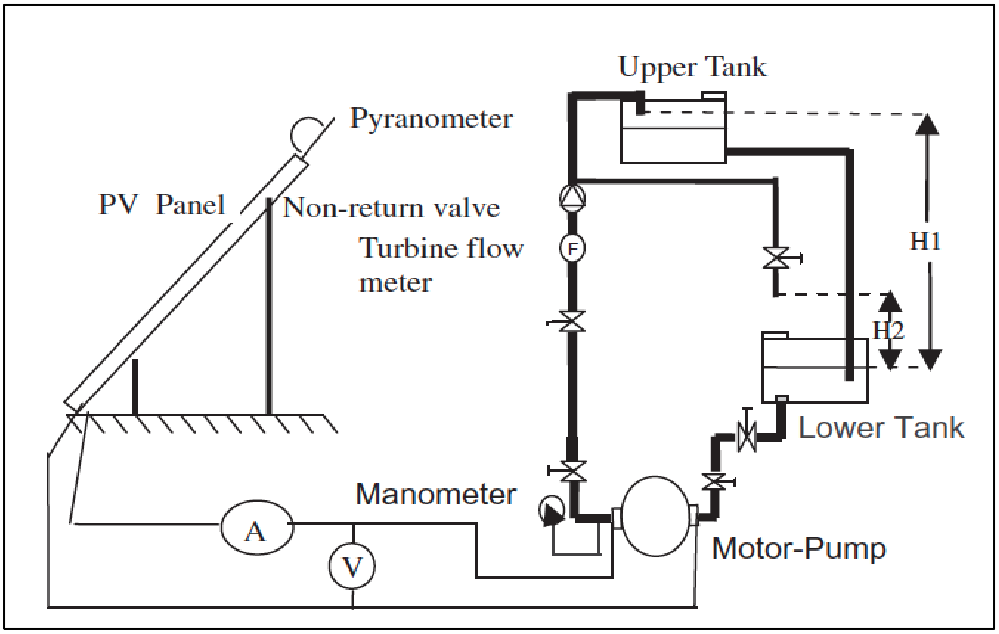

Figure 2.2: Schematic Diagram of PV Pumping system (Mokeddem et al., 2011).

2.2.2. CAZRI PV Drip Irrigation System, India

CAZRI (Central Arid Zone Research Institute) developed a solar PV pumping system in Jodhpur, India (Pande et al.,2003) presented the design and development of this solar PV pumping, which delivered water using a drip irrigation mechanism in an orchard field. This pumping system was designed to irrigate 5 hectares. Rainwater is the common source of irrigation in Jodhpur, India, which lies in an arid climatic zone of Rajasthan. The delivery of water using a drip irrigation system was especially considered due to the geographical location and its climatic conditions. Jodhpur's terrain is mostly a desert that receives very little rainfall. Due to these reasons, the judicious and efficient use of water for irrigation was one of the important considerations in designing this pumping system. Jodhpur receives an average solar insolation of 6 kWh m^{-2} day^{-1} incident on a horizontal surface. Solar water pumping consists of a PV array rated at 900 watts, a centrifugal pump directly coupled to an 800 watt DC motor and water-harvesting tank. The tilt angle of the PV panels from horizontal was kept at 4° and 48° in the summer and winter seasons respectively. PV panels were ground mounted and the orientation of the panels was manually adjusted to track sun towards the east, south and west directions during different times of day.

A performance evaluation of this PV pumping system was carried out for different solar energy incident on the PV array. It was noted that the PV array required a minimum of 400 W/m^2 to run the pump with a flow rate output of 1.75 l/s. The maximum discharge of the pump was recorded to be 3.8 l/s at 900 watts/m^2 of irradiance. In order to get more solar power, the orientation of the PV array was manually changed to three different positions during the day. PV panels were kept pointed towards the east up till 11:30 am, later oriented towards south until to 1:35 pm and then subsequently towards the west till sunset. The manual tracking of the panels enabled the system to receive more than 800 W/m^2 of irradiance for an average of 7 hours in winter and 9 hours in summer. Pressure and head versus discharge of the pump was also studied. Discharge of water increased from 1 to 2 l/s with a decrease in head from 14 to 11.5 m. The pump developed the pressure between 70 and 100 kPaG at an irradiance ranging from 600 W/m^2 to 900 W/m^2. With the pressure of the pump between 70 and 100 kPa, drippers discharged was recorded to be at 3.6 to 3.8 L/h at various locations during different times of the day.

It was observed that output of the PV array was reduced to 45 % due to dust accumulation, which is very common in arid climatic zones. Moreover, a significant reduction in discharge was also noted from the drippers because of clogging. Therefore, drippers needed regular cleaning to maintain the required discharge. Performance evaluation of this PV pumping system showed that PV irrigation is suitable in arid climatic zones using drip irrigation methods for orchards.

2.2.3. Badia PV Water Pumping Project

Al-Smairan (2012) presented a comparative case study of PV water-pumping systems for remote areas versus diesel powered pumping systems. PV water pumping systems were established in 1989 to carryout research in solar pumping systems by the Renewable Energy Research Center, Mafraq, Jordan. This PV pumping system is located in Badia, Jordan, where Bedouins surround the site and use this facility to supply water for domestic livestock. The site location lies in a semi-arid climatic region and receives the highest solar radiation in the country with an average daily solar radiation of 5.3 kWh/m2/day. The average monthly solar insolation for this site is shown in Figure 2.4. This PV water pumping system was designed to match daily water requirement of 45 m^3/day. Water was pumped from a groundwater well with a depth of 174 m; however, the pumping head was 105 m. Based on the hydraulic and climatic data, the total energy required by the pump required a PV array size of 12.875 kWh/day and 5.02 kWp (kilowatts peak power). The size of the PV array was increased from 5.02 to 5.94 kW to compensate for output losses because of heat and dust accumulation on the panels.

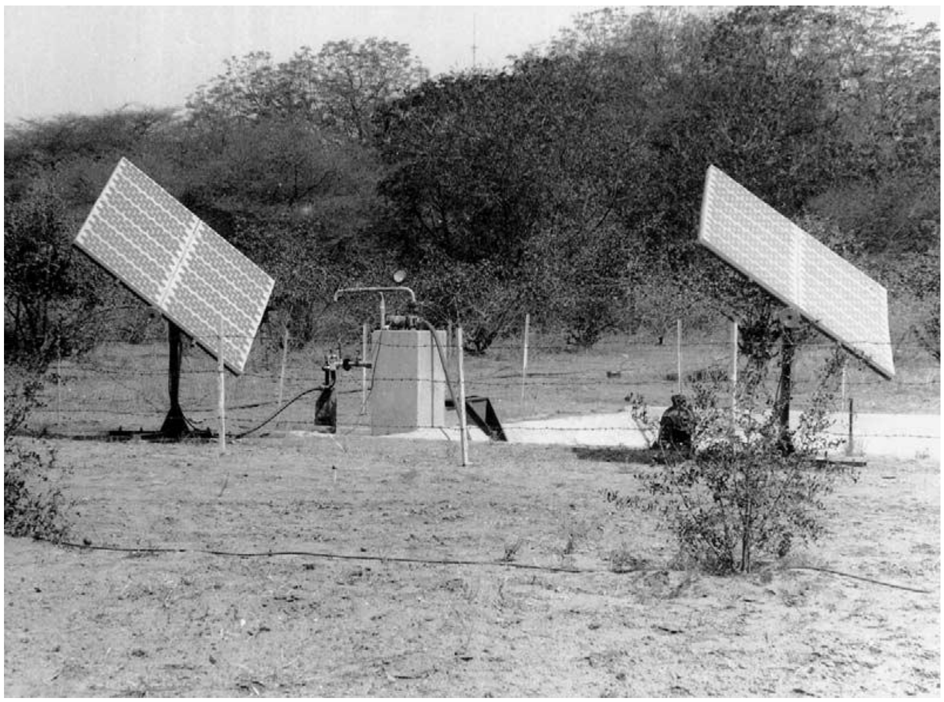

Figure 2.3: PV Pumping system at Jodhpur [Pande et al., (2003)].

The overall system consisted of 108 PV panels facing due south, one 3 phase, 5.5 kW, submersible AC pump and one 7.5 kVA inverter. This system is shown in Figure 2.5. Two water tanks, each with a capacity of 55 m^3 were used to store the pumped water. These water tanks served the similar purpose of batteries in a way that energy was stored by pumping water into tanks instead of storing electrical energy in batteries. The size of the water tanks was taken to be 2.5 times of the actual water requirement for 2 to 3 days.

In addition to evaluating this water pumping station using PV panels, it was also evaluated using diesel-pumping system. A 10 kW diesel engine was considered to pump an equivalent amount of water as the PV system. The diesel engine required 25 liters of fuel for 6 hours to pump 45 m^3 of water in a day.

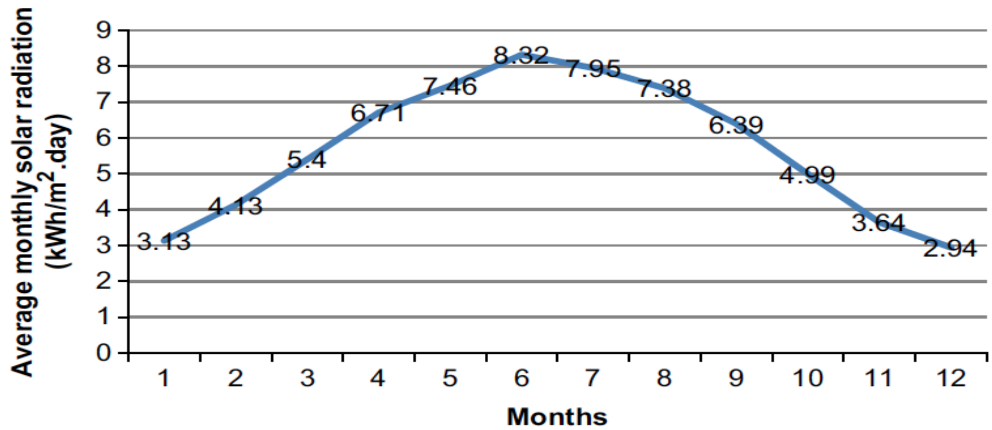

Figure 2.4: Average Solar Insolation for Badia, Jordan (Al-Smairan, 2012).

Figure 2.5: 5.5 kW PV Water Pumping System in Badia, Jordan (Al-Smairan, 2012).

Al-Smairan (2012) presents a present value cost analysis for both the PV and the diesel pumping systems. The purpose is to propose most economical pumping system for the same hydraulic capacity. Results showed that the pumping cost per cubic meter of water for the diesel and the PV pumping systems was \$0.58 and \$0.20 respectively. It is evident that

PV pumping systems are cost-effective over diesel pumps for remote locations and regions where grid lines are not available.

2.2.4. Ritem Solar PV Water Pumping System

Odeh et al. (2006) developed a simulation prototype for PV water pumping systems in TRNSYS (Transient Energy Simulation Software). This model was validated compared with field data of a PV water pumping system installed at Ritem, Jordan. This PV water pumping system used 90 PV modules rated at a peak power of 4.5 kWp, a 2.2 kW motor directly coupled to a centrifugal pump, a 3.5-kVA DC/AC inverter and used a 55 m^3 water tank for storage as shown in Figure 2.6. A data logger by Nes Modas (Mobile Data Acquisition System) was used to collect the data from the Ritem PV water pumping system. Data was collected every 2 seconds and processed every hour for a year duration, which included DC current and voltage of the PV array, dynamic head, flow rate and solar insolation incident on the PV modules. This energy simulation was developed to assess the performance of the PV water pumping system. A simulation model was supplied weather data for Ritem, Jordan and used actual specifications of the installed devices and components such as the PV array capacity, motor-pump assembly, pumping head, water tank and AC-DC inverter.

Simulations were run to evaluate the impact of the solar insolation, size of PV array and pumping head on the overall performance of the PV water pumping system. The simulated results were higher than the measured field data. Certain real-time external factors of shading, dust accumulation, PV-pump mismatch, and spectral losses were not taken into account, which resulted in overestimated performance of the PV water pumping system. The actual field measured data showed that annual water volume pumped was 2.6% lower than simulated outputs. Whereas, the actual total annual powered produced by the PV array was 5.7 % lower than simulated data.

It was concluded that the size of the PV array is critical to the overall performance of the system and greatly affects the overall efficiency of system. A larger PV array size decreased the efficiency of the system as the PV array produced more power than required by the pump; and hence, excess power could not be utilized. A small increase in PV array size over that required by the pump had a trivial impact on the cost of water pumped per cubic meter. However, a slight decrease in size of the PV array extensively increased the cost of pumped water by up to 94 %. To design an efficient PV water pumping system, a proper design insolation point must be determined to avoid a mismatch between the PV array and the pump. The design insolation point is a level of solar irradiance at which the pump operates at its rated speed. Thus, the size of the PV array could be optimized by determining the average duration of solar irradiance above the design insolation point at that given location and the number of hours of pumping required in a day. At locations where solar irradiance is lower than the design insolation point for many hours of the pumping operation, the size of the PV array needs to be increased to achieve the needed power to run a the pump.

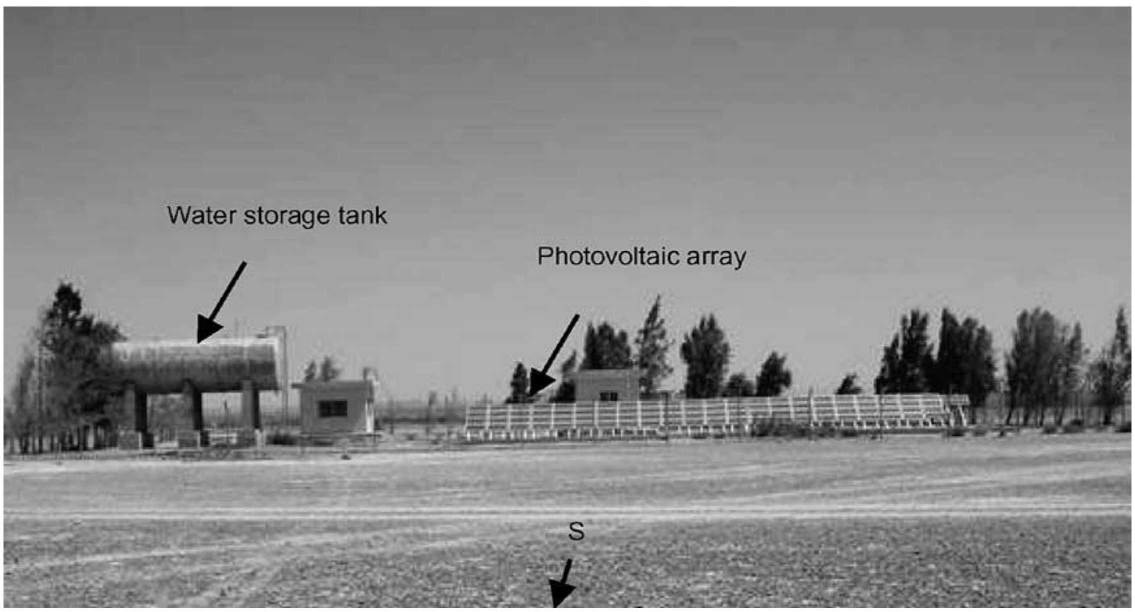

Figure 2.6: 4.5 kW PV Water Pumping System at Ritem, Jordan (Odeh et al. ,2012).

The influence of pumping head on efficiency of the overall system, subsystem and PV array were obtained for various static heads. The PV array, DC/AC inverter and motor-pump assembly were considered as constituents of a subsystem in this simulation work. As shown in the Figure 2.7, the optimum efficiency was different for the PV array, general system and subsystem for different static heads. The PV array operated at maximum efficiency at static head of 12 m; whereas, the complete system and subsystem operated at maximum efficiency at a static head of 28 m. From Figure 2.7 it can be seen that the efficiency of the entire system is low, in the 2 to 4% range. It would be nice to increase this number; however, it must be remembered that the energy being used by the system is free.

What is most important is the initial cost of the system. If this can be made to be very small, than PV pumping systems will be the way to perform irrigation. While it is reasonable to assume that the highest operating efficiency will deliver the lowest initial costs, this is not necessarily true. Conversely it is true that lower overall efficiencies will require larger PV arrays. This generally will result in higher costs.

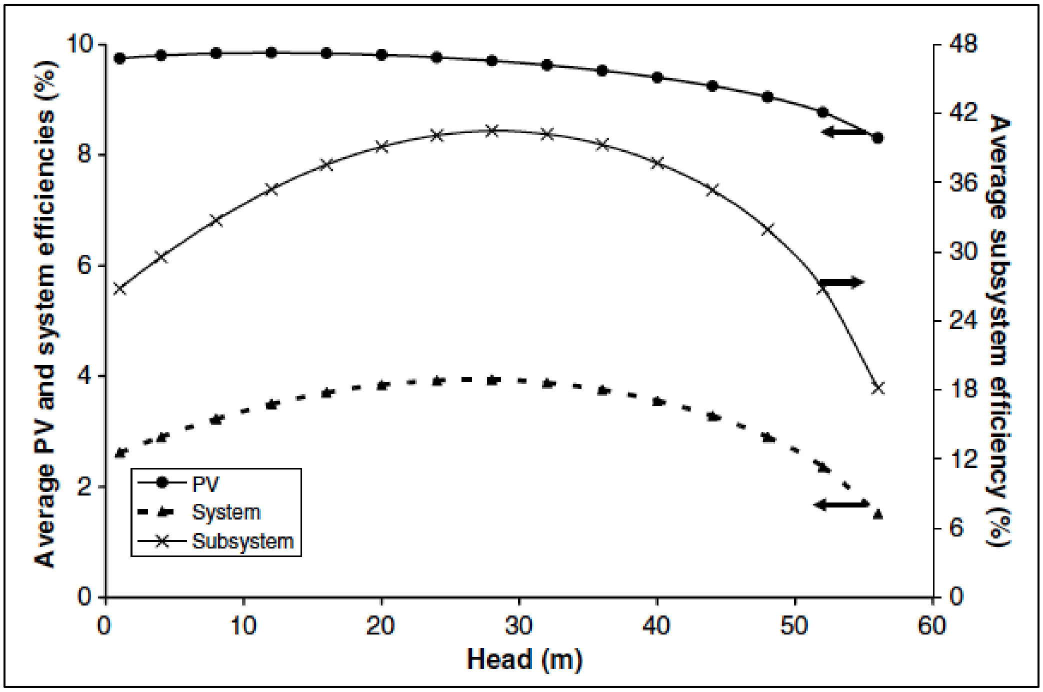

Figure 2.7: System, subsystem and PV efficiency versus static head (Odeh et al., 2012)

2.3. Summary

In the literature reviewed, various sizes of PV water pumping systems were studied. It can be seen that most of these PV water pumping system have been running successfully for more than 15 years in arid and semi-arid climatic zones. PV power is obviously a feasible and suitable option for water pumping applications in desert regions. Inaccessibility to grid lines and increasing fuel cost make PV water pumping systems attractive and economically viable in remote locations. All of the PV water pumping systems studied in this section did not use batteries for energy storage due to their high cost for large pumping capacities. In place of batteries, elevated storage tanks were used to store and deliver water when irrigation was required. This arrangement of using elevated storage tanks instead of batteries does not allow PV pumping systems to be run at their optimum efficiency point. This is due to the reason that motor-pump assembly is operating at reduced load conditions under diurnal variable solar irradiance. Directly coupled PV water pumping systems installed at Oran, Algeria demonstrated their success for lower flow rate applications. Jodhpur's PV water pumping system with drip delivery showed the reliability of using PV sourced pumping for cultivating orchard fields.

Pumping head, solar insolation, sizes of PV array and motor-pump assembly are important factors to design efficient PV pumping systems. Proper sized and best matched between PV array and motor-pump assembly are essential to operate a PV water pumping system at its maximum efficiency. It was shown in some of the studies mentioned above that at locations with higher insolation; PV sizing can be reduced to a design insolation point, which makes the complete system much more efficient and reduces the cost.

Chapter 3

Photovoltaic Irrigation System Experimental Setup

This chapter describes the experimental setup of a solar driven photovoltaic (PV) irrigation system. The overall PV irrigation system is divided into three major subsystems: a power subsystem, a data acquisition (DAQ) subsystem and an irrigation subsystem. The power subsystem includes the PV panels, solar tracker, batteries and maximum power point tracker (MPPT) - charge controller. Note that the MPPT and charge control are one unit in this system and will be referred to as the MPPT-charge controller in this thesis. The DAQ subsystem uses different sensors that measure the current, voltage, solar insolation, temperature, pressure and flow rate at a number of points throughout the PV irrigation system. DAQ cards sold by National Instruments were used to acquire data from the sensors.

The acquired data is processed and stored on personal computer using a LabVIEW program written specifically for this thesis project. The irrigation subsystem consists of a water pump, tubing and a water filter. The design and specifications of the equipment and devices used in this PV irrigation system are discussed in this chapter. The overall PV irrigation system will be discussed first and then each of the three subsystems will be discussed.

3.1. Overview of the PV Irrigation System

This PV irrigation system is an ongoing project that was originally started in 2011 as a Mechanical Engineering Senior Design project at Wright State University in Dayton, Ohio (Hull, 2011). Later in 2012, another group of Mechanical Engineering Senior Design students from Wright State University added the DAQ subsystem to the PV irrigation system (Rowland, 2012). In 2013, a third Mechanical Engineering Senior Design Group from Wright State University designed and built a vertical axis solar tracker (Strickalnd, 2013).

While these three senior design groups did some impressive design and construction work on the PV irrigation system, a great deal of work was still required in troubleshooting the DAQ subsystem, calibrating the DAQ subsystem, fixing broken parts, integrating the solar tracker into the PV irrigation system, and getting the entire system installed on the roof of the Russ Engineering Building at Wright State University. Originally this system was fixed mounted on the roof of Dennis Hance's garage in Piqua, Ohio. The PV irrigation system was originally designed to irrigate 0.25 acres of Hance's grape field. The PV irrigation system was then relocated to the fluids lab at Wright State University for troubleshooting problems associated with the DAQ subsystem and rewriting the software used to automatically collect data. After the DAQ system was made to work effectively and calibration work was done, the entire PV irrigation was installed on the roof of Russ Engineering Building at Wright State University and used to complete the main goal of this thesis work. That is to collect data on the performance of the PV irrigation system in Dayton, Ohio. It should be mentioned that nothing is being irrigated with this system; water is simply pumped in an out of a storage tank. Data has been collected for about two months from July to August and results are presented and discussed in the next chapter of thesis.

The overall schematic diagram of PV irrigation system is shown in Figure 3.1. Components or devices associated with power system are represented by red color. And, sensors and devices used by data acquisition subsystem are marked by light grey color. Whereas, parts used in irrigation subsystem are denoted by blue color.

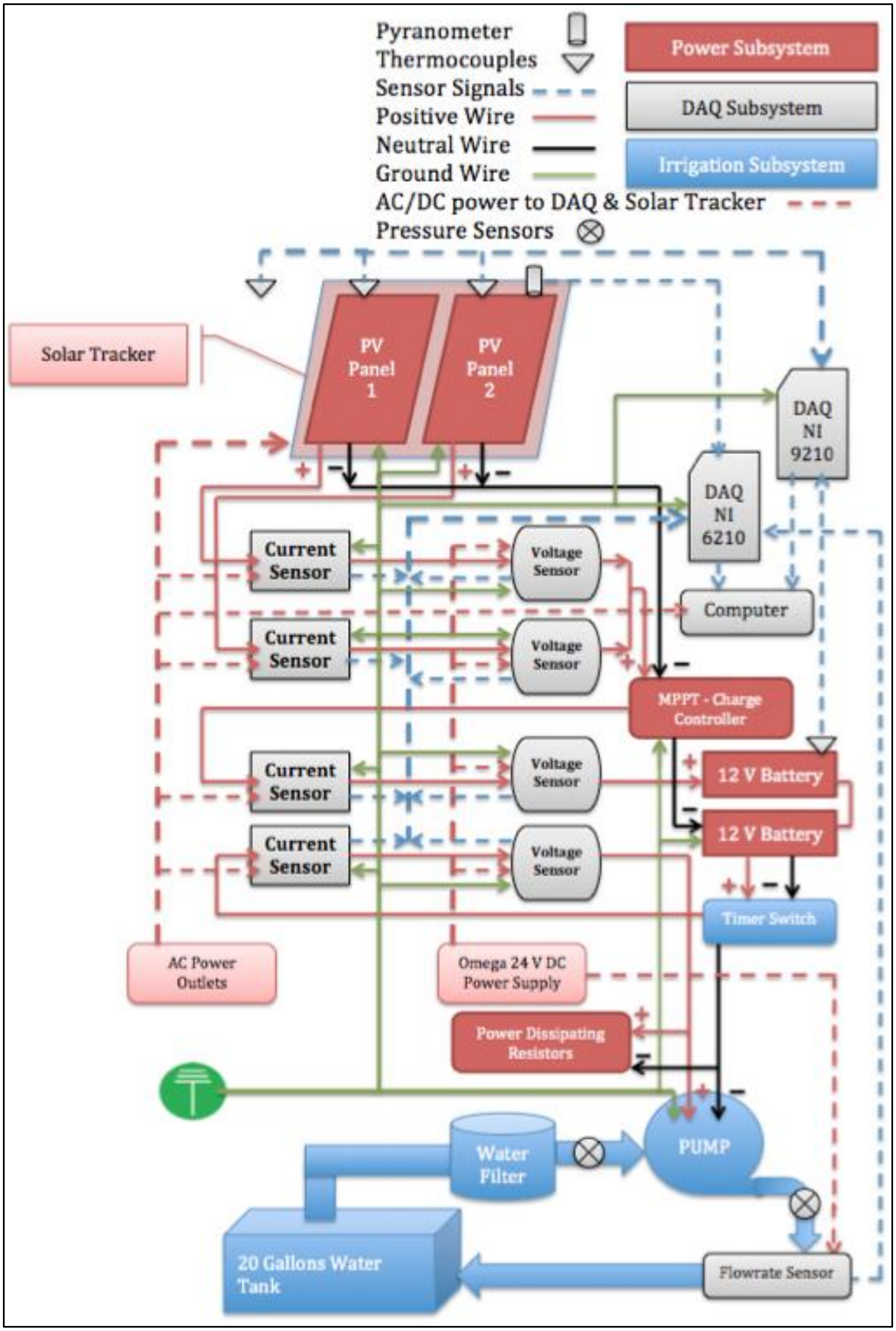

Figure 3.1: Overall schematics of PV Irrigation system.

Figure 3.2: Solar powered irrigation system on the roof of the Russ Engineering Building at Wright State University.

The overall PV irrigation system is shown in Figure 3.2. As mentioned above this system is divided into three major subsystems. The key pieces of equipment of the PV irrigation system are two 224 watt PV modules connected in a parallel arrangement. Each of these PV modules measures 0.99 x 1.64 meters for a total collection area of 3.25 m^2. The PV irrigation system is designed for complete off-grid application that stores power from the PV panels in two 12 volt batteries and delivers this power to a water pump. The batteries allow the system to pump water when the sun is not available. The PV modules convert solar energy into electricity by the photoelectric affect and store this energy in two batteries wired in a series arrangement. The batteries when fully charged, can deliver up to 100 amps-hour of energy at 24 volts.

As part of this thesis work a MPPT charge controller was added to the existing power subsystem. The MPPT-charge controller is connected in line between the solar panels and battery bank. The MPPT-charge controller installed with this system performs two different functions. First, it regulates the charge and voltage produced by the solar panels and delivers only safe voltages and currents to the batteries. This is done to prevent the batteries from overcharging. Secondly, the MPPT-charge controller tracks the voltage and current point at which the PV panels develop maximum power; this maximizes overall output of the PV irrigation system. Moreover, PV modules used in this system are mounted on a single-axis solar tracker to increase the amount of direct solar energy captured during the day over that captured with the fixed orientation design used on the system when it was located in Piqua, Ohio (Hull, 2011).

The irrigation subsystem of the overall PV irrigation system consists of a 100 watt, direct current centrifugal pump that operates at 24 volts, and is powered by the battery bank. This system was originally designed to pump rainwater from a tank and deliver it to grape plants using a drip irrigation system. However, due to the lack of a rainwater harvesting facility at the current location of this system, the pump only recirculates water via tubing and a tank. Since, the system was designed to irrigate with rainwater, a water filter is installed on the suction side of the pump to avoid the passage of debris and other fragments through the pump. In addition, a timer-switch is used for automatic operation of the pump, which takes 24-volt power from the batteries. For automatic operation of the pump, the required hours of daily pumping can be fed into the control settings of the timer to operate the pump on a weekly basis.

The existing DAQ subsystem used in this PV irrigation system uses several sensors to measure the current, voltage, temperature, pressure, flow rate and solar insolation. This instrumentation subsystem uses four current sensors and four voltage transducers to track the current and voltage from each panel, the battery bank and the pump. For temperature measurement, four thermocouples are used to measure the temperature of the two PV panels, the outside air temperature, and the surface temperature of the batteries. Solar insolation is an important parameter to track the performance of the PV modules; a pyranometer is installed at the same tilt angle as the PV panels to measure the solar insolation impinging on the PV modules. In addition, a flow rate meter is used at the discharge side of the pump to gauge the water flow rate produced by the pump. The original DAQ subsystem used two electrical pressure transducers, one installed at the suction side and one installed at the discharge side to measure the pressure rise across the pump. At the initial location of this system, water collected in the flow lines froze to ice in the winter season and damaged both pressure transducers. To keep costs down, the broken pressure transducers were replaced by two bourdon tube pressure gauges, which had to be manually read.

Figure 3.3: Solar powered irrigation system being raised to the roof of the Russ Engineering Building.

In order to properly install this system on the roof of the Russ Engineering Building, the base or foundation of the solar translator was built using sixteen 2 by 4 boards as shown in Figure 3.2. These boards were then loaded down with 60 pound sand bags to keep the system from being moved by the wind. Permanent anchoring to the roof of the Russ Engineering Building was not done to avoid putting holes in the roof. Officials at Wright State University wanted to avoid piecing the roof to avoid future rainwater leakage problems. This meant the most feasible option was to mount this solar system by applying sufficient weight to its foundation. The PV irrigation system uses a solar tracker that moves from east to west. Because of this, the wind affect has to be taken into account in all directions and sufficient weight had to be applied on each side of the board base to prevent this system from tipping over in high speed winds. Solar panels have a sailing area of 3.25 m^2 and to counter wind speeds up to 70 mph, four sand bags weighing a total of 240 lbs. were put on all four sides of the translator. Thus 960 pounds of sand is used to hold the PV irrigation system in place. Movement of all equipment, as well as the solar panels, onto the roof of the Russ

Engineering Building was facilitated with the help of the NEC building construction crew and their long reach lift vehicles as shown in Figure 3.3.

Data acquisition cards by National Instruments have been employed in the DAQ subsystem to acquire the data from the above-mentioned sensors. Data acquired by DAQ cards are sent to the LabVIEW software, which processes this data and stores it in a computer. Moreover, the MPPT-charge controller has its own data collection system. The MPPT-data recorder stores the array voltage, array current and power output of the PV array. The MPPT-charge controller data recorder also acquires the data such as battery voltage, battery current and power delivered to the battery bank. The MPPT-charge controller data acquisition provided an additional validation of the existing DAQ subsystem instrumentation.

It is important to note that the PV array is rated at 448 watts; which is more than the 100 watts required by the water pump. This oversize was designed into the system so that the batteries could be charged while the pump is running. This oversize was also designed into the system so that additional power would be available to run power tools. Because of this oversizing of the solar panels, the MPPT-charge controller would prevent the solar panels from delivering power to the batteries for a good portion of the day. This meant that the performance of the PV panels was greatly degraded, because there was no place to deliver all the power that the PV panels could produce in the Dayton sun. Thus a technique was needed to drain power from the batteries at faster rate than the pump could do. To do this, an additional load of 350 watts was connected to the PV irrigation system using four power-dissipating resistors wired in parallel to the pump. This enabled us to see the maximum performance of the PV panels for longer portions of the day. All the components and devices of the power subsystem, DAQ subsystem and irrigation subsystem are properly grounded to a common ground source.

3.2. Power Subsystem

The PV modules, solar tracker, MPPT- charge controller and batteries are the components, which make up the power subsystem of this PV irrigation system. The working mechanisms and specifications of these devices are discussed in this section.

3.2.1. Solar Panels

The system uses two ND-224UC1 PV modules manufactured by the Sharp Electronics Corporation and are shown in Figure 3.4. Each module measures 0.99 x 1.64 meters and consists of 60 polycrystalline silicon cells connected in series, which can produce maximum power (P_{max}) of 224 watts at standard test conditions (STC). STC refers to standard test conditions for PV modules which are 25° C, 1000 watts-m^{2} of solar insolation and a non-dimensional air mass (AM) of 1.5. It is important to note that operating temperatures of these PV modules are usually higher than 25° C; at higher temperatures than 25° C PV panels produce less than their rated power output at a solar insolation of 1000 watts-m^{-2} and their efficiency drops due to this temperature affect.

Figure 3.4: Photovoltaic modules used in the PV irrigation system.

The efficiency of these modules is 13.74 %, which can produce a maximum power voltage (V_{pm}) and current (I_{pm}) of 29.3 Volts and 7.66 amps respectively at STC conditions. The open circuit voltage (V_{oc}) and short circuit current (I_{sc}) of this module is 36.6 volts and 8.33 amps respectively. Both modules are connected in parallel via multiple contact locking connectors, MC4 connectors, to maintain approximately 28 volts. So that the performance of each individual PV panel can be measured, the individual positive side wires from each panel run through current sensors and are linked together before they are connected to the MPPT-charge controller. Similarly, negative wires from the panels are also linked together via MC4 connectors, but they are connected right after the panels' outlet. Subsequently, positive and negative wires from the PV array are connected to relevant terminals of the MPPT-charge controller.

3.2.2. Solar Tracker

The single-axis solar tracker of this system follows the sun's position throughout the day from east to west moving around a vertical axis with a tracking range of 140 degrees (see Figure 3.5). This solar tracker moves in discrete steps and tracks the sun's azimuthal angle.

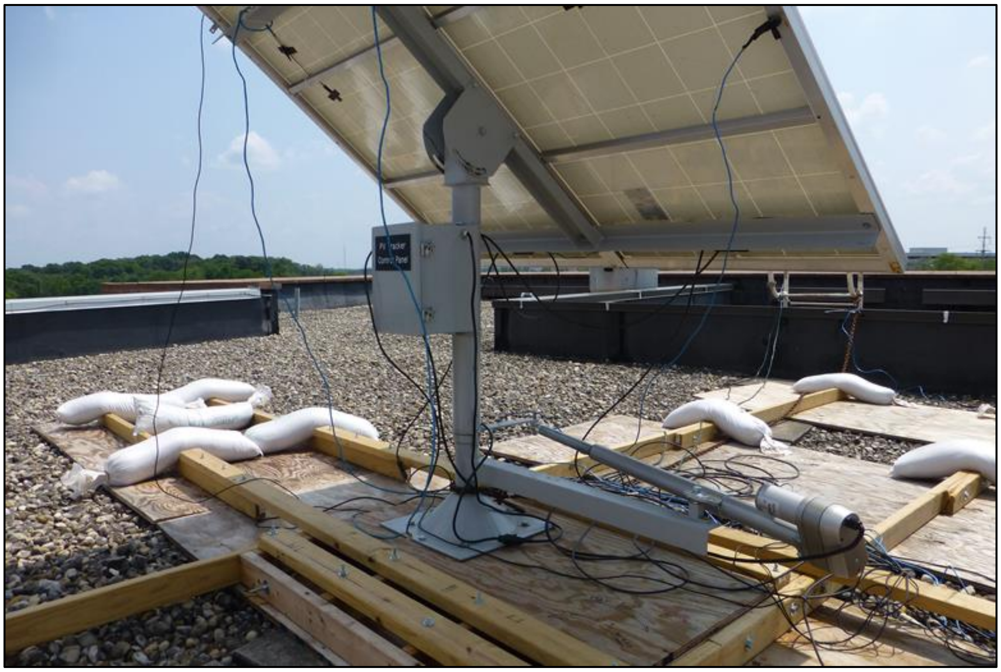

Figure 3.5: Single axis solar translator.

The solar tracker is equipped with an AC powered Altronix 2-channel programmable timer, which actuates a 24 volt DC motor at a current of less than 4 amps. Having two channels of this programmer allows the motor to actuate in forward and reverse paths; this allows the tracker to rotate in east and west directions.

The timer in the solar tracker can execute 50 events in one direction and every event can actuate the motor for 1 to 15 seconds. Each second corresponds to a rotation of 1.25 degrees. The azimuthal angle of the sun was calculated every thirty minutes for Dayton, OH; it has been fed into the clock setting of the timer. The timer is programmed to execute 32 events from east to west at 30 and 15 minute intervals based on the sun's azimuthal angle.

The timer is programmed to reset and adjust the position of the solar tracker to due east at night and it starts tracking the sun the next day from sunrise to sunset. The solar tracker also allows manual adjustment of the altitude angle of the panels from 0 to 60 degrees from a horizontal surface. The solar tracker enables this system to receive more direct solar energy and increases the efficiency of collection by 25% for the Dayton, Ohio area (Strickland et al. 2013).

3.2.3. Batteries

This solar PV irrigation system is designed for a complete off-grid application, which stores the power generated by the solar panels in batteries. The system uses two sealed lead acid 12 volt, deep cycle batteries, manufactured by Werker. Each battery can deliver 100 amp-hours of energy at 12 volts. These batteries are wired in a series arrangement to supply power to the pump and MPPT-charge controller and can deliver 100 amp-hours of energy at 24 volts. Batteries can deliver continuous power to the pump for 58.8 hours of pumping operation. This provides the backup power for the pump to run for more than two days in case of overcast weather.

3.2.4. MPPT – Charge Controller

The solar PV irrigation system uses a TS 45 maximum power point tracker (MPPT) and changer controller that regulates the current and voltage coming from the PV array and adjusts the voltage and current delivered to the batteries. This MPPT-charge controller is shown in Figure 3.6. The purpose of using this device was to increase the energy harvest from the PV array and to protect the batteries from overcharging. Based on the rated power of our panels, this MPPT-charge controller was the suitable choice to work within the range of our system. The controller uses a tracking algorithm that tracks and maintains PV output at the array peak power production point. This MPPT-charge controller can supply a maximum of 45 amps current from the PV array to the batteries. Since, our PV array consists of only two PV panels connected in parallel, the MPPT- charge controller can deliver a maximum current of 17.32 amps. The MPPT controller has four terminal connectors; two terminals feed the positive and negative leads from the PV array and the other two terminals are connected to the positive and negative terminals of the batteries.

Figure 3.6: Maximum power point tracker (MPPT) – charge controller.

The controller is also equipped with voltage and current sensors to measure the voltage and current from the batteries; this feature enables the controller to optimize the charging operation of the batteries and improve the system performance. The controller features adjustable switch settings that can be set to achieve a desired maximum voltage depending upon the voltage of the PV array and battery bank.

This controller operates in three different charging stages, which are MPPT, absorption and float stage. Each stage is executed depending upon the charge and voltage level of the battery bank. The MPPT stage provides the maximum current that a PV array can supply and stores the maximum amount of power into the battery bank until the battery bank voltage has reached its maximum level. This stage occurs when the battery bank charge level is below 50%. Once the battery bank voltage reaches to the maximum point that the batteries can handle, the MPPT stage changes to the absorption stage. In this stage the MPPT limits the input current at the maximum voltage the battery bank can handle. After the batteries are fully charged, the controller changes the absorption stage to the float stage; at this point no current is delivered to the batteries: this stage prevents the batteries from long-term overcharge. Three LED lights of green, yellow and red display the current state of charge of the batteries. LED indicators also indicate if there is any fault in the system.

3.2.5. Power Dissipating Resistors

The nominal load of the pump is small compared to the rated power output of the PV array. This was designed this way so that the pump could run for long periods where there was no sun. During actual PV system operation, the battery bank reaches its float stage fairly quickly at low solar insolation levels. Once the battery is at its float stage, the MPPT restricts the flow of current from the PV array to the battery bank. At this point, the PV array produces no power or very small amounts of power at any insolation level. To overcome this condition of the system, power-dissipating resistors were connected as a dummy load to allow the PV panels to harvest the maximum amount of power possible for a greater portion of the day. Therefore, four resistors (see Figure 3.7) with an equivalent resistance of 1.96 ohms were connected to the battery in parallel to the pump. One of the four resistors used in this system cannot be seen in this figure. These resistors can dissipate power up to 305 watts in addition to the pump load.

3.3. Irrigation Subsystem

The irrigation subsystem of this PV irrigation system primarily consists of a water pump, water tank, some tubes and a timer for automatic operation of the pump.

3.3.1. Pump

A 100-watt centrifugal, positive displacement Dankoff solar pump is used in this system for water irrigation. This pump requires a 24 volt DC supply, which comes from the battery bank. This pump is capable of lifting water a 450 feet vertical height. This pump can deliver 4320 gallons of water per day at a flow rate of 3 gallons per minute and requires 50 watts of power to develop pressures of 25 and 2 psi at the discharge and the suction side respectively. The current draw and flow characteristics of this pump are shown in Figure 3.8. Although, power of pump is rated at 100 watt by manufacturer but at current design, it consumes approximately 50 watt of power.

Figure 3.7: Power-dissipating resistors connected in parallel.

Figure 3.8 shows that in order to maintain a consistent flow rate, the current draw from the pump rises with increase in the pump head. Because our Solar PV system has been placed on the roof of the Russ Engineering Building for experimental data collection, the pump only recirculates the water in a 20 gallon water tank and there is very little load placed on the pump. In order to gauge the pressure rise across the pump two pressure gauges have been installed; one at the inlet and one at the outlet of the pump. The irrigation subsystem, such as the pump and tubing are housed in one covered wooden along with the power dissipating resistors.

3.3.2. Tubing and Water Tank

Tubing and PVC pipes are used at the suction and discharge side of the pump to circulate the water in a 20 gallon tank as shown in Figure 3.9. The PVC pipe used at the suction side measures 5.7 feet in length and 3/4 inch in diameter. A water filter has been installed at the suction side of the pump to eliminate the passage of debris through the pump. T-joints have been used at the inlet and outlet of the pump to facilitate the installation of pressure sensors or gauges. Elbow joints and connectors link several pieces of PVC pipe together from the water tank to the inlet of the pump. At the discharge section, a flexible pipe that measures 5 feet in length and 3/4 inch in diameter connects the pump and the water tank through the flow rate meter.

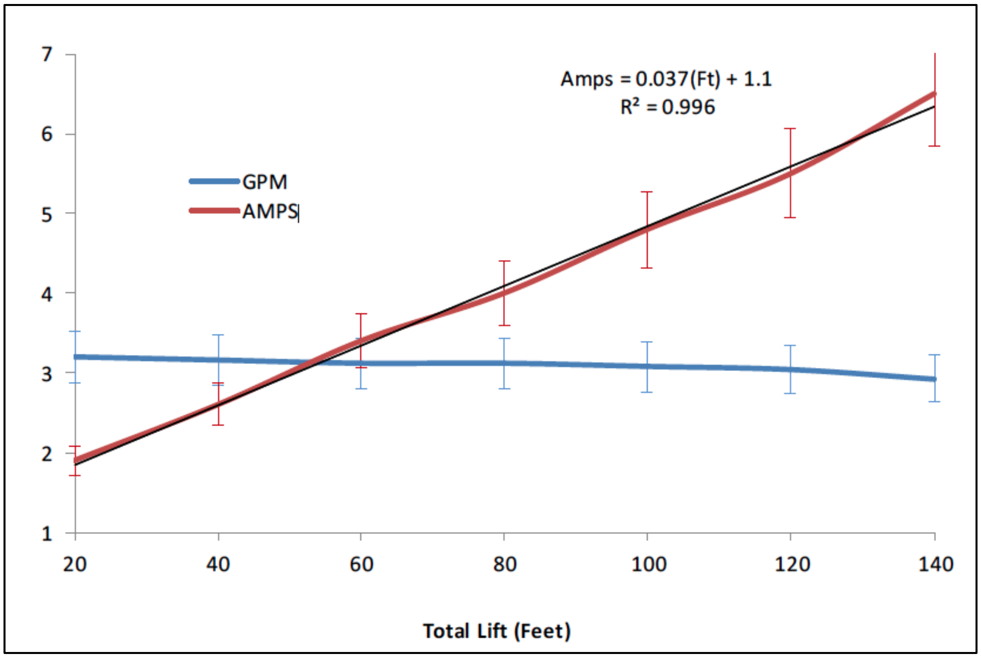

Figure 3.8: Current draw and flow rate characteristics of the pump (Rowland et al., 2012).

3.3.3. Timer

A programmable, 24 volt DC timer switch by Brazix is installed for automatic operation of the pump (see Figure 3.10). It can be programmed to switch on and off up to 6 different times in a 24 hour time period. The timer uses three modes of operation, which are on, off and auto. In the auto mode, the timer operates the pump at preset times determined by the user. Then, there are two on and off modes that enable the user to manually switch on and switch off the pump anytime during the day. Once, the timer is operating in on or off mode, the timer overrides the events programmed in automatic mode. In our PV system the timer is connected in such a way that it operates the resistors and the pump at the same time. The recommended current to operate this timer is 15 amps; therefore, a 15 amp fuse is installed inline between battery and timer for its protection. This matches the current requirement of the pump and resistors because the total current draw from the batteries to the pump and resistors does not exceed 14.5 amps.

Figure 3.9: Irrigation subsystem of solar PV irrigation system.

The timer has four electrical port connectors labeled A, B, 1 and 2. Ports A and B are connected one-to-one to the positive and negative terminals on the battery; while the 1 and B ports are connected to the positive and negative terminals on the pump. Terminal 2 is connected to port A. Battery life quickly depreciates if it is discharged below 30 percent of its total charge level. At times when the solar insolation is low, the rate of power consumption by the pump and resistors remains higher than the PV array output. For this operating situation the batteries get discharged quickly. Therefore, the timer has to be switched on and off manually to prevent the charge level of the batteries from dropping below 30%. The intermittent nature of solar insolation does not allow us to run the pump and resistors on a preset automatic mode using the timer and thus manual operation of the pumps and resistors was performed.

3.4. Data Acquisition Subsystem

The DAQ subsystem consists of sensors, data acquisition cards and a computer. All the diagnostic instruments along with the MPPT-charge controller, batteries and computer are housed in a wooden box, covered with a plastic sheet to keep the equipment dry when it rains. Calibration tests were performed on most of the sensors to ensure that accurate output is obtained.

Figure 3.10: 24 volts DC programmable switch.

The objective of employing this DAQ subsystem was to measure the following quantities associated with the PV irrigation system:

- voltage delivered by each PV panel,
- current delivered by each PV panel,
- power delivered by each PV panel,
- power delivered to batteries,
- power delivered to pump,
- surface temperature of PV panels,
- ambient temperature,
- battery temperature,
- water flow rate from pump,
- water pressure at the inlet and exit from pump, and
- solar insolation incident on PV panels.

3.4.1 Current Sensors

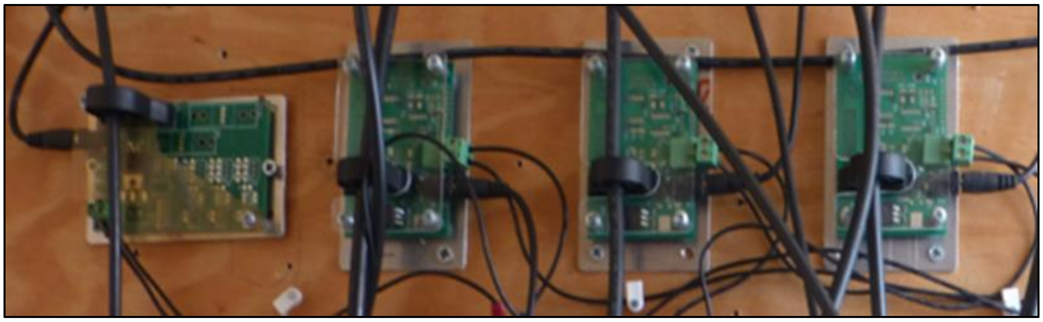

Figure 3.11: Four H - ACDC current sensors.

Four H-ACDC-70 current sensors (see Figure 3.11) have been used in this DAQ subsystem to measure the current delivered by each PV panel and current delivered to the batteries and the pump. Current sensors use hall-effect transducers to sense the electric current by measuring the magnetic field around the wire. Sensors have a current sensing range of ±70 amps with a response time of 3 microseconds. According to manufacturer specifications, this current sensor can generate an output signal with an accuracy of ±3% of full-scale, which is 2.2 amps. In order to enhance the accuracy and minimize the error in the output, these current sensors have been calibrated against a hand held Extech multi-meter with a 20 amp sensing range. The current range for calibration of these sensors was from – 3 to + 14 amps. After calibration, these sensors are estimated to have an uncertainty of ± 0.7 %, which is an error of 0.5 amps. The sensitivity and accuracy of these sensors can be improved by increasing the number wire loops through the doughnut sensor. The linear relationship between input current and output signal in volts obtained during the calibration process is shown in Figure 3.12. The voltage output from these current sensors is on the order of millivolts, which is small and can be affected by any electrical noise present in the vicinity of the sensors. For this reason, the output signals from the current sensors show small fluctuations.

3.4.2. Voltage Transducers

The DAQ subsystem has four voltage transducers by CR magnetics, to measure the voltage of each PV panel, the battery bank and the pump. The output range of these voltage transducers is 150 volts and the input power is 15 mA at 24 DC volts, which is supplied by an Omega 24 volt, DC power supply.

The voltage transducers generate an output signal ranging from 0 to 10 volts DC, which is proportional to the input voltage being measured. The voltage transducers have been calibrated against a hand held Fluke voltmeter and they generate very accurate output signals with an uncertainty of ± 0.04 %. These voltage transducers can be seen in Figure 3.13.

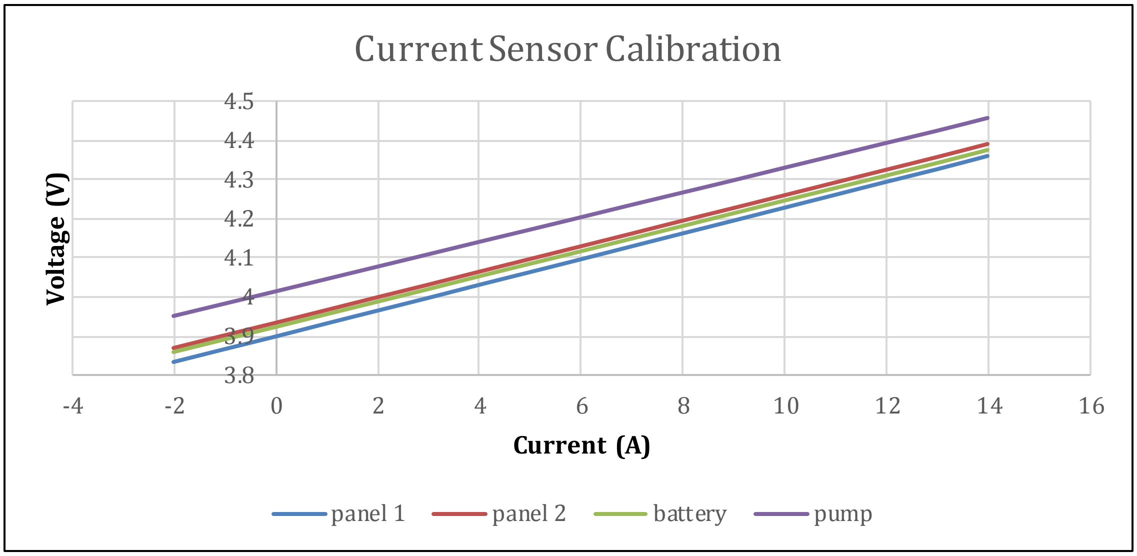

Figure 3.12: Current sensor calibration results.

Figure 3.13: CR531150 magnetic voltage transducers.

3.4.3. Thermocouples

Temperature measurement is also very important in this project. The efficiency of the PV modules is a function of their nominal operating cell temperature (NOCT). Once the solar insolation increases, PV panels get hot and their efficiency drops. Ambient temperature is also significant, because outside air temperature can also affect the temperature of the solar panels. Moreover, it is important to record temperature changes in the batteries, as they get charged and discharged. This information is helpful in understanding the performance of this system.

Figure 3.14: Thermocouples installed on backside of PV panels.

So as to assess the temperature effect on operation of this solar PV irrigation system, it was required to measure the surface temperature of the solar panels, the batteries and the ambient temperature. Two thermocouples are installed on the back sheets of the two PV panels as shown in Figure 3.14. The other two thermocouples record the ambient and surface temperature of the batteries. These thermocouples are calibrated at the reference temperature of an ice-water mixture in equilibrium and the outside air temperature. The outside air temperature was measured with an independent thermocouple. It has been determined that that the output of these thermocouples has an uncertainty of ± 5%.

3.4.4. Pyranometer

Solar insolation is an important parameter in this project to assess the efficiency of PV panels. An Apogee SP-110 pyranometer is installed at the same tilt angle as the PV panels to measure the solar insolation impinging on the PV modules as shown in Figure 3.15 (a).

Figure 3.15: (a) Apogee SP – 110 pyranometer (b) Pyranometer under sensitivity test.

This pyranometer is a self-powered sensor with a sensitivity of 0.20 mV per W/m^2 and generates an output signal with an uncertainty of ±5%. The pyranometer is pre-calibrated by the manufacturer and its sensitivity varies with ambient temperature. We do not have any device to calibrate this sensor with reference to some known source of radiation and thus we are relying on the manufacturers ratings.

In order to understand the angular sensitivity of the pyranometer; a test was done. The pyranometer was fixed at one end of an adjustable protractor, facing exactly at the azimuthal angle of the sun as shown in Figure 3.15 (b). The output of pyranometer was recorded every second and averaged over a period of one minute; this output in Watts/m^2 has been plotted as function of angle from 0 to 180 degrees. The test result is shown in Figure 3.16; the black dot represents the altitude angle of the sun for Dayton, Ohio at the time this test was conducted, which is at 60°. The pyranometer detects a maximum solar insolation of 969 Watts/m^2 at this point because the sensor is facing directly towards the sun. The results shown in Figure 3.16 show that the pyranometer has a cosine type of sensitivity to the direction of the sun's solar irradiation. This is exactly what is expected. The close symmetry of the results around the altitude angle of the sun was also expected.

3.4.5. Pressure Sensors

The DAQ subsystem uses two Bourdon tube pressure gages to measure the water pressure at the inlet and outlet ports of the pump. There is no electrical signal from these pressure gages and thus their output cannot be read and stored using the computer. The pressure from these gages has been recorded manually during the pumping operation. For most of the pump's operation there was a pressure of -2 psig at the inlet port and +25 psig at outlet port. Thus the pump was developing a 27 psi pressure head.

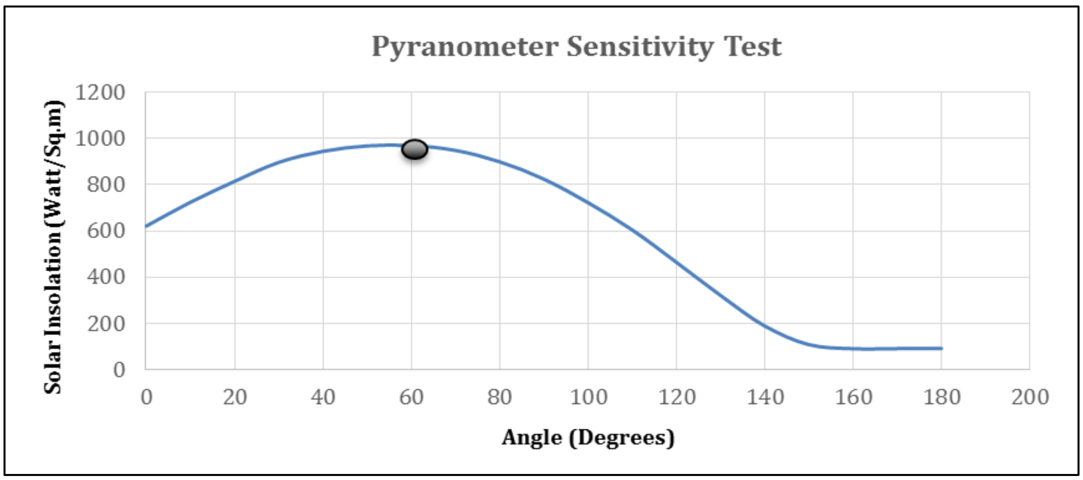

Figure 3.16: Pyranometer output as function of its altitude angle. The altitude angle of the sun is shown with a black dot to be 60º.

3.4.6. Flow Rate Sensor

To measure water flow rate the DAQ subsystem uses an A-712 flow rate sensor by Dyer Instruments that is installed at the outlet of the pump as shown below in Figure 3.17.This flow rate sensor delivers its output signal as a voltage and thus is compatible with our DAQ devices. Originally a hall-effect flow sensor was used that had an output signal in frequency. The present flow rate sensor is more convenient and economical than the hall effect flow meter. The present flow meter is capable of sensing water flow rates from 0 to 5 gallons per minute and requires a 24 volts DC power supply to produce output signals from 1 to 10 DC volts with an accuracy of ± 5%. The flow rate sensor was checked against a bucket and stop watch method to ensure its accuracy.

Figure 3.17: A-712 flow rate sensor.

3.4.7. Data Acquisition (DAQ) devices

All outputs from the sensors, except the pressure gages, were sent to a DAQ device and delivered to the computer to be manipulated and stored. In this regard, two USB plug-in DAQ devices, i.e. NI 6210 and NI 9210, by National Instruments are used to sense output voltage signals of the various sensors and convert the sense voltage to a digital signal. The NI 6210 module can support up to 16 channels but we are only using 10 channels. Ten channels are required to sense the voltage output signals from four current sensors, four voltage transducers, one flow rate sensor and one pyranometer. While, it is possible to feed signals of thermocouples to the NI 6210 module, the output signals generated by thermocouples are small and signal amplification is required for noise elimination. In order to minimize noise effects, the NI 9210 thermocouple input DAQ module is used. This module is specially designed to read thermocouple outputs and using signal conditioning to cancel out unwanted noise and deliver a digital signal to the computer. This device is capable of reading the 4 output signals using 8 differential input modes of the four thermocouples mounted on the PV irrigation system. The NI 6210 and NI 9210 DAQ modules are shown in Figure 3.18.

Figure 3.18: Data acquisition (DAQ) devices NI 9210 and NI 6210.

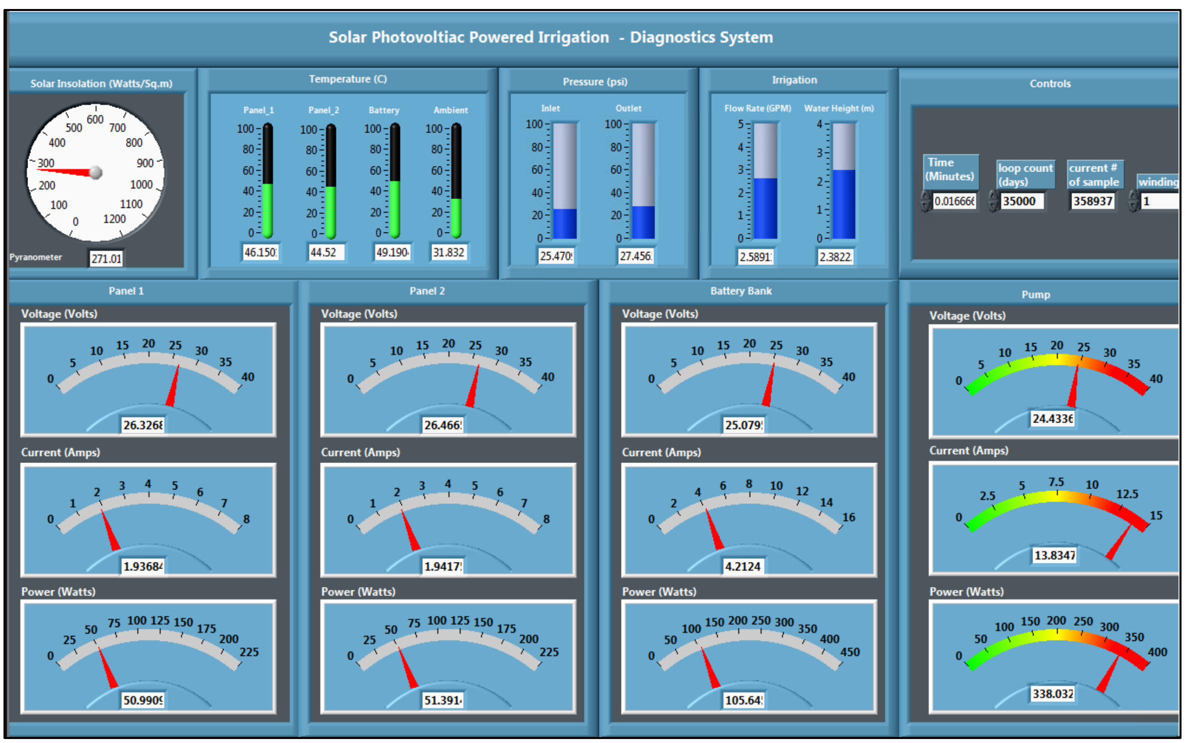

Figure 3.19: Front panel of LabVIEW program.

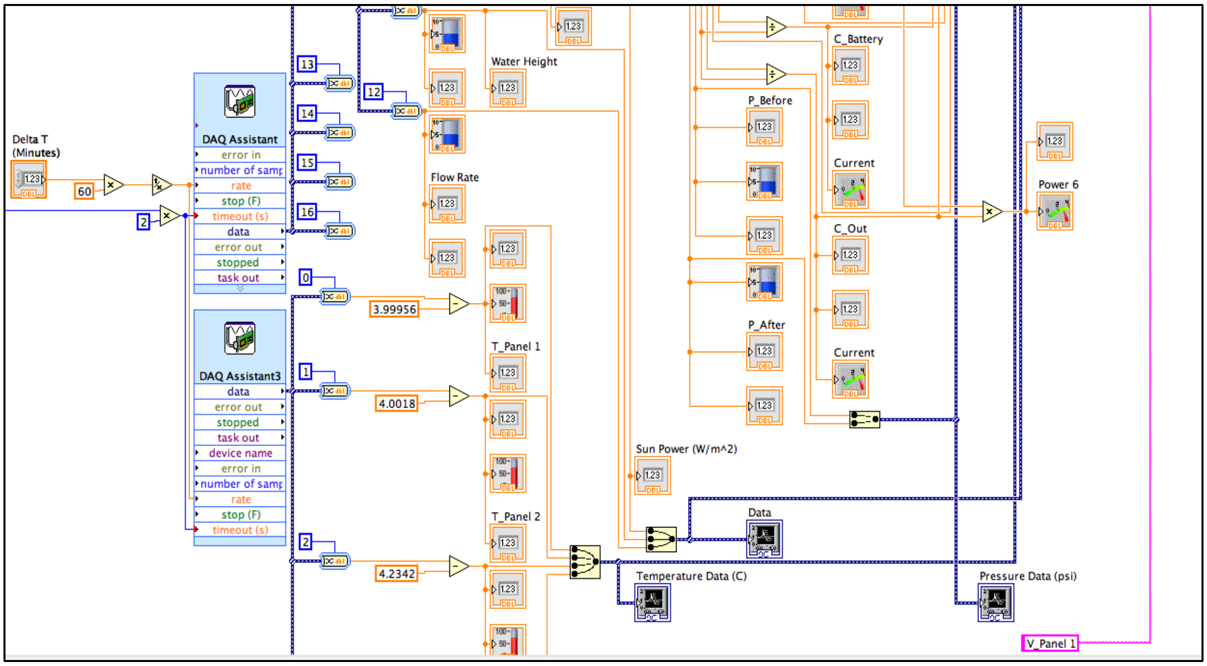

Figure 3.20: Block diagram of LabVIEW program.

3.4.8. LabVIEW software

DAQ devices such as the NI 6210 and the NI 9210 acquire data from the sensors and transmit this data to the computer. In order for the computer to understand and accept these data, LabVIEW software is used. In addition to programing the computer on how to accept the data from the DAQ devices, the LabVIEW software allows us to control the data acquisition process and to manipulate the signals acquired from the sensors. A LabVIEW program has been developed, which processes the acquired data and presents this data in a graphical user interface (GUI) format. Control of the system is also on the GUI. The GUI displays the output data of all the installed sensors in an easy and interactive mode. Figures 3.19 and 3.20 show the front panel and block diagram of the LabVIEW software developed as part of this Masters Thesis work. The front panel of this software is mainly used to display the output of the sensors. All the sensors used in this DAQ system provide output signals in volts; the block diagram of LabVIEW is used to convert the voltage signals into the desired units such as current, voltage, temperature, flowrate, or solar insolation. The conversion and calibration factors obtained during the calibration tests of the various sensors have been coded into the LabVIEW program so that accurate results are displayed on the GUI. LabVIEW software has been programmed to acquire data every second and stores this data in excel files in computer for later use if needed. It is easy to change the period between data acquisition events from a second to any time desired with a simple input value. In this work we have obtained data on the second time interval.

Chapter 4

Results

This chapter presents a large number of results on the performance of the PV irrigation system discussed in the prior chapters of this thesis. In this work, various measurable quantities associated with the PV irrigation system have been obtained as a function of the time of day and of the configuration of the PV irrigation system. Four different configurations were studied. These configurations differ by the orientation of the solar panels relative to the sun and the way in which power is dissipated from the batteries. The four configurations studied are:

1. azimuthal solar tracking at an inclination angle of 40° with both the water pump and power dissipating resistors being used to consume the power generated by the PV array,
2. azimuthal solar tracking at an inclination angle of 30° with both the water pump and power dissipating resistors being used to consume the power generated by the PV array,
3. a fixed solar array pointing due south at an inclination angle of 40° with both the water pump and power dissipating resistors being used to consume the power generated by the PV array, and

4. azimuthal solar tracking at an inclination angle of 40° with only the water pump being used to consume the power generated by the PV array, where the water pump is run 24 hours a day.

Results from each of these four configurations are given in each of the four subsections directly below. The first three configurations listed above deal with the orientation of the solar panels relative to the sun and the last configuration deals with the dissipation of power from the system. Of course different orientations of the solar panels relative to the sun will enable different electrical energy production by the solar panels; however, it must be realized that the power dissipation from the batteries also causes different amounts of power to be delivered from the solar panels. When the batteries are fully charged, the MPPT-charge controller stops delivery of electrical energy from the solar panels; and thus no current flows from the solar panels. The panels still produce voltage, but no current is produced. This proved to be a difficult issue to deal with because the batteries should not be discharged less than 30% of full charge. This means how much the pump and power dissipating resistors can be run is limited and depends on the amount of solar insulation on the panels. Thus a crude manual process was used to switch the pump and power dissipating resistors in and out of the circuit. Because this process was not well refined, there are a number of times when the batteries became fully charged and the sun was still shining brightly. This means the results in this chapter will show at times when the solar irradiation is high, but no power is flowing from the solar panels to the batteries. For the first three configurations tested in this work the pump and dissipating resistors were switched into the circuit one or two times a day.

For the first three configurations of the PV irrigation system listed above, the pump and power dissipating resistors were connected in parallel and were operated using the same timer switch. Once the timer switch is turned on, both the pump and resistors draw and dissipate power. Thus, for the first three PV irrigation system configurations listed above, switching on the pump implies that both the pump and power dissipating resistors are turned on. For the fourth configuration listed above, where only the water pump is being run, no power dissipating resistors were used.

All of the data presented in this chapter were taken towards the end of July and throughout the month of August in the year of 2014. The location of the system during the time these measurements were made is on the roof of the Russ Engineering Building located on the Wright State University campus, which is located in Dayton, Ohio. Each of the four configurations was run for approximately one week with the data acquisition subsystem recoding measurements every second, 24 hours a day. This means that data is taken when the sun is down, as well as with the sun up. While night time results are not very interesting, it was easy to let the system run 24 hours a day since all data acquisition was automatically done. In addition, nighttime results will be presented in the plots that follow and serve as a good division between the results for each day. While second level data acquisition is rather quick for solar PV systems, this quick of a data acquisition process does allow the reader to see some electrical phenomena that is occurring in the system. For some of the results presented in this chapter the data has been averaged to the minute level. Because of clouds, the solar energy striking the panels can vary on the minute level.

For all four configurations tested plots of voltages, currents, powers, temperatures and energy production are presented in their own subsections. The voltages and currents are presented for each PV panel in the system, for that going to the batteries, and for that going to the pump and dissipating resistors. Temperatures are presented for each PV panel, the batteries, and the surrounding air temperature. Power flows are presented for the PV array and the batteries. Energy production is presented for the PV array. For the first configuration presented additional subsections are introduced for the solar irradiation, the water flow rates from the pump, and the PV array efficiency. The solar insolation section is not duplicated for the remaining three configurations because the solar irradiation results are plotted on plots for the voltage, current, and temperature and a separate section for these results is not required after and explanation of the solar insulation behavior has been given. The water mass flow rate and PV efficiency results are not duplicated with the remaining three configurations because these results are essentially the same for all four configurations tested. The pump was always run with the same pressure head and thus the flow rates did not change. The PV efficiency for the remaining three cases can be found in Appendix C and the reader can verify that plotting this quantity versus solar irradiation looks similar for all configurations.

To produce the plots and perform some data manipulation a MATLAB data manipulation code has been written. This is essential due to the large amount of data that has been collected. Initially, Microsoft EXCEL software was tried to process this data; but EXCEL software has its own limitations and it cannot process more than 32,000 data points. Whereas, the data collected consisted of 1.9 million data points in only a 24 hour time period, a MATLAB code was specifically written to process this data and produce graphical results.

Moreover, PV panels receive maximum solar energy if they are facing directly at the sun. The solar tracker employed in this PV irrigation system has been used to track sun for increased collection of solar energy throughout the day. This allows PV array to capture most solar radiation and produces maximum energy. Since altitude angle of sun is higher in summer, orienting PV panels' tilt relatively lower to altitude angle of sun can increase energy production. The best practice is to adjust PV array tilt at complement angle of sun's altitude angle. The altitude angle refers to sun's angular position from horizontal surface and it changes with time during the day. But in following work, altitude angle is referred to sun position at which sun moves and stays maximum amount of time during the solar noon. To harvest maximum amount of solar energy for PV irrigation system, altitude angle of sun was determined for Dayton, OH for the month of August, which is about at 60°. Thus by adjusting the tilt angle at 30° would allow PV array to capture maximum solar radiation in August. Note that the 60° is not the maximum altitude angle of sun in August for Dayton, OH. It can be as high as 68° but it was positioned in such a way that panels could still track sun in the morning and evening, when sun is lower in the sky.

Since solar insolation is ultimate driving force in the operation of the PV irrigation system and solar insolation affects parameters such as voltage, current, power and temperature it is presented in a number of the plotted results shown below. Therefore in the plots shown below the voltage, current, power and temperature have been plotted on the primary y-axis as function of time, located on the x-axis, and the solar insolation is plotted on the secondary y-axis. Results obtained in each case have been discussed separately and performance outputs of individual parameters in these cases have been graphically represented.

4.1. Azimuthal Solar Tracking at an Inclination Angle of 40° with both Water Pump and Power Dissipating Resistors

For this set of results the solar tracker was employed to track the sun from east to west while the inclination angle of the PV array was kept at 40°. The PV irrigation system was tested in this configuration for 12 days from July 28th to August 8th, 2014. The results taken from measurements obtained from July 28th to August 3rd, 2014 are presented in this subsection and the results obtained from the measurements taken from August 4th to August 8th, 2014 are presented in Appendix C. This was done so the plotted results can be seen more clearly and the results presented for the other three cases are only for one week.

4.1.1. Voltages

Voltage outputs versus time recorded by the data acquisition subsystem at various points such as panel 1, panel 2, the batteries and the pump are shown in Figure 4.1 for seven days from July 28 to August 3. In addition to results from the data acquisition subsystem developed for the PV irrigation system, there is an array voltage measurement made by the MPPT data logger, labeled "V MPPT Array", and battery voltage measurement made, labeled "V MPPT Battery", that are shown on these plots. Some of these curves placed on this graph cannot be seen because they lie on top of one another. This is true of the voltages labeled panel 1, panel 2, and V MPPT Array, and the curves labeled V battery and V MPPT Battery. The V MPPT Array voltage lies over Panel 1 and Panel 2 voltages and the V MPPT Battery voltage lies over the V battery voltage. These curves should lie over the other and this serves as a verification check on these measurements.

The solar insolation sensed by the pyranometer is also plotted in Figure 4.1 on the secondary y-axis. This is the dark black line on the graph. It can be seen that the solar insolation has oscillations throughout the day. These oscillations are due to clouds going in front of the sun. When the sun is unobstructed and shining directly on the solar panels more than 1000 W/m^2 of solar energy hits the panels.

The pump was operated once or twice every day throughout this week depending on the solar radiation. The reader can easily determine when the pump is running by looking at the yellow pump voltage line. The pump voltage is about 25 volts when the pump is on and 0 volts when the pump is off. In order to conserve battery life, pumping was turned off somewhere before the batteries were discharged to the 30% level.

Voltage outputs during the 2nd and 6th day of this week have been enlarged in Figures 4.2 and 4.3, respectively, from that shown in Figure 4.1. During the night, when there is no solar insolation, the voltage output of the PV array drops to zero volts. As the sun rises the voltage rises quickly to the 30 to 35 volt level where it stays until power is drawn from the panels; that is the pump is turned on. It can be seen that the panel voltages are not a strong function of the solar irradiation magnitude, once some minimum level of solar energy is impinging on the panels. This is best seen between hours 128 and 130 where the solar insolation drops from 790 watts/m^2 to 250 watts/m^2 and the array voltage drops by 1 to 2 volts. The biggest effect on the solar panel voltage is the load placed on the panels. When the pump is running the voltage drops to about 27 volts. The PV array delivers a voltage of about 35 volts when the load is disconnected and the batteries are fully charged. This is close to the PV panels' specifications for open circuit voltage; as the open circuit voltage (V_{oc}) at standard testing conditions is given as 36.6 volts.

From Figures 4.1, 4.2 and 4.3 it can be see that the data acquisition subsystem senses the voltage output of each panel. The voltage output of each panel should be the same as the PV array voltage since both panels are connected in parallel. This is clearly shown in the results as the voltage outputs of panel 1, panel 2 and the MPPT Array voltage are the same, except for some spikes that show up in the panel voltages at times when the load is connected and the pump is running. Fluctuations or spikes observed in the voltage output of panel 1 and panel 2 at times when the load is connected is due to the MPPT–charge controller making adjustments to the power output from the PV array. At some instances the MPPT-charge controller drops the current and increases the voltage of the PV array while monitoring charge and voltage level of the batteries. If the battery voltage and charge level increases then the MPPT-charge controller decreases the PV power output. As it can be seen from the plotted results, the MPPT data logger does not record and display such fluctuations. More than likely the MPPT data logger filters its voltage measurements. Our data acquisition system tracks these spikes or fluctuations in the voltage outputs.

When the results of Figure 4.2 are averaged over a period of one minute the results of Figure 4.4 are obtained. This averaging process smooth the results and makes them a little easier to view. For example the rapid oscillations seen in the array voltages in Figure 4.2 and discussed in the paragraph above are no longer present and the voltages labeled panel 1, panel 2, and V MPPT Array lie on top of one another. In addition, the V MPPT Battery voltage lies over the V battery voltage. It is very easy to see that when the pump is turned on the PV panel / array voltage drops and when the pump is turned off the panel / array voltage increases. The voltage output of the PV panels is usually maintained between 33 to 36 volts during the day, when there is no load on the PV array and the batteries are fully charged. If the batteries are not fully charged then the PV array voltage is lower, because power is being delivered from the panels to the batteries.

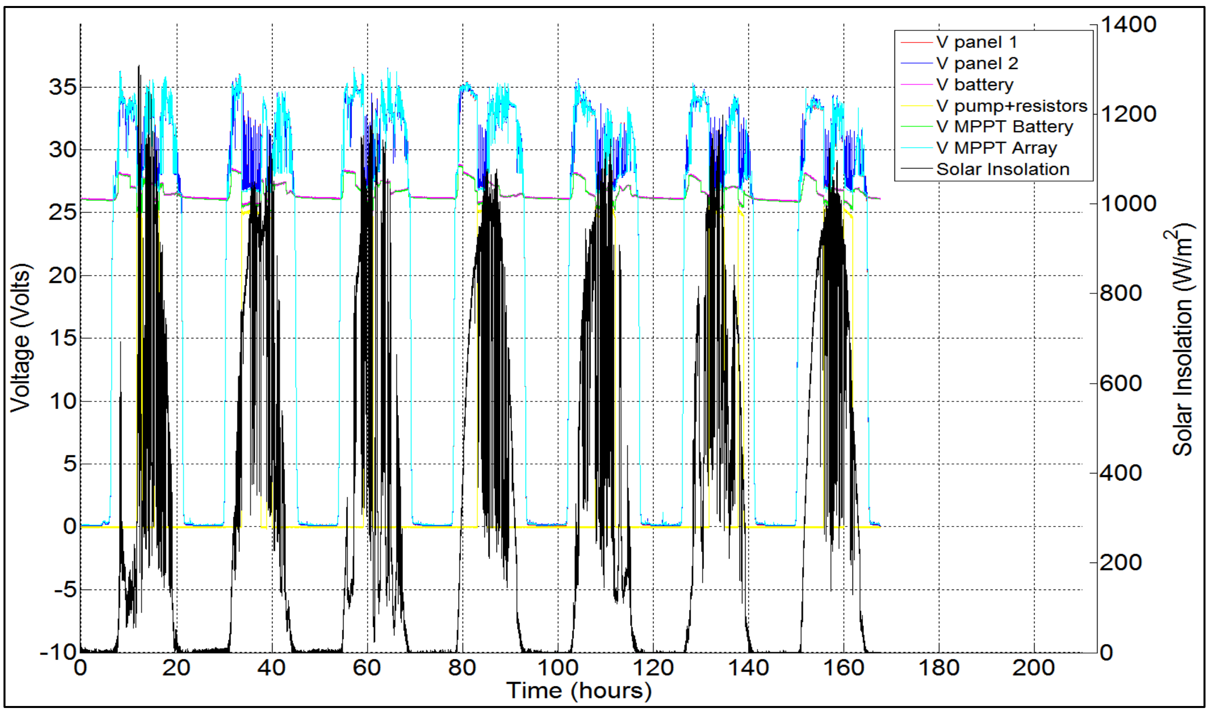

Figure 4.1: Voltage and solar insolation versus time for PV array inclination at 40° and sun tracking for seven days of operation from July 28 to August 3, 2014.

4.1.2. Currents

Current and solar insolation versus time recorded by the data acquisition subsystem and MPPT data logger are shown in Figure 4.5 through Figure 4.7. The current output of each panel, PV array, battery, pump and resistors acquired by the data acquisition subsystem are represented as C panel 1, C panel 2, C array, C battery and C pump+resistors respectively. Current outputs recorded by the MPPT data logger for the PV array and battery are represented as C MPPT Array and C MPPT Battery respectively. In figures 4.5 through 4.7 the current results labeled C MPPT array should be equal to the current results from the sum of the C panel 1 and C panel 2. While this sum is not shown on these graphs there is good agreement between these results, within the 0.7% full scale accuracy of the current meters used. In addition the current curves C MPPT battery and C battery should be the same; within the accuracy of the current sensors used they are the same.

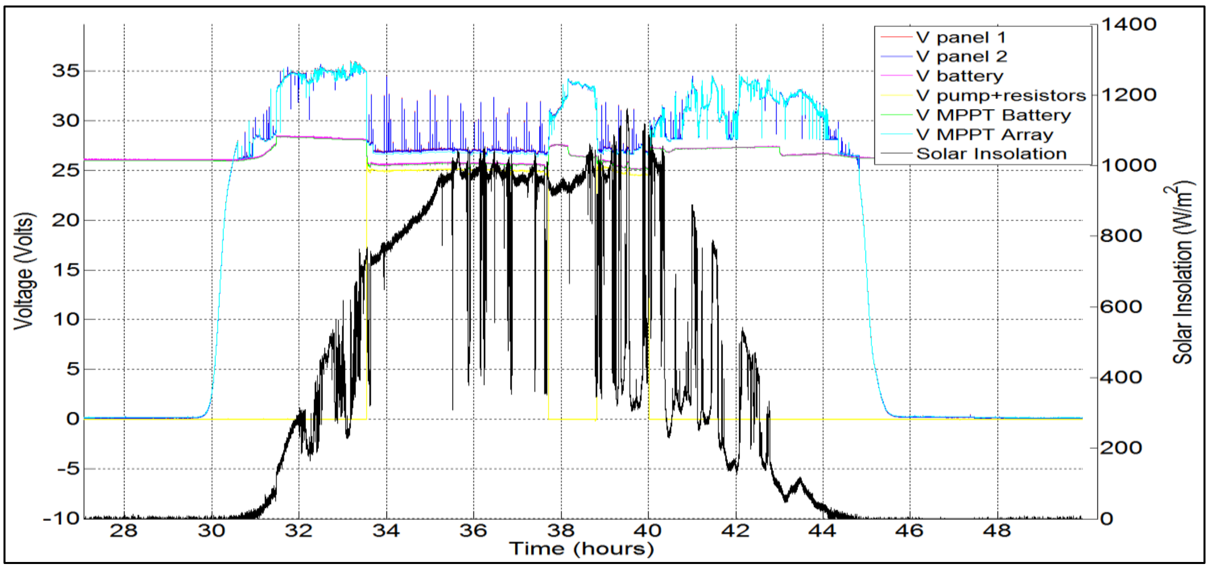

Figure 4.2: Voltage and solar insolation versus time for PV array inclination at 40° and sun tracking for operation hours from 28 to 48 on July 29, 2014.

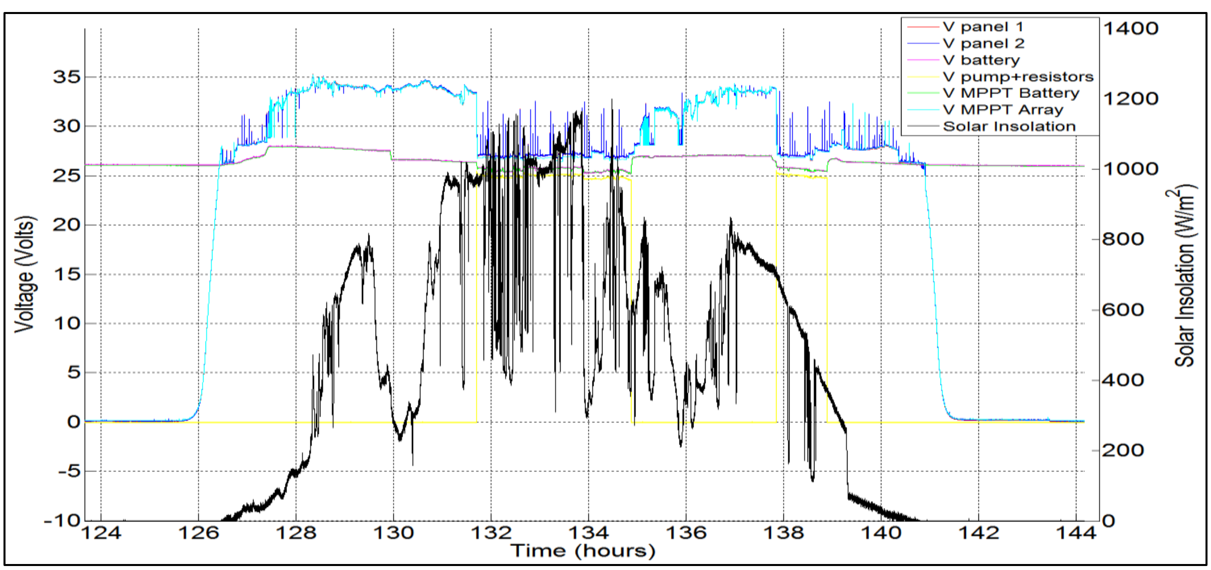

Figure 4.3: Voltage and solar insolation versus time for PV array inclination at 40° and sun tracking for operation hours from 124 to 144on August 2, 2014.

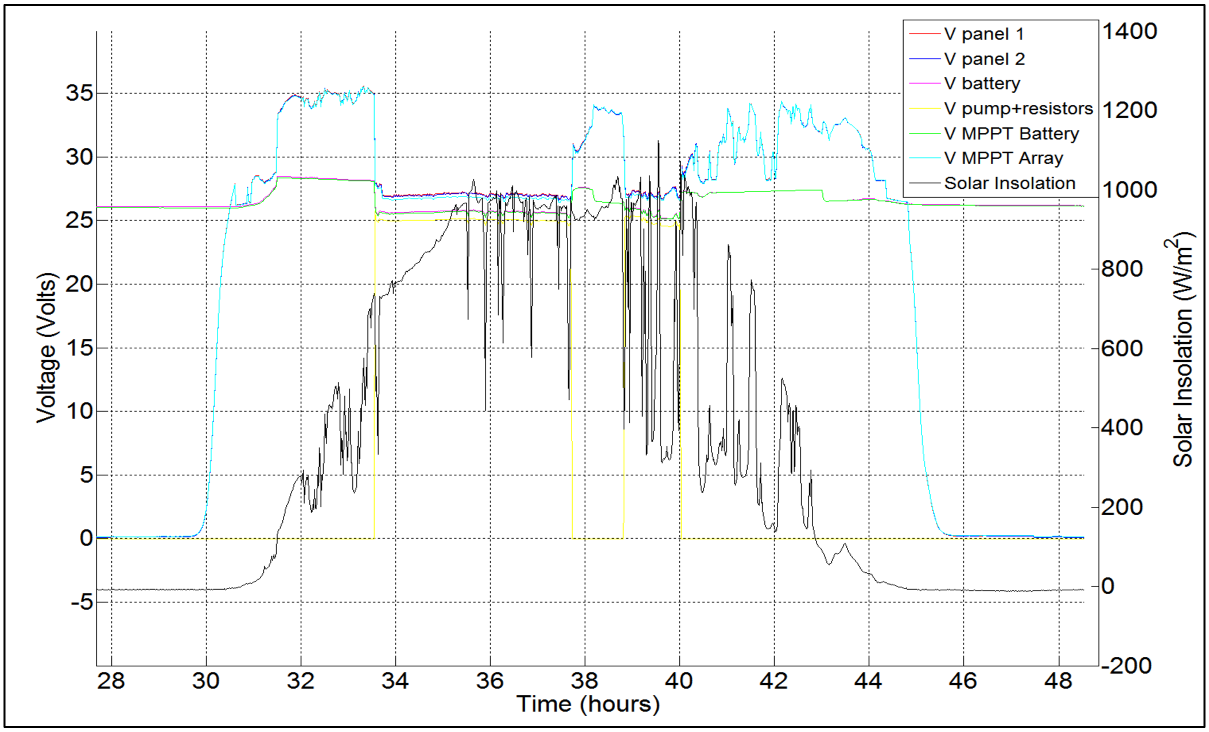

Figure 4.4: Voltage and solar insolation versus time averaged over one minute time intervals for PV array inclination at 40° and sun tracking for operation hours from 28 to 48 on July 29, 2014.

In Figure 4.5, the current data acquired throughout the week from July 28th to August 3rd is shown. Current outputs recorded on July 29th, 2014 and August 2nd, 2014 for 20 hours of operation are shown in Figures 4.6 and 4.7 respectively. The maximum power current (I_{pm}) of each panel is 7.66 amps at 1000 watts/m^2 of solar insulation and an ambient temperature of 25^{o}C according to the manufactures specification sheet. Since the PV panels are connected in parallel, the rated maximum power current (I_{pm}) of the PV array should be 15.32 amps.

As the solar insolation rises during the 31st hour (see Figure 4.6); so does the current output of the PV array. After a period of time current starts to decrease until it reaches a point where no current is delivered close to the 34th hour, even though solar insolation is high enough to generate current. This is due to the batteries becoming fully charged by the 34th hour. If there is no place for the current from the PV panels to go, they are shut down by the MPPT-charge controller. Once the pump is switched on slightly before the 34th hour there is a place for the panel current to go and the PV array starts delivering current proportional to the solar insolation. As the intensity of the solar insolation rows, the current output of the PV array also increases. After 4 hours of pumping operation the batteries got discharged to the 30% level and the pump was switched off during the 37th hour. Once the pump was switched off, the array current began to drop as the batteries got charged back to their float stage.

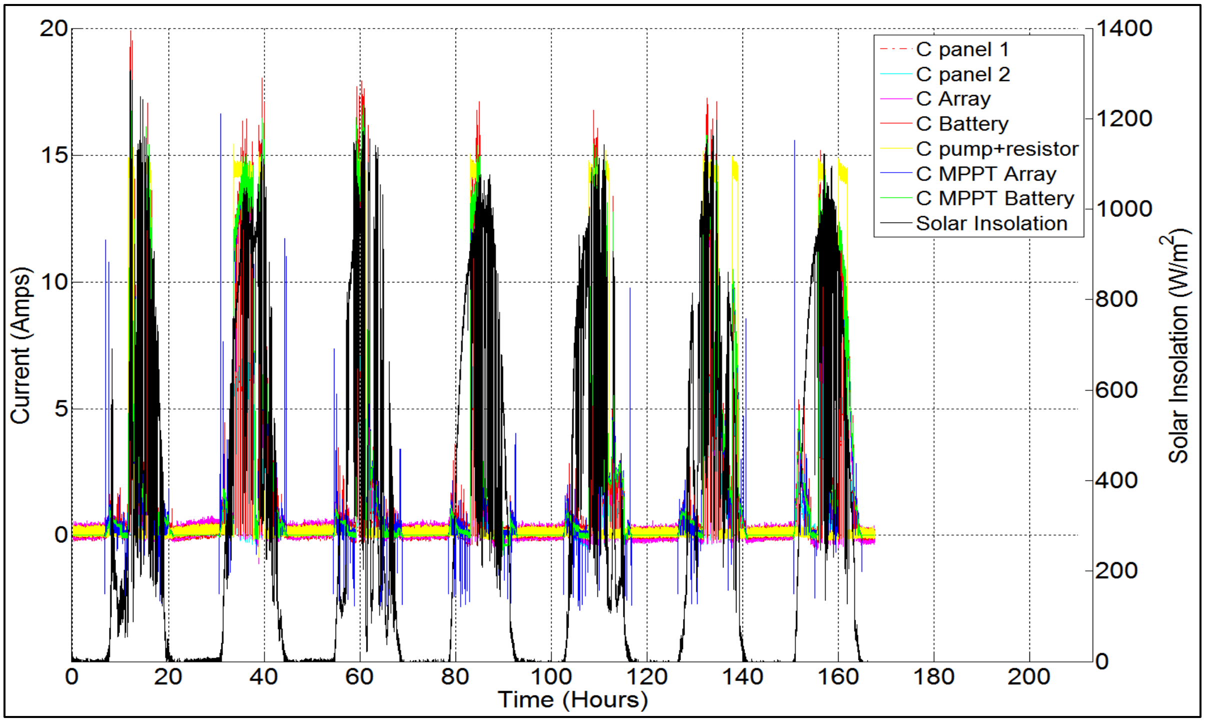

Figure 4.5: Current and solar insolation versus time for PV array inclination at 40° and sun tracking for seven days of operation from July 28 to August 3, 2014.

In Figure 4.6 note that the solar insolation is continuously above 900 watts/m^2 from end of hour 36 to the end of hour 39, but the current output of the panels still drops to zero slightly before hour 38 ends. This is where the charge controller portion of the MPPT-charge controller comes into play. The primary purpose of the charge controller is to regulate the battery voltage and current to ensure that the batteries do not get over charged. When a load is connected to the batteries, the MPPT-charge controller switches back to MPPT operation to deliver power to the batteries and balance the power consumption from the batteries with power input to the batteries from the PV array. When the load is removed and the batteries are still fully charged, there is no longer a need for PV power. As a result the controller restricts the power output from the array. If the batteries do not require maximum power to maintain proper charge, the MPPT–charge controller does not draw maximum power. The pump was switched back on after the batteries have been fully charged at the 37th hour. After the 39th hour the solar insolation varied and the PV array could not generate enough power to balance the power draw from the batteries. Thus, the batteries got discharged in approximately one hour. Since the resistors are connected along with the pump; the current draw from both the pump and resistors is 14.5 amps. If only the pump were connected the current draw would be considerable less at approximately 1.8 amps. The power draw of the pump and power dissipating resistors when the batteries are fully charged is about 360 watts. More detailed information on powers will be given in the next section. Note that similar trends in current flows can be seen in Figure 4.7.

In Figures 4.5 through 4.7 the C MPPT Array curves recorded by the MPPT data logger show large spikes at sunrise and sunset. These same spikes do not seem to be present in the C Array, C panel 1and C panel 2 curves as obtained by the PV irrigation system data acquisition sensors. It is known why the MPPT data logger registers these spikes. It is known that there are capacitors and inductors inside the MPPT and there could be some large current discharges at times. It may be that the data acquisition current sensors do not have the response time to detect these current spikes.

The PV array current as a function of solar insolation is shown in Figure 4.8. To generate this plot, the weeklong data shown in Figure 4.5 is processed in a way to eliminate all PV array currents when the pump and power dissipating resistors are not on. Then the current outputs of the PV array are plotted versus solar insolation. As expected, the PV array current is nearly linearly dependent on the solar insolation. Increasing solar insolation increases the PV array current. Moreover, the number of data samples are higher at solar insolation levels from 650 watts/m^2 to 1050 watts/m^2. This occurs because the pump was mostly run in relatively good weather conditions, at higher solar insolation. Thus the data reduction procedure eliminated many of the lower solar insulation results. As per the PV panel's manufacturers specifications, the maximum power current (I_{pm}) from the PV array should 15.32 amps at standard test conditions, 1000 watts/m^2 and an ambient temperature of 25 ^oC. . However, the PV array at 1000 watts/m^2 solar insolation is delivering current from 12 to 13.7 amps. As will be described in the next section this is probably due to the

MPPT not being able to operate at the maximum power point of the PV array because of the charge state of the batteries.

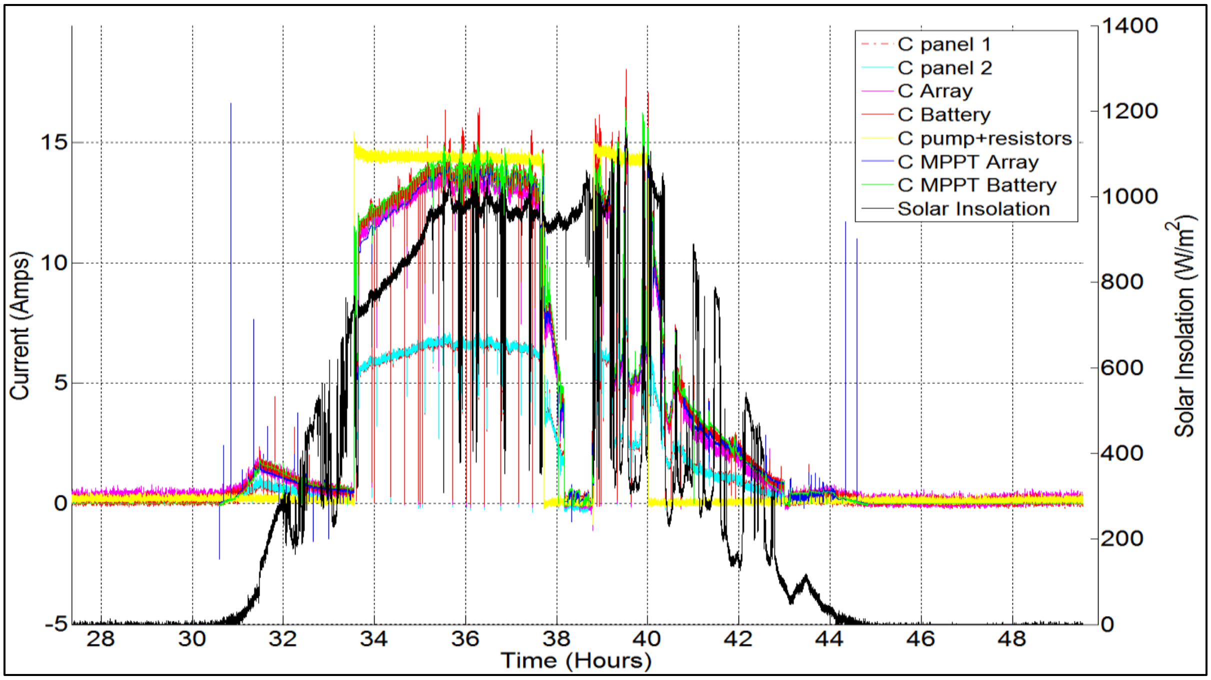

Figure 4.6: Current and solar insolation versus time for PV array inclination at 40° and sun tracking for operation hours of 28 to 48 on July 29, 2014.

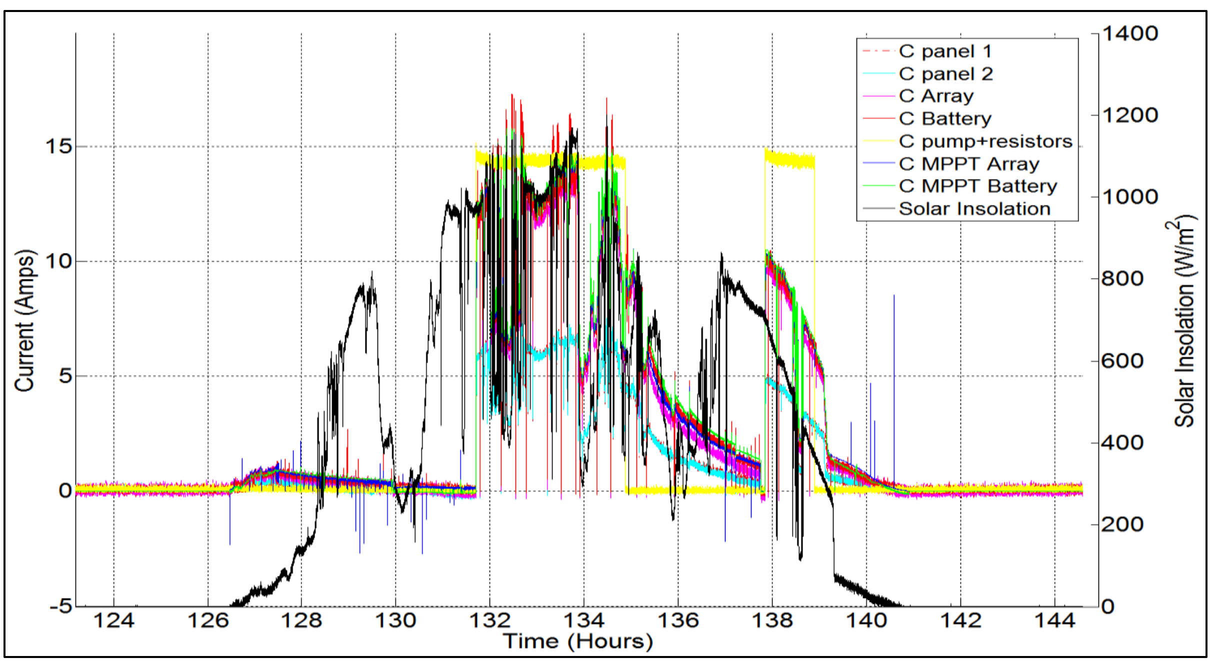

Figure 4.7: Current and solar insolation versus time for PV array inclination at 40° and sun tracking for operation hours from 124 to 144 on August 2, 2014.

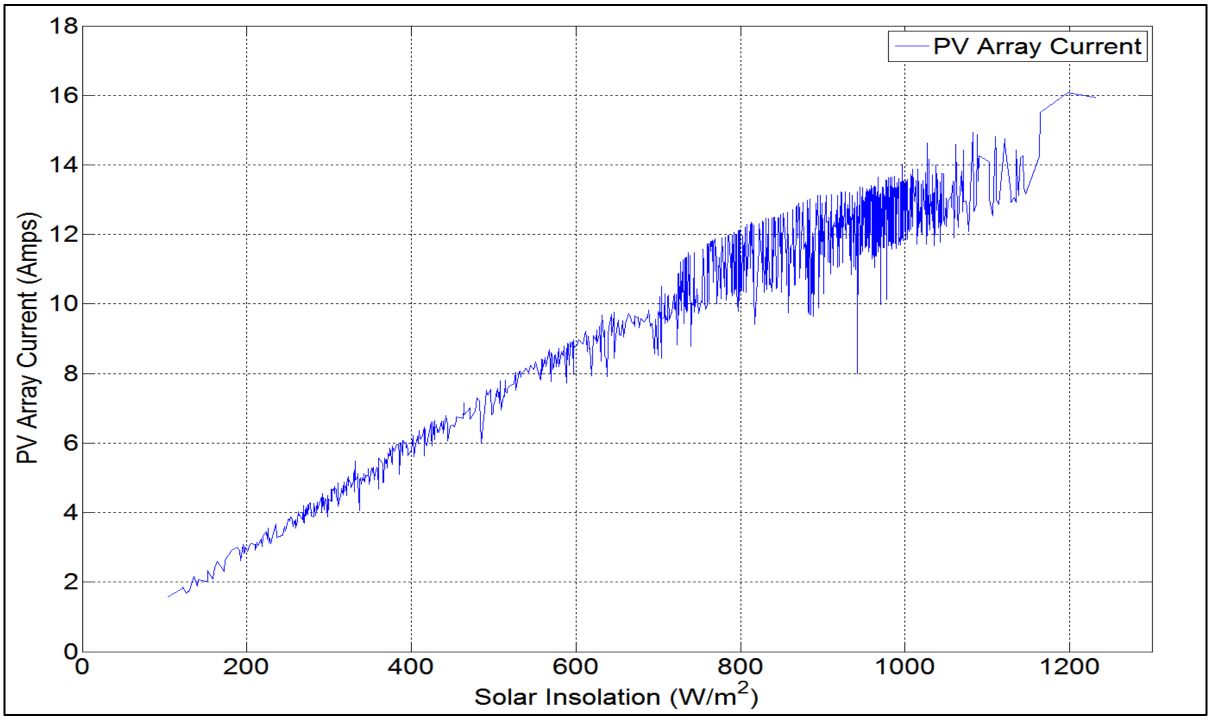

Figure 4.8: PV array current as a function of solar insolation for PV array inclination at 40° and sun tracking.

4.1.3. Power

Power and solar insolation versus time recorded by the data acquisition subsystem and MPPT data logger are shown in Figures 4.9 through Figure 4.11. Power results from panel l, panel 2, PV array and pump with power dissipating resistors are denoted by P panel 1, P panel 2, P Array and P Pump+resistors respectively. Whereas, the curve labeled MPPT Array Power is power delivered by the PV array recorded by the MPPT data logger. Power output data obtained throughout the week from July 28 to August 3, 2014 are shown in Figure 4.9. The power outputs recorded on July 29, 2014 and August 2, 2014 for 20 hours of operation are shown in Figures 4.10 and 4.11 respectively.

Each panel can produce a maximum power (P_{max}) of 224 watts at standard test conditions (STC). Thus, the PV array can produce a maximum power of 448 watts. The combined power consumption by the pump and resistors is about 360 watts. The pump requires only 55 watts if separately connected to a 24 volt battery bank and the resistors can dissipate 305 watts. As discussed in the preceding section the power dissipating resistors were added to increase power load on the batteries and thus allow the PV panel to deliver power to the batteries for a greater period of time. The MPPT-charge controller maintains the power balance between the power being delivered to the batteries from the PV array and the power delivered from the batteries to the pump and resistors. Solar insolation has a direct relationship for PV array power. When the load is connected, the power delivered by the PV array increases with increasing solar insolation (see Figures 4.10 and 4.11). As can be seen in these figures the P array and P MPPT Array power results approximately coincide with each other.

PV array power output as a function of solar insolation is shown in Figure 4.12. This shows that the power output of the PV array is almost linearly proportional to the solar insolation, just like the current was in Figure 4.8. At a solar insolation of 1000 watts/m^2 the power generated by the PV array is approximately at 350 watts. The maximum power (P_{max}) of the PV array should be 448 watts. This reduction in power generation by the PV array at this insolation level is more than likely due to the MPPT not being able to operate at the maximum power point of the PV array because of the charge state of the batteries. The load on the array is about 350 watts and this is approximately what the panels are delivering. There may also be a small temperature effect here. It has been found during this study that increasing solar insolation results in increase in PV array temperature, which reduces the efficiency of PV array.

4.1.4. Temperatures

Temperature and solar insolation versus time recorded by the data acquisition subsystem are shown in Figures 4.13 through 4.15. Four thermocouples installed in this PV irrigation system generated this temperature data with an uncertainty of ±5%. Two of these sensors were installed at the backside of each PV panel denoted as T panel 1 and T panel 2. One of the thermocouples was used to record the ambient temperature represented as T Ambient and another was installed on the battery bank denoted by T battery. Temperature data obtained during the week from July 28 to August 3, 2014 are shown in Figure 4.13. The temperature outputs obtained on July 29, 2014 and August 2, 2014 for 20 hours of operation are shown in Figures 4.14 and 4.15 respectively.

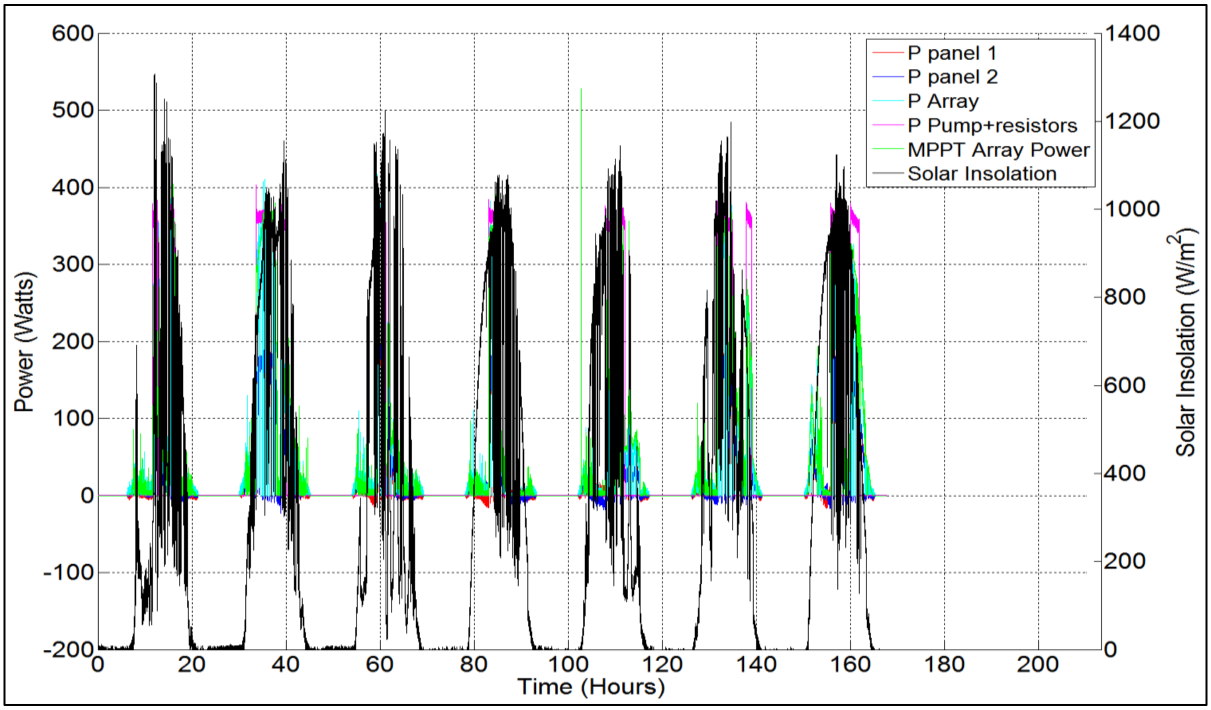

Figure 4.9: Power and solar insolation versus time for PV array inclination at 40° and sun tracking for seven days of operation from July 28 to August 3, 2014.

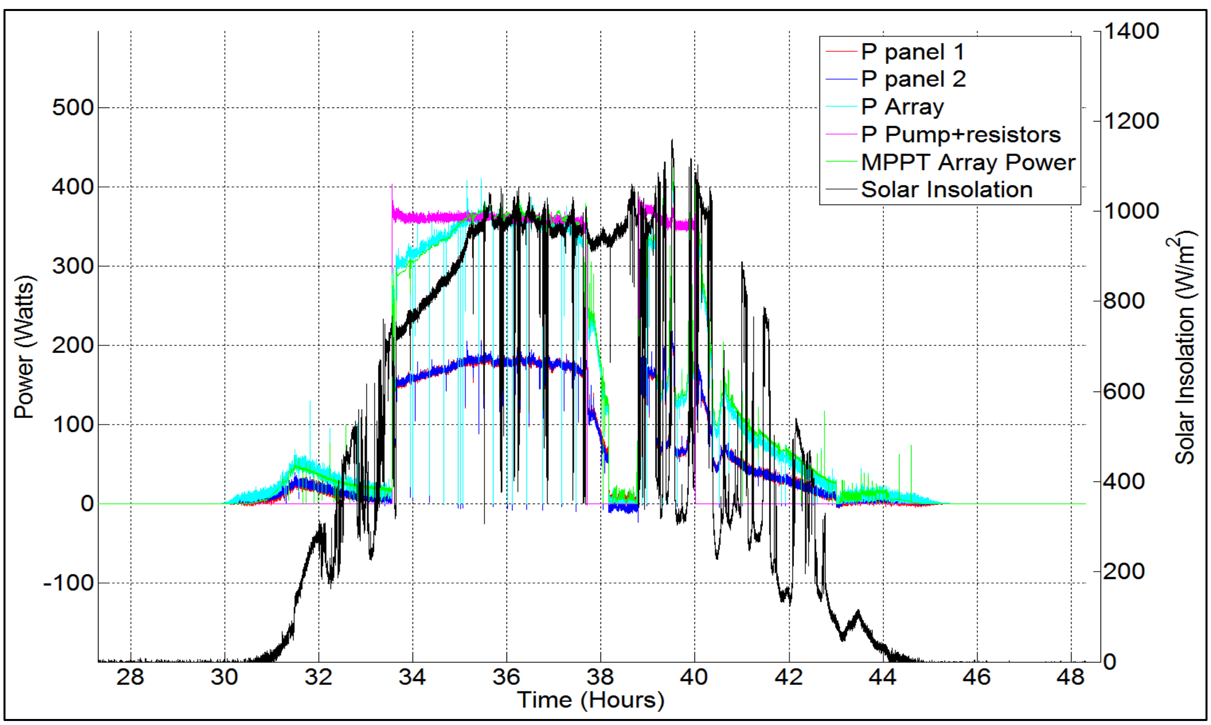

Figure 4.10: Power and solar insolation versus time for PV array inclination at 40° and sun tracking for the hours of operation from 28 to 48 on July 29, 2014.

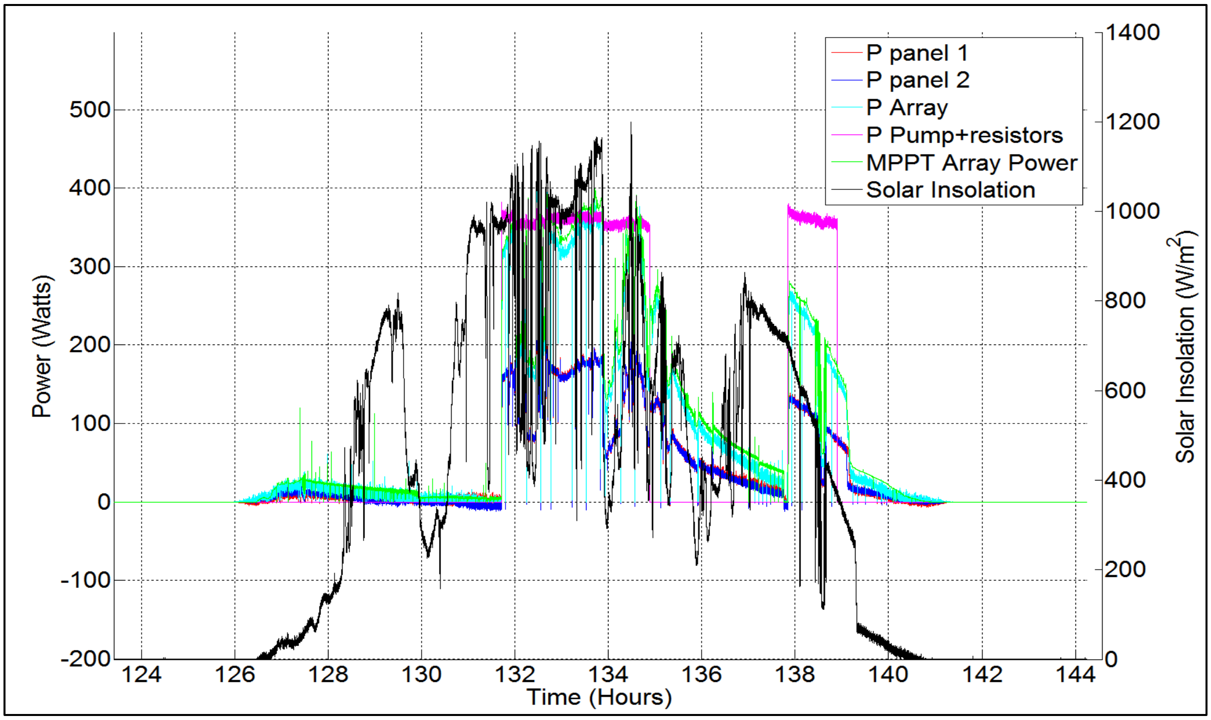

Figure 4.11: Power and solar insolation versus time for PV array inclination at 40° and sun tracking for the hours of operation from 124 to 144 on August 2, 2014.

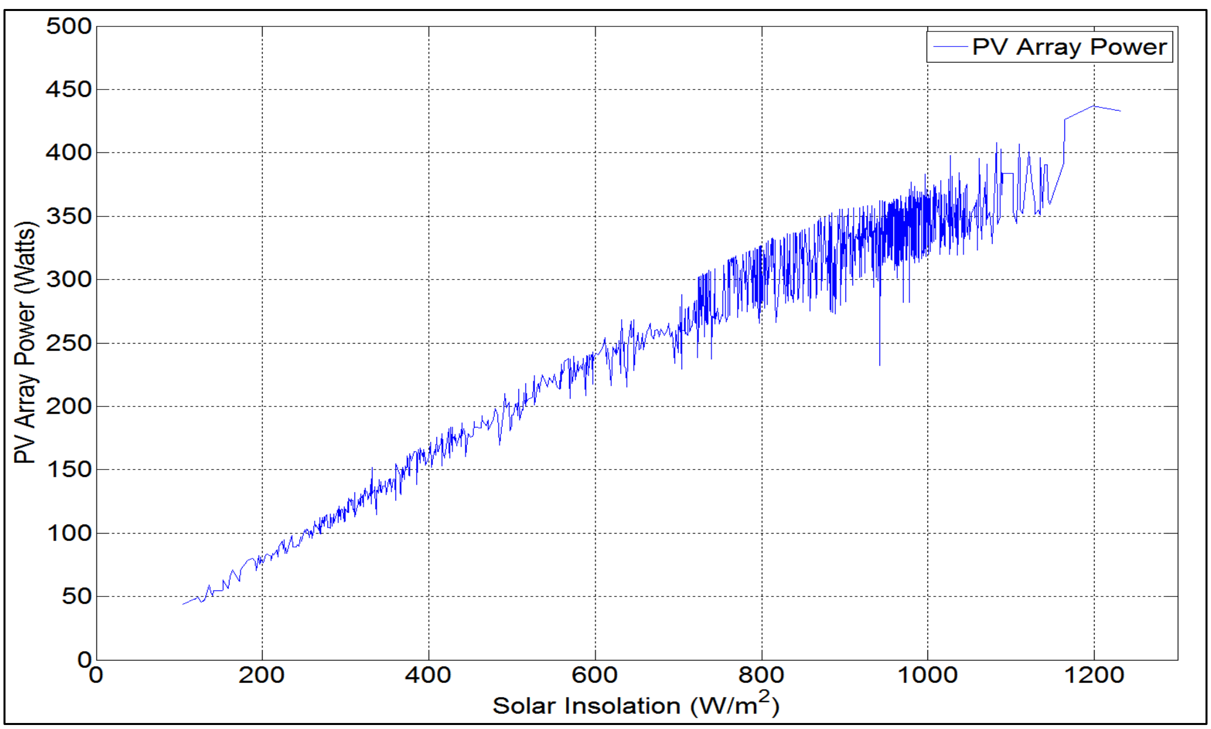

Figure 4.12: PV array power as a function of solar insolation for PV array inclination at 40° and sun tracking.

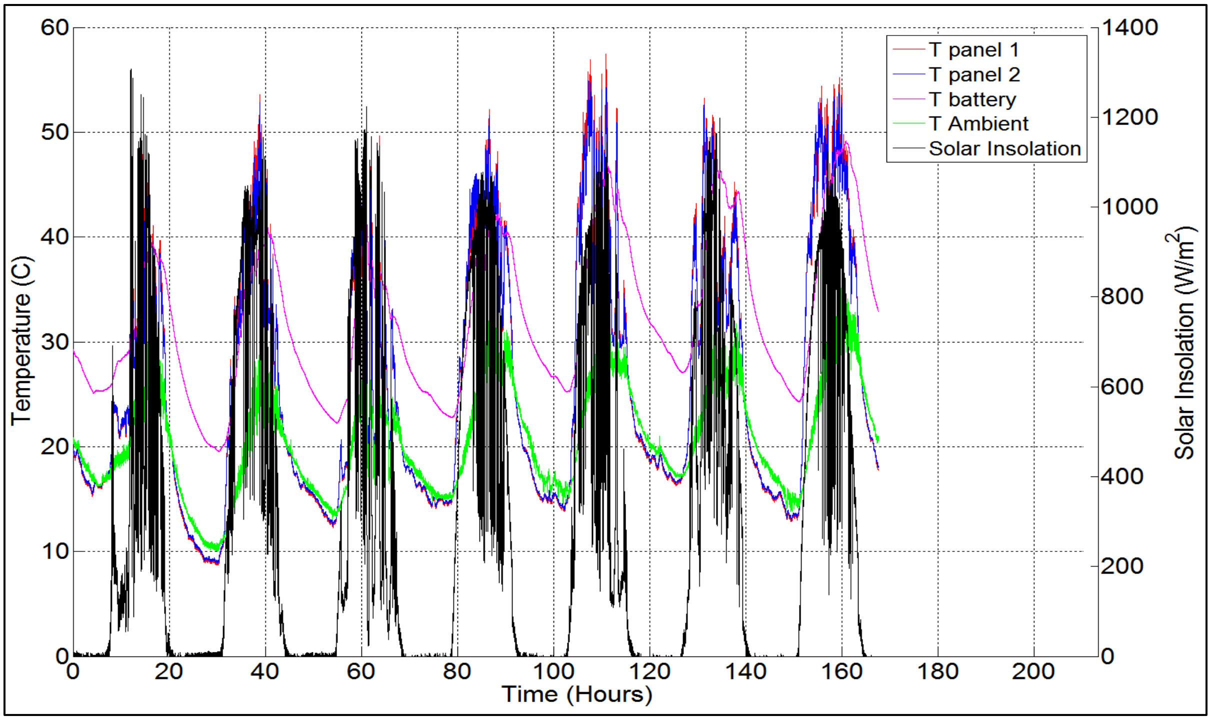

Figure 4.13: Temperature and solar insolation versus time for PV array inclination at 40° and sun tracking for seven days of operation from July 28 to August 3, 2014.

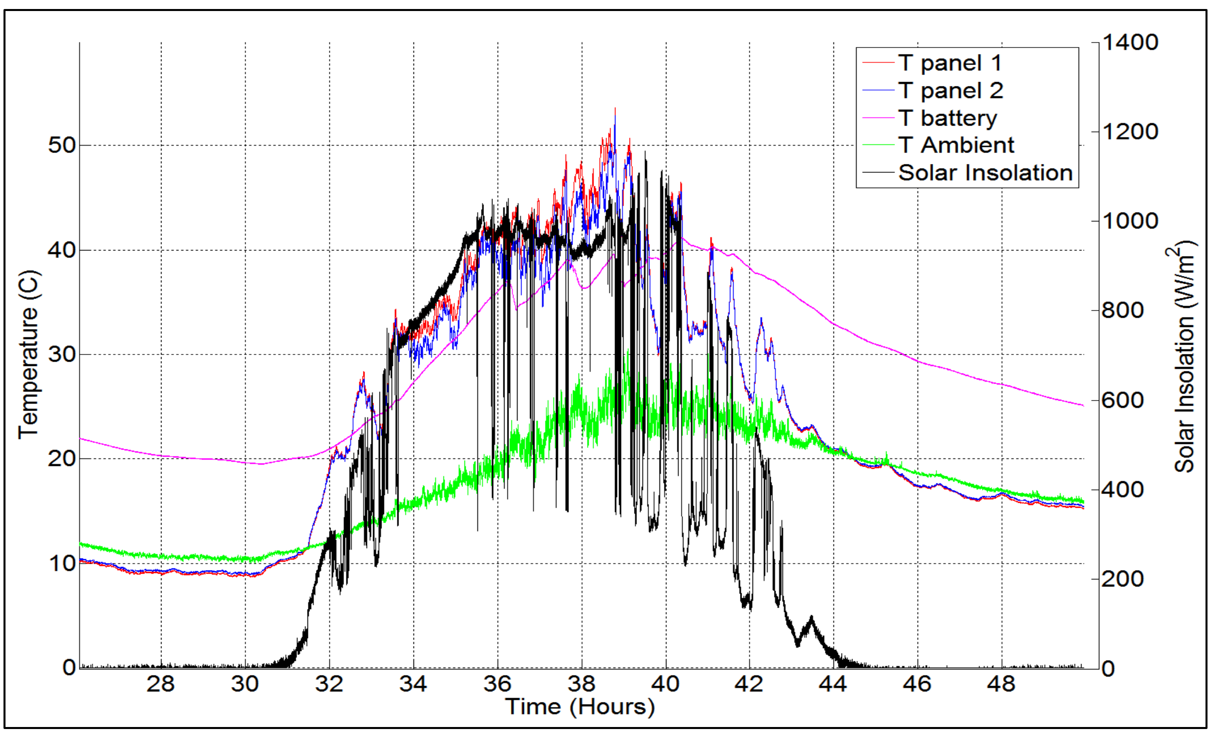

Figure 4.14: Temperature and solar insolation versus time for PV array inclination at 40° and sun tracking for the hours of operation from 124 to 144 on August 2, 2014.

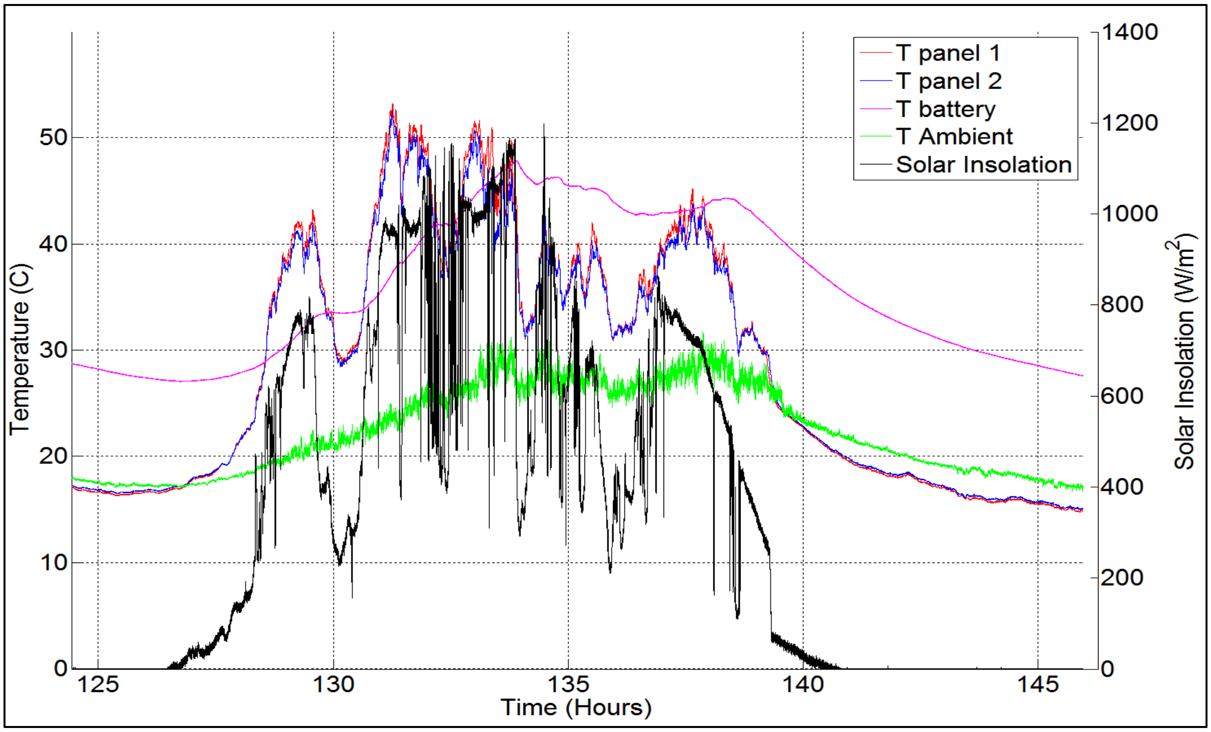

Figure 4.15: Temperature and solar insolation versus time for PV array inclination at 40° and sun tracking for the hours of operation from 125 to 145 on August 2, 2014.

The highest temperature for the PV panels was recorded as approximately 53° C on August 1, 2014, which is 5th day during this week as seen in Figure 4.13. From the temperature results, it can be seen that the temperature of PV panels has a direct relationship with solar insolation (see Figures 4.14 and 4.15).

As the solar insolation level changes throughout the day, the PV temperature follows this change. For example, in Figure 4.15 the solar insolation dips are clearly noticeable through the 130th to 138th hour of operation. Both the panel temperatures follow these dips in solar irradiation well. These results suggest that higher amounts of solar insolation result in increasing the PV array temperature. This is reasonable for a large fraction of the solar insolation impinging on the PV panels gets converted to thermal energy. It is also interesting to notice that the range of ambient temperatures encountered during these tests has very little effect on the PV panel temperatures. The PV panel temperatures have to increase with increasing ambient temperature, but for the range of ambient temperatures seen in these tests. This effect is hidden by the relationship of the PV panel temperature to solar insolation.

The battery temperature results are seen to follow the ambient temperature. This can be seen in Figures 4.13 through 4.15. The battery temperatures are about 10 °C higher than the ambient temperatures. The question that remains to be answered is why is there a 10 °C temperature difference between the batteries and the ambient temperature. At first it might be this because the batteries are charging or discharging; however this would mean the 10 °C difference in battery and ambient temperature should go away at night. Results in Figure 4.13 do not show this happening. It is believed that the batteries and other equipment in the box where the batteries are located heat up the air in the box, and thus the heat capacity of the items in the box is enough to keep the box temperature 10 °C above ambient for the night.

4.1.5. Solar Insolation

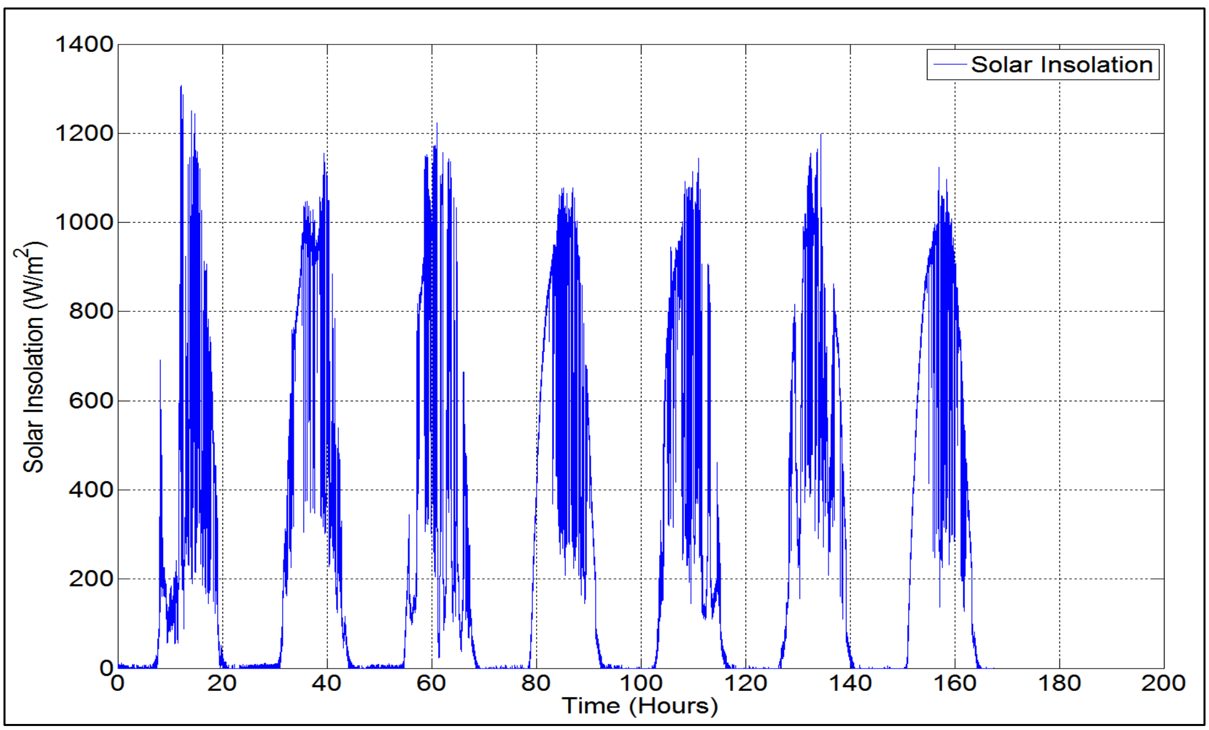

Figure 4.16: Solar insolation versus time for PV array inclination at 40° and sun tracking for seven days of operation from July 28t to August 3, 2014.

Solar insolation versus time on the second and minute time intervals acquired by the pyranometer are shown in Figures 4.16 and 4.17 respectively. A pyranometer is used in the data acquisition subsystem to generate solar insolation output signals with an accuracy of

± 5% on full scale. This corresponds to an error in power readings of ±50 watts. At some instances the pyranometer senses solar insolation up to 1200 watts/m^2 as shown in Figure 4.16 on the first day of these measurements. This is a high solar insolation, but it is possible. It also must be remembered that these are second level values and the results averaged over 1 minute are lower as shown in Figure 4.17 do not show as high of peaks. To obtain 1200 watts/m^2 the sun must have been high in sky, the cloud cover must have been nonexistent, and the humidity ratio of the air must have been low. While we did not calibrate our pyranometer, we did not have the equipment to do so, it has been calibrated by the manufacturer. There is no assurance that the pyranometer's calibration is unchanged since it has been purchased. All we can say is the solar insolation measured values do look reasonable.

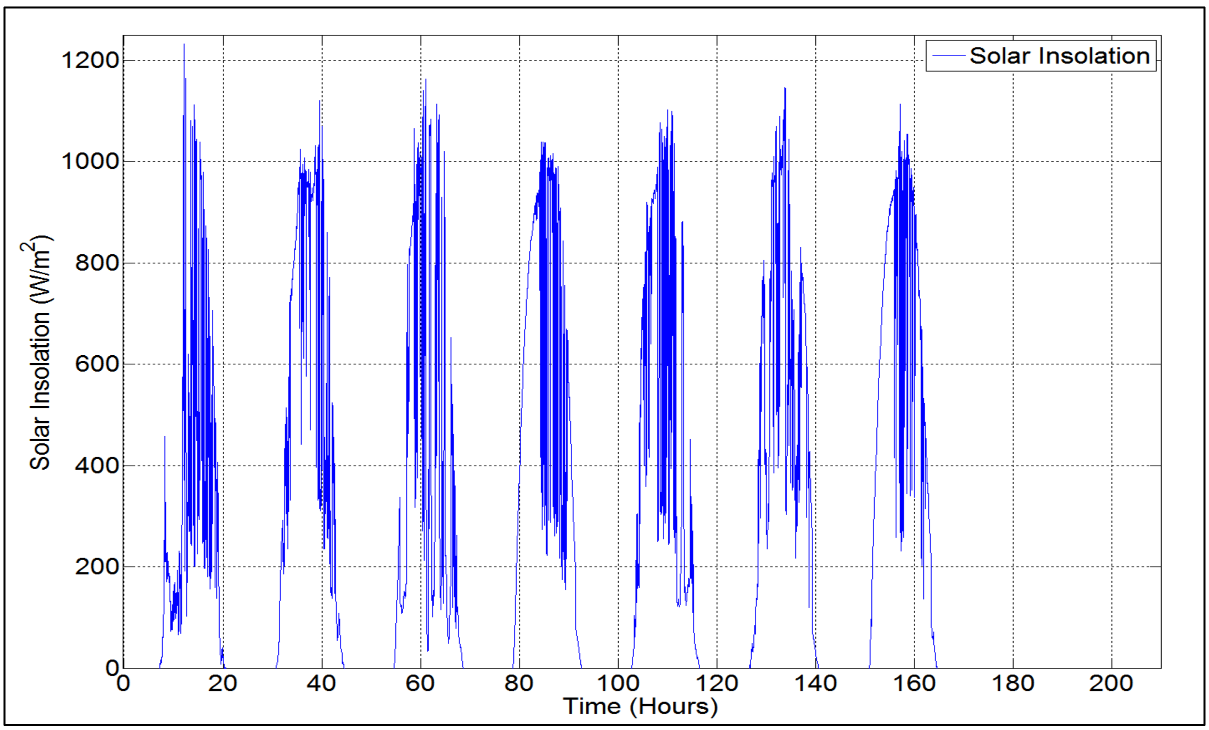

Figure 4.17: Solar insolation versus time for PV array inclination at 40° and sun tracking for seven days of operation from July 28 to August 3, 2014.

4.1.6. Flowrate

Water flowrate through the pump versus time for a weeklong operation from July 28, 2014 to August 3, 2014 is shown in Figure 4.18. The pump produces a flowrate of approximately 2.8 gpm (gallons per minute) at a pressure rise across the pump 27 psi. The pressure at the inlet and exit of the pump were determined with Bourdon tube gages, which had to be read manually. These were checked periodically and seen to give a consistent pressure rise across the pump of 27 psi. These flow rates and pressure rises were obtained for all PV irrigation configurations studied as part of this thesis work. Thus these plots will not be shown for the other configurations discussed in the subsections to follow.

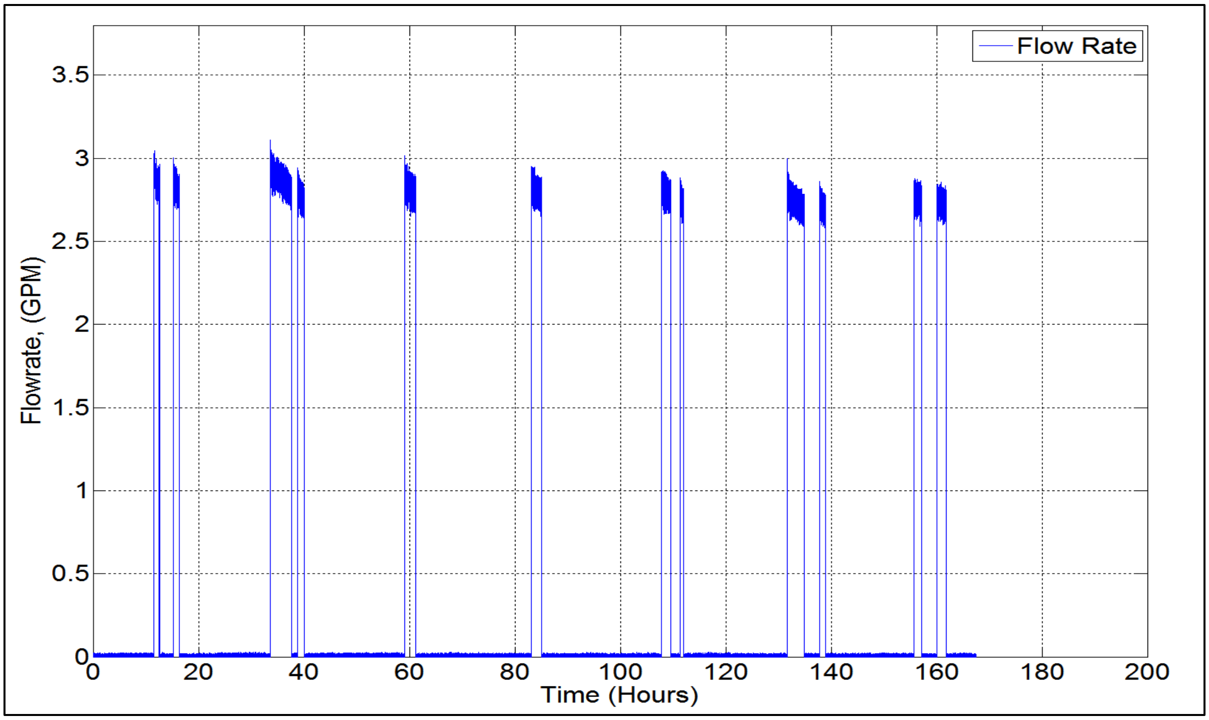

Figure 4.18: Flowrate versus time for PV array inclination at 40° and sun tracking for seven days of operation from July 28 to August 3, 2014.

4.1.7. PV Array Efficiency

The efficiency of the PV modules used in this PV irrigation system is given as 13.74 % at standard test conditions (STC). In order to assess the efficiency of the PV panels during operation the electrical power output of the PV panels had to be divided by the amount of solar radiation striking the panels. This has been done and the results are presented in Figures 4.19 through 4.21.

The efficiency of the PV array is a function of the solar insolation impinging on PV array. The calculated efficiencies of the PV array at the beginning and end of each day go above 100 % (see Figure 4.19), which is not physically possible. These results are short lived and are more than likely due to power storage in the MPPT-charge controller or the uncertainties in solar insolation measurement or PV panel current measurement at these low values. However, the efficiency results get better when the solar insolation is higher. Once the PV load is connected the PV array operates with an efficiency of 12 to 13 % as shown in Figure 4.20, which is actually showing the same results shown in Figure 4.19 except the data has been zoomed to show that PV array efficiency is about 12 percent when load is connected. If a load is not connected the MPPT – charge controller does not allow the PV array to produce power even though solar insolation is available. This causes the PV array efficiency to be small.

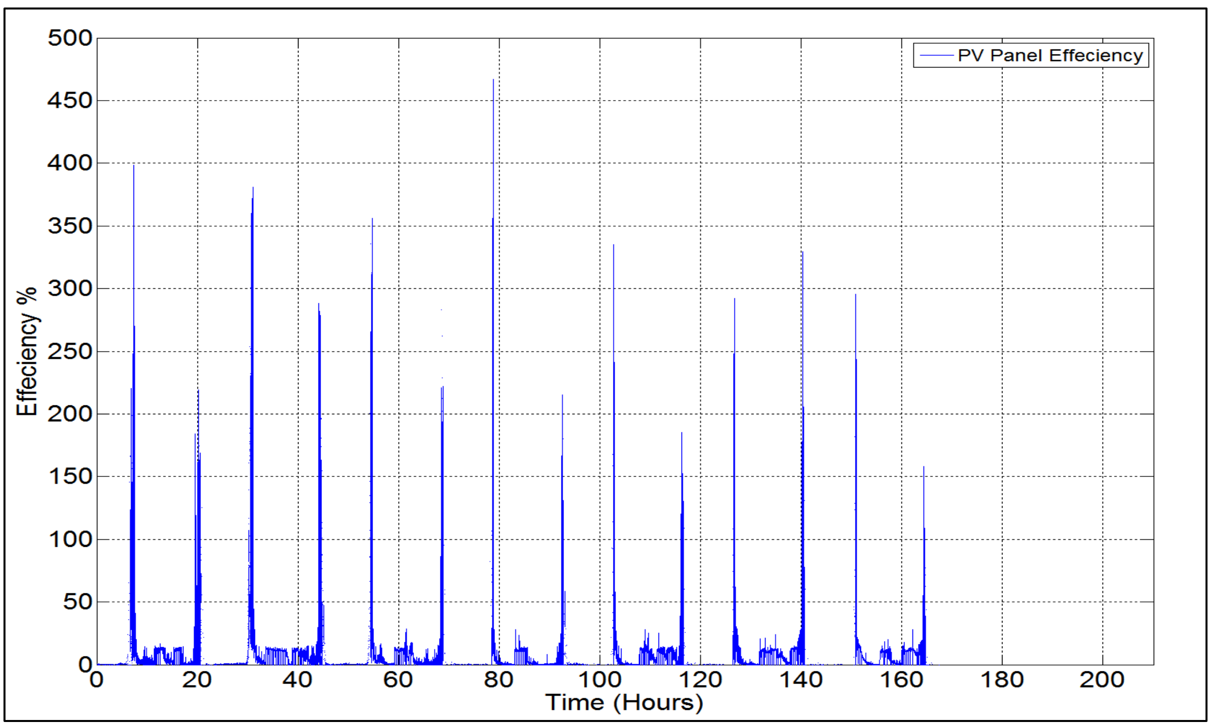

Figure 4.19: PV array efficiency versus time for PV array inclination at 40° and sun tracking for seven days of operation from July 28 to August 3, 2014.

Moreover, PV efficiency is also a function of temperature of the PV array. This has been shown in Figure 4.21, in which the PV efficiency is presented as a function of solar insolation and temperature. The PV array operates at an efficiency of 12 to 13%. The temperature of PV panels increases with increasing solar insolation. This increase in the PV panels' temperature decreases the PV efficiency. At solar insolation values above 800 watts/m^2 the PV array efficiency tends to decrease from 12 to 10 percent.

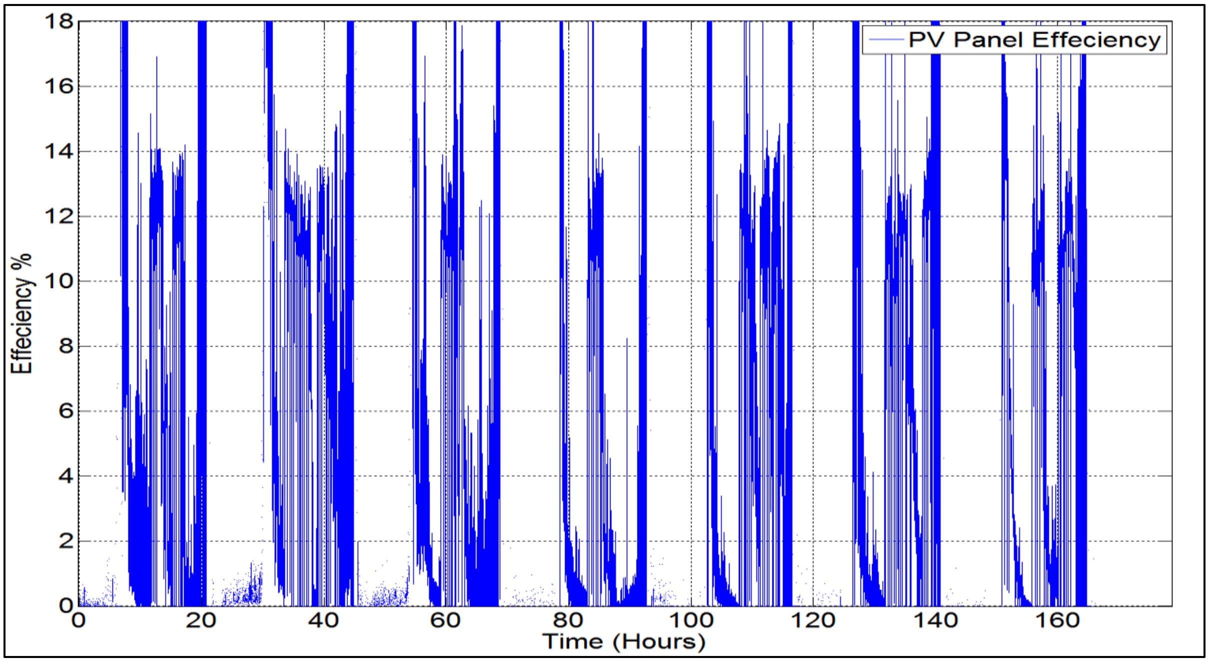

Figure 4.20: Zoomed in view of PV array efficiency versus time for PV array inclination at 40° and sun tracking for seven days of operation from July 28 to August 3, 2014.

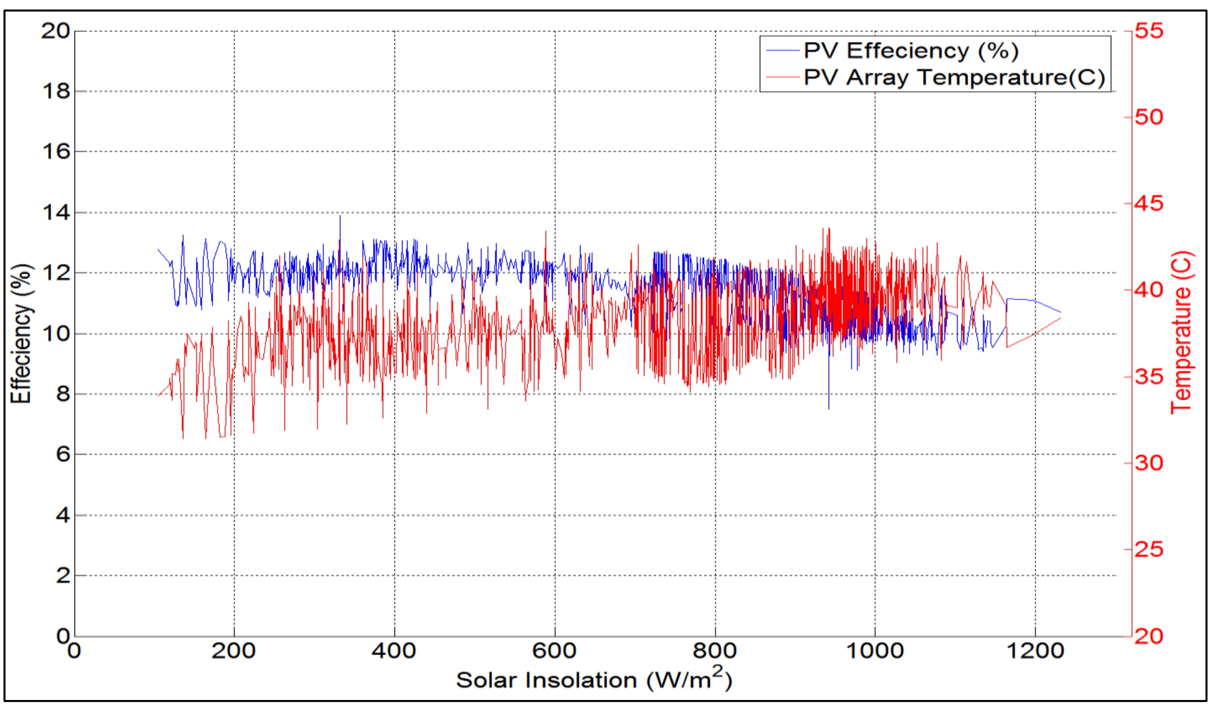

Figure 4.21: PV array efficiency and panel temperature as a function of solar insolation for PV array inclination at 40° and sun tracking for seven days of operation from July 28 to August 3, 2014.

4.1.8. PV Array Energy Generation

It is important to evaluate energy generated by the PV array on a daily basis and compare it with total solar energy incident on the PV array. Figure 4.22 shows daily PV energy generation as grey bars and solar energy incident on PV array is shown via the blue line The amount of energy generated by the PV array should be read off the left y-axis and the amount of solar energy impinging on the panels should be read off the right axis. The first day of this week was bad in terms of weather conditions, as it rained on this day for four hours in the early morning and the weather remained mostly overcast for rest of the day. Thus a low 0.834 kW-h of energy were generated on this day. Whereas, the total solar energy incident on the PV array was 14.22 kW-h. It can be concluded that even in bad weather conditions the PV array can generate some kW-h energy. The highest solar energy collected by the PV array was 26.65 kW-h on the seventh day of this week. However, on this day, the pump was run for a short duration of time that is why the PV energy production was low at 1.23 kW-h. On the 2nd day of the week, the PV array generated a maximum energy of 2.13 kW-h, while the total energy incident on PV array was 24.57 kW-h.

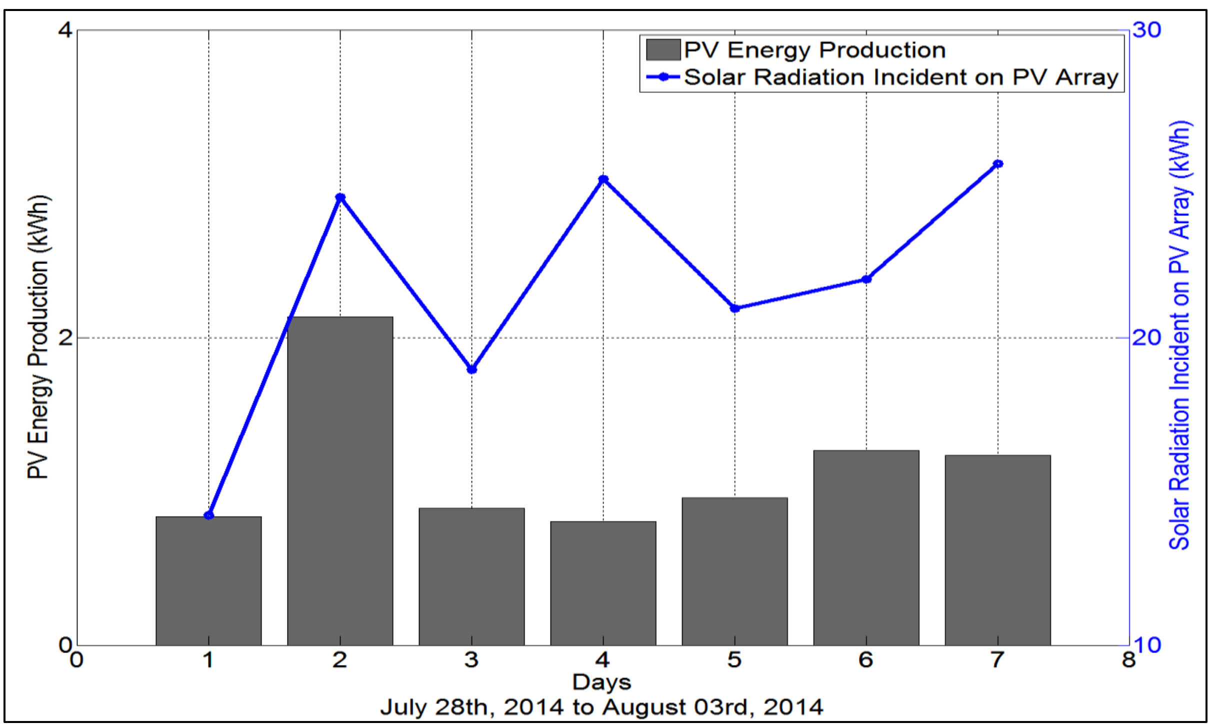

Figure 4.22: PV energy production for PV array inclination at 40° and sun tracking for seven days of operation from July 28 to August 3, 2014.

These total energy results, as well as the results presented in other subsections, indicate the importance of a proper sizing of the solar panels relative to the required load. If the load is much more than the solar panels can deliver than there will not be power available for pumping water. If the load is much smaller than the energy that can be delivered by the solar panels, some of the energy generating capacity of the system will be lost causing the system to operate at a reduced efficiency overall.

4.2. Azimuthal Solar Tracking at an Inclination Angle of 30° with both Water Pump and Power Dissipating Resistors

In this subsection the solar tracker was employed to track the azimuthal angle of the sun with a PV panel inclination angle of 30°. It was expected that by orienting the PV array at a 30° tilt, the energy production would increase. At 30° tilt faces the panels more directly at the sun since the attitude angle of the sun is about 60° during the middle of the day in the summertime. The PV irrigation system was tested at these conditions for 7 days from August 9, 2014 to August 15, 2014. Moreover, resistors remained connected to the batteries in similar way as in the previous test. Results will be presented in a similar order as done in Section 4.1, except the solar irradiation and mass flow rate sections will be eliminated.

4.2.1. Voltages

Voltage and solar insolation outputs versus time for panel 1, panel 2, batteries and pump with resistors are shown in Figure 4.23. Like the results in Section 4.1 the V MPPT battery and V MPPT Array voltages recorded by the MPPT data logger are also shown. Voltage outputs for the 2nd, 5th and 7th day during this week are shown in Figures 4.24 to 4.26. By orienting the PV array at 30°, solar insolation was increased and at some instances the pyranometer sensed as much as 1300 watts/m^2 (see Figure 4.23), which is a level not measured when the panels were tilted at 40°. At a 40° tilt the solar insolation outputs mostly fluctuated between 1000 to 1200 watts/m^2. On August 16, 2014 the pump ran for more than 9 hours continuously as the PV array received good solar insolation almost all day.

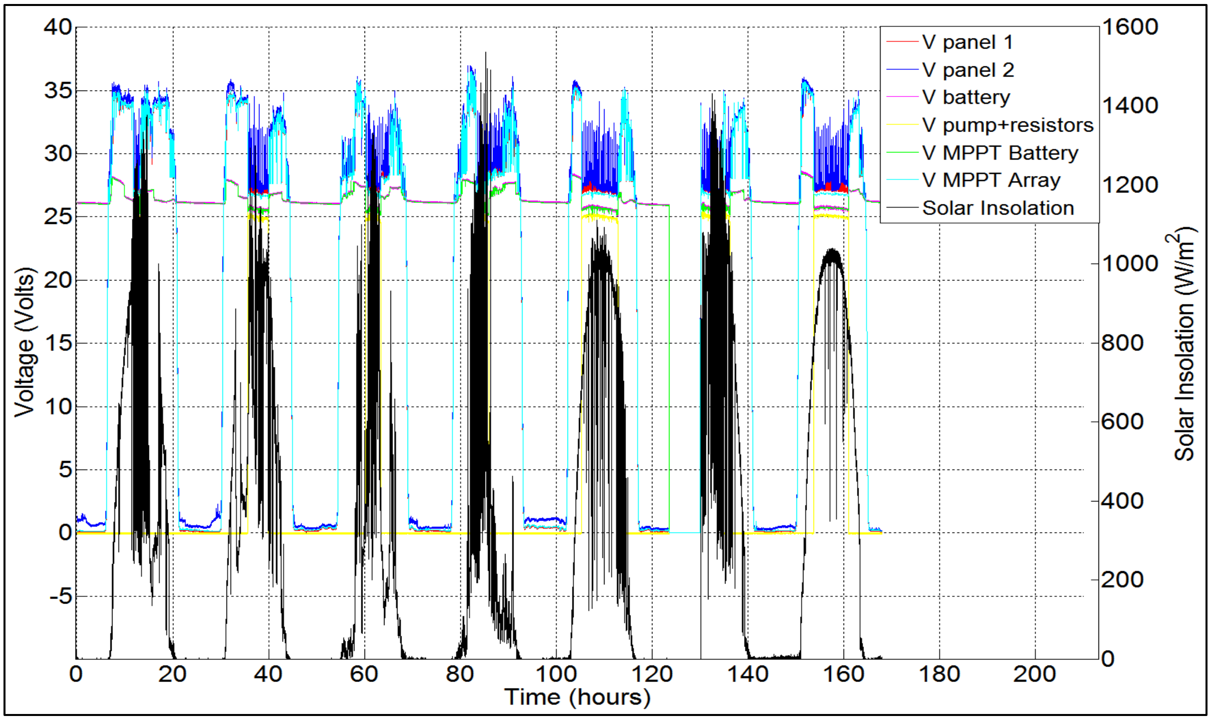

Figure 4.23: Voltage and solar insolation versus time for PV array inclination at 30° and sun tracking for seven days of operation from August 9 to August 15, 2014.

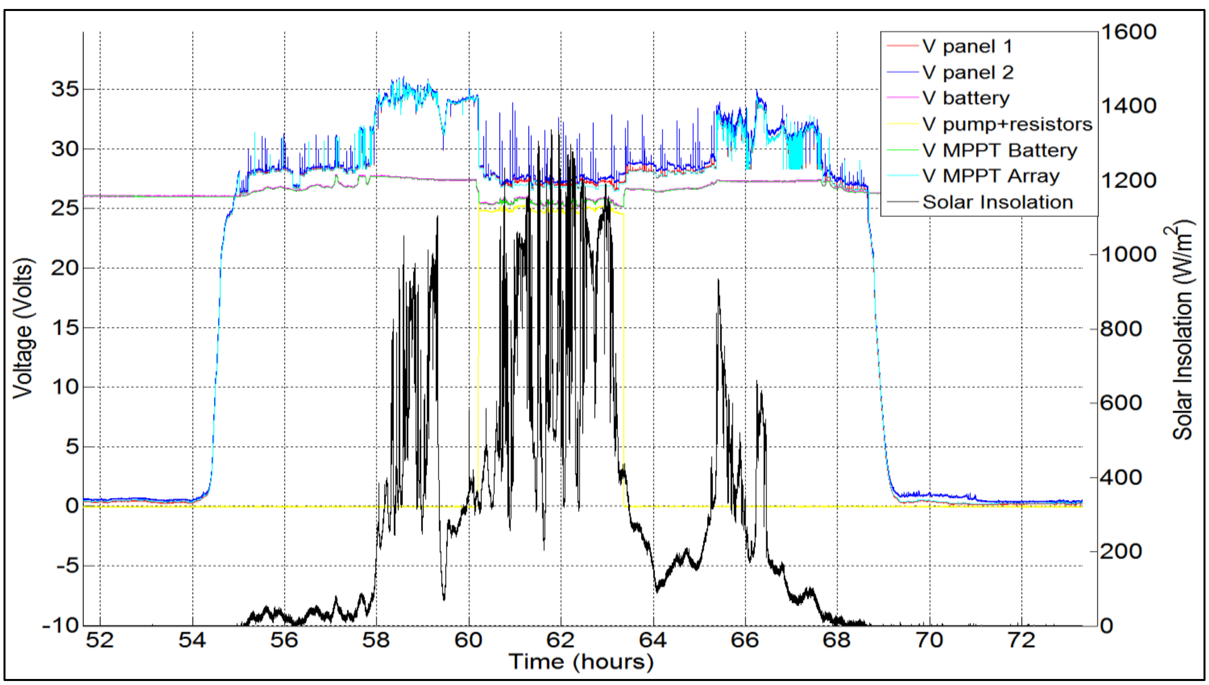

Figure 4.24: Voltage and solar insolation versus time for PV array inclination at 30° and sun tracking for operation hours from 52 to 72 on August 11, 2014.

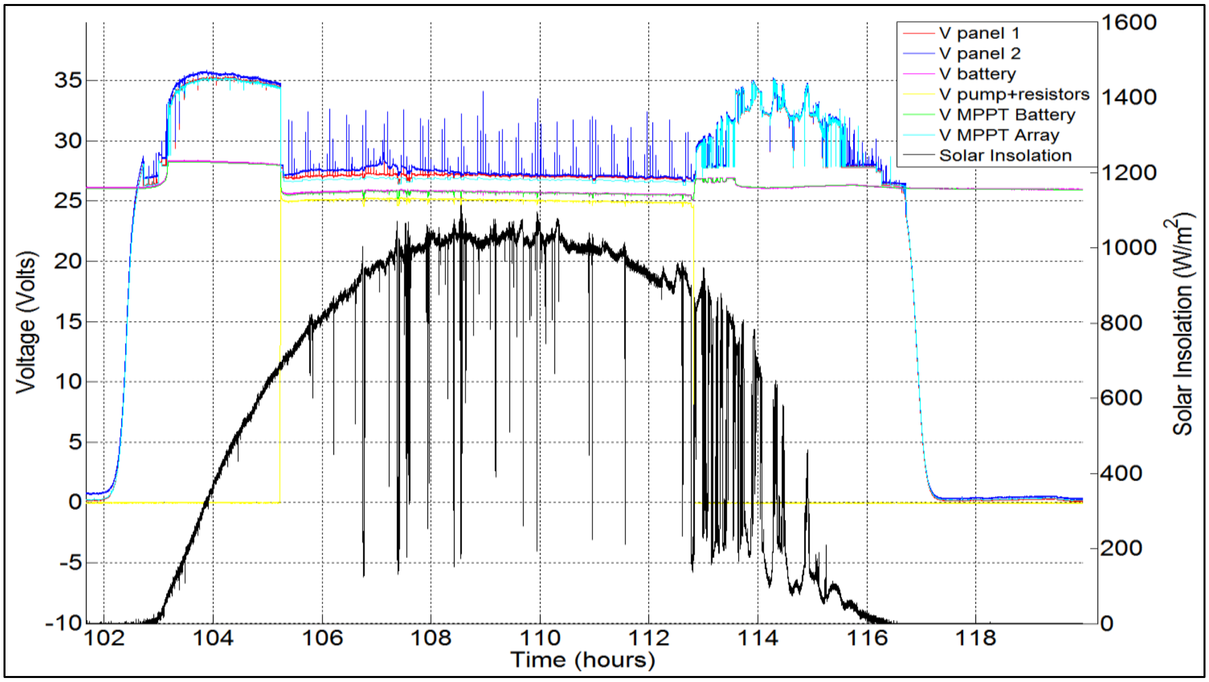

Figure 4.25: Voltage and solar insolation versus time for PV array inclination at 30° and sun tracking for operation hours from 102 to 118 on August 13, 2014.

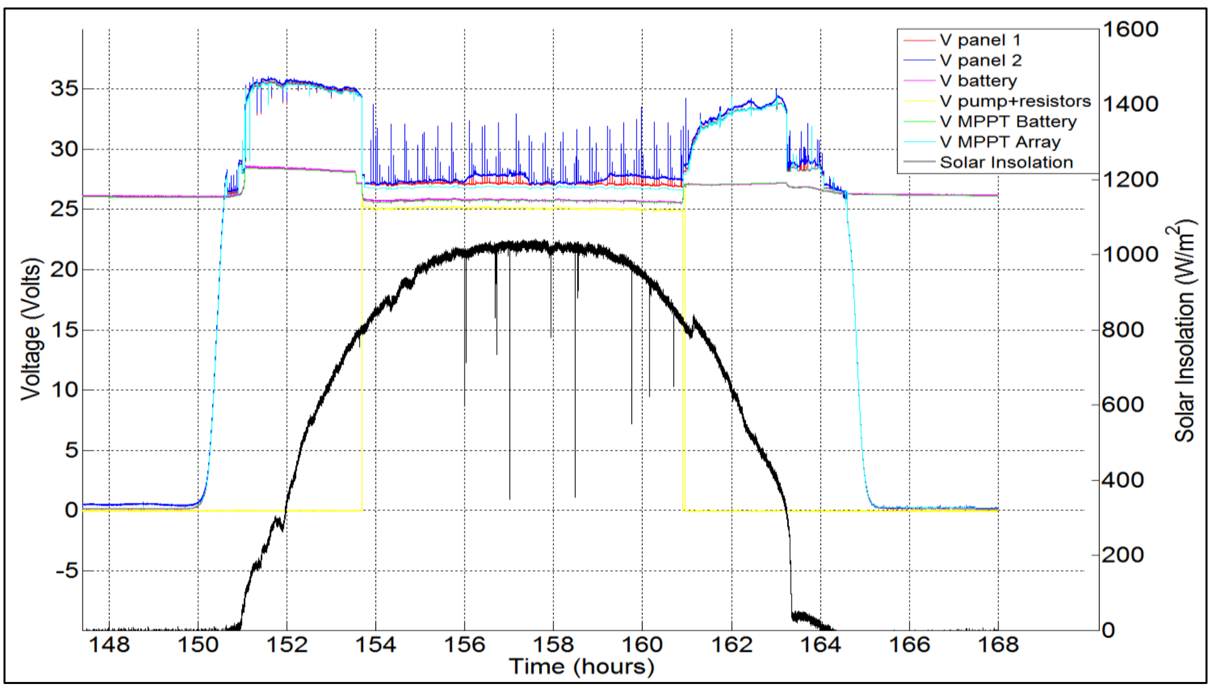

Figure 4.26: Voltage and solar insolation versus time for PV array inclination at 30° and sun tracking for operation hours from 148 to 168 on August 15, 2014.

Voltage outputs of PV panel 1 and panel 2 show fluctuations or spikes when the pump and resistors are connected, these fluctuations in voltage are similar to voltage data shown in the test taken at a 40° tilt. The PV array produced a maximum voltage of 36 volts when the load was disconnected. Since the solar insolation remained lower during the early morning for 3 hours from the 55th to 58th hour (see Figure 4.24). As a result the voltage outputs of the PV array were lower as well. Later when the solar insolation became higher, the voltage increased to 36 volts. During this test, the voltage output from PV panel 1 and 2 slightly differed from each other during 157th and 160th hour as shown in Figure 4.26.

4.2.2. Currents

Current and solar insolation versus time recorded throughout the week by the data acquisition subsystem and MPPT data logger are shown in Figure 4.27. Current outputs and insolation data for individual days is shown in Figures 4.28 through 4.30.

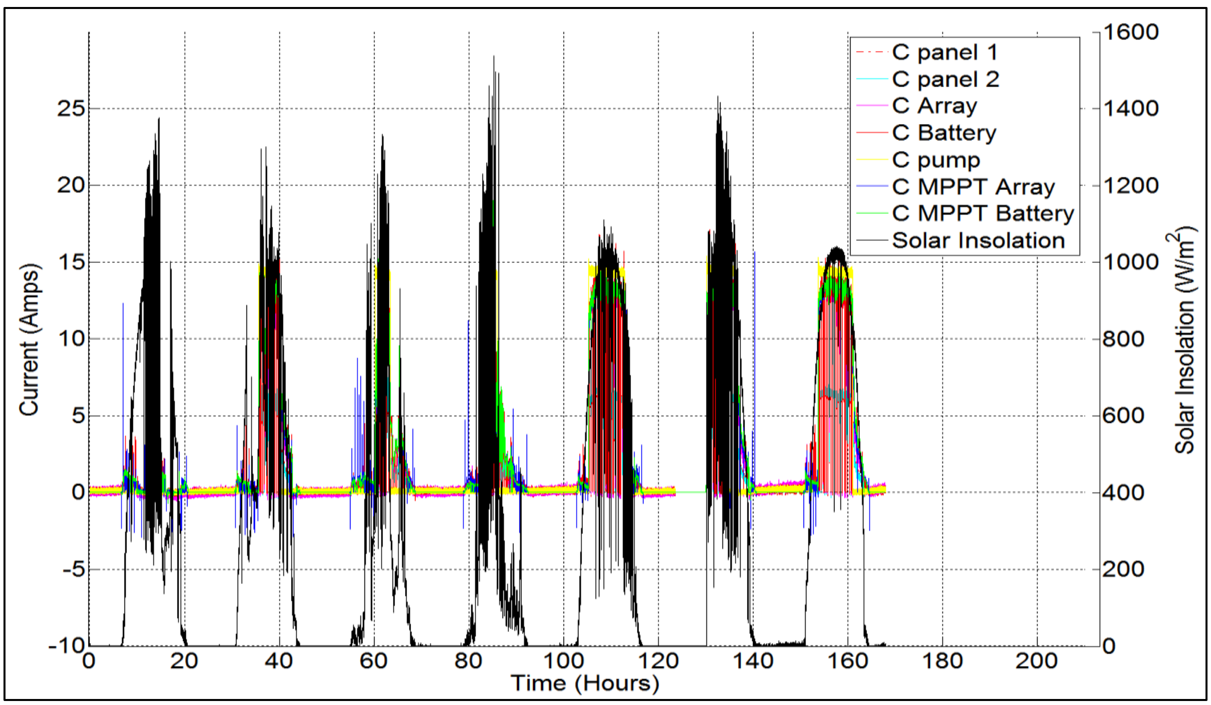

Figure 4.27: Current and solar insolation versus time for PV array inclination at 30° and sun tracking for seven days of operation from August 9 to August 15, 2014.

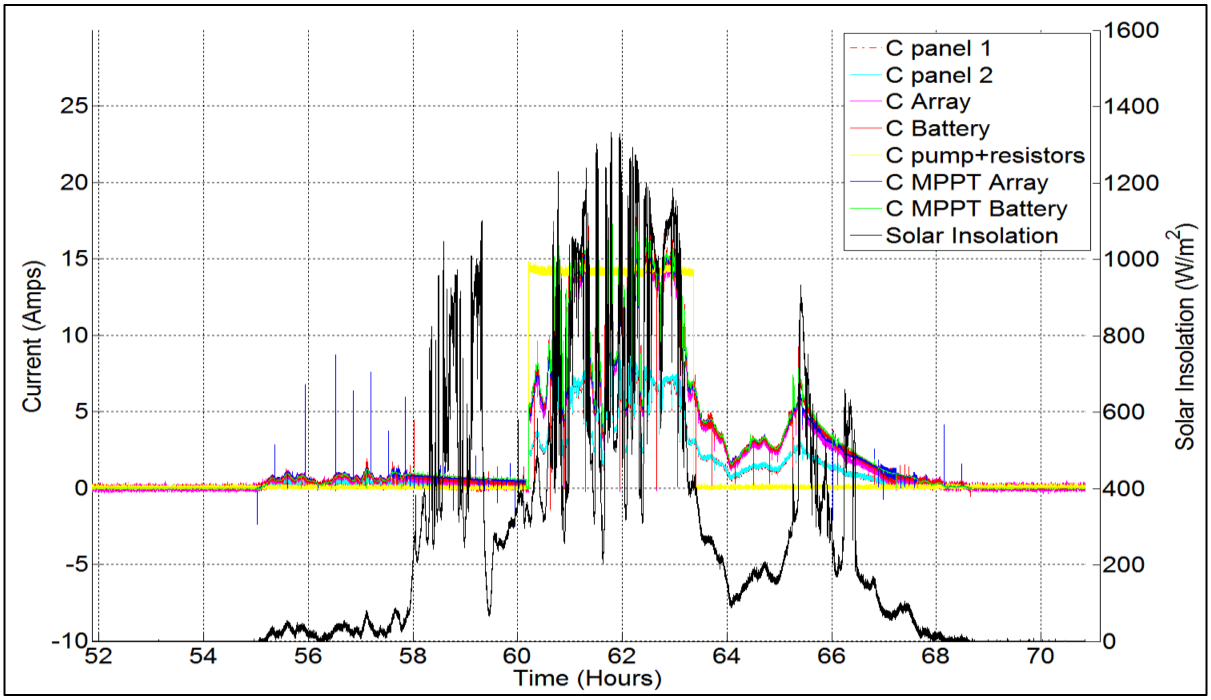

Figure 4.28: Current and solar insolation versus time for PV array inclination at 30° and sun tracking for operation hours from 52 to 72 on August 11, 2014.

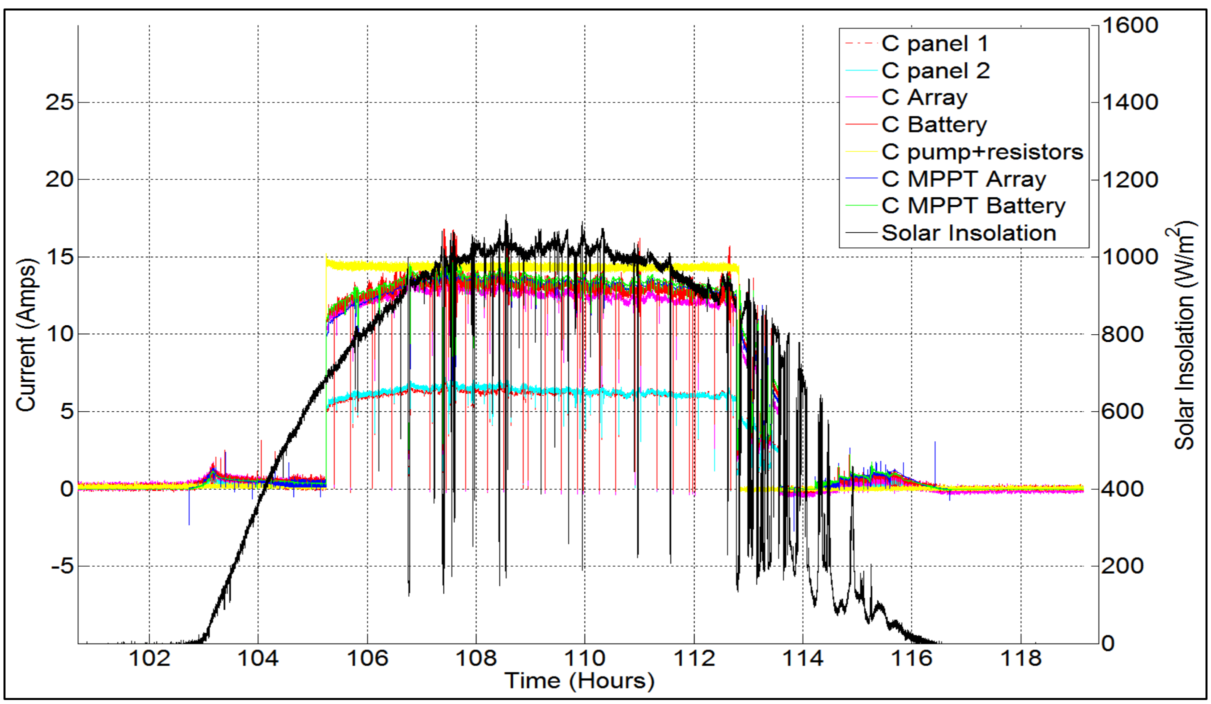

Figure 4.29: Current and solar insolation versus time for PV array inclination at 30° and sun tracking for operation hours from102 to 118 on August 13, 2014.

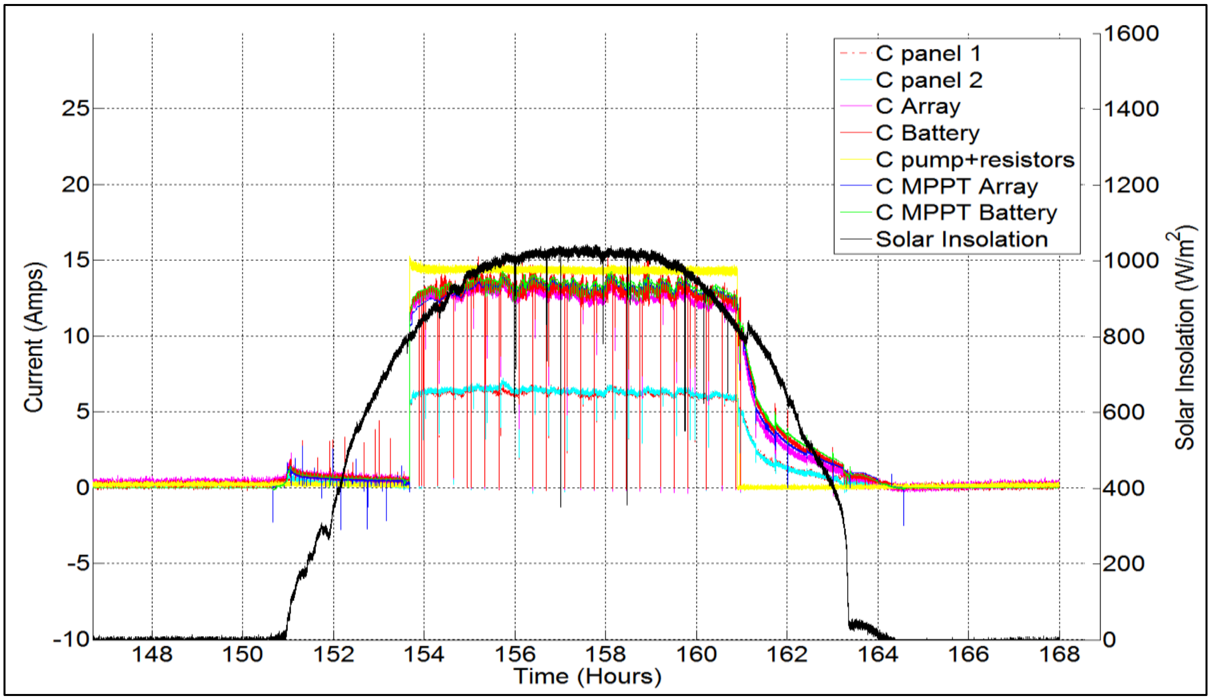

Figure 4.30: Current and solar insolation versus time for PV array inclination at 30° and sun tracking or operation hours from148 to 168 on August 15, 2014.

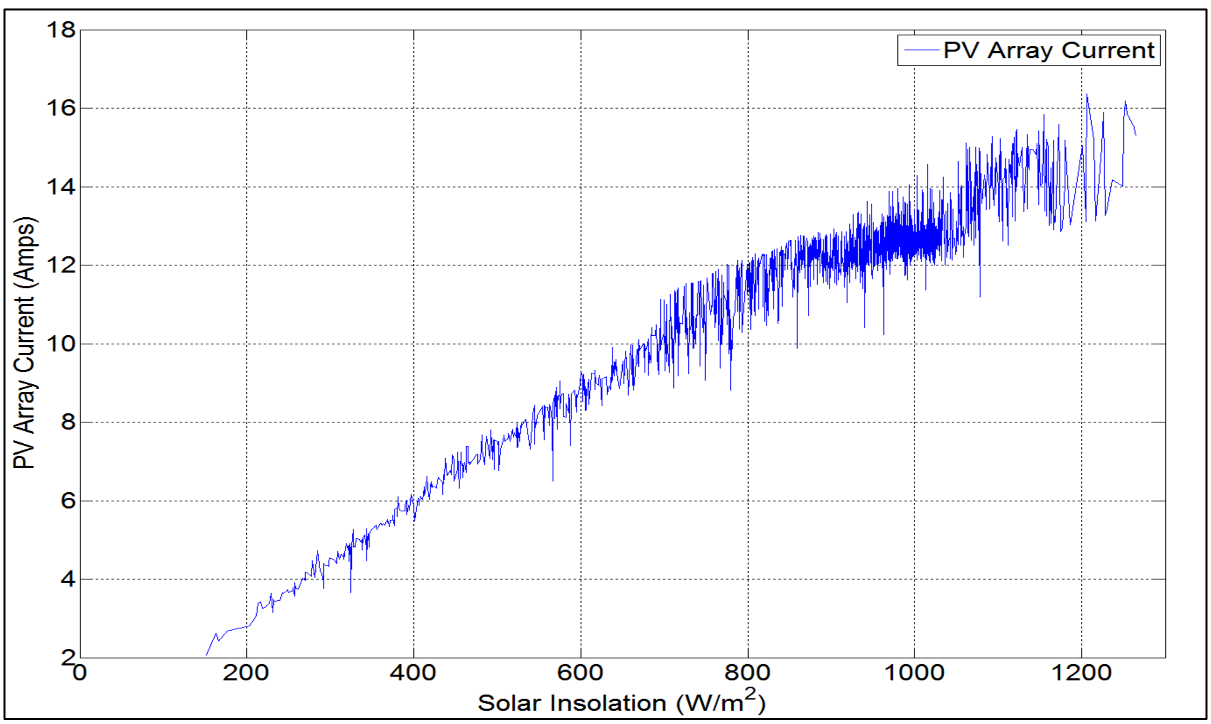

Figure 4.31: PV array current as a function of solar insolation for a PV array inclination at 30° and sun tracking.

On August 16th, the second day of the week, the pump was run for only 2 hours from 60th to 63rd hour (see Figure 4.28) due to bad weather conditions. As it can be seen the solar insolation fluctuated due to rain in the early morning and cloud cover in the afternoon. On the 5th and 7th days of the week, the weather was clear and continuous pumping was done for more than 7 hours. On a very clear day with no clouds at all, the PV panels can continuously deliver approximately 12 amps for more than 7 hours as shown in Figure 4.30. The impact of the PV array surface orientation at 30° inclination, in comparison to current outputs recorded with PV array oriented at 40°, is not so visible in Figures 4.27 to 4.30. However, current outputs recorded at 30° inclination have increased from 13 amps to approximately 15 amps by comparing Figures 4.8 and 4.31. Moreover, it can also be noticed that the number of data samples between 1000 to 1200 watts/m^2 increased for the 30° orientation as compared to the 40° orientation.

4.2.4. Powers

Power and solar insolation versus time recorded by the data acquisition subsystem and the MPPT data logger with the PV orientation at 30° inclination angle are shown in Figures 4.32 to 4.34. Power results from panel l, panel 2, PV array and pump with resistors are denoted by P panel 1, P panel 2, P Array and P Pump+resistors respectively. The PV array has continuously generated more than 300 watts of power while the pump is running for more than 7 hours as shown in Figures 4.33 and 4.34. The pump and the resistors draw power from the batteries at approximately 360 watts. The effects of orientation at two different PV array inclination angles are not visible in these two figures. However, a noticeable increase in power output can be seen when PV array is oriented at 30° by comparing Figure 4.35 with Figure 4.12. At a 40° tilt the PV array output did not exceed more than 410 watts with the exception of three data points. At a 30° tilt the PV array generated more than 420 watts at insolation levels higher than 1100 watts/m^2.

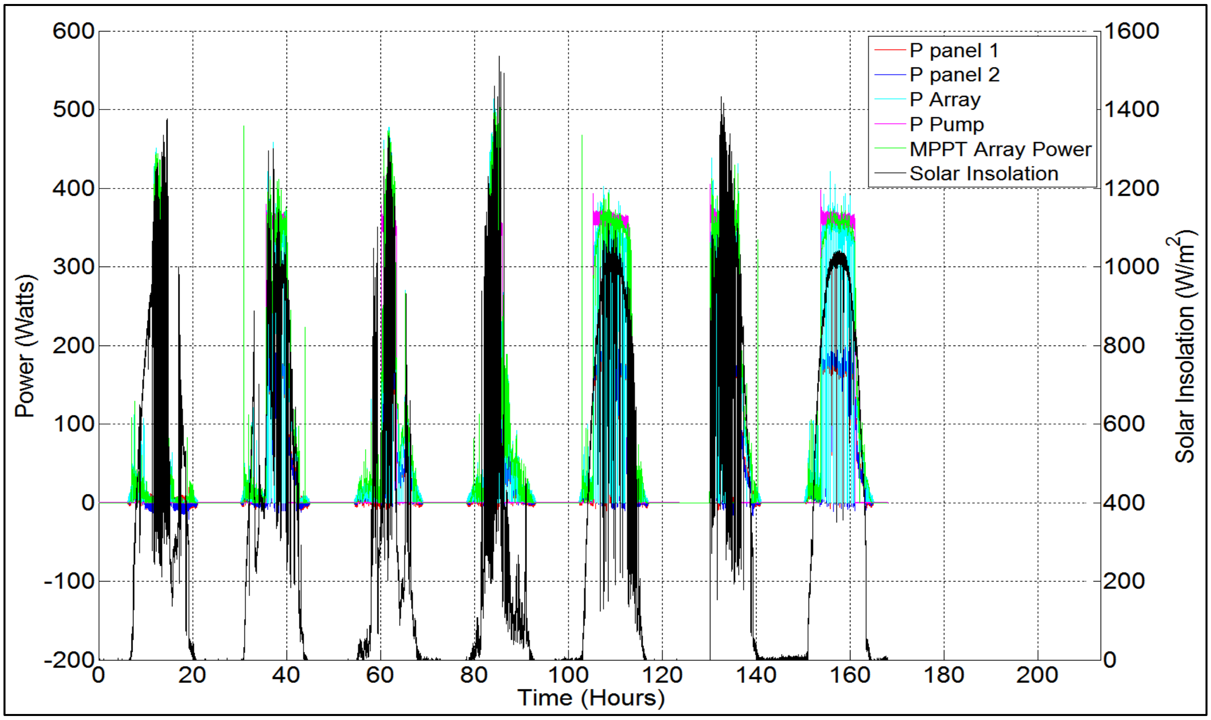

Figure 4.32: Power and solar insolation versus time for PV array inclination at 30° and sun tracking for seven days of operation from August 9 to August 15, 2014.

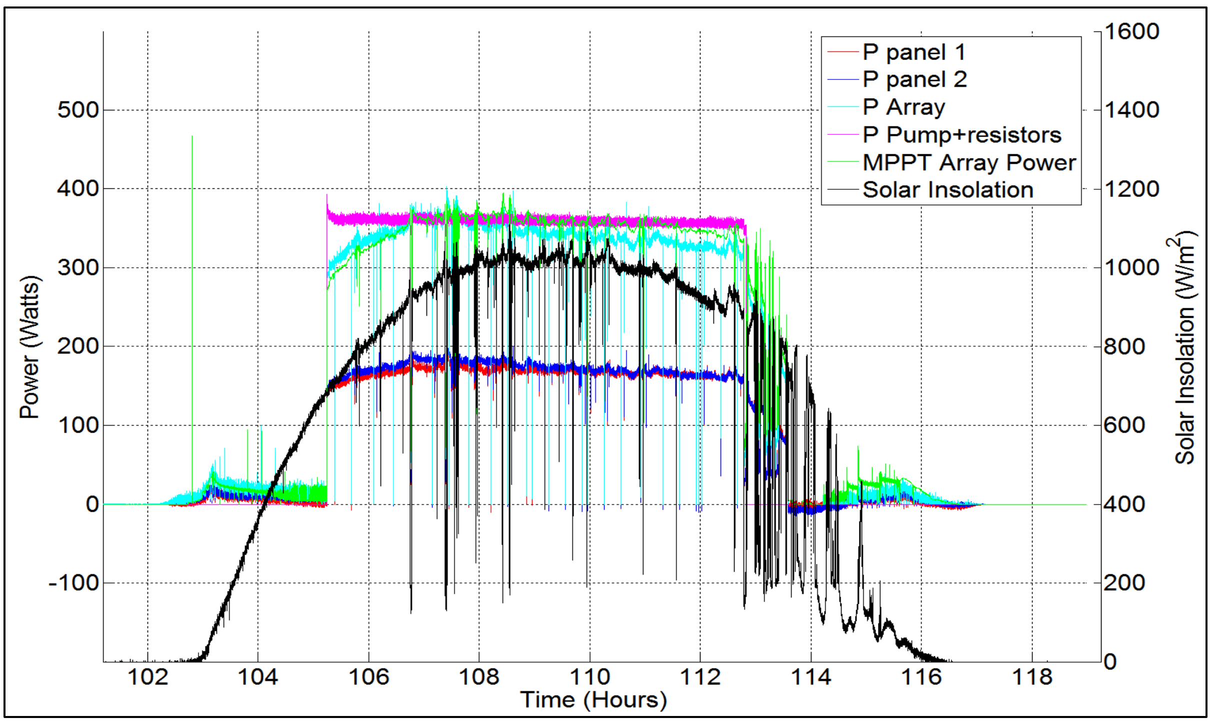

Figure 4.33: Power and solar insolation versus time for PV array inclination at 30° and sun tracking for the hours of operation from 102 to 118 on August 13, 2014.

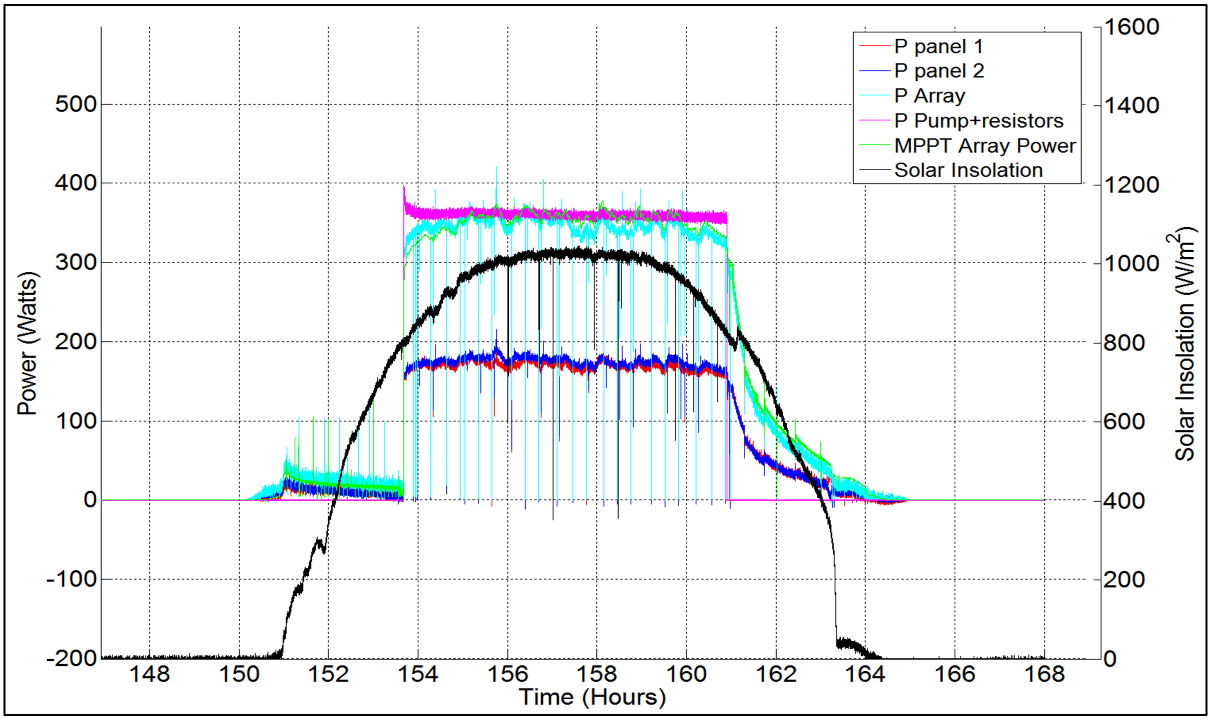

Figure 4.34: Power and solar insolation versus time for PV array inclination at 30° and sun tracking for the hours of operation from 148 to 168 on August 15, 2014.

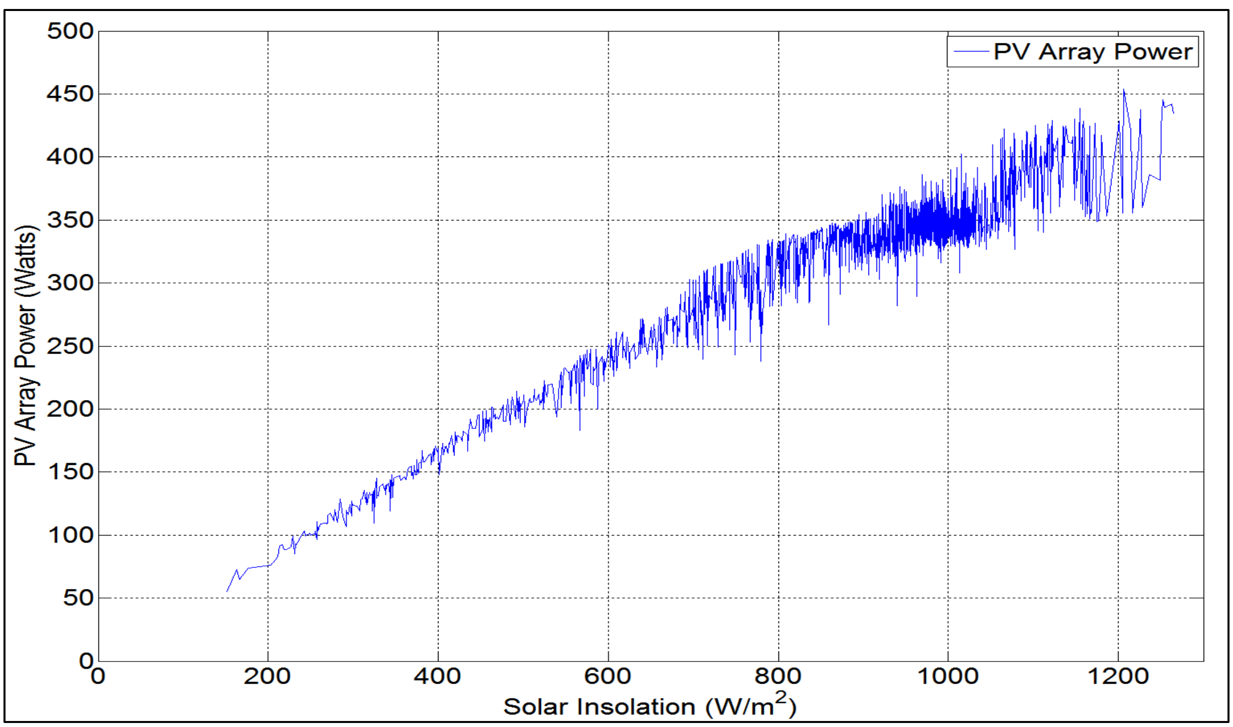

Figure 4.35: PV array power as a function of solar insolation for a PV array inclination of 30° and sun tracking.

4.2.4. Temperatures

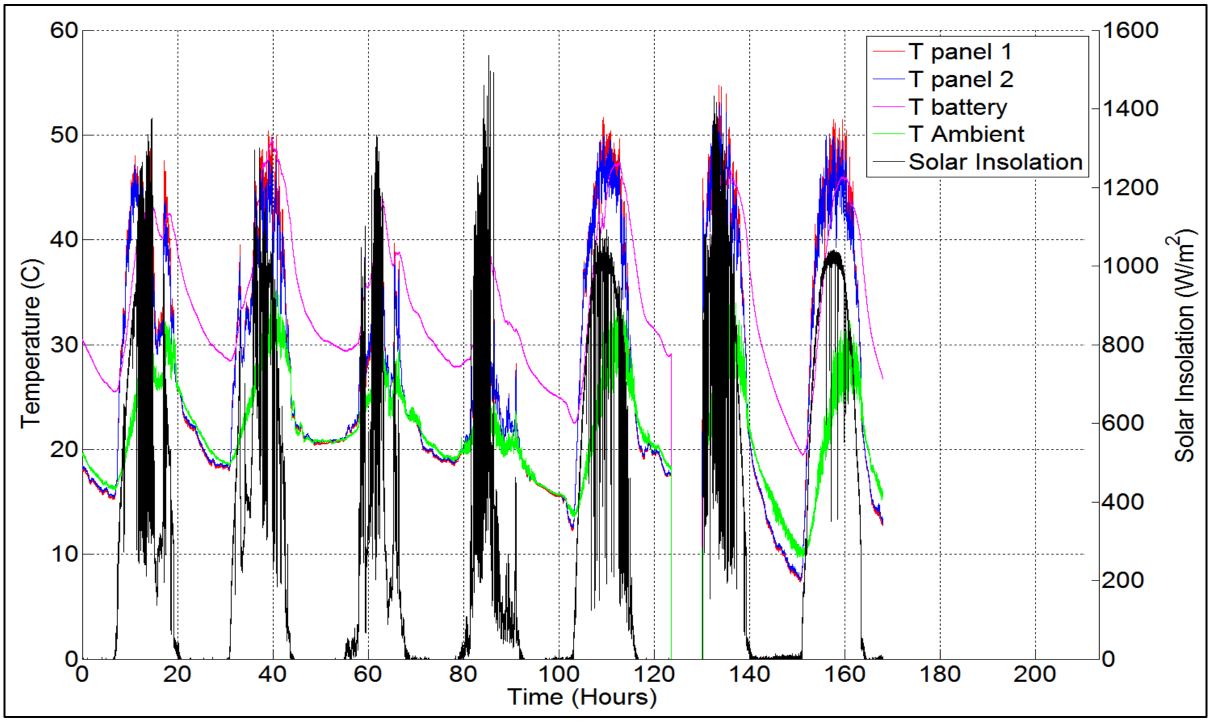

Figure 4.36: Temperature and solar insolation versus time for PV array inclination at 30° and sun tracking for seven days of operation from August 9 to August 15, 2014.

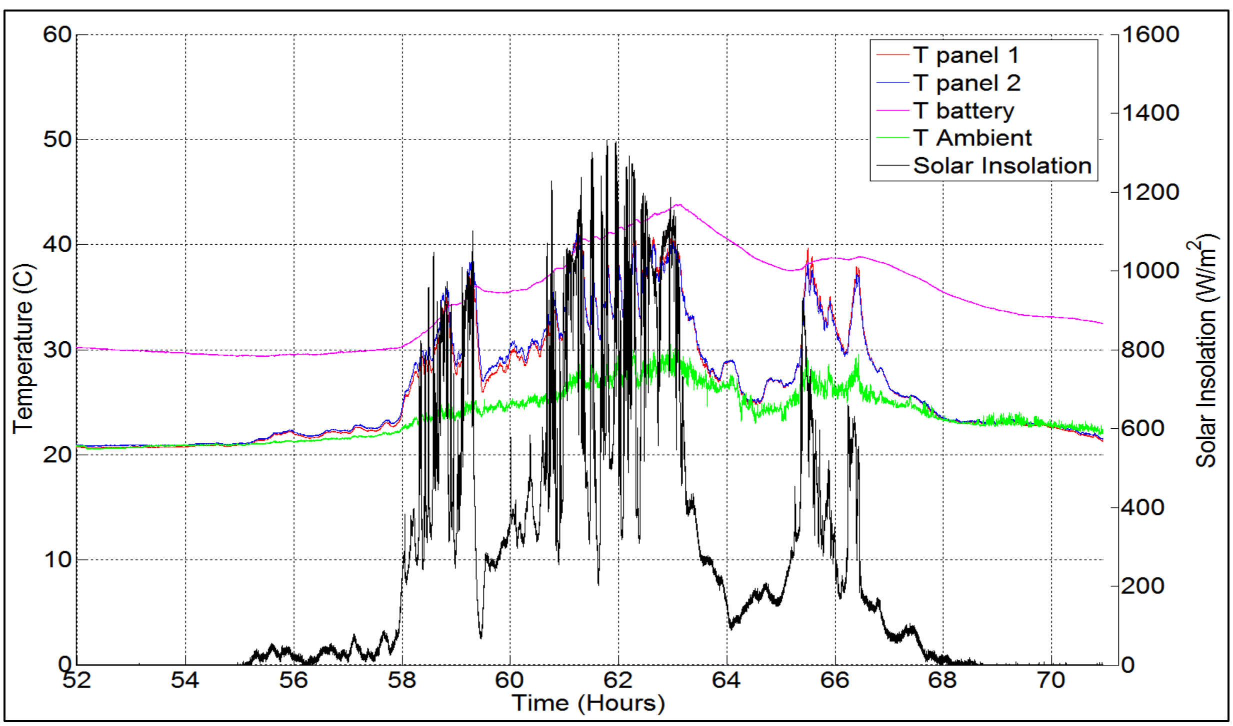

Figure 4.37: Temperature and solar insolation versus time for PV array inclination at 30° and sun tracking for the hours of operation from 52 to 72 on August 11, 2014.

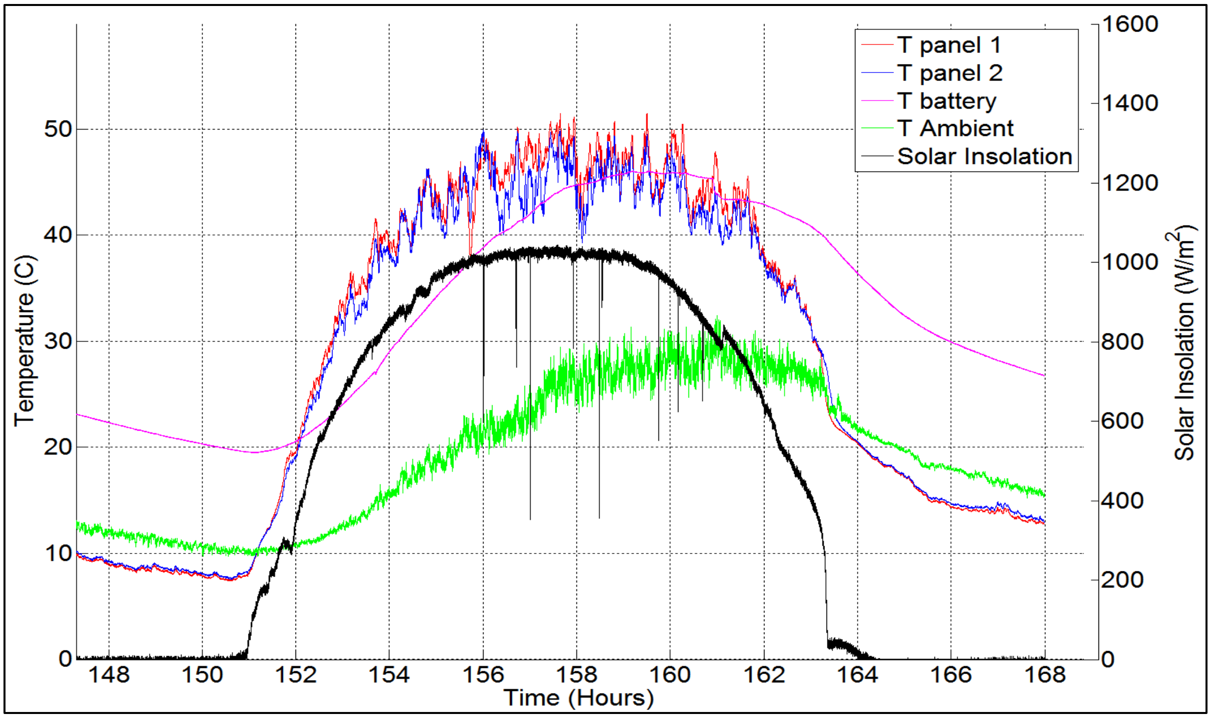

Figure 4.38: Power and solar insolation versus time for PV array inclination at 30° and sun tracking for the hours of operation from 148 to 168on August 15, 2014.

Data such as temperature and solar insolation versus time, recorded throughout the week at a PV array inclination angle of 30° is shown in Figures 4.36. The temperature and insolation data for individual days for August 11 and August 15 are shown in Figures 4.37 and 4.38 respectively. As solar insolation is suddenly changing from high to low or low to high, in the result, the temperature of each panel is also changing in response to the solar insolation (see Figure 4.37). On the other hand, on a very clear day, the temperature of the PV panels follows the same pattern as the solar insolation as shown in Figure 4.38. The impact of temperature on efficiency of PV panels is discussed in next subsection.

4.2.5. PV Array Efficiency

By orienting the PV panels at an inclination angle of 30° with sun tracking, the PV array operates at an efficiency of 12 to 13 % within the range of 200 to 800 watts/m^2 of solar insolation as shown in Figure 4.39. As the solar insolation exceeds 800 watts/m^2; the PV array efficiency drops to 10%. As can be seen from Figure 4.39 the efficiency of the PV array decreases as the solar insolation increases. This is because the temperature of the panels increases as shown in Figures 4.36 to 4.38 and in Figure 4.39. However there is a small anomaly in the temperature versus solar radiation behavior at 1050 watts/m^2 and it can be noticed that the PV array efficiency gets higher until it reaches 1180 watts/m^2, where temperature tends to rise back up to 44°C.

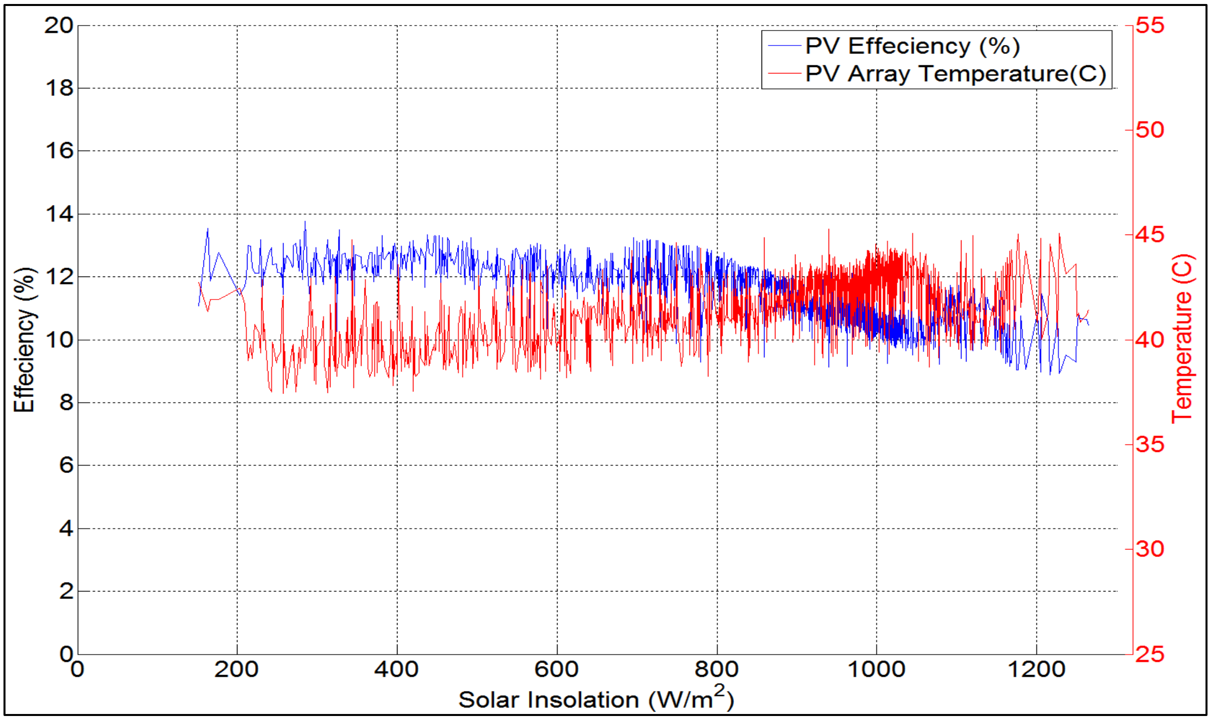

Figure 4.39: PV array efficiency and panel temperature as a function of solar insolation for PV array inclination at 30° and sun tracking for seven days of operation from August 9 to August 15, 2014.

4.2.6. PV Array Energy Generation

Energy production results by the PV array oriented at 30° inclination and with sun tracking for the week from August 9 to August 15 are shown in Figure 4.40. By comparing these results with energy output at 40° inclination, it can be seen that the highest solar energy incident on the PV array at 40° inclination was 26.65 kW-h. Whereas, highest solar energy incident at 30° inclination is 29.18 kW-h on 7th day of the week, which is about 2.5 kW-h more energy collected at the 30° inclination than the 40° inclination. The PV array generated 2.65 kW-h energy at this 29.18 kW-h of solar energy incident on the panels. The second highest solar energy incident on PV array at 30° tilt was 28.95 kW-h on 5th day, when the PV array generated its highest energy of 2.72 kW-h. Moreover, lowest solar energy collected by the PV array was 12.34 kW-h at which PV array generated 1.08 kW-h. The lowest energy production was observed on 1st day of this week when the PV array generated only 0.6 kW-h, although a sufficient amount of solar energy was collected by the PV array. The lower energy production on this day is due to the pump not being run for long periods of time. Since there was no energy consumed by the pump and resistors, the charge level of the batteries was almost full and the PV array did not convert available solar energy into electricity.

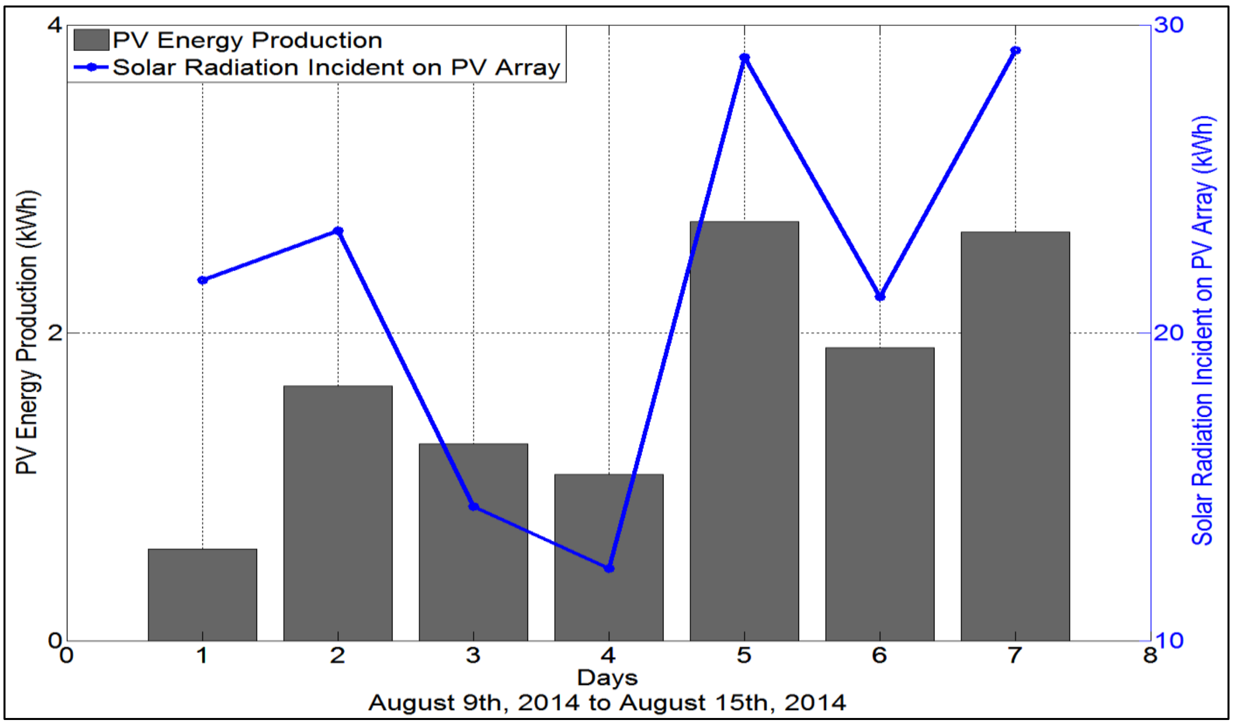

Figure 4.40: PV array energy production for PV array inclination at 30° and sun tracking for seven days of operation from August 9 to August 15, 2014.

4.3. Fixed, Due South Orientation at an Inclination Angle of 40° with both Water Pump and Power Dissipating Resistors

In this test the orientation of the PV array is fixed facing due south with an inclination angle of 40°. Since many solar PV systems use a fixed orientation it was desired to test our system with a fixed orientation. Results acquired under such an orientation of the PV array will give some indication of the differences between fixing the orientation of the PV panels and tracking the azimuthal position of the sun. Like in the previous two configurations, in this configuration of the PV array both the pump and the power dissipating resistors are connected to the battery bank. Results such as voltage, current, power and PV energy recorded throughout the week from August 23 to August 29, 2014 are presented. Please note that on 4th day during the data collection period shown in this section, MPPT data logger ceased and did not respond. Therefore, it did not collect data on 4th and 5th day. But, LabVIEW or data acquisition subsystem designed with this project was still operational. Thus, LabVIEW recorded data for 4th and 5th day during this time period. Whereas, on 6th and 7th day LabVIEW also ceased to respond. That is the reason there are blanks on 6th and 7th day, which means data was not collected during these two days. However, data was collected for three more days after LabVIEW and MPPT data logger had shut down. This could be noticed in measurements recorded such as voltages, currents, temperatures, powers and PV energy production in this section.

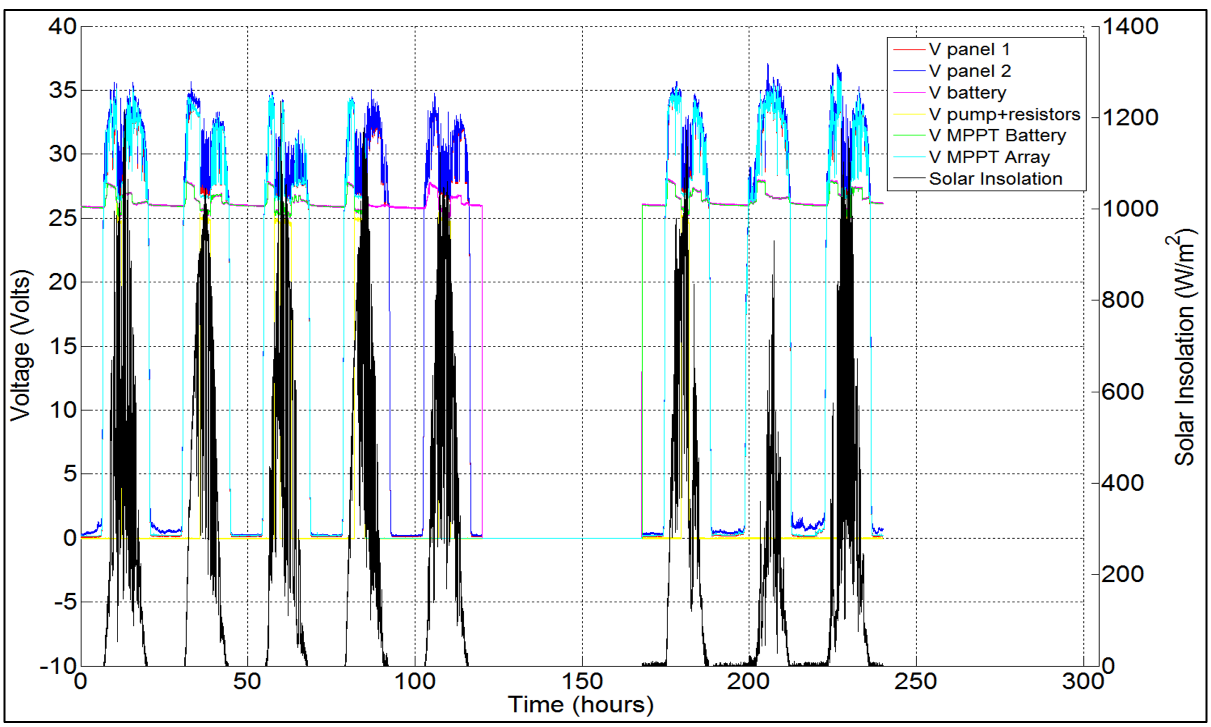

Figure 4.41: Voltage and solar insolation versus time for PV array with azimuthal orientation fixed due south and inclination fixed at 40°for ten days of operation from August 23 to September 1st, 2014.

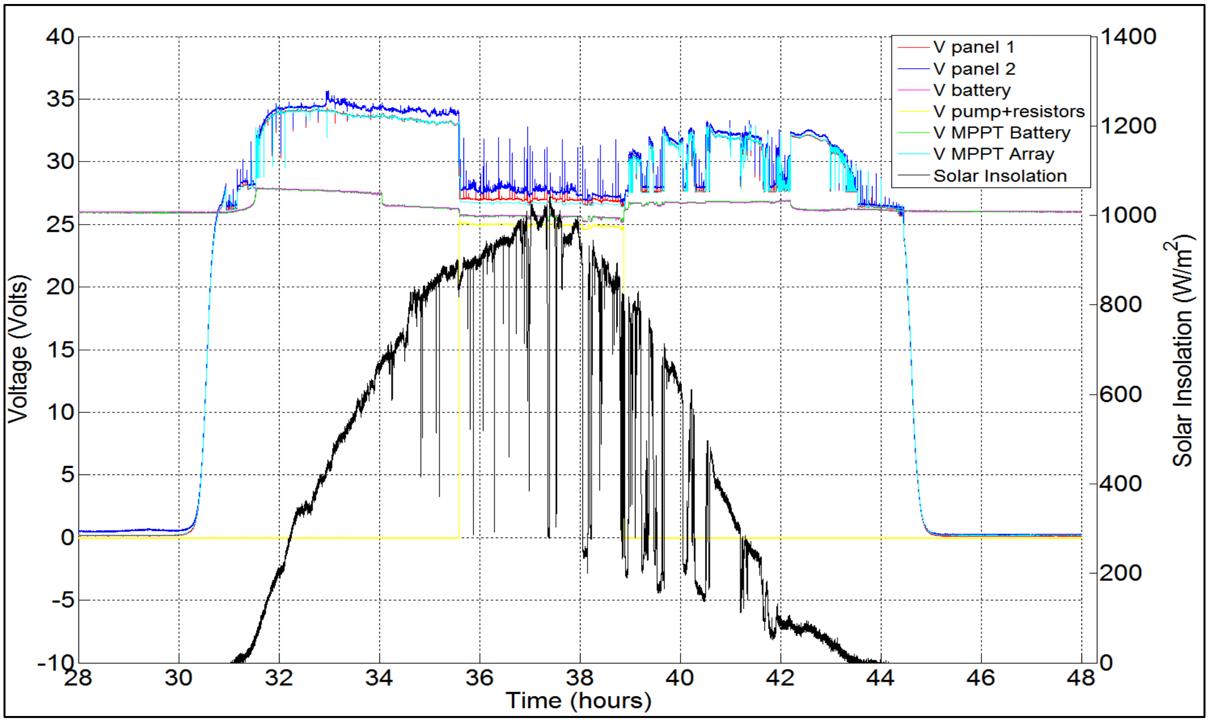

Figure 4.42: Voltage and solar insolation versus time for PV array with azimuthal orientation fixed due south and inclination fixed at 40° for the hours of operation from 28 to 48 on August 24, 2014.

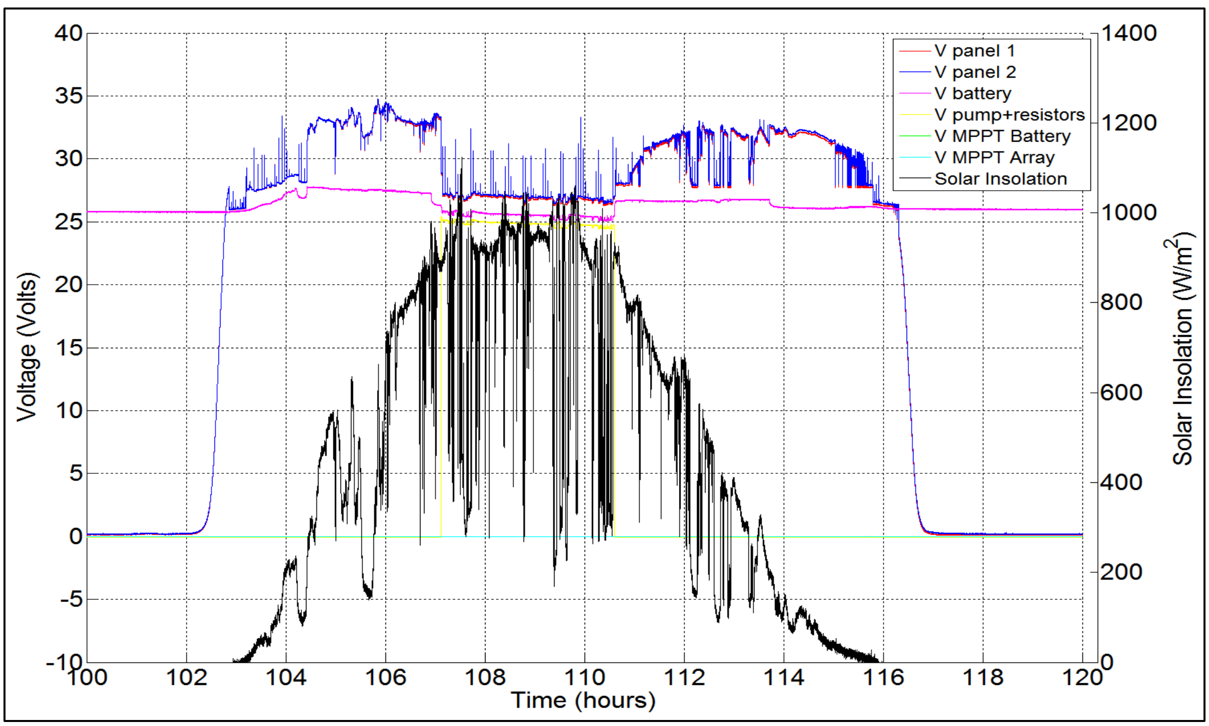

Figure 4.43: Voltage and solar insolation versus time for PV array azimuthal orientation fixed due south and inclination fixed at 40° for the hours of operation from 100 to 120 on August 27, 2014.

4.3.1. Voltages

Voltage and solar insolation recorded for the PV array with a due south fixed orientation with an inclination angle of 40° are shown in Figures 4.41 to 4.43. These curves are similar to those in Figures 4.1 to 4.4 for case that uses solar tracking with a inclination angle of 40°, but the peaks in solar insolation values are slightly smaller with the PV panels having a fixed orientation. The voltage results are also similar to those in Figures 4.23 to 4.26 for the case of solar tracking with an inclination angle of 30°, however, the peaks of the solar insolation for the 30° inclination angle case are even higher than the 40° inclination angle case. The voltage profiles are also similar.

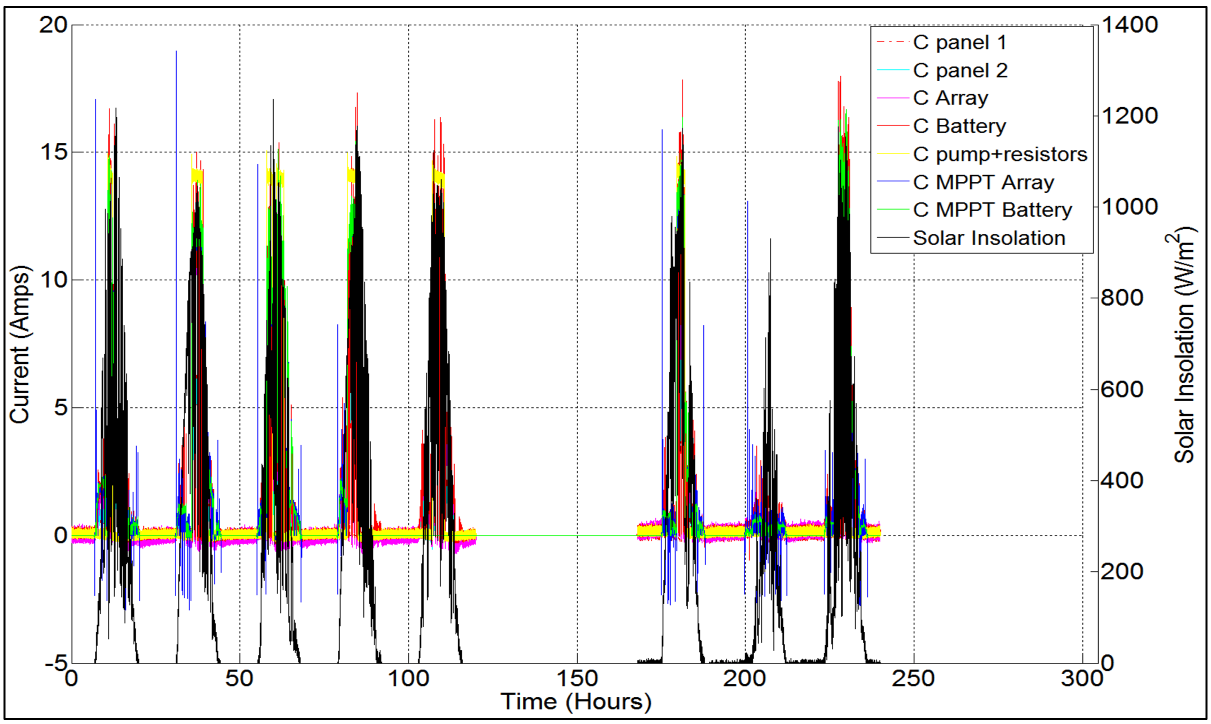

Figure 4.44: Current and solar insolation versus time for PV array with azimuthal orientation fixed due south and inclination fixed at 40° for ten days of operation from August 23 to September 1st, 2014.

4.3.2. Currents

Current and solar insolation recorded for the PV array with a fixed orientation due south at an inclination angle of 40° are shown in Figures 4.44 to 4.46. Current outputs show similar behavior as observed in the previous two cases that employed solar tracking.

However, as the PV array is fixed, less solar energy is impinged on the PV array in the morning and evening hours. As a result the PV panels deliver less current during the day. Thus the batteries get discharged at a quicker rate. Because the current draw of the resistors and pump from the batteries is higher than the current supplied by the PV array; except during solar noon at which the PV panels are directly facing the sun. Due to this reason the load has to be disconnected in a shorter period of time as compared to the cases when the solar tracker was operational.

4.3.3. Powers

Power and solar insolation versus time recorded for the PV array with fixed orientation due south at an inclination angle of 40° are shown in Figures 4.47 to 4.48. Like current, the PV array generates less power at a fixed orientation during the morning and evening hours and on an overall basis. The PV array power as a function of solar insolation has been shown in Figures 4.49 and 4.50 on second and minute time intervals respectively.

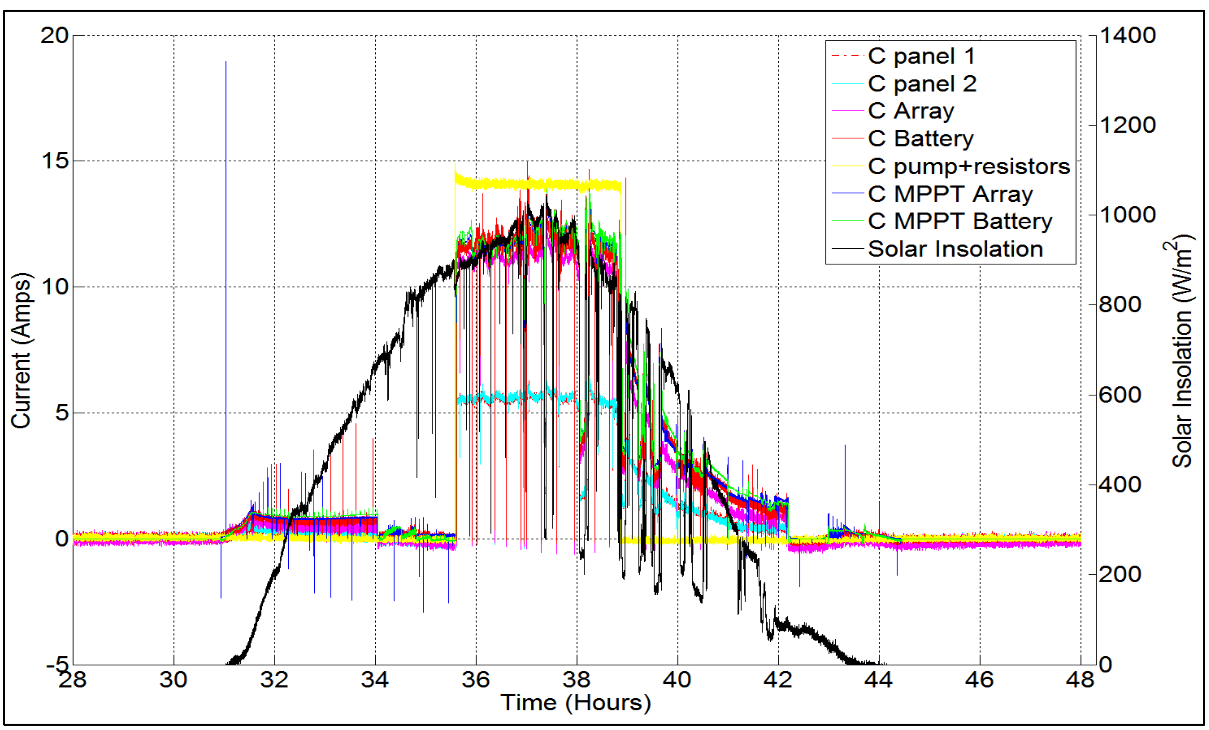

Figure 4.45: Current and solar insolation versus time for PV array with azimuthal orientation fixed due south and inclination fixed at 40° for the hours of operation from 28 to 48 on August 24, 2014.

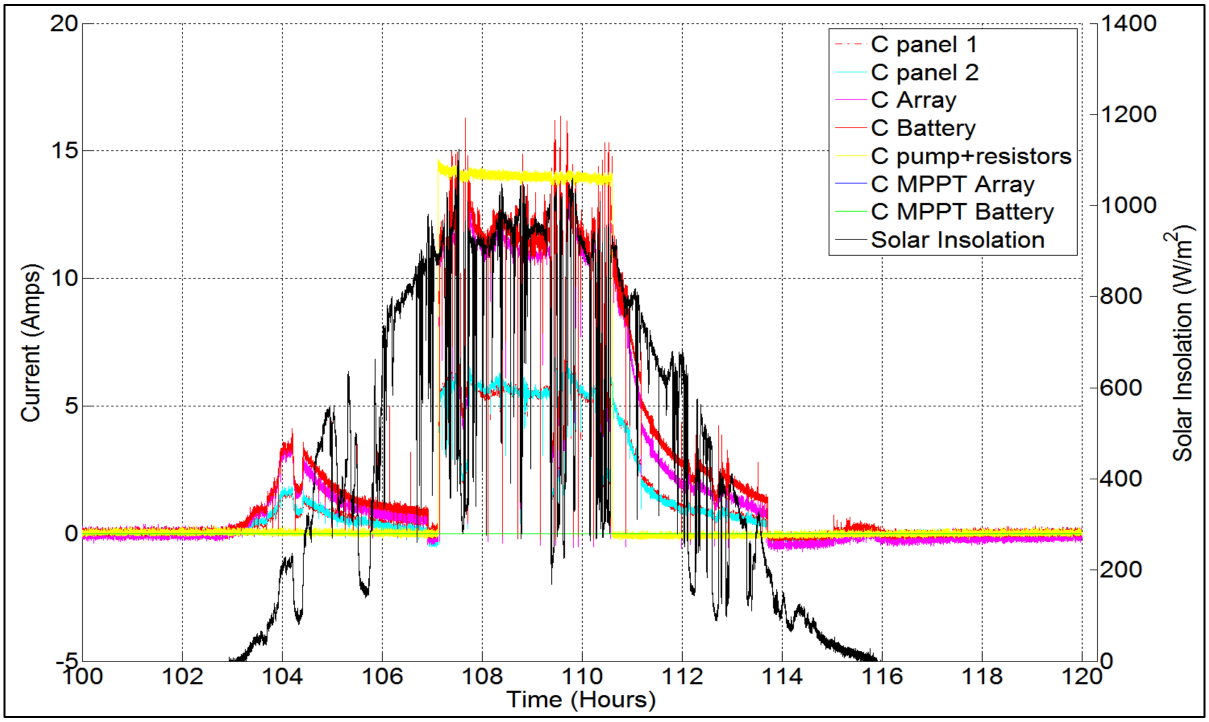

Figure 4.46: Voltage and solar insolation versus time for PV array with azimuthal orientation fixed due south and inclination fixed at 40°for the hours of operation from 100 to 120 on August 27, 2014.

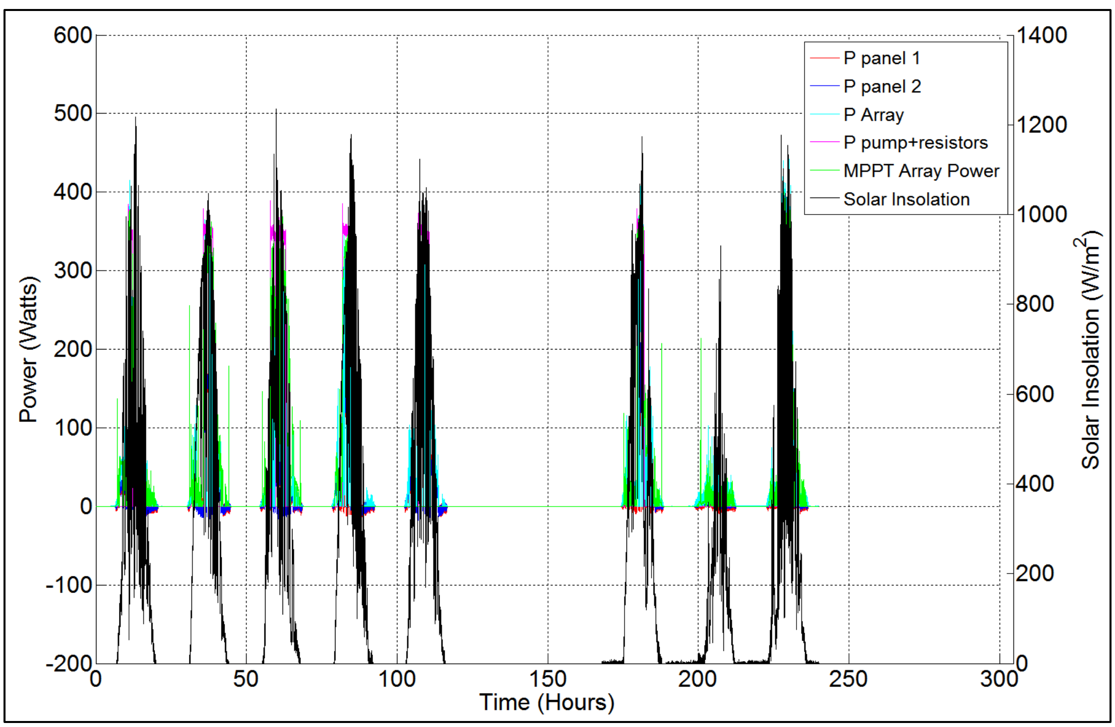

Figure 4.47: Power and solar insolation versus time for PV array with azimuthal orientation fixed due south and inclination fixed at 40°for ten days of operation from August 23 to September 1st, 2014.

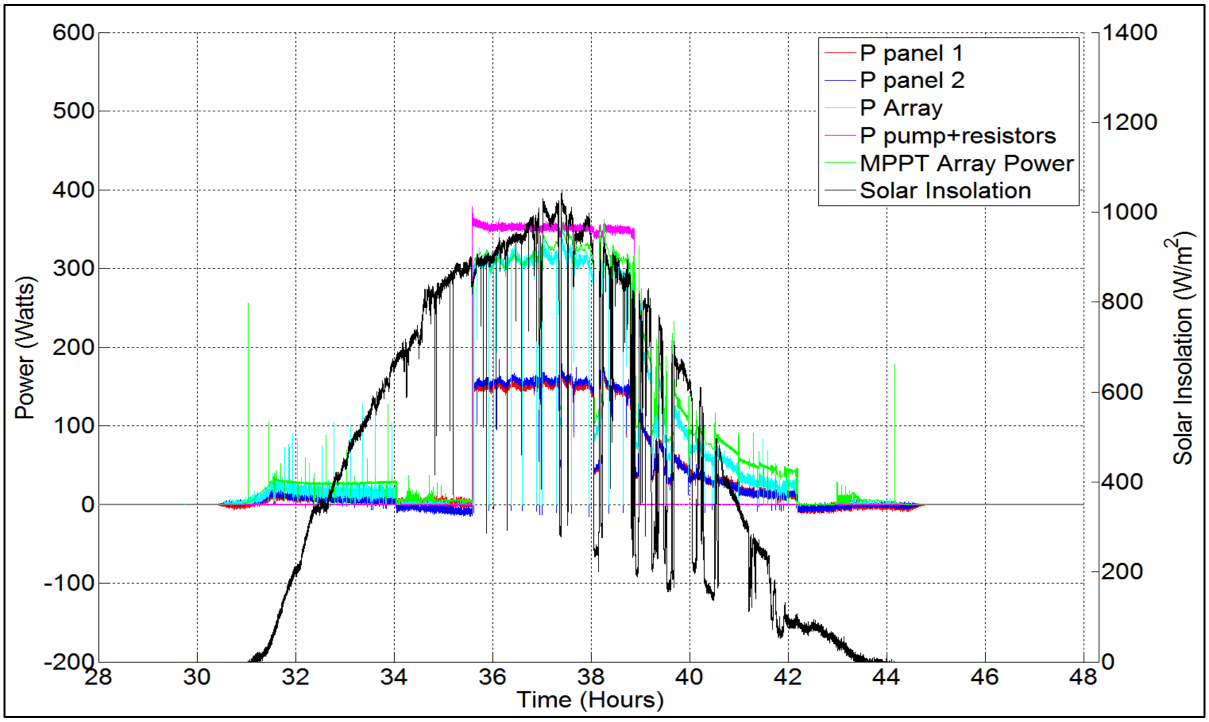

Figure 4.48: Power and solar insolation versus time for PV array for PV array with azimuthal orientation fixed due south and inclination fixed at 40°for the hours of operation from 28 to 48 on August 24, 2014.

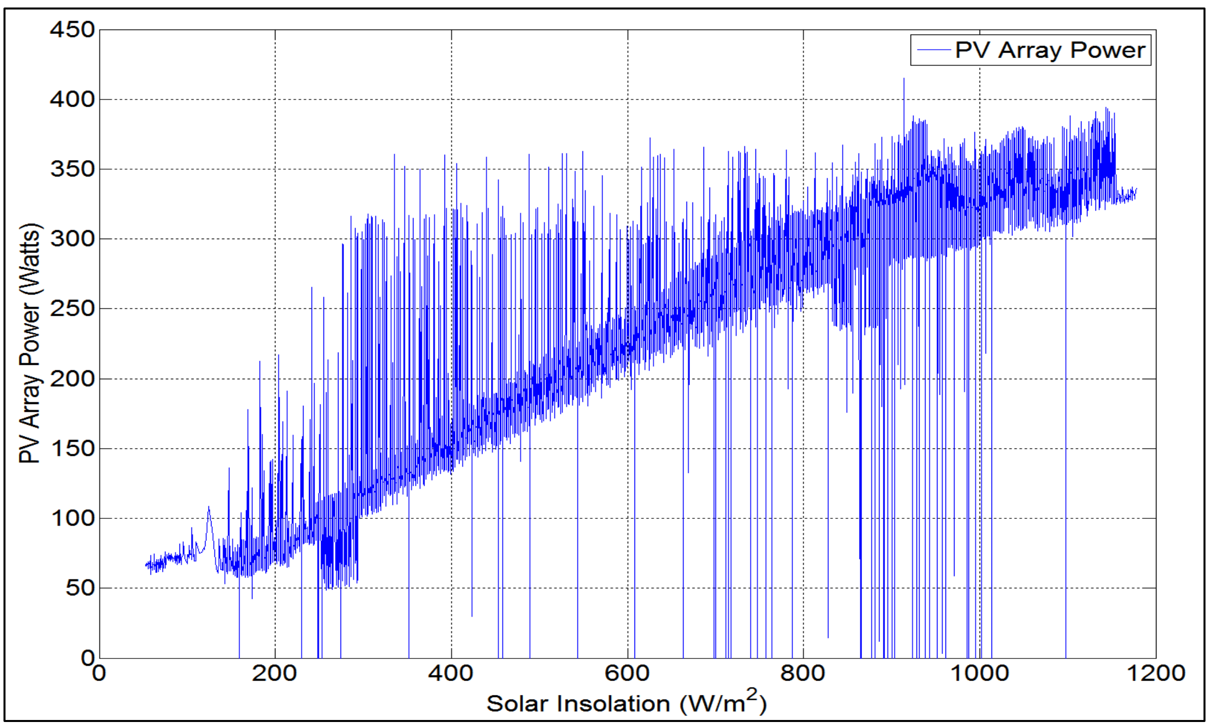

Figure 4.49: PV array power as a function of solar insolation recorded on the second time interval with azimuthal orientation fixed due south and inclination fixed at 40°.

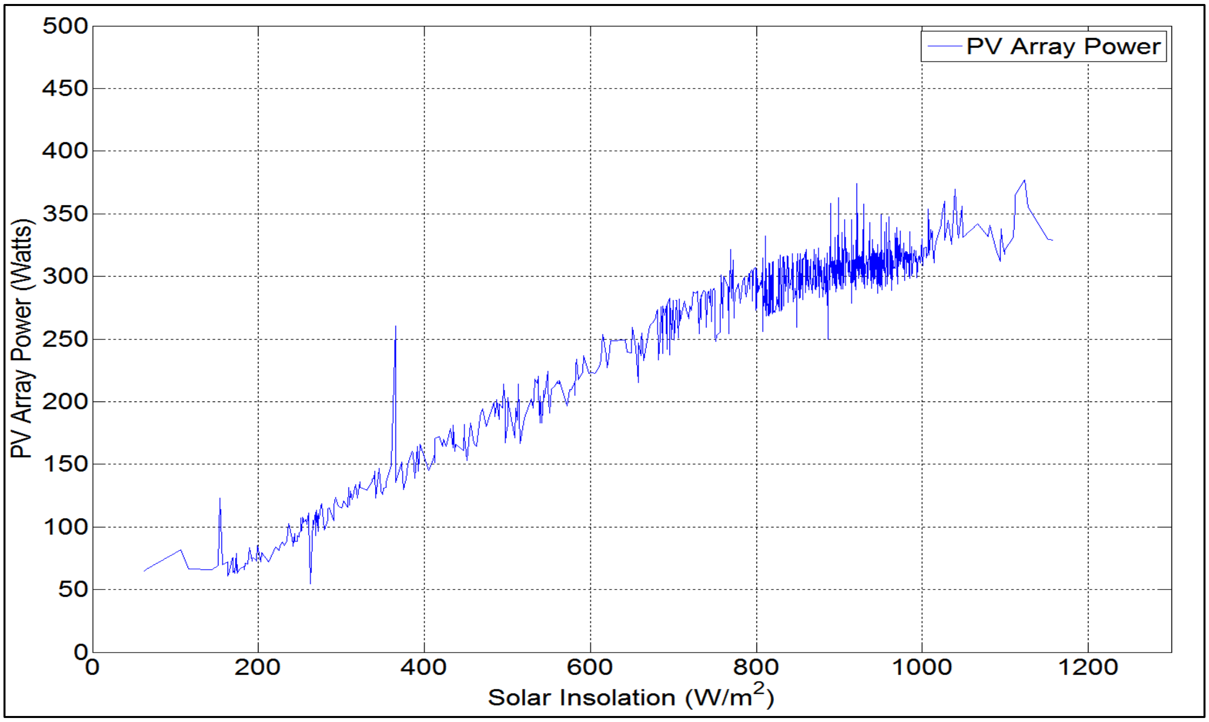

Figure 4.50: PV array power as a function of solar insolation averaged over a period of one minute with azimuthal orientation fixed due south and inclination fixed at 40°.

As previously shown, there is an approximate linear relationship of the PV array power with solar insolation. In comparing the PV output power in Figure 4.50 to that in Figure 4.12 for the PV array with solar tracking at an inclination angle of 40° it is seen that the fix orientation produces a little less power. The spikes seen in Figure 4.49 are due to the electrical behavior of the MPPT–charge controller, which is using some capacitors to store and release power at some instances while, it also shuts the power off at some other instants, even at higher solar insolation. This data was recorded every second, that is how our data acquisition system has been able to track these spikes. However, after averaging this data over a period of one minute the spikes are gone as shown in Figure 4.50.

4.3.4. Temperatures

Temperature and insolation recorded for the PV array at fixed orientation due south at 40° inclination are shown in Figures 4.51 through 4.53. Just like the PV array temperature increases with increasing solar insolation for the cases with solar tracking the temperature also increases with solar insolation for the fixed orientation. Since the solar insolation behaves differently at fixed orientation, the temperature also behaves in a different way.

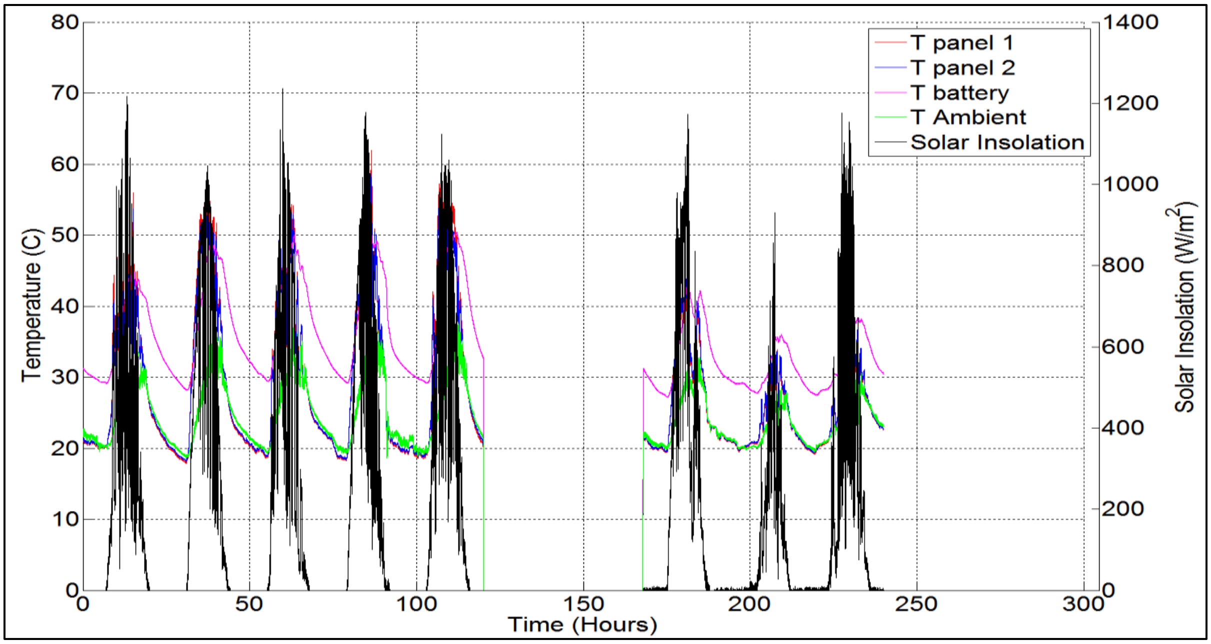

Figure 4.51: Temperature and solar insolation versus time for PV array with azimuthal orientation fixed due south and inclination fixed at 40°for ten days of operation from August 23 to September 1st, 2014.

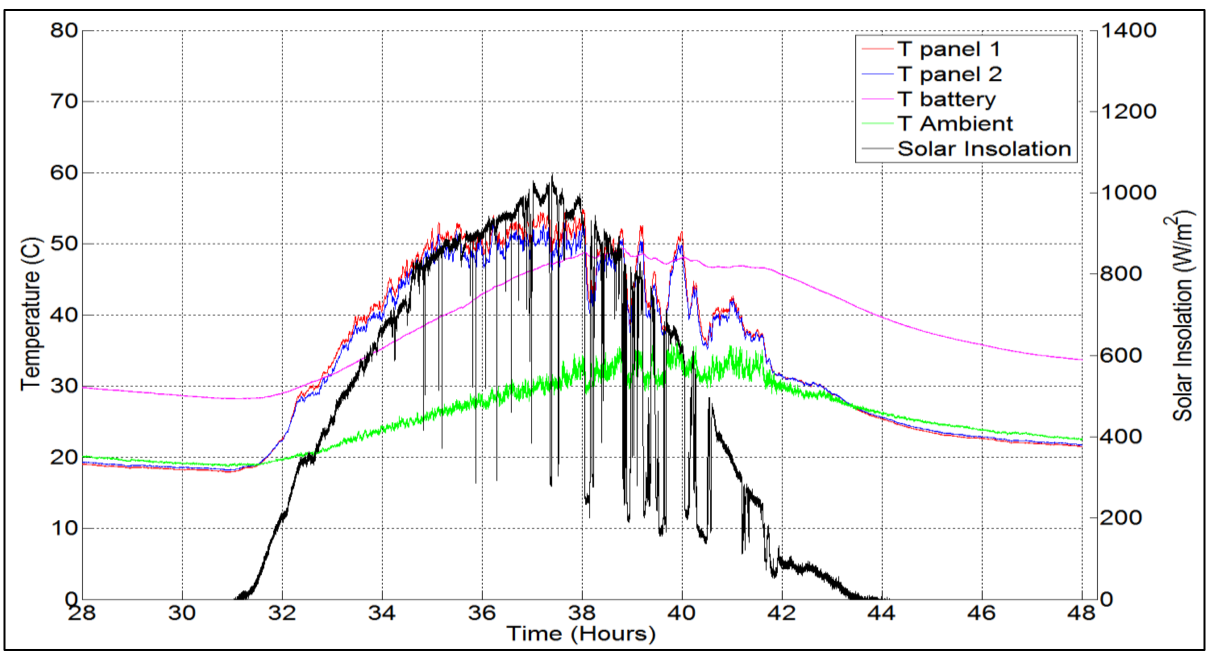

Figure 4.52: Temperature and solar insolation versus time for PV array with azimuthal orientation fixed due south and inclination fixed at 40° for the hours of operation from 28 to 48 on August 24, 2014.

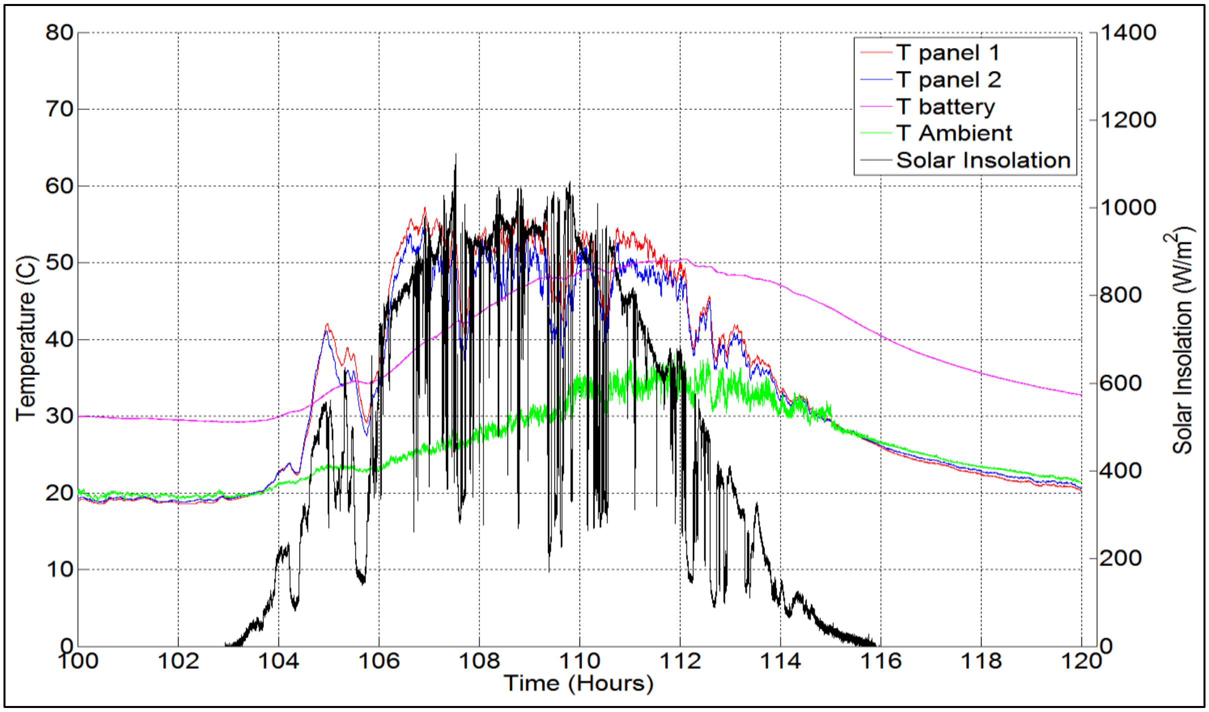

Figure 4.53: Temperature and solar insolation versus time for PV array with azimuthal orientation fixed due south and inclination fixed at 40°for the hours of operation from 100 to 120 on August 27, 2014.

The temperature of the PV array with sun tracking stays at a maximum level for several hours as the PV array is constantly tracking and facing towards the sun for many hours. At a fixed orientation the solar insolation increases up to a vertex point, maintaining it for a short while and then quickly starts to decrease. Therefore, the PV array reaches a maximum temperature at maximum solar insolation for short period of time. And, at the same time as the sun's position is moving away from the PV panels, the PV array does not generate as much energy as in the case of the PV array with sun tracking.

4.3.5. PV Array Energy Generation

As expected the PV array collects less solar energy in a fixed orientation and as a result, it generates less energy as shown in Figure 4.54. It has been observed that the PV irrigation system with sun tracking on a good sunny day receives approximately 25 kW-h (see Figures 4.22 and 4.40); for a fixed orientation, the solar energy incident on the PV array did not exceed more than 21 kW-h during the week. This is approximately 5 kW-h of less energy collected by the PV array with solar tracking and inclination angle of 40°. Thus, it can be concluded that employing solar a tracker in a PV irrigation system would increase energy collection by about 25%. Maximum energy incident on PV array was 20.63 kW-h on 2nd day of the week and on this day the PV array generated 1.23 kW-h. This is not the maximum energy generation during this week. Because the pump did not run for the optimum time; as the batteries got fully charged, preventing the PV array from converting more of the solar energy into electrical energy. The highest energy generation by fixed PV array was on the 5th day; on this day PV array generated 1.36 kW-h from 19.93 kW-h of solar energy incident on the PV array. As mentioned earlier that data was not collected on 6th and 7th day as LabVIEW ceased to collect data. Therefore, PV energy production and solar radiation incident on PV array show zero outputs on 6th and 7th day. This does not mean that there was no solar energy collected by PV array on these two days. This is simply because data could not be acquired and MATLAB cannot manipulate any results on these days. Whereas, as on 9th day during this time period, solar energy was the lowest as it rained and weather was cloudy most of the day. Due to this reason pump was not switched on at all; pump and resistors have not consumed any power from the battery bank.

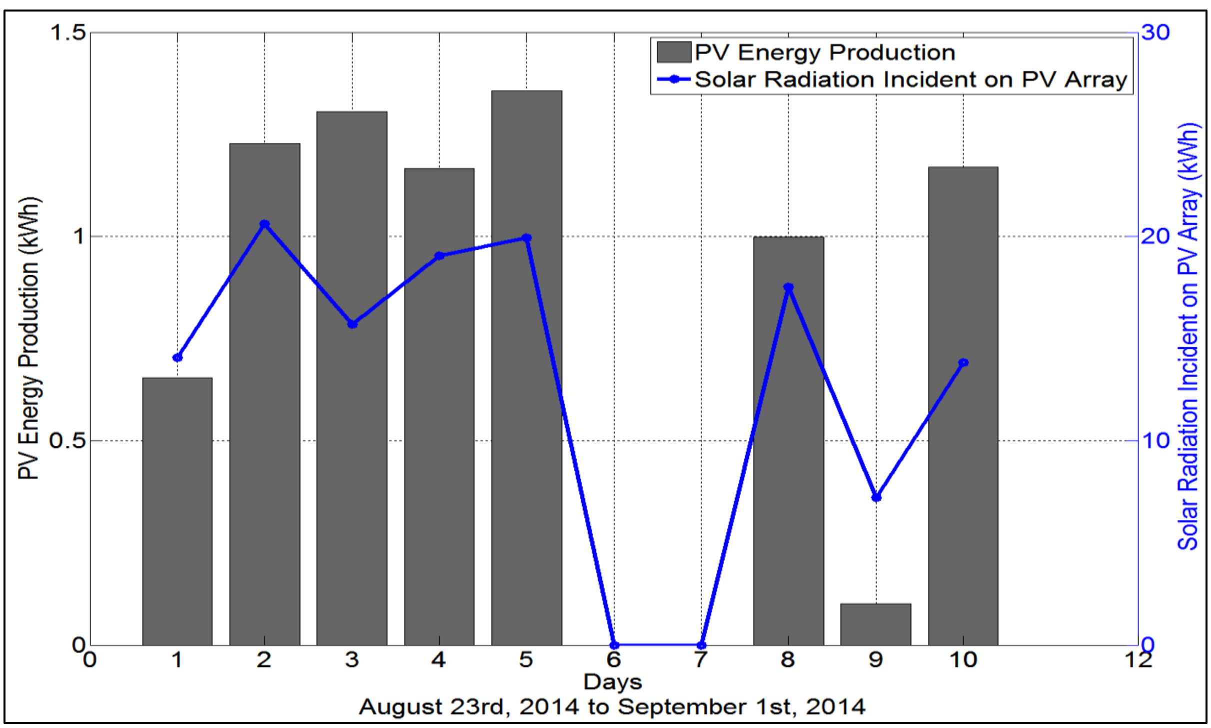

Figure 4.54: PV energy production for PV array with azimuthal orientation fixed due south and inclination fixed at 40° for ten days of operation from August 23 to September 1st, 2014.

4.4. Azimuthal Solar Tracking at an Inclination Angle of 40° with Continuous Running of the Water Pump and no Power Dissipating Resistors

Since the original goal for this solar system was to perform irrigation, it was desired to test the system with only the pump and no power dissipating resistors. The pump was allowed to run 24 hours a day for this entire test to show that the panels were sized large enough to run this pump continuously, as long as the solar insolation is reasonable. Another benefit to running this configuration is that behavior of the system under a continuous, lower magnitude load can be seen. During this test, the pump is run continuously for a week from August 16, 2014 to August 22, 2014. The PV array has an inclination angle of 40° and the azimuthal angle of the sun is tracked from east to west during the day. The weather was relatively bad for this week as it rained a few days and the sky was mostly cloudy. Bad weather conditions mean lower solar energy collection and lower energy production by the PV array. Despite low energy production and running the pump continuously for a whole week, the batteries did not drain to 30% level and the pump did not stop at any point during the operation. Of course this is because the pump only draws 50 watts of power from the batteries. It has been earlier determined that fully charged batteries can deliver continuous power to the pump for 58.8 hours. Thus, if the weather is bad for two consecutive days and the PV array does not produce energy at all, the batteries would still be able run this pump for more than two days. This was exactly the design criterion while designing this project in 2011.

4.4.1. Voltages

In this test, when the pump is running continuously, the battery voltage drops to 25 volts during the night time (see Figure 4.55) as the pump is drawing out power. As the PV array starts generating power the next day; the batteries get charged while increasing the battery voltage to 26 or more volts depending on the solar insolation at that point during the day. It can be seen that when the solar insolation is very low and it does not exceed more than 700 watts/m^2 (see Figure 4.56) at any point during the day, the array voltage stays below 30 volts. This occurs because there is insufficient solar insolation available for the PV array to produce enough energy to charge the batteries fully and increase the battery voltage to its maximum point of 27 volts. On a day when better solar insolation is available (see Figure 4.57); the maximum voltage that the batteries can handle is attained during the 105th hour, at this point the MPPT-charge controller changes the MPPT stage to absorption stage where the array voltage is increased, while the array current is tapered down to zero. That is why, after the batteries have reached their maximum voltage; the array voltage exceeds 30 volts, which is not similar in the case shown in Figure 4.56. This could be better comprehended by looking at current outputs for this same day in the next section in Figure 4.60. As it is clearly showing that after batteries have attained maximum voltage, current is gradually reducing down until it reaches a point where no current is being delivered by the PV array. This means that batteries have been fully charged and the MPPT–charge controller is in float stage.

Moreover, spikes or fluctuations in voltage outputs observed during the 98th and 100th hours, which are at night, are due to lightening as shown in Figure 4.57. These lightning flashes are not registered by the pyranometer. As it can be seen that array voltage reaches 16 volts at some instances as a result of electromagnetic energy from lightening flashing across the sky. There is no current being produced during this lightening event because the voltage produced is not sufficient to drive current into the batteries.

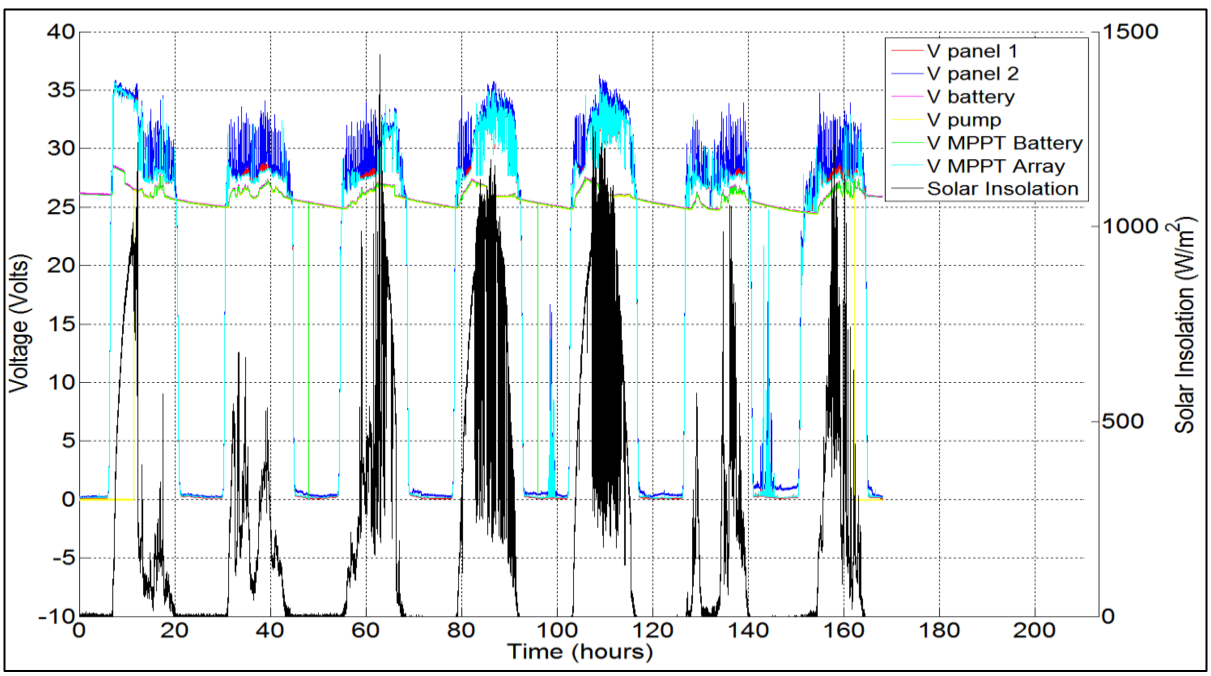

Figure 4.55: Voltage and solar insolation versus time with continuous pumping with no power dissipating resistors for PV array inclination at 40° and sun tracking and sun tracking for seven days of operation from August to August 22, 2014.

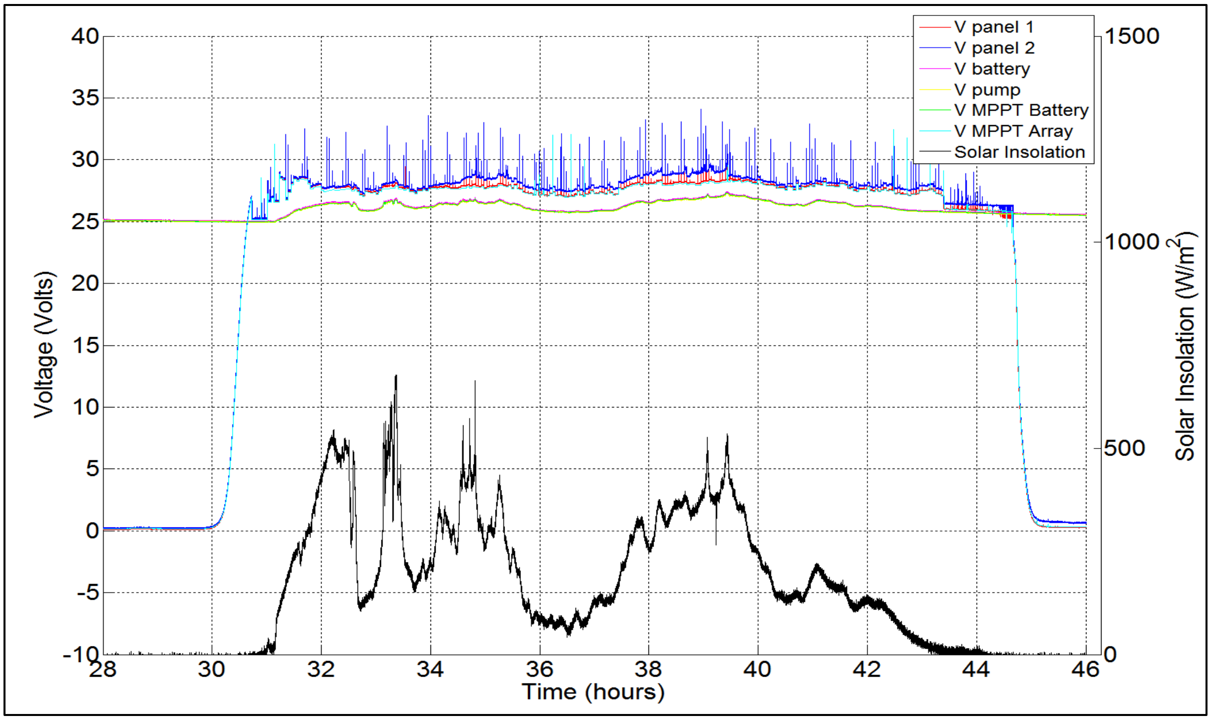

Figure 4.56: Voltage and solar insolation versus time for continuous pumping and PV array inclination at 40° and sun tracking through 28 to 46 hours of operation on August 17th, 2014.

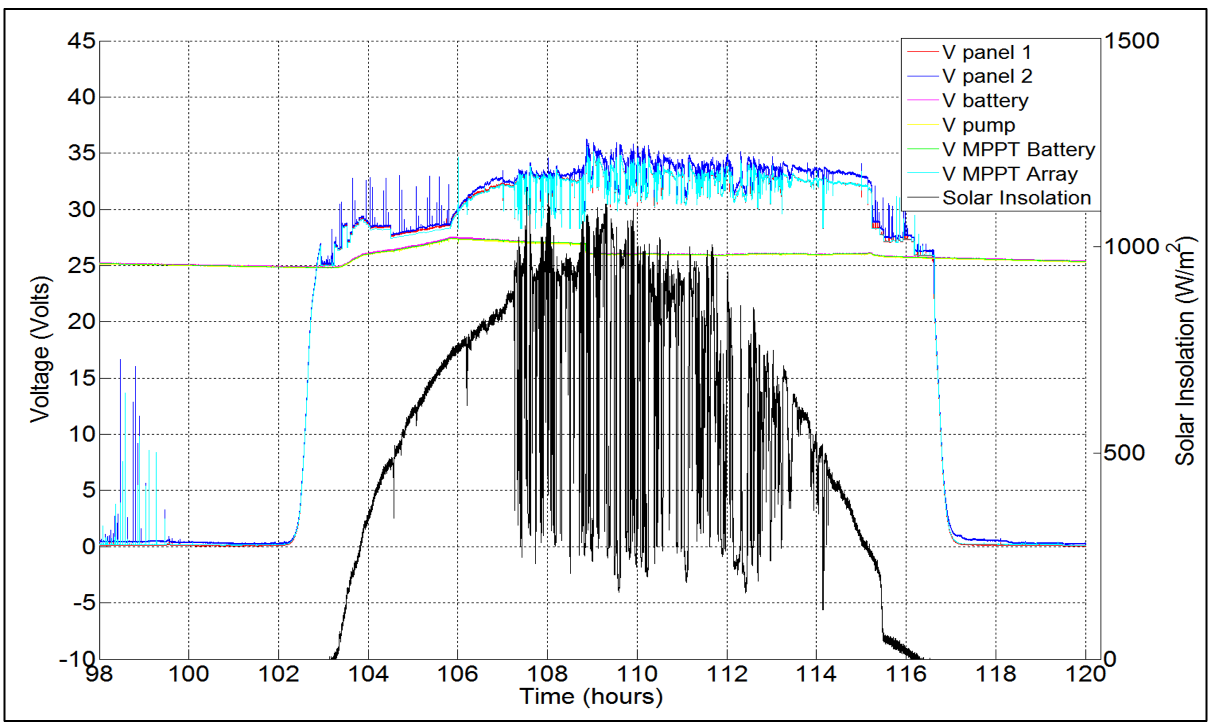

Figure 4.57: Voltage and solar insolation versus time for continuous pumping and PV array inclination at 40° and sun tracking through 98 to 120 hours of operation on August 20th, 2014.

4.4.2. Currents

The pump used in this PV irrigation system draws 1.8 amps from the batteries. In the other configurations studied, when the resistors were also connected to batteries, the total current draw was 14.5 amps. As shown in Figures 4.58 through 4.60 the pump is continuously drawing 1.8 to 2 amps. Since the solar insolation was low most of the days in this week, the maximum current produced by the PV array did not exceed 13 amps. Another reason the maximum current draw is low is the lower load demand produced by just the pump.

4.4.4. Powers

The power flows as a function of time of the PV panels and pump are shown in Figures 4.61 through 4.63. As discussed earlier, in this arrangement the power load on the batteries is low and the batteries are only supplying 50 watts of power to the pump. For the other three configurations the pump and the power dissipating resistors drew 360 watts from the batteries. The other unusual aspect of for the test of this configuration is the solar insulation was low most of the week. As the solar insolation mostly remained lower than 500 watts/m^2, the PV array generally generated less than 200 watts (see Figure 4.62). However, on a higher solar insolation day (see Figure 4.63), the PV array power generation increases with increasing solar insolation during the early hours of the day and the power generation of the PV array continues to increase until the voltage level of batteries reaches its absorption voltage, which is 27 volts. So at this point, the MPPT-charge controller gradually reduces the power generation from the PV array. Once, the batteries get fully charged at the 109th hour, the MPPT-charge controller completely shuts the power supply off from the PV array.

4.4.3. Temperatures

Temperature outputs recorded for this reduced load configuration with sun tracking at 40° inclination and continuous running pump indicate similar behavior as recorded in the other three configurations shown in this thesis. The difference would be that less solar insolation is absorbed in this configuration and thus the panel temperatures are not quite as high on a number of days during the week.

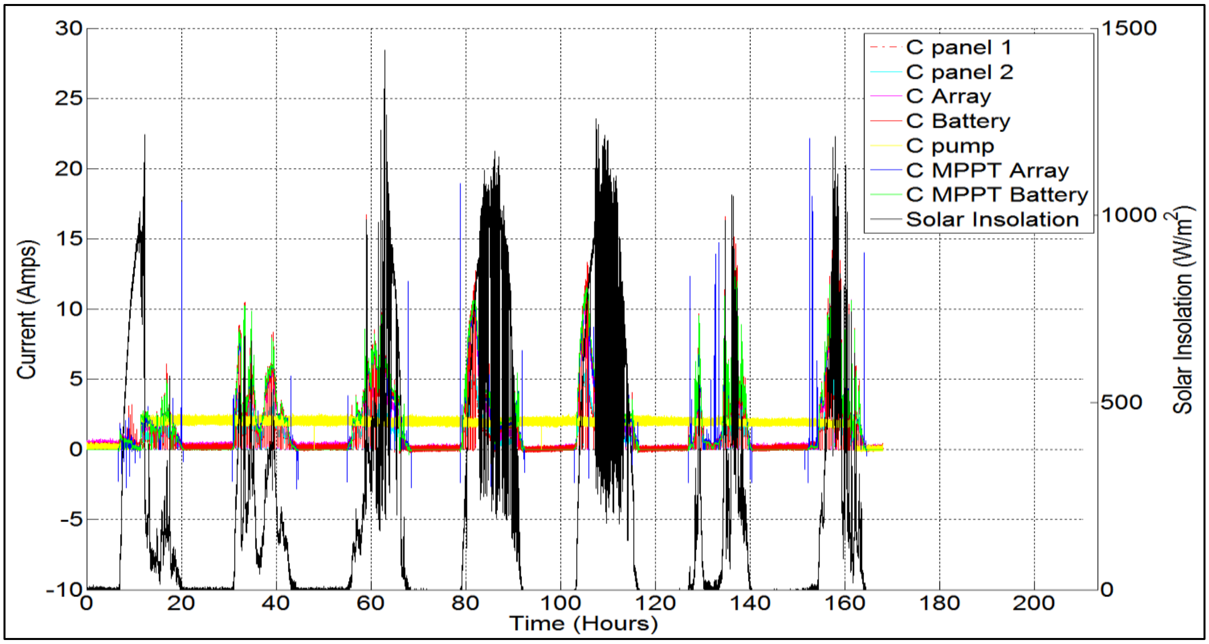

Figure 4.58: Current and solar insolation versus time for continuous pumping and PV array inclination at 40° and sun tracking for seven days of operation from August 16th, to August 22nd, 2014.

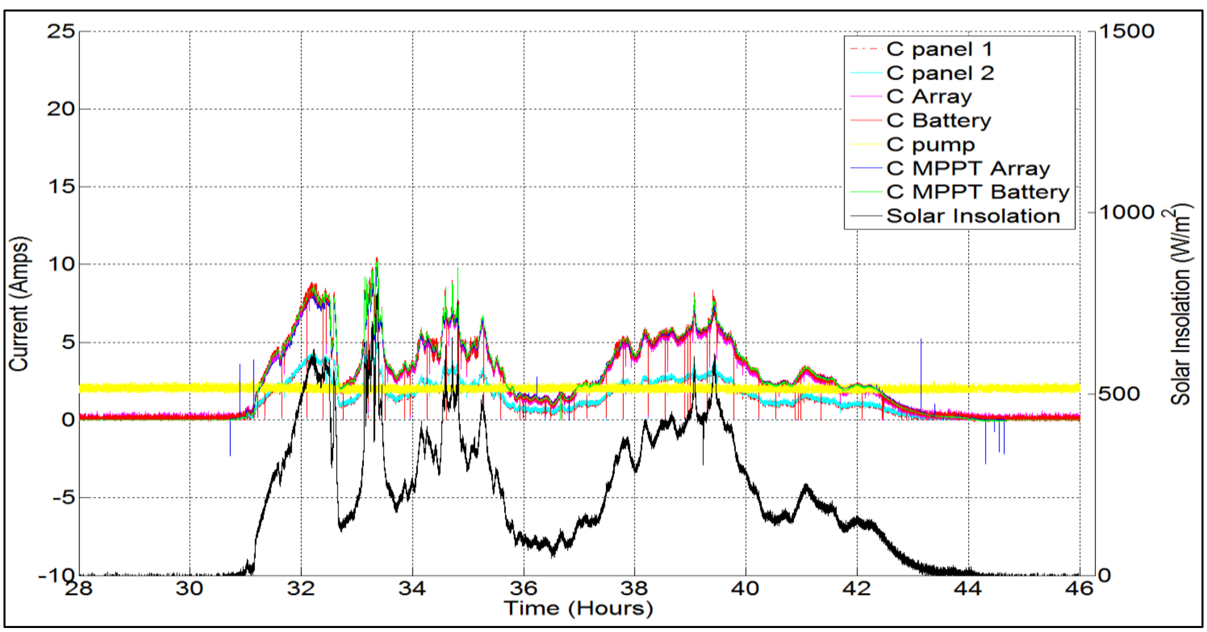

Figure 4.59: Current and solar insolation versus time for continuous pumping and PV array inclination at 40° and sun tracking through 28 to 46 hours of operation on August 17th, 2014.

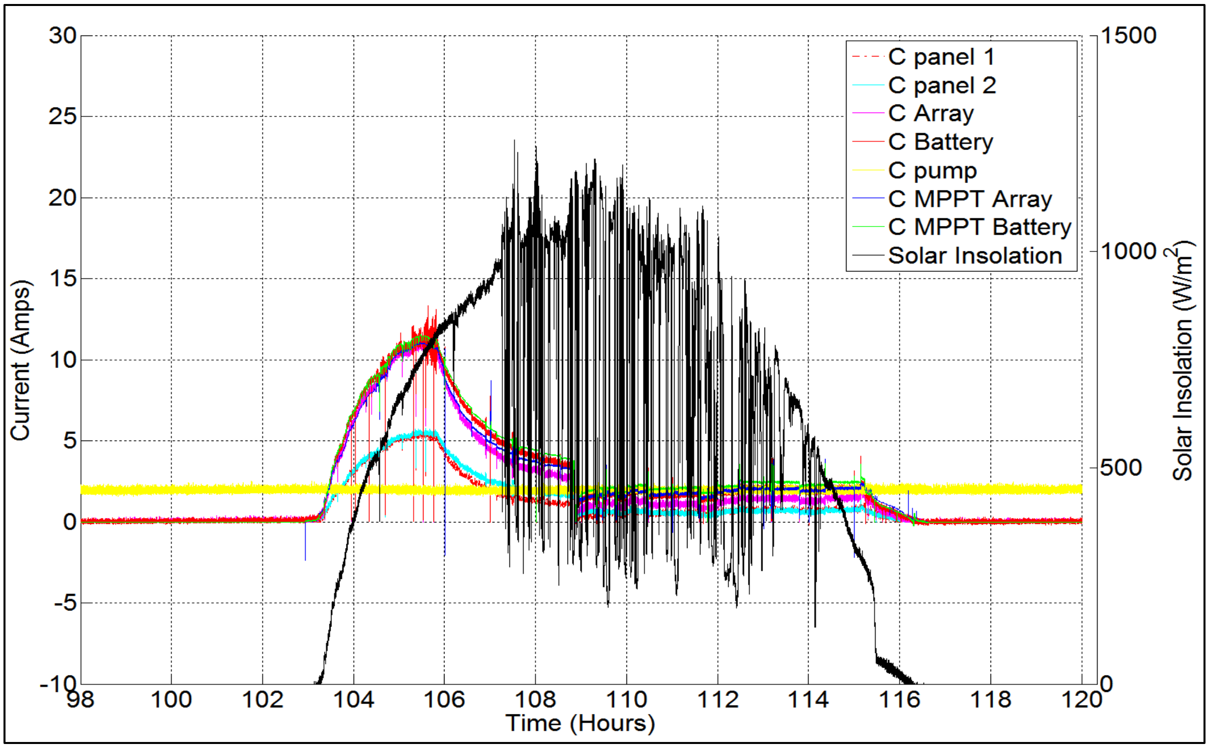

Figure 4.60: Current and solar insolation versus time for continuous pumping and PV array inclination at 40° and sun tracking through 98 to 120 hours of operation on August 20th, 2014.

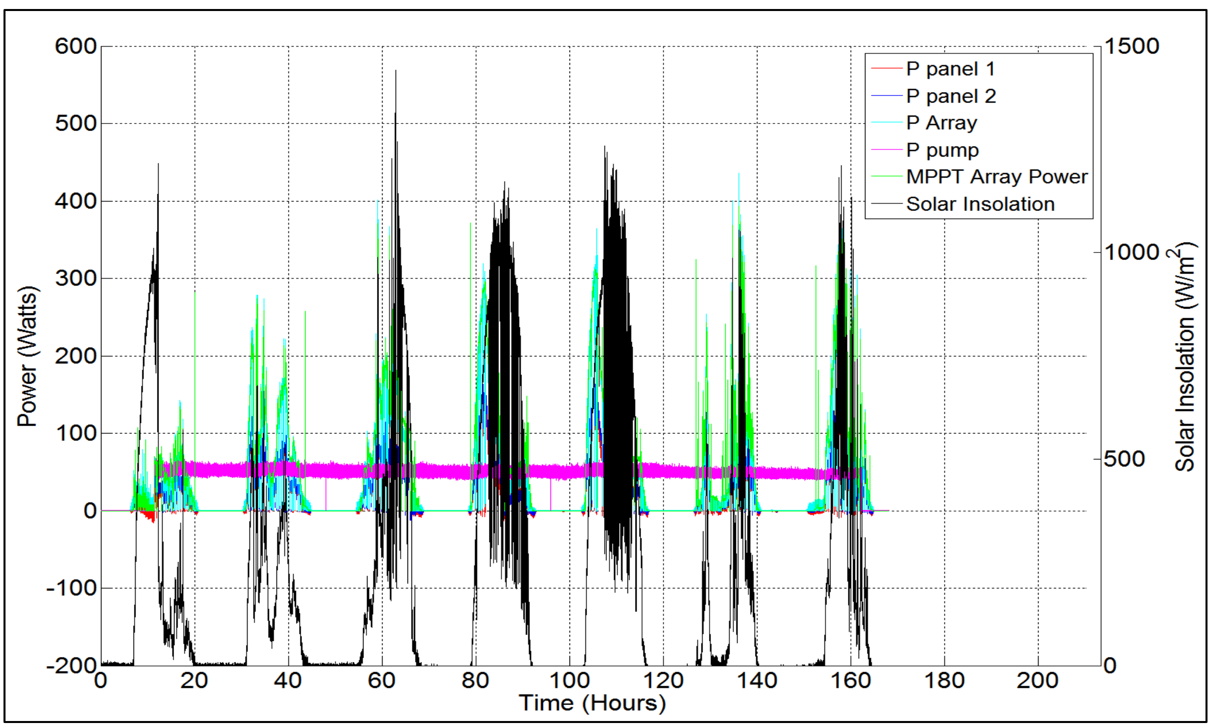

Figure 4.61: Power and solar insolation versus time for PV array inclination at 40° and sun tracking for seven days of operation from August 16^{h}, to August 22nd, 2014.

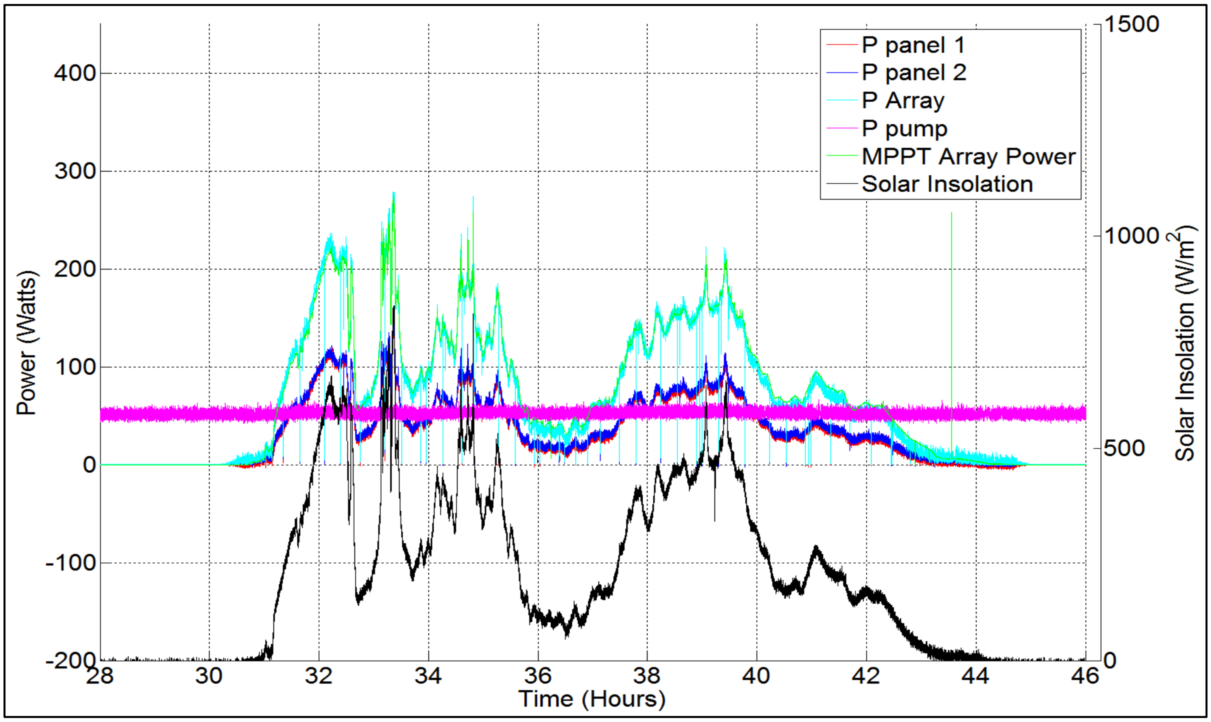

Figure 4.62: Power and solar insolation versus time for PV array inclination at 40° and sun tracking through 28 to 46 hours of operation on August 17th, 2014.

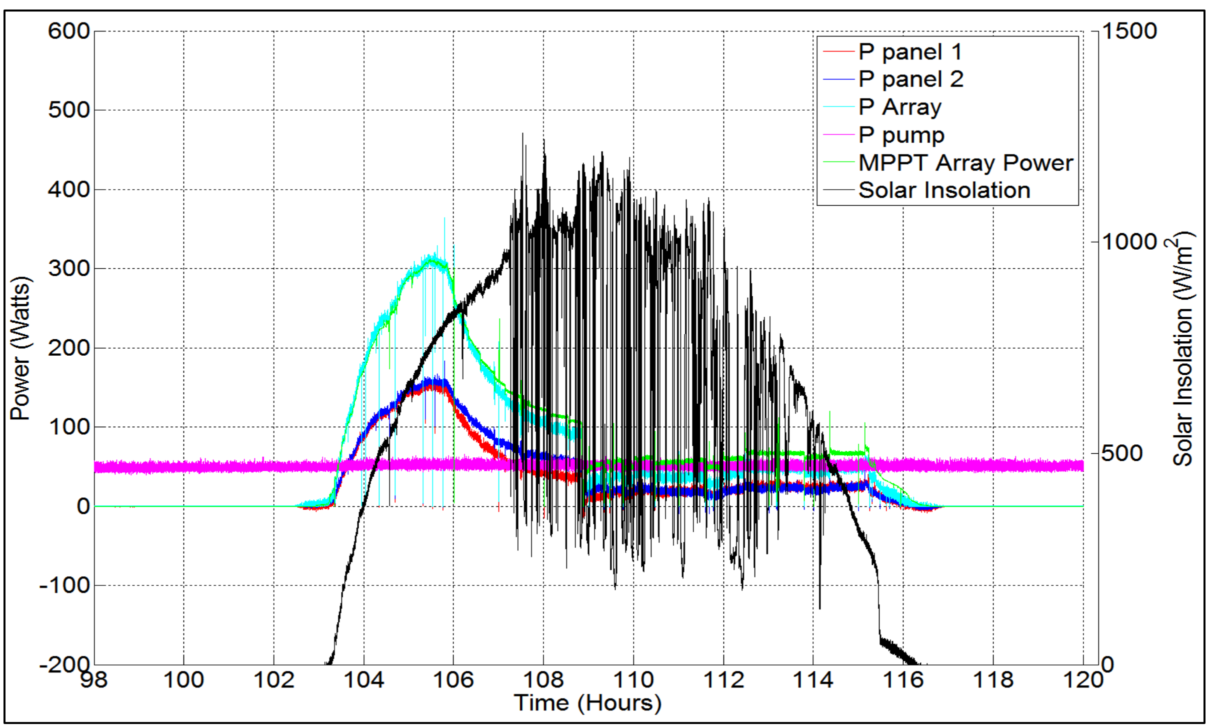

Figure 4.63: Power and solar insolation versus time for PV array inclination at 40° and sun tracking through 28 to 46 hours of operation on August 17th, 2014.

4.4.3. PV Array Energy Production

To assess the performance of the PV irrigation system at this reduced load condition, the energy generated by the PV array is shown in Figure 4.67. To aid in understanding the results in Figure 4.67 the solar insolation values throughout the week are given in Figure 4.68. Evidently, by comparison of these two figures, it can be perceived that higher solar insolation leads to higher energy collection and more energy generation by the PV array. On the first day of this week, the energy generated by the PV array is lowest because the pump was switched on just a little before mid-noon. As the batteries were fully charged, the MPPT-charge controller did not allow the PV array to generate power from early morning until mid-noon. This is why the system generated its lowest energy of 0.462 kW-h. The total solar energy incident on the PV array on this day was 15 kW-h. Interestingly, on the 2nd day of this week, the PV array generated higher amounts of energy, 1.22 kW-h, despite having significantly lower total solar energy incident on the PV array, 9.348 kW-h. This is due to the pump running continuously during the previous night and by the next morning the batteries were discharged less than 50 %. Consequently, the MPPT-charge controller sensed lower charge and voltage level of the batteries; therefore, allowing the PV array to generate as more energy to charge the batteries. It has been observed that for reduced load situations, the PV array generates little over than 1 kW-h of energy on daily basis. Of course this cannot happen in situations where the solar energy is very low, as seen on 6th day. Thus it can be concluded that at reduced load, the PV array generates close to 1 kW-h of energy on daily basis, regardless of whether total solar energy incident on the PV array is high or low. This means the PV irrigation system does not utilize all the solar energy available to it during the day and part of solar energy available is just being wasted. At higher load demands the PV array generated 2.13 kW-h of energy at 24.57 kW-h of solar energy incident on the PV array as shown in Figure 4.22.

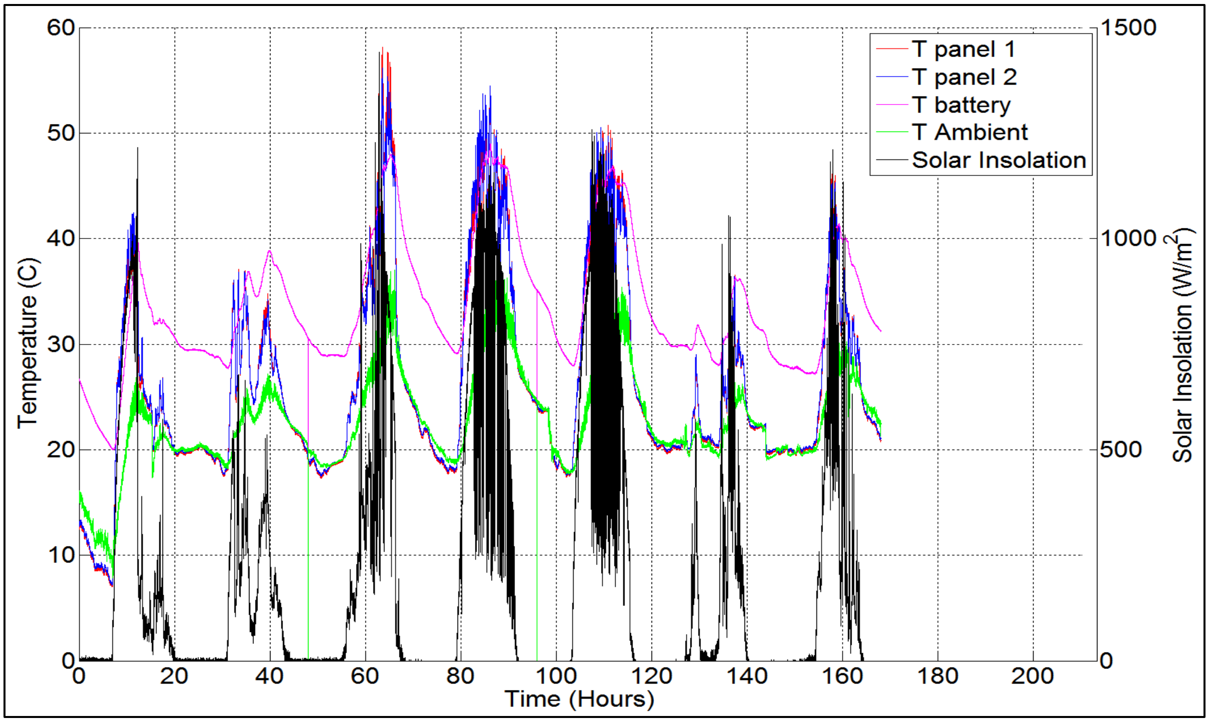

Figure 4.64: Temperature and solar insolation versus time for continuous pumping and PV array inclination at 40° and sun tracking for seven days of operation from August 16^{h}, to August 22nd, 2014.

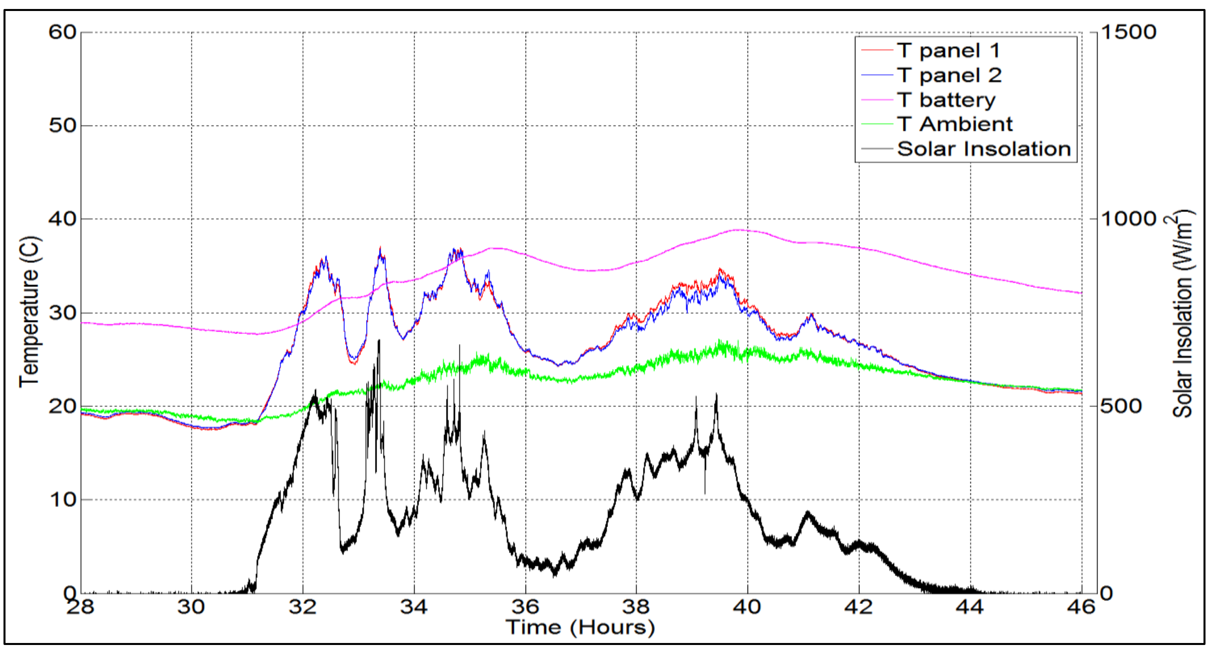

Figure 4.65: Temperature and solar insolation versus time for continuous pumping and PV array inclination at 40° with sun tracking through 28 to 46 hours of operation on August 17th, 2014.

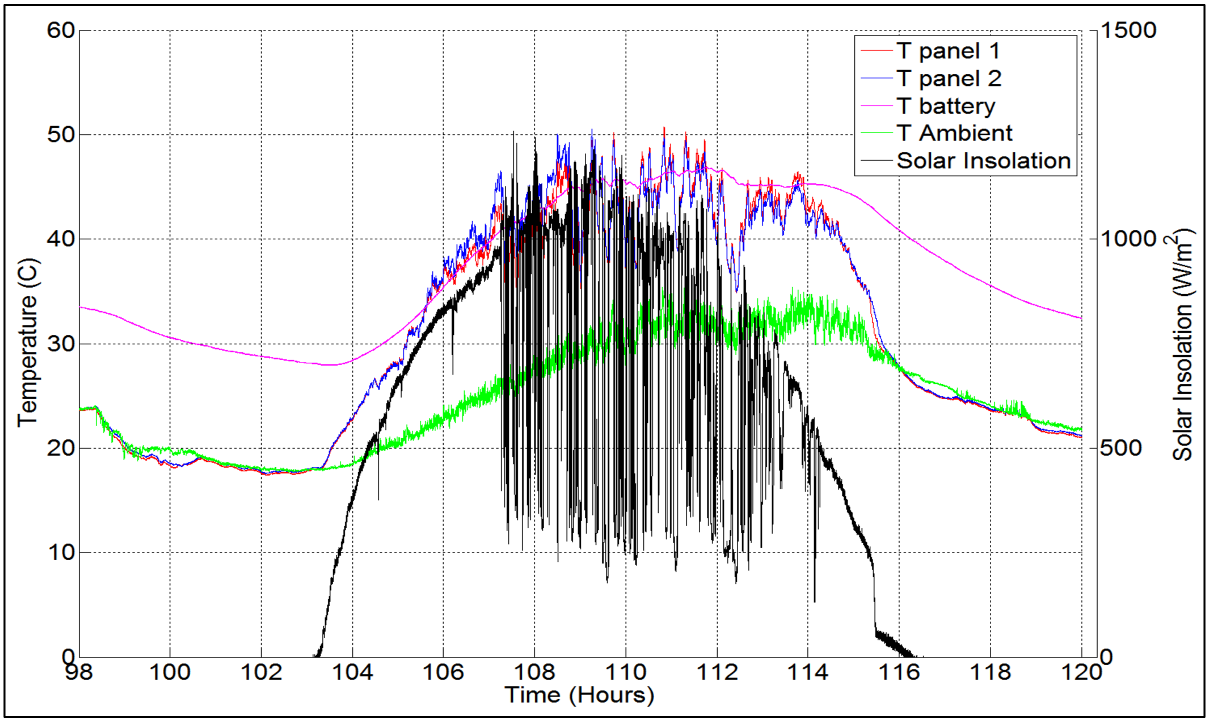

Figure 4.66: Temperature and solar insolation versus time for continuous pumping and PV array inclination at 40° and sun tracking through 98 to 120 hours of operation on August 17th, 2014.

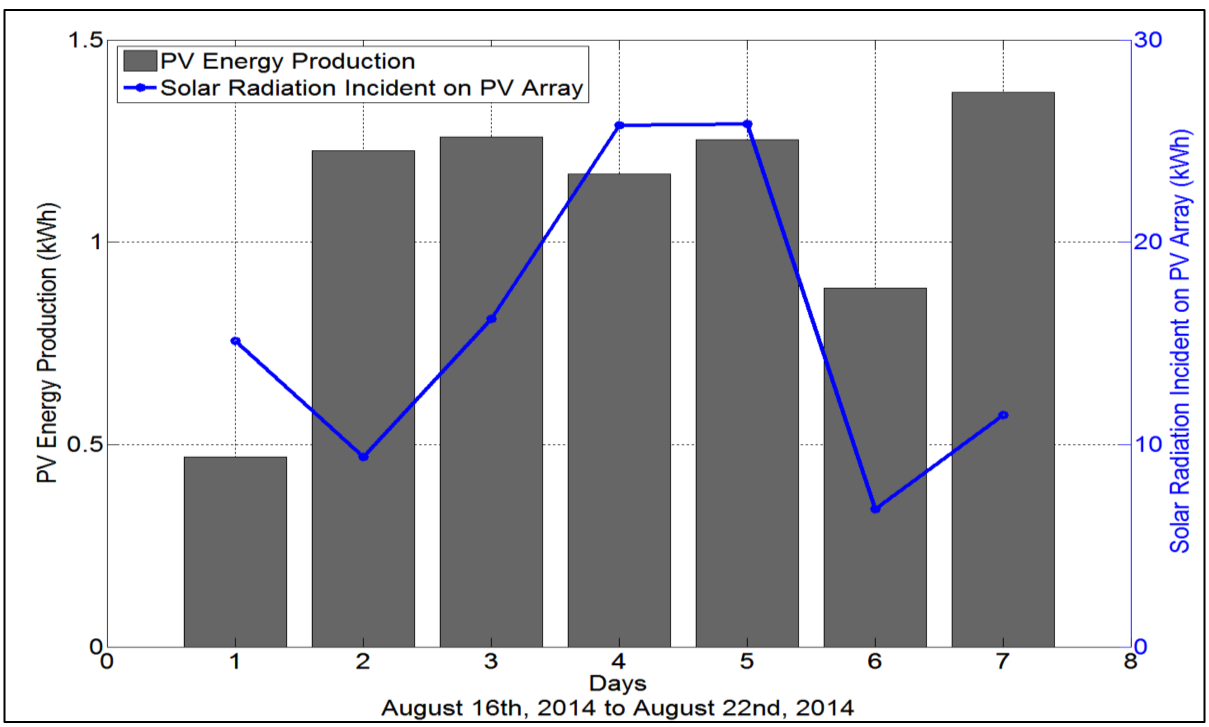

Figure 4.67: PV energy production for continuous running pump for PV array inclination at 40° and sun tracking for seven days of operation from August 16th, to August 22nd, 2014.

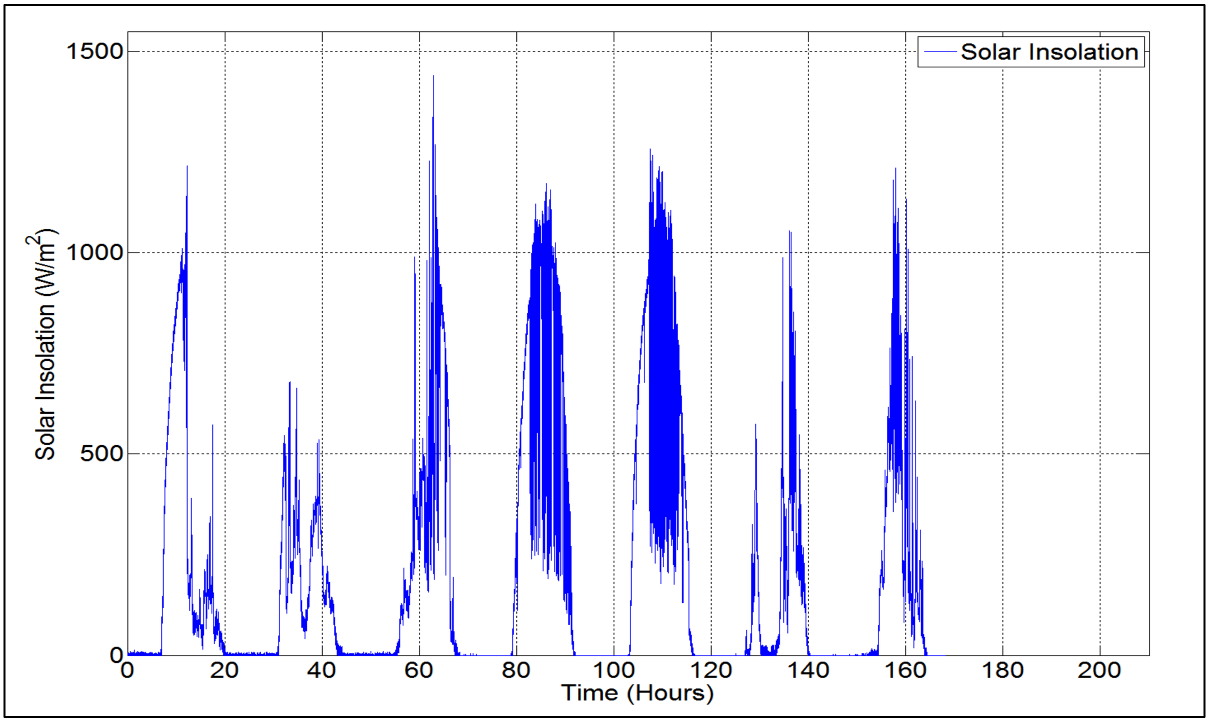

Figure 4.68: Solar insolation versus time for PV array inclination at 40° and sun tracking for seven days of operation from August 16th, to August 22nd, 2014.

The PV irrigation system was operated under four different conditions such as PV array with sun tracking inclined at 40° and 30°, fixed orientation facing due south inclined at 40°, and a reduced load condition with sun tracking at 40° inclination. As observed during these tests the PV array with sun tracking generates 25% more energy than PV array at fixed orientation. Moreover, the PV array oriented at 30° with sun tracking collected 3 to 4 kW-h more energy than at 40°. While at a reduced load condition, the PV array did not generate more than 1.3 kW-h of energy, even though when there was a high solar energy incident on the PV array. From these observations, it can be stated that PV irrigation system performs best at 30° inclination with sun tracking. However, it needs to be realized that a 30° inclination angle is just for summer and in order for PV array to generate optimum energy throughout the year the 40° inclination that matches the latitude coordinate of Dayton, OH should be implemented.

Chapter 5

Conclusions

This thesis presents the research work carried out on a PV (photovoltaic) irrigation system. This work involved integrating three previously developed solar systems developed as part of the Wright State Senior Design course. The three senior design projects were:

1. design and build a solar powered irrigation system,
2. design and build a DAQ (data acquisition system) for the solar powered irrigation system, and
3. design and build a solar translator.

In this thesis each of these three parts are referred to as a subsystem. Because the DAQ subsystem did not work correctly, getting this subsystem to work properly was the first step in this thesis work. As part of this step a new LabVIEW data acquisition program was written to take data automatically, quickly and accurately for long periods of time. This program implemented a graphical user interface format to make the program easy to use. After getting the DAQ subsystem working correctly, the solar powered irrigation subsystem, the DAQ subsystem, and the solar translator subsystem were integrated into one system that is referred to as the PV irrigation system. A maximum power point tracker MPPT–charge controller was added to the solar powered irrigation subsystem and connected inline between the PV modules and the battery bank. Power dissipating resisters were added in parallel to the water pump so that higher loads could be placed on the system. This system was installed on the roof of the Russ Engineering Building, which is located on the Wright State University campus in Dayton, Ohio. Voltages, currents, and temperatures were each measured at four different locations on the system. Solar insolation levels on the PV panels were measured with a pyranometer and water flow rates through the pump were measured with a flow rate sensor. Measurements on the system performance were collected every second, 24 hours a day, for periods of about a week over the time period from July 28 to September 1st, 2014.

The end goal of this research was to acquire data on this PV irrigation system and evaluate its performance for different operating configurations. Four different operating configurations were studied:

1. azimuthal solar tracking at an inclination angle of 40° with both the water pump and power dissipating resistors being used to consume the power generated by the PV array,
2. azimuthal solar tracking at an inclination angle of 30° with both the water pump and power dissipating resistors being used to consume the power generated by the PV array,
3. a fixed solar array pointing due south at an inclination angle of 40° with both the water pump and power dissipating resistors being used to consume the power generated by the PV array, and
4. azimuthal solar tracking at an inclination angle of 40° with only the water pump being used to consume the power generated by the PV array, where the water pump is run 24 hours a day.

The first configuration listed above tilts the PV array at the latitude coordinate of its location. This is the inclination angle that is supposed to capture the most solar energy over the course of a year. The latitude coordinate of Dayton, OH is 39.75 and thus the panels were tilted at 40°. Data was collected on this configuration of the PV irrigation system for more than a week. Results obtained during this test suggest that the PV array, which measures 3.25 m^{-2}, can intercept more than 26 kW-h of energy on a summer day in Dayton, Ohio. With this amount of solar energy impinging on the PV panels, the PV array can generate more than 2 kW-h of energy.

Since the sun's position is higher in the sky in summer the inclination angle of the PV panels reduced to 30° in an attempt to collect more solar energy. Thus, the PV array was given an inclination angle of 30° with sun tracking enabled. Measurements were made for a week and, as expected, the PV array intercepted slightly more solar energy, 29.18 kW-h on a sunny day. As a result the PV array generated a little more electrical energy, 2.72 kW-h. This was the highest recorded energy generated during the whole data collection period. These results support the conventional knowledge that inclination angles smaller than the latitude of where the panels are located will collect more solar energy and thus produce more electrical energy.

It was also desired to determine the performance of PV array irrigation in a fixed orientation. Therefore, PV array was fixed oriented at an inclination angle of 40°, pointed due south, and data was collected for one week. Results obtained at this condition were clearly different than those obtained with azimuthal solar tracking. Solar energy intercepted by the PV array and the energy generated were lower than the sun tracking operating configuration. It was observed that at fixed position of the PV array, the maximum solar energy intercepted was a little higher than 20 kW-h. This is lower than the energy collected by the PV array with azimuthal solar tracking. The maximum electrical energy generated by the fixed PV array was 1.36 kW-h.

Lastly, it was desired to test the performance of the PV irrigation system under reduced load conditions. In order to do this, the power-dissipating resistors initially connected to the batteries, in parallel with the water pump, used in the first three operating configurations were removed. Thus, the load on a battery bank was reduced substantially to a 50 watt pump. This test was performed with the pump operating continuously, 24 hours a day, for the whole week. This test showed that there is more than adequate PV array capacity and battery capacity to run this small pump for one week, even if it is a cloudy week. In essence the PV array and battery bank is oversized for the pump used in the system. This was consciously done in the original design, because extra power was to be available for running power tools and other electrical equipment. There is sufficient energy storage in the battery bank, two batteries that supply 100 amps-hour of energy at 24 volts to power the 50-watt pump for more than two days without recharge. During the daytime for this test, when solar insolation is available, the batteries got completely charged. During the night, the power draw from the pump discharged batteries by up to 50 %. Another interesting finding is this operating configuration of the PV irrigation system generated the least amount of energy compared to other three operating conditions. This was due to the low power draw of the pump from batteries. Since the batteries remained fully or almost fully charged for a portion of the day, the MPPT-charge controller limited and power generation from PV array.

In addition to the conclusions drawn above, the results collected as part of this thesis work showed that the efficiency of the PV array was reduced when the PV array attained higher temperatures. Results also demonstrated that temperature of PV array were in a direct relationship with the solar insolation. As the temperature of the PV array increased the efficiency of the PV array was reduced. The dominant factor determining the PV array temperature was the amount of solar insolation impinging on the panels.

References

Al-Smairan, M., “Application of photovoltaic array for pumping water as an alternative to diesel engines in Jordan Badia, Tall Hassan station: Case study”. *Renewable and Sustainable Energy Reviews* (2012), Vol. 16, pp. 4500–4507.

Bloomberg New Energy Finance, United States. *PV Market Outlook 1977 – 2013* (2013)

Brian, D and Clark, R., “Determining the Optimum Solar Water Pumping System for Domestic Use, Livestock Watering or Irrigation”. *American Solar Energy Society (ASES) National Solar Conference* (2009). May 11-16, 2009.

Burney, J., Woltering, L., Burke, M., Naylor, R., and Pasternak, D., “Solar-Powered drip Irrigation Enhances Food Security in in the Sudano-Sahel”. *Proceedings of the National Academy of Sciences of United States of America* (2010) Vol. 107. No. 5.

Cuadros, F., Lopez, F., Marcos, F. and Coello, J. “A procedure to size solar-powered irrigation (photoirrigation) schemes”. *Journal of Solar Energy* (2004), Vol. 76, pp. 465–473.

Dahl, S. and Chorkendorff, I., “Solar-fuel generation: Towards practical implementation”. *Nature Materials*. (2012) Vol. 11, 100–101. doi:10.1038/nmat3233

Energy Information Administration, United States. World Energy Outlook (2013)

Hamidat, A. and Benyoucef, F., “Systematic procedures for sizing photovoltaic pumping system, using water tank storage”. *Energy Policy* (2009), Vol. 37, pp. 1489-1501.

Hamidat, A., Benyousef, B. and Hartani, T., “Small-scale irrigation with photovoltaic water pumping system in Sahara regions”. *Journal of Renewable Energy* (2008), Vol. 28, pp. 1081–1096.

Hull. B, Papie, J, Ashcraft, S. and Blommel, N., *Clean Renewable Irrigation System*, Senior Design Project Report, Department of Mechanical and Materials Engineering, Wright State University, Dayton Ohio. (2011).

International Energy Agency, France. *World Energy Outlook* (2013)

Kelley, L., Gilbertson, E., Sheikh, A., Eppinger, S. and Dubowsk, S., “On the feasibility of solar-powered irrigation”. *Renewable and Sustainable Energy Reviews* (2010) Vol. 14, No. 9, 2669-2682.

Kolhe, M., Kolhe, S. and Joshi, J., “Economic viability of stand-alone solar photovoltaic system in comparison with diesel-powered system for India”. *Journal of Energy Economics* (2002), Vol. 24, pp. 155-165.

Mahmoud, E. and Nather, S., “Renewable energy and sustainable developments in Egypt: photovoltaic water pumping in remote areas”. *Journal of Applied Energy* (2003), Vol. 74, pp.141–147.

Meah. K., Fletcher, S. and Ula, S., “Solar photovoltaic water pumping for remote locations”. *Renewable and Sustainable Energy Reviews* (2008), Vol. 12, pp. 472–487.

Mokeddem, A., Mioun, A., Kadri, D., Hiadsi, S. and Raja, I., “Performance of a directly-coupled PV water pumping system”. *Journal of Energy Conservation and Management* (2011), Vol. 52, pp. 3089–3095.

Odeh, I., Yohanis, B. and Norton, B., “Influence of pumping head, insolation and PV array size on PV water pumping system performance”. *Journal of Solar Energy* (2006), Vol. 80, pp. 51–64.

Odeh, I., Youanis, Y. and Norton, B., “Economic Viability of Solar Photovoltaic Water Pumping System”. *Journal of Solar Energy* (2006), Vol. 80, pp. 850–860.

Pande, P., Singh, A., Ansar, S., Vyas, S. and Dave, B., “Design development and testing of a solar PV pump based drip system for orchards”. *Journal of Renewable Energy* (2003), Vol. 28, pp. 385-396.

Purohit, P., “Financial Evaluation of Renewable Energy technologies for irrigation water pumping”. *Energy Policy* (2006), Vol. 35, pp. 3134–3144.

REN21, Renewable Energy Policy Network for 21st Century, France. *Renewables Global Futures Report* (2013)

Rowland, J., French, A., and Chernesky, B., *Solar Irrigation Instrumentation System*, Senior Design Project Report, Department of Mechanical and Materials Engineering, Wright State University, Dayton Ohio. (2012).

Smil, V., “Agricultural Energy Costs: National Analysis”. *Energy in Farm Production*. (1992) Vol. 6, 85-100.

Stickelman, M., Townsend, J. and Wilmoth, S., *PV Panel Orientation Device*, Senior Design Project Report, Department of Mechanical and Materials Engineering, Wright State University, Dayton Ohio. (2013).

US DOE, Department of Energy, United States. *Building a New Energy Future with Wind Power* (2013)

US DOE, Department of Energy, United States. *Revolution Now: The Future Arrives for Four Clean Energy Technologies* (2013)

Vanek, Francis M. and Albright, Louis D., "Energy Systems Engineering: Evaluation and Implementation". McGraw – Hill, (2008).

Wenham, S., Green, M., Mureil, W., Corkish, R. and Sproul, A., "Applied Photovoltaics", 3rd Edition. Earthscan (2011)

World Energy Council, United Kingdom. "World Energy Scenarios: Composing Energy futures to 2050". (2013).

Appendix – A: Equipment Data Sheets

Data Sheet 1: Sharp Electronics, "224 watt Multipurpose Module," ND-224UC1 datasheet, 2008.

SHARP

solar electricity

224 WATT

MULTI-PURPOSE MODULE

NEC 2008 Compliant

ND-224UC1

MULTI-PURPOSE 224 WATT MODULE FROM THE WORLD'S TRUSTED SOURCE FOR SOLAR.

Using breakthrough technology, made possible by nearly 50 years of proprietary research and development, Sharp's ND-224UC1 solar module incorporates an advanced surface texturing process to increase light absorption and improve efficiency. Common applications include commercial and residential grid-tied roof systems as well as ground mounted arrays. Designed to withstand rigorous operating conditions, this module offers high power output per square foot of solar array.

Business leaders install this module in large commercial applications, demonstrating financial astuteness and environmental stewardship.

ENGINEERING EXCELLENCE
High module efficiency for an outstanding balance of size and weight to power and performance.

DURABLE
Tempered glass, EVA lamination and weatherproof backskin provide long-life and enhanced cell performance.

RELIABLE
25-year limited warranty on power output.

HIGH PERFORMANCE
This module uses an advanced surface texturing process to increase light absorption and improve efficiency.

Sharp multi-purpose modules offer industry-leading performance for a variety of applications.

Improved Frame Technology

SHARP: THE NAME TO TRUST
When you choose Sharp, you get more than well-engineered products. You also get Sharp's proven reliability, outstanding customer service and the assurance of our 25-year limited warranty on power output. A global leader in solar electricity, Sharp powers more homes and businesses than any other solar manufacturer worldwide.

BECOME POWERFUL

224 WATT

ND-224UC1

NEC 2008 Compliant
Module output cables now 12 AWG with locking connectors

ELECTRICAL CHARACTERISTICS	
Maximum Power (Pmax)*	224 W
Tolerance of Pmax	+10%/-5%
Type of Cell	Polycrystalline silicon
Cell Configuration	60 in series
Open Circuit Voltage (Voc)	36.6 V
Maximum Power Voltage (Vpm)	29.3 V
Short Circuit Current (Isc)	8.33 A
Maximum Power Current (Ipm)	7.66 A
Module Efficiency (%)	13.74%
Maximum System (DC) Voltage	600 V
Series Fuse Rating	15 A
NOCT	47.5°C
Temperature Coefficient (Pmax)	-0.485%/°C
Temperature Coefficient (Voc)	-0.36%/°C
Temperature Coefficient (Isc)	0.053%/°C

*Measured at (STC) Standard Test Conditions: 25°C, 1 kW/m² insolation, AM 1.5

IV CURVES

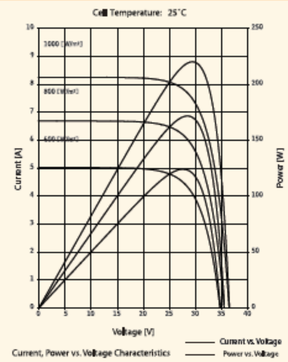

MECHANICAL CHARACTERISTICS	
Dimensions (A x B x C below)	39.1" x 64.6" x 1.8"/994 x 1640 x 46 mm
Cable Length (I)	43.3"/1100 mm
Output Interconnect Cable**	12 AWG with MC4 Locking Connector
Weight	44.1 lbs / 20.0 kg
Max Load	50 psf (2400 Pascals)

**A safety lock clip (Multi Contact part number PV-SSH4) may be required in readily accessible locations per NEC 2008 690.33 (C)

QUALIFICATIONS	
UL Listed	UL 1703
Fire Rating	Class C

WARRANTY

25-year limited warranty on power output
Contact Sharp for complete warranty information

Design and specifications are subject to change without notice.
Sharp is a registered trademark of Sharp Corporation. All other trademarks are property of their respective owners. Contact Sharp to obtain the latest product manuals before using any Sharp device. Cover photo: Solar installation by Pacific Power Management, Auburn CA.

DIMENSIONS

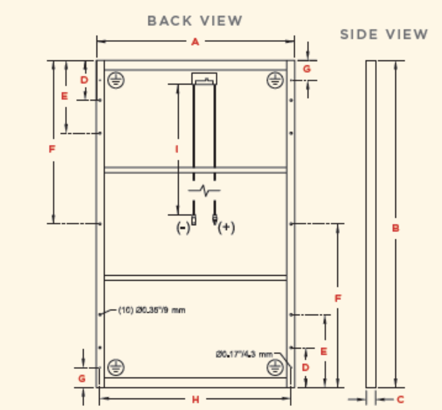

A	B	C	D	E
39.1"/994 mm	64.6"/1640 mm	1.8"/46 mm	7.9"/200 mm	14.4"/365 mm

F	G	H	I
32.3"/820 mm	3.9"/100 mm	37.7"/958 mm	43.3"/1100 mm

Contact Sharp for tolerance specifications

SHARP ELECTRONICS CORPORATION
5901 Bolsa Avenue, Huntington Beach, CA 92647
1-800-SOLAR-06 • Email: sharpsolar@sharpusa.com
www.sharpusa.com/solar

08L-033 • PC-11-08

Data Sheet 2: Morningstar, "Tristar MPPT," TS MPPT 30-45-60 datasheet, 2014.

MORNINGSTAR
World's Leading Solar Controllers & Inverters

TRISTAR MPPT™

SOLAR CONTROLLER WITH MAXIMUM POWER POINT TRACKING

Product shown with optional meter.

Morningstar's **TriStar MPPT** solar controller with TrakStar Technology™ is an advanced maximum power point tracking (MPPT) battery charger for off-grid photovoltaic (PV) systems up to 3kW. The controller provides the industry's highest peak efficiency of 99% and significantly less power loss compared to other MPPT controllers.

The TriStar MPPT features a smart tracking algorithm that maximizes the energy harvest from the PV by rapidly finding the solar array peak power point with extremely fast sweeping of the entire I-V curve. This product is the first PV controller to include on-board Ethernet for a fully web-enabled interface and includes up to 200 days of data logging.

Key Features and Benefits

Maximizes Energy Harvest

Our TrakStar MPPT Technology features:

- Better peak power point tracking than other MPPT controllers
- Very fast sweeping of the entire I-V curve
- Recognition of multiple power points during shading or mixed PV arrays
- Excellent performance at sunrise and low solar insolation levels

Extremely High Reliability

- Robust thermal design and no cooling fans
- Parallel circuit design provides less stress and longer life for electronic components
- No mechanical relays
- Extensive electronic protections including PV short circuit protection
- Epoxy encapsulated inductors and conformally coated printed circuit boards

Very High Efficiency

- Peak efficiency of 99%
- Proprietary tracking algorithm minimizes power losses
- Low self-consumption
- Continuous operation at full power to 45°C without need to de-rate
- Selected electronic devices with higher ratings to minimize losses from heating

Extensive Networking and Communications Capabilities

Enables system monitoring, data logging and adjustability. Uses open standard MODBUS™ protocol and Morningstar's MS View software.

- Meterbus: communications between compatible Morningstar products
- Serial RS-232: connection to a personal computer
- EIA-485: communications between multiple devices on a bus
- Ethernet: fully web-enabled interface to a local network or internet; view from a web browser or send email/text messages.

Metering and Data Logging

- Optional TriStar meter and remote meter provides detailed operating data, alarms and faults
- Three LED's display system status
- Up to 200 days of data logging via meters or communications ports

System Status:

53.60V	28C	54.2A
2867W		MPPT

Data Logging:

Today Batt 46.4Vmin	Day:-1 Batt 47.2Vmin
Today Solar 58.9Amax	Day:-1 Solar 56.8Amax
Today Solar 107.2Vmax	Day:-1 Solar 105.5Vmax

TRISTAR MPPT™ SOLAR CONTROLLER

TRAKSTAR™ MAXIMUM POWER POINT TRACKING

TECHNICAL SPECIFICATIONS

Electrical

		TS-MPPT-30	TS-MPPT-45	TS-MPPT-60
• Maximum Battery Current		30 amps	45 amps	60 amps
• Nominal Maximum Solar Input	12 Volt	400 Watts	600 Watts	800 Watts
	24 Volt	800 Watts	1200 Watts	1600 Watts
	48 Volt	1600 Watts	2400 Watts	3200 Watts

	TS-MPPT-30, 45 and 60
• Peak Efficiency	99%
• Nominal System Voltage	12, 24, 36 or 48 volts DC
• Max. Solar Open Circuit Voltage	150 volts DC
• Battery Operating Voltage Range	8-72 volts DC
• Maximum Self-consumption	2.7 Watts
• Transient Surge Protection	4500 Watts/port

Electronic Protections

- **Solar:** Overload, Short Circuit, High Voltage
- **Battery:** High Voltage
- **High Temperature**
- **Lightning and Transient Surges**
- **Reverse Current at Night**

Battery Charging

• Charging algorithm	4-stage
• Charging stages	Bulk, Absorption, Float, Equalize
• Temperature Compensation	
Coefficient	−5mV/°C/cell (25° ref)
Range	−30°C to +80°C
Set points	Absorption, Float, Equalize, HVD

Note: Remote Temperature Sensor is included.

Mechanical

• Dimensions	29.1 x 13.0 x 14.2 cm 11.4 x 5.1 x 5.6 inch
• Weight	4.2 kg / 9.2 lbs.
• Max. Wire Size	35 mm² / 2 AWG
• Conduit knockouts	M20; ½, 1, 1 ¼ inch
• Enclosure	Type 1 (indoor and vented) IP20

Environmental

• Ambient Temperature	–40°C to +45°C
• Storage Temperature	–55°C to +100°C
• Humidity	100% non-condensing
• Tropicalization	Epoxy encapsulation Conformal coating Marine rated terminals

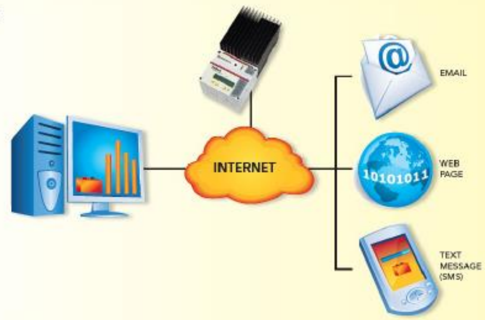

Communication Ports

	TS-MPPT-30	TS-MPPT-45	TS-MPPT-60
• MeterBus	Yes	Yes	Yes
• RS-232	Yes	Yes	Yes
• EIA-485	No	No	Yes
• Ethernet	No	No	Yes

Options

- TriStar Meter-2 (TS-M-2)
- TriStar Remote Meter-2 (TS-RM-2)
- Meter Hub (HUB-1)
- Relay Driver (RD-1)

Certifications

- CE Compliant
- ETL Listed (UL1741)
- cETL (CSA C22.2 No. 107.1-01)
- FCC Class B Part 15 Compliant
- Complies with (NEC) U.S. National Electric Code
- RoHS Compliant
- Manufactured in a certified ISO 9001 facility

WARRANTY: Five year warranty period. Contact Morningstar or your authorized distributor for complete terms.

AUTHORIZED MORNINGSTAR DISTRIBUTOR:

MORNINGSTAR
World's Leading Solar Controllers & Inverters
www.morningstarcorp.com

 PRINTED IN USA 224E-R4-1/14

Data Sheet 3: Dankoff Solar, "Dankoff Solar Slowpump," 1300 -2600, datasheet, 2014.

Dankoff Solar Slowpump™

Dankoff Solar

1300
1400
2500
2600
Series

Use solar-electric power to provide 200–2,600 Gallons per Day (750–10,000 ltrs.) from shallow water sources. Slowpump can push water as high as 450 vertical feet (137m).

Solar Slowpump was the world's first commercially available low power solar pump. It was developed by Windy Dankoff in 1983, in response to those who said "that's impossible". Thousands of Slowpumps have been installed worldwide by ranchers, homeowners, missionaries, health workers, government agencies, etc. Some of our oldest Slowpumps are still in daily service.

Slowpump is not submersible, but can draw water from shallow wells, springs, cisterns, tanks, ponds, rivers, and streams, and push it as high as 450 vertical feet and through miles (kilometers) of pipeline. Slow pumping minimizes the size and cost of the solar array, wire and piping.

Slowpump is less expensive than submersible DC pumps, and made in a much wider range of sizes. Wearing parts typically last 5 to 10 years. Overall life expectancy is 15 to 20 years.

1300 and 2600 Series Solar Slowpumps

Construction & Features

- Rotary vane mechanism (positive displacement) made of forged brass, carbon-graphite and stainless steel
- NSF® approved for drinking water
- Handles sea water, dissolved minerals
- Survives most freezes
- Permanent magnet, DC motor
- AC models use a low-surge PM motor that greatly reduces starting surges, inverter and wire size requirements
- Installation and Service Manual is highly detailed and illustrated

"The Slowpump #2507-24V is supplying water for a work camp on the outer island of Onotoa. It's supplying water for 60 people. The well is one half mile [800m] away from the camp."

B.C., Ministry of Works and Energy,
Kiribati, South Pacific

"I have been very happy with the 1308 Solar Slowpump!... We are using it in a 5 meter deep hand dug well in a valley, and pumping 200 meters distant and 50 meters vertically."

"These pumps work great. ... Even during low light levels when the motor is turning slowly, a small amount of water can be pumped. ... The manual is easy to read. Windy's troubleshooting section is excellent. ... Not only have these pumps stood the test of time, but small changes have made them even better."

B. Schultze
product review in *Home Power Magazine #42*

"Over the last five years, we've found the Slowpump to

Solar Slowpump™ Performance Chart

1300 & 2500 Series 1/4 HP • PV or Battery 12, 24V • 115Vac

Total Lift		Pump # 1322		1310		1308		1304		1303		2505		2507	
Feet	Meters	GPM	Watts	GPM	Watts	GPM	Watts	GPM	Watts	GPM	Watts	GPM	Watts	GPM	Watts
20	6	0.51	27	0.92	29	1.25	30	1.75	37	2.50	48	3.25	52	4.00	57
40	12	0.51	32	0.92	41	1.25	48	1.75	53	2.50	60	3.23	69	3.95	78
60	18	0.51	36	0.89	46	1.20	54	1.68	64	2.40	78	3.15	90	3.90	102
80	24	0.49	40	0.88	51	1.20	60	1.64	73	2.30	93	3.10	106	3.90	120
100	30	0.49	45	0.88	57	1.20	66	1.64	82	2.30	105	3.08	124	3.85	144
120	36	0.48	50	0.88	61	1.20	70	1.62	90	2.25	121	3.02	142	3.80	165
140	42	0.47	56	0.88	66	1.20	75	1.60	100	2.20	138	2.92	166	3.65	195
160	48	0.47	62	0.87	74	1.20	84	1.60	112	2.20	153	2.85	187		
180	54	0.47	66	0.86	82	1.18	93	1.57	122	2.15	165	2.75	205		
200	60	0.45	74	0.85	89	1.16	101	1.56	133	2.15	180				
240	72	0.44	90	0.83	105	1.14	117	1.54	152	2.15	204				
280	84	0.41	102	0.81	120	1.12	135	1.51	175						
320	96	0.41	120	0.79	138	1.10	153	1.48	196						
360	108	0.41	134	0.76	154	1.05	171								
400	120	0.40	150	0.73	176	1.00	198								
440	132	0.39	168	0.70	202										

performance at 15 or 30V (PV-Direct voltage)
For battery, subtract 20% from Flow & Watts

24V pump may be run at 12 volts to yield 1/2 flow at 1/2 watts.
Actual performance may vary ±10% from specifications.

LPM = GPM X 3.8

1300
1400
2500
2600
Series

Dankoff Solar Slowpump™

1400 & 2600 Series 1/2 HP • Battery 24V, 48V • PV-Direct 36V • 115Vac

Max Voltage: 29V or 58V on Battery Models

Pump# ⟶		1408		1404		1403		2605		2607	
Feet	Meters	GPM	Watts	GPM	Watts	GPM	Watts	GPM	Watts	GPM	Watts
160	48									4.30	283
180	54							3.35	280	4.25	305
200	60							3.33	296	4.20	338
240	72					2.55	266	3.30	331	4.05	396
280	84					2.50	302	3.25	373	4.00	444
320	96			1.66	255	2.50	338	3.20	410		
360	108			1.62	280	2.50	374	3.16	450		
400	120			1.64	312	2.50	406				
440	132	1.10	269	1.66	342	2.50	451				

Order pumps using these item numbers

Pump #	12V	24V	36VPV or 48VBatt
1322	22207	22208	
1310	22205	22206	
1308	22203	22204	
1304	22201	22202	
1303	22209	22210	
2505	22211	22212	
2507	22213	22214	
1408		22220	22221
1404		22222	22223
1403		22224	22225
2605		22226	22227
2607		22228	22229

Voltage option 115Vac—for any above, ADD Item 22219

Suction Capacity
- 20 vertical feet (6 m) at sea level– subtract 1 ft. for every 1000 ft. altitude (1 m for every 1000 m). Pump should be placed as low as possible.

Filtration Requirement
- This pump CANNOT tolerate dirt. Water MUST be filtered clear. If water is very dirty, improve the source or consider a different pump.

PV-Direct (non-battery) Requirements
- The rated power of the PV array must exceed pump watts by 20% or more.
- A Linear Current Booster (controller) is required to start and run in low light
- Solar Tracker (optional) will increase daily yield (40-55% in summer)

Accessories
- **#20242 Intake Strainer/Foot Valve:** Monel metal screen, stops coarse debris
- **#20235 Inline Filter:** (10") Uses standard filter cartridges
- **#20237 Intake Filter/Foot Valve:** (30") Replaces Intake Strainer and Inline Filter with a single unit, may be lowered into a shallow well or stream
- **Spare Filter Cartridges:** (5 or 10 micron spun fiber)
  #20236 10" 2–pack
  #20238 30" 3–pack
- **Dry Run Switch:** Prevents pump damage if source runs dry
  #20240 for 1300/1400 Series
  #20241 for 2500/2600 Series
- **#20308 Close Elbows** for use in 6-10" well casings (150-250 cm)
- **Linear Current Booster** (LCB) required for PV-Direct: Specify voltage and current (amps = watts from chart divided by volts)

Fittings
- 1300/1400 Series: 1/2" female
- 2500/2600 Series: 3/4" male

Dimensions (1300/2500 Series)
- 5.7 x 15.5" (14 x 39 cm)
- Weight 16 lbs (7 kg)

Warranty
1 year against defects in materials and workmanship

Available From: SC Solar 1-866-856-9819

Available From:
SC Solar
146 Rental Court
Rock Hill, SC 29732
Phone: 803-980-4320 Email: erik@scsolar.com

version 4/2000

Data Sheet 4: Measure-Current.Com, “HB ACDC,” HB ACDC datasheet, Oct, 2010.

Measure-Current.com HB-ACDC Series Datasheet


HB-ACDC
1 Channel Current Sensor

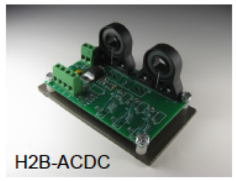
H2B-ACDC
2 Channel Current Sensor

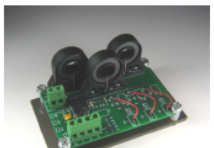
H3B-ACDC
3 Channel Current Sensor

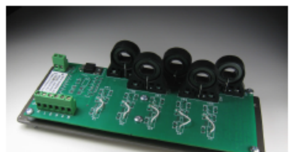
H5B-ACDC
5 Channel Current Sensor

The HXB-ACDC-XX fixed offset, fixed gain series Hall effect current sensor transducer board delivers output voltage proportional to the amount of current detected in the wire being measured.

This type of sensor is often by system designers due to it's ability to provide electrical isolation from the line being monitored and also allows the end user to to strengthen the signal by simply looping the line through the sensor as many times is desired.

The HXB-ACDC-XX series differs from the HA-ACDC-XX series because it has a fixed offset / fixed gain output. It is a low cost solution and is well suited for data logging and instrumentation / data acquisition. This sensor is fed by a precision voltage regulator with a high quality linear response CSLA series Hall effect transducer made by Honeywell.

Assembled in the USA, Lead free ROHS compliant.
Assembled in the USA, Lead free ROHS compliant.
Various mounting options are availble along with different options & Accessories available as a kit. Quantity discounts also available. (For more details see ordering guide)

Features

- Voltage polarity protection on supply excitation input.
- Wide input power range
- Linear output
- AC or DC current sensing
- Over current protection
- Fast response time
- Output voltage isolation from input
- Minimum energy dissipation
- Maximum current limited only by conductor size
- Adjustable performance and built-in
- Adjustable performance and built-in temperature compensation assures reliable operation
- Accurate, low cost sensing
- Operating temperature range -25 °C to 85 °C
- Sturdy open frame mounting

Typical Applications

- Data Acquisiton hw / sw inlcuding LabVIEW
- Solar panel monitoring
- Bicycle generator monitoring
- Wind turbine monitoring
- Battery charging
- Variable speed drives
- Overcurrent protection
- Ground fault detectors
- Current feedback control systems
- Robotics
- UPS and telecommunication power supplies
- Welding power supplies
- Automotive - Battery management systems
- Wattmeters

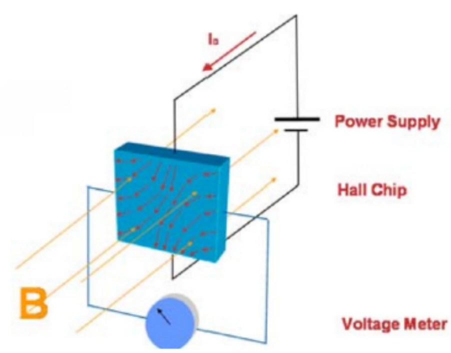

Measure-Current.com HB-ACDC Series Datasheet

SPECIFICATIONS

Product Type	Inductive Analog Current Sensor
Sensed Current Type	ac or dc
Sensed Current Range	HxB-ACDC -72 ±72 A; HxB-ACDC -125 ±125 A
Package Type	PCB Bottom Mount
Output Type	HxB-ACDC -72 ~ 1.64 to 6.35; HxB-ACDC -125 ~ 1.55 to 6.45
Sensitivity (N = Number of Turns)	HxB-ACDC -72 32.7 mV N ±3.0 mV N; HxB-ACDC -125 19.6 mV N ±1.3 mV
Default Offset Output (Zero Amps)	4.0 DC ± 0.15
Supply Current	20 mA max.
Supply Voltage (Input excitation voltage range)	6.0 Vdc to 12.0 Vdc
Power Connector	2.5mm ID power plug or screw terminals
Offset Shift	±0.02
Response Time	3 µs
Operating Temperature	-25 °C to 85 °C [-13 °F to 185 °F]
Storage Temperature	-40 °C to 100°C [-40 °F to 212 °F]
Sensor Housing Material	PBT Polyester
Mounting	Screws into panel or DIN rail option
Availability	Global
Weight	3.4 oz mounted to plate 1.4 oz not mounted
Series Name	HB-ACDC-XX
Sensor Inside Dimensdion	0.43"

Note: This sensor outputs an AC signal for AC Current measurements.

Data Sheet 5: CR Magnetics, “DC Voltage Transducer,” CR 5311 datasheet, 2004.

DC Voltage Transducer

DIN RAIL / PANEL MOUNT, RMS

The **CR5300** Series, DC Voltage Transducers and Transmitters, are designed to provide an output DC signal that is proportional to the input DC voltage. These devices are especially suited for applications with a current shunt to monitor DC current.

Single Element
1 - 200 VDC Input Range

Applications

Power Supply over/under sensing
Battery chargers and systems
Mobile applications
Power sensing

Features

Output isolated from input
Available with 0-5 VDC, 0-10 VDC or 4 - 20 mADC outputs
35mm DIN rail or panel mount
Connection diagram printed on case

Regulatory Agencies

Recognized to UL 61010B-1
Recognized to CAN/CSA-C22.2, No. 61010-1-2004
Meets requirement of IEC 61010-1 and BS EN 61010-1

If you need a relay output, use a **CR3395**.
See Section for Details.

C Transducers

E199795

CR5310 with Resistor Application is shown below (optional).

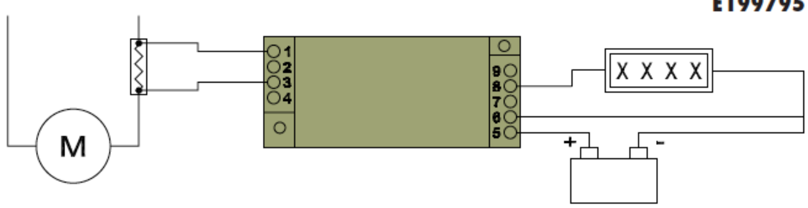

Add suffix for input range

1	-	0-1 VDC
5	-	0-5 VDC
10	-	0-10 VDC
50	-	0-50 VDC
150	-	0-150 VDC
200	-	0-200 VDC

Ranges available up to and including 600 VDC

* **UL Recognized up to 300 Vdc**

PART NUMBERS

CR5310	▪		Single Element with 5 VDC output
CR5311	▪		Single Element with 10 VDC output
CR5320	▪		Single Element with 4 - 20 mADC output

NOTE: CR5300 Series is available with 12V Power Supply. Use same application as 24V Power Supply.
Example Part Number: CR5310-300-12V

DIN RAIL / PANEL MOUNT, RMS

SPECIFICATIONS

Basic Accuracy:...................... 0.5 %	Supply Voltage:.............................. 24 VDC ±10%
Calibration:............................ RMS Calibrated	Frequency Range:........................ DC only
Thermal Drift:......................... 200 PPM/°C	Output Load:...... ±5 or ±10 VDC...... 2 K Ω or greater
Operating Temperature:.......... 0°C to +50°C	4-20 mADC.......... 0 - 300 Ω
Installation Catagory:.............. CAT II	Supply Current:
Pollution Degree:.................... 2	CR5310:......................Typical 10mA Max 15mA
Response Time:.................... 250 ms. max.,0-90% FS	CR5320:......................Typical 35mA Max 35mA
Altitude:................................ 2000 Meters Max.	Torque Specs.:................ 3.0 inch lbs. (0.4Nm)
MTBF:........................... Greater than 100 K hours	Weight:.............................0.5 lbs.
Insulation Voltage:.................. 2500 VDC	

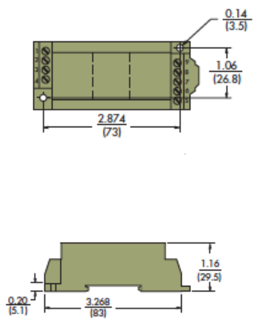

Dimensions for All CR5300 Series (shown)

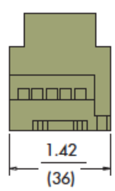

OUTLINE DRAWING

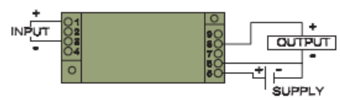

CR5310 5 VDC Output
CR5311 10 VDC Output

CR5320 4 - 20 mADC Output

CONNECTION DIAGRAM

C

Transducers

NOTE: The building installation must have a switch or circuit-breaker that is in close proximity and within easy reach of the operator. The switch or circuit breaker shall be marked as the disconnecting device for the equipment.

CR Magnetics, Inc. 3500 Scarlet Oak Blvd. St. Louis MO USA 63122 V: 636-343-8518 F: 636-343-5119
Web: http://www.crmagnetics.com E-mail: sales@crmagnetics.com

Data Sheet 6: Apogee, "Pyranometer," SP 110, datasheet, 2013.

Measure Shortwave Radiation Reaching the Earth's Surface

The SP-series silicon cell pyranometers are available in self-powered voltage, amplified voltage, and current output options. They are calibrated to measure total shortwave radiation. This cosine-corrected sensor is designed to maintain its accuracy when radiation comes from low zenith angles. This accuracy is shown in the graph below. The SP-110 closely matches the Kipp & Zonen CM21.

The cosine response and accuracy of the pyranometer have met with the high standards of Campbell Scientific, one of the world's leaders in environmental instrumentation. Campbell Scientific installs Apogee pyranometers on weather stations such as the ET107.

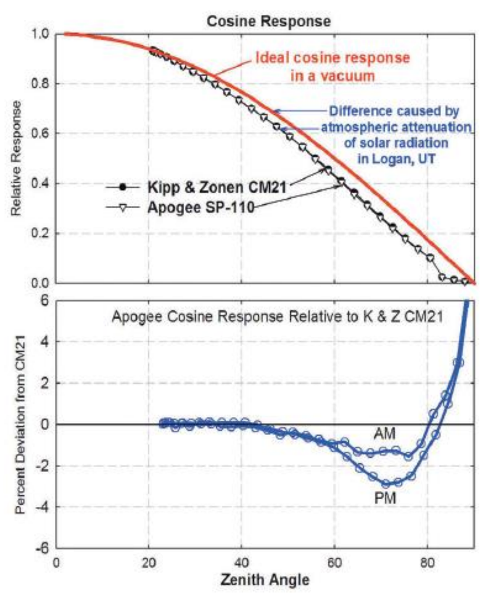

Related Product

AL-100

A plate used to keep the sensor heads level.

Specifications

Cosine Directional Response
- 45° zenith angle: ± 1%
- 75° zenith angle: ± 5%

Absolute Accuracy
- ± 5%

Uniformity
- ± 3%

Repeatability
- ± 1%

Spectral Range
- 380 to 1120 nanometers

Output
SP-110 and SP-230
- Responsivity = 0.2 mV per W m^{-2}, Full sunlight = 220 mV (1100 W m^{-2})
- Calibration Factor = 5.0 W m^{-2} per mV
- Range = 0 to 350 mV (0 to 1750 W m^{-2})

SP-212
- Responsivity = 2 mV per W m^{-2}, full sunlight = 2.2 V (1100 W m^{-2})
- Calibration Factor = 0.5 W m^{-2} per mV
- Range = 0 to 2.5 V (0 to 1250 W m^{-2})

SP-215
- Responsivity = 4 mV per W m^{-2}, full sunlight = 4.4 V (1100 W m^{-2})
- Calibration Factor = 0.25 W m^{-2} per mV
- Range = 0 to 5 V (0 to 1250 W m^{-2})

SP-214
- Responsivity = 0.013 mA per W m^{-2}, full sunlight = 18.1 mA (1100 W m^{-2})
- Calibration Factor = 78 W m^{-2} per mA
- Range = 4 to 20 mA (0 to1250 W m^{-2})

Power Requirement
SP-110 = None, self-powered
SP-212 = 2.5 to 5.5 VDC
- Current Draw = nominal 300 µA

SP-215 = 5 to 5.5 VDC
- Current Draw = nominal 300 µA

SP-214 = 5 to 36 VDC
- Current Draw =2 mA quiescent current, 22 mA = max current at 1250 W m^{-2}

SP-230 = 12 VDC for integrated heater
- Current Draw = 15 mA

Response Time
- Less than 1 millisecond

Long Term Drift
- Less than 3% per year

Temperature Response
- 0.1 % / °C

Field of View
- 180°

Operating Environment
- -40 to 60 C
- 0 to 100% relative humidity
- Designed for continuous outdoor use
- Can be submerged in water

Materials
- Anodized aluminum with cast acrylic lens

Mass
- 70 g (with 5 m lead wire)

Cable
- 5 meters of twisted-pair, shielded wire with Santoprene jacket
- Custom lengths available

Warranty
- 1 year against defects in materials and workmanship

Measurements

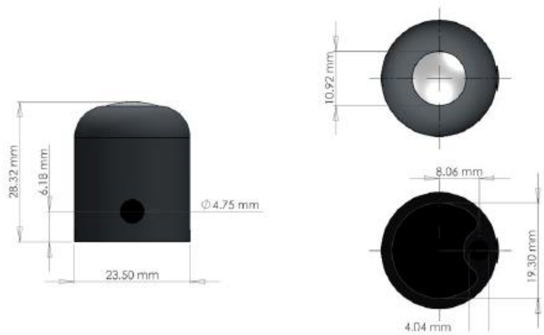

Scan to call us

www.apogeeinstruments.com

Scan for more information on SP sensors

Data Sheet 7: Dyer Instruments, "Flow Indicator," A - 712datasheet, 2011.

Bulletin F-47

Series SFI-800 & SFI-801 Sight Flow Indicator

Specifications - Installation and Operating Instructions

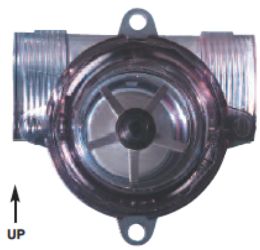

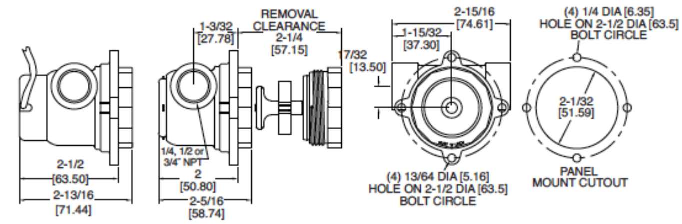

SFI with A-711 Option SFI Model Only

The Series SFI-800 Sight Flow Indicator provides protection for expensive equipment and systems, accommodating fluid temperatures as high as 212°F (100°C) and pressures up to 150 psi (10.34 bar). This sight flow indicator is composed entirely of FDA/NSF-ratable materials. It is exceptionally corrosion-resistant and can handle de-ionized water and many acids, bases and salts. (Consult B. P. Amoco's Extensive "Chemical Guide" for further information on the Udel P1700 Polysulfone resin).

The Series SFI-801 Sight Flow Indicator is similar to the SFI-800 except it is made of UV stablized materials. It can be used in outdoor applications where indication of water flow or control is needed. The materials are not FDA approved.

Three output options are available for the SFI-800 and 801:

The A-711 is a unique, patent pending sensor that outputs two pulse voltage signals proportional to flow rate. Pulse outputs are a 5 VDC pulse and a pulse of the input supply voltage used, which can be 8 to 28 VDC. This sensor can be used to monitor flow rate and flow totalization.

The A-712 is a sensor that outputs a linear 1 to 10 VDC signal proportional to flow rate. This sensor can be used to monitor flow rate.

The A-713 is a flow switch with open collector outputs. One output is active above setpoint and the other output is active below setpoint. The setpoint can be changed by pressing a button at the desired flow rate.

SPECIFICATIONS
Service: Compatible fluids.
Wetted Materials:
Body: SFI-800: Polysulfone, SFI-801: UV Stabilized Polycarbonate;
Window: SFI-800: Polysulfone, SFI-801: UV Stabilized Polycarbonate;
Rotor: SFI-800: White Polysulfone, SFI-801: Red UV Stabilized PBT;
Rotor Pin: 316 SS;
Thrust Washers: 300 Series SS;
O-ring: SFI-800: Fluoroelastomer (NSF Grade), SFI-801:Buna-N.
Temperature Limits: SFI-800: -20 to 212°F (-28 to 100°C); SFI-801: -20 to 130°F (-28 to 55°C).
Pressure Limits: SFI-800: 150 psi (10.34 bar); SFI-801: 125 psi (8.62 bar).
Viscosity Max: 200 SSU.
Weight: SFI-800: 3.35 oz (95 g); SFI-800-A711: 5.0 oz (142 g).

ELECTRICAL SPECIFICATIONS (for A-711 Option Only)
Temperature Limits: -20 to 212°F (-28 to 100°C).
Power Requirements: 8 to 28 VDC.
Output Signal: White lead: 5 VDC. Green lead: 8 to 28 VDC equal to supply voltage. Pulsed output with frequency rate proportional to flow rate.
Accuracy: ±5% of F.S.
Frequency Output Range: 0 to 100 Hz.
Electrical Connections: Black lead - Ground; White lead: 5 VDC out pulse; Green lead: 8 to 28 VDC out pulse; Red lead: 8 to 28 VDC supply.

ELECTRICAL SPECIFICATIONS (for A-712 Option Only)
Temperature Limits: -20 to 212°F (-28 to 100°C).
Power Requirements: 15 to 28 VDC.
Output Signal: White lead: 1 to 10 VDC.
Accuracy: ±5% of F.S.
Electrical Termination: Black lead: Ground; Red lead: 15 to 28 VDC input; White lead: 1 to 10 VDC output.

ELECTRICAL SPECIFICATIONS (for A-713 Option Only)
Temperature Limits: -20 to 212°F (-28 to 100°C).
Power Requirements: 8 to 28 VDC.
Output Signal: White lead: Normally open switch; Green lead: Normally closed switch. Both open collector, 100 mA max, 28 VDC max.
Electrical Connections: Black lead: Ground; White lead: Normally open; Green Lead: Normally closed; Red lead: 8 to 28 VDC.

W.E. ANDERSON DIV., DWYER INSTRUMENTS, INC.
P.O. BOX 358 • MICHIGAN CITY, INDIANA 46361 U.S.A.
Phone: 219/879-8000
Fax: 219/872-9057
www.dwyer-inst.com
e-mail: info@dwyer-inst.com

INSTALLATION

1. Select an indoor location (SFI-800 only) that is free from excess vibration, within the specified temperature limits, and away from direct sunlight. (SFI-800 is adversely affected by ultraviolet light.)

Note: The SFI-801 is rated for indoor or outdoor use and is not affected by ultraviolet light.

2. When mounting horizontally, make sure the "belly" of the indicator is on the bottom. This will prevent entrapped bubbles from collecting and degrading performance.

3. All Series 800 and 801 units may be panel mounted using the (4) four holes integrated into the body.

4. Use plumbers tape thread sealant. Do not use pipe dope compounds, which can craze and crack the polysulfone housing. Hand tighten system pipe fitting. If additional torque is needed to seal pipe joint, use strap wrench on fitting.

5. If using solvent-based glues like PVC cement, in the piping system, do so with the meter's body removed until glue has cured, then purge the system before reinstalling. Do not solder brass fittings with the body installed, because the heat generated to solder the brass fittings will damage the flowmeter.

6. Incoming flow may be connected to either port. However, for best performance a straight section of pipe with a minimum of 10 times the tube diameter should be used on the inlet side.

MAINTENANCE

With all mechanical type sensing units, a minimal amount of cleaning is required. However if a 150-micron filter is used, reduced cleaning can be expected.

The Series SFI-800 Dwyer® Sight Flow Indicator utilizes a patent pending sensing design, no magnets are molded inside the impeller, to attract ferrous material. This greatly reduces the necessary maintenance when used in mechanical systems with ferrous residuals. If residuals are found inside the unit, clean with mild detergent. Inspect for impeller wear. If impeller vibration is noticeable, or if the unit produces an oscillation (whirring or buzzing) sound, replace the impeller.

The Series SFI-800 & SFI-801 Sight Flow Indicators are not field serviceable and should be returned if repair is needed (field repair should not be attempted and may void warranty). Be sure to include a brief description of the problem plus any relevant application notes. Contact customer service to receive a return goods authorization number before shipping.

CAUTION: Be sure that the window locking mechanism is in the locked position. This would be at the 6 o'clock position, when mounted on the horizontal plane with the belly down.

A-711, A-712, or A-713 SENSOR OPTION INSTALLATION

This procedure is for customers who purchased an SFI-800, 801 Sight Flow Indicator and want to add the A-711, A-712, or A-713 Sensor Option.

1. Orient the sight flow indicator with the "belly" down. The sensor "pocket" should be in the 6 o'clock position (as one is facing the unit).

2. Position the A-711, A-712, or A-713 sensor with the wire cable leads at 3 o'clock and the exposed sensor portion at 6 o'clock.

3. Allow the sensor package to rest on the four (4) tabs on the back of the sight flow indicator.

4. Firmly and evenly press the sensor onto the back of the sight flow indicator.

5. The assembly will only go on one way. The sensor is not intended for removal.

6. Follow electrical installation for lead termination.

ELECTRICAL INSTALLATION (for A-711 Option Only)

1. Connect the RED wire from the sensor to the positive 8 to 28 VDC power supply output.

2. Connect the BLACK wire from the sensor to the negative or ground connection of the power supply output.

3. Connect the WHITE wire to get a 5 VDC digital pulse where the frequency of the pulse is proportional to the flow rate.

4. Connect the GREEN wire to get an 8 to 28 VDC pulse where the frequency of the pulse is proportional to the flow rate. The voltage level will be equal to the supply voltage (on the RED wire) minus approximately 0.7 volts.

CAUTION: DO NOT Connect the white and green leads together. Any unused output connections should remain disconnected.

OUTPUT SIGNALS (for units with A-711 Option)

White Wire Connection:

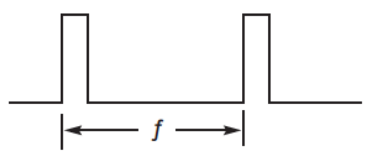

GPM = $\frac{\text{Freq (Hz)}}{4.5}$ for SFI-800-1/2"-A711

GPM = $\frac{\text{Freq (Hz)}}{1.7}$ for SFI-800-3/4"-A711

GPM = $\frac{\text{Freq (Hz)}}{4.5}$ for SFI-801-1/2"-A711

GPM = $\frac{\text{Freq (Hz)}}{1.7}$ for SFI-801-3/4"-A711

Green Wire Connection:

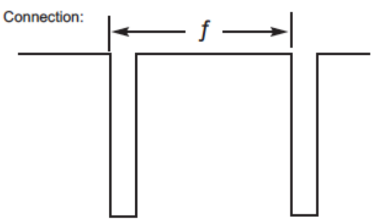

GPM = $\frac{\text{Freq (Hz)}}{4.5}$ for SFI-800-1/2"-A711

GPM = $\frac{\text{Freq (Hz)}}{1.7}$ for SFI-800-3/4"-A711

GPM = $\frac{\text{Freq (Hz)}}{4.5}$ for SFI-801-1/2"-A711

GPM = $\frac{\text{Freq (Hz)}}{1.7}$ for SFI-801-3/4"-A711

ELECTRICAL INSTALLATION (for A-712 Option Only)

1. Connect the RED wire from the sensor to the positive 15 to 28 VDC power supply output.

2. Connect the BLACK wire from the sensor to the negative or ground connection of the power supply output.

3. Connect the WHITE wire to receive the 1 to 10 VDC linear output (see equations below).

GPM = $\frac{\text{Output Voltage}}{0.50}$ for SFI-800-1/2"-A712

GPM = $\frac{\text{Output Voltage}}{0.25}$ for SFI-800-3/4"-A712

GPM = $\frac{\text{Output Voltage}}{0.49}$ for SFI-801-1/2"-A712

GPM = $\frac{\text{Output Voltage}}{0.27}$ for SFI-801-3/4"-A712

ELECTRICAL INSTALLATION (for A-713 Option Only)

1. Connect the RED wire from the sensor to the positive 8 to 28 VDC power supply output.

2. Connect the BLACK wire from the sensor to the negative or ground connection of the power supply output.

3. Connect the WHITE wire to the load that is energized when flow rate is above setpoint (high flow). Connect other end of load to the positive end of the power source. This wire may be left unconnected.

4. Connect the GREEN wire to the a load that is energized when flow rate is below setpoint (low flow). Connect other end of load to the positive end of the power source. This wire may be left unconnected.

5. Adjust flow rate to desired setpoint and press the push to set button. The setpoint light will flash to indicate setpoint has been changed. The setpoint light will then turn on above setpoint and off below setpoint.

Example of Wiring Diagram

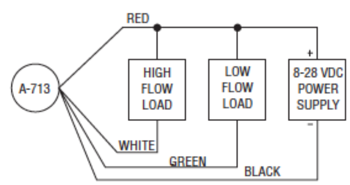

Printed in U.S.A. 9/11

FR# 83-443156-00 Rev. 5

W.E. ANDERSON DIV., DWYER INSTRUMENTS, INC.
P.O. BOX 358 • MICHIGAN CITY, INDIANA 46361 U.S.A.

Phone: 219/879-8000
Fax: 219/872-9057

www.dwyer-inst.com
e-mail: info@dwyer-inst.com

Data Sheet 8: National Instruments, "Thermocouple Input Module," NI 9210, datasheet, Dec. 2007.

Technical Sales
United States
(866) 531-6285
info@ni.com

NI 9211

4-Channel, 14 S/s, 24-Bit, ±80 mV Thermocouple Input Module

- 4 thermocouple or ±80 mV analog inputs
- 24-bit resolution; 50/60 Hz noise rejection
- Hot-swappable operation
- -40 to 70 °C operating range
- NIST-traceable calibration

Specifications

Specifications Documents

- Specifications
- Data Sheet

Specifications Summary

General	
Product Name	NI 9211
Product Family	Industrial I/O
Form Factor	CompactDAQ , CompactRIO
Part Number	779001-01
Operating System/Target	Real-Time , Windows
Measurement Type	Temperature , Thermocouple , Voltage
Isolation Type	Ch-Earth Ground Isolation
RoHS Compliant	Yes

Signal Conditioning	Cold-junction compensation
Analog Input	
Channels	4 , 0
Single-Ended Channels	0
Differential Channels	4
Resolution	24 bits
Sample Rate	14 S/s
Max Voltage	80 mV
Maximum Voltage Range	-80 mV , 80 mV
Minimum Voltage Range	-80 mV , 80 mV
Simultaneous Sampling	No
Analog Output	
Channels	0

Digital I/O	
Bidirectional Channels	0
Input-Only Channels	0
Output-Only Channels	0
Counter/Timers	
Counters	0
Physical Specifications	
Length	9 cm
Width	2.3 cm
I/O Connector	Screw terminals
Minimum Operating Temperature	-40 °C
Maximum Operating Temperature	70 °C
Minimum Storage Temperature	-40 °C
Maximum Storage Temperature	85 °C
Timing/Triggering/Synchronization	
Triggers cDAQ Chassis	No

Data Sheet 9: National Instruments, "Multifunction DAQ," NI 9210, datasheet, 2008.

NATIONAL INSTRUMENTS

Technical Sales

(866) 531-6285
orders@ni.com

Requirements and Compatibility | Ordering Information | Detailed Specifications | Pinouts/Front Panel Connections

For user manuals and dimensional drawings, visit the product page resources tab on ni.com.

Last Revised: 2012-05-07 16:20:50.0

Bus-Powered M Series Multifunction DAQ for USB - 16-Bit, up to 400 kS/s, up to 32 Analog Inputs, Isolation

- Up to 32 analog inputs at 16 bits, up to 400 kS/s (250 kS/s scanning)
- Up to 2 analog outputs at 16 bits
- Up to 32 TTL/CMOS digital I/O lines
- Two 32-bit, 80 MHz counter/timers
- NI-PGIA 2 and NI-MCal calibration technology for improved measurement accuracy
- NI signal streaming for 4 high-speed data streams on USB
- Bus-powered design
- Available with CAT I isolation

Requirements and Compatibility

OS Information

- Linux®
- Mac OS X
- Windows 2000/XP
- Windows 7
- Windows Vista x64/x86

Driver Information

- NI-DAQmx
- NI-DAQmx Base

Software Compatibility

- ANSI C/C++
- LabVIEW
- LabWindows/CVI
- Measurement Studio
- SignalExpress
- Visual Basic .NET
- Visual C#

Comparison Tables

Family	Connector	Analog Inputs	Resolution (bits)	Max Rate (kS/s)	Analog Outputs	Resolution (bits)	Max Rate (kS/s)	Digital I/O	Isolation
USB-6210	Screw	16	16	250	-	-	-	4 DI/4 DO	-

Analog Input	
Number of channels	
USB-6210/6211/6212/6215/6216	8 differential or 16 single ended
USB-6218	16 differential or 32 single ended
ADC resolution	16 bits
DNL	No missing codes guaranteed
INL	Refer to the AI Absolute Accuracy Tables
Sampling rate	
Maximum	
USB-6210/6211/6215/6218	250 kS/s single channel, 250 kS/s multichannel (aggregate)
USB-6212/6216	400 kS/s single channel, 400 kS/s multichannel (aggregate)

Minimum	0 S/s
Timing accuracy	50 ppm of sample rate
Timing resolution	50 ns
Input coupling	DC
Input range	±10 V, ±5 V, ±1 V, ±0.2 V
Maximum working voltage for analog inputs (signal + common mode)	±10.4 V of AI GND
CMRR (DC to 60 Hz)	100 dB
Input impedance	
Device on	
AI+ to AI GND	>10 GΩ in parallel with 100 pF
AI- to AI GND	>10 GΩ in parallel with 100 pF
Device off	
AI+ to AI GND	1200 Ω
AI- to AI GND	1200 Ω
Input bias current	±100 pA
Crosstalk (at 100 kHz)	
Adjacent channels	-75 dB
Non-adjacent channels	-90 dB
Small signal bandwidth (-3 dB)	
USB-6210/6211/6215/6218	450 kHz
USB-6212/6216	1.5 MHz
Input FIFO size	4,095 samples
Scan list memory	4,095 entries
Data transfers	USB Signal Stream, programmed I/O
Overvoltage protection (AI <0..31>, AI SENSE)	
Device on	±30 V for up to two AI pins
Device off	±20 V for up to two AI pins
Input current during overvoltage condition	±20 mA max/AI pin

Settling Time for Multichannel Measurements	
Accuracy, full scale step, all ranges	
USB-6210/6211/6215/6218	
±90 ppm of step (±6 LSB)	4 µs convert interval
±30 ppm of step (±2 LSB)	5 µs convert interval
±15 ppm of step (±1 LSB)	7 µs convert interval
USB-6212/6216	
±90 ppm of step (±6 LSB)	2.5 µs convert interval
±30 ppm of step (±2 LSB)	3.5 µs convert interval
±15 ppm of step (±1 LSB)	5.5 µs convert interval

Analog Output

USB-6210	0
USB-6211/6212/6215/6216/6218	2
DAC resolution	16 bits
DNL	±1 LSB
Monotonicity	16 bit guaranteed
Maximum update rate	
1 channel	250 kS/s
2 channels	250 kS/s per channel
Timing accuracy	50 ppm of sample rate
Timing resolution	50 ns
Output range	±10 V
Output coupling	DC
Output impedance	0.2 Ω
Output current drive	±2 mA
Overdrive protection	±30 V
Overdrive current	2.4 mA
Power-on state	±20 mV
Power-on glitch	±1 V for 200 ms
Output FIFO size	8,191 samples shared among channels used
Data transfers	USB Signal Stream, programmed I/O
AO waveform modes:	

Appendix – B: MATLAB Data Manipulation Program

```
%% MATLAB Data Manipulation Program
% Khalil Raza

%% Inputs
solar_roof = combine_august23rd_sep1st;                    % Workspace File
Name
average_minute = 1;                                        % Average minutes
PV_array_area = 3.2868;                                    % sqaure meter
polyfit_variable = 3;

%% Average Data in Specified Minutes
nAvg = average_minute*60;

for m=1:36,
    for n=1:nAvg:(floor(length(solar_roof)/nAvg)*nAvg),
        average_data(floor(n/nAvg)+1,m)=mean(solar_roof(n:n+(nAvg-1),m));
    end
end

%% Get Variables From Data (Seconds)

% LabViEW DAQ Parameters
time_daq            = solar_roof (:,1);         %time Stamp
V_panel_1           = solar_roof (:,3);         %Voltage Panel 1
V_panel_2           = solar_roof (:,4);         %Voltage Panel 2
V_battery           = solar_roof (:,5);         %Voltage Battery
V_pump              = solar_roof (:,6);         %Voltage Pump
C_panel_1           = solar_roof (:,7);         %Current Panel 1
C_panel_2           = solar_roof (:,8);         %Current Panel 2
C_battery           = solar_roof (:,9);         %Current Battery
C_pump              = solar_roof (:,10);        %Current Pump
T_panel_1           = solar_roof (:,11);        %Temperature Panel 1
T_panel_2           = solar_roof (:,12);        %Temperature Panel 2
T_battery           = solar_roof (:,13);        %Temperature Battery
T_ambient           = solar_roof (:,14);        %Ambient Temperature
P_panel_1           = solar_roof (:,20);        %Power Panel 1
P_panel_2           = solar_roof (:,21);        %Power Panel 2
P_battery           = solar_roof (:,22);        %Power Battery
P_pump              = solar_roof (:,23);        %Power Pump
solar_insolation    = solar_roof (:,17);        %Solar Insolation
flow_rate           = solar_roof (:,19);        %flow rate
Pressure_inlet      = solar_roof (:,15);        %Inlet Pressure
Pressure_outlet     = solar_roof (:,16);        %Outlet Pressure
C_array             = C_panel_1+C_panel_2;
P_array             = V_panel_2.*C_array;
solar_insolation(solar_insolation<0) = 0;

% MPPT Parametes
MPPT_array_voltage        = solar_roof (:,24);
MPPT_array_current        = solar_roof (:,25);
MPPT_input_array_power    = solar_roof (:,26);
```

```
MPPT_output_array_power   = solar_roof (:,27);
MPPT_battery_voltage      = solar_roof (:,28);
MPPT_battery_current      = solar_roof (:,29);

% PV Effeciency
insolation_PV_array = solar_insolation.*PV_array_area;
P_array(P_array<0) = 0;
PV_effeciency = (P_array./insolation_PV_array)*100;

%% Solar Energy Incident on PV Modules
% Solar Insolation Impinging on Panels
insol_per_kw = solar_insolation./1000;
uSum = 3600;
for mm=1:1,
    for u=1:uSum:(floor(length(insol_per_kw)/uSum)*uSum),

solar_insolation_kWh(floor(u/uSum)+1,mm)=mean(insol_per_kw(u:u+(uSum-
1),mm));
    end
end

dSum = 24;
for dd=1:1,
    for d=1:dSum:(floor(length(solar_insolation_kWh)/dSum)*dSum),

solar_insolation_kWh_day(floor(d/dSum)+1,dd)=sum(solar_insolation_kWh(d:d+
(dSum-1),dd));
    end
end

solar_energy_incident = solar_insolation_kWh_day.*PV_array_area;
xaxis(:,1) = [1:size(solar_insolation_kWh_day,1)]' * 1;
ptime = xaxis;

% Energy Output By Solar Panels

PV_power_kW = P_array./1000;
pSum = 3600;
for pp=1:1,
    for p=1:pSum:(floor(length(PV_power_kW)/pSum)*pSum),
        PV_energy_kWh(floor(p/pSum)+1,pp)=mean(PV_power_kW(p:p+(pSum-
1),pp));
    end
end

eSum =24;
for ee=1:1,
    for e=1:eSum:(floor(length(PV_energy_kWh)/eSum)*eSum),
        PV_energy_kWh_day(floor(e/eSum)+1,ee)=sum(PV_energy_kWh(e:e+(eSum-
1),ee));
    end
end


%% Get Variables From Data (Average)
```

```
% LabViEW DAQ Parameters
atime_daq            = average_data (:,1);        %time Stamp
aV_panel_1           = average_data (:,3);        %Voltage Panel 1
aV_panel_2           = average_data (:,4);        %Voltage Panel 2
aV_battery           = average_data (:,5);        %Voltage Battery
aV_pump              = average_data (:,6);        %Voltage Pump
aC_panel_1           = average_data (:,7);        %Current Panel 1
aC_panel_2           = average_data (:,8);        %Current Panel 2
aC_battery           = average_data (:,9);        %Current Battery
aC_pump              = average_data (:,10);       %Current Pump
aT_panel_1           = average_data (:,11);       %Temperature Panel 1
aT_panel_2           = average_data (:,12);       %Temperature Panel 2
aT_battery           = average_data (:,13);       %Temperature Battery
aT_ambient           = average_data (:,14);       %Ambient Temperature
aP_panel_1           = average_data (:,20);       %Power Panel 1
aP_panel_2           = average_data (:,21);       %Power Panel 2
aP_battery           = average_data (:,22);       %Power Battery
aP_pump              = average_data (:,23);       %Power Pump
asolar_insolation    = average_data (:,17);       %Solar Insolation
aflow_rate           = average_data (:,19);       %flow rate
aPressure_inlet      = average_data (:,15);       %Inlet Pressure
aPressure_outlet     = average_data (:,16);       %Outlet Pressure
aC_array             = aC_panel_1+aC_panel_2;     %Array Current
aP_array             = aV_panel_2.*aC_array;      %Array Power

% MPPT Parameters
aMPPT_array_voltage        = average_data (:,24);
aMPPT_array_current        = average_data (:,25);
aMPPT_input_array_power    = average_data (:,26);
aMPPT_output_array_power   = average_data (:,27);
aMPPT_battery_voltage      = average_data (:,28);
aMPPT_battery_current      = average_data (:,29);

% PV Effeciency
ainsolation_PV_array = asolar_insolation.*PV_array_area;
aP_array(aP_array<0) = 0;
aPV_effeciency = (aP_array./ainsolation_PV_array)*100;
%% Sort Data WRT Solar Insolation; pump is ON (Seconds)
pump_on = solar_roof;

ntime_daq            = pump_on (:,1);        %time Stamp
nV_panel_1           = pump_on (:,3);        %Voltage Panel 1
nV_panel_2           = pump_on (:,4);        %Voltage Panel 2
nV_battery           = pump_on (:,5);        %Voltage Battery
nV_pump              = pump_on (:,6);        %Voltage Pump
nC_panel_1           = pump_on (:,7);        %Current Panel 1
nC_panel_2           = pump_on (:,8);        %Current Panel 2
nC_battery           = pump_on (:,9);        %Current Battery
nC_pump              = pump_on (:,10);       %Current Pump
nT_panel_1           = pump_on (:,11);       %Temperature Panel 1
nT_panel_2           = pump_on (:,12);       %Temperature Panel 2
nT_battery           = pump_on (:,13);       %Temperature Battery
nT_ambient           = pump_on (:,14);       %Ambient Temperature
nP_panel_1           = pump_on (:,20);       %Power Panel 1
nP_panel_2           = pump_on (:,21);       %Power Panel 2
```

```
nP_battery            = pump_on (:,22);         %Power Battery
nP_pump               = pump_on (:,23);         %Power Pump
nsolar_insolation     = pump_on (:,17);         %Solar Insolation
nflow_rate            = pump_on (:,19);         %flow rate
nPressure_inlet       = pump_on (:,15);         %Inlet Pressure
nPressure_outlet      = pump_on (:,16);         %Outlet Pressure
nC_array              = nC_panel_1+nC_panel_2;
nP_array              = nV_panel_2.*nC_array;

% MPPT Parametes
nMPPT_array_voltage         = pump_on (:,24);
nMPPT_array_current         = pump_on (:,25);
nMPPT_input_array_power     = pump_on (:,26);
nMPPT_output_array_power    = pump_on (:,27);
nMPPT_battery_voltage       = pump_on (:,28);
nMPPT_battery_current       = pump_on (:,29);

% PV Effeciency
nsolar_insolation(nsolar_insolation<0) = 0;
ninsolation_PV_array = nsolar_insolation.*PV_array_area;
nP_array(nP_array<0) = 0;
nPV_effeciency = (nP_array./ninsolation_PV_array)*100;

% A = [0 2 3 4 5 6 ; 11 0 0 0 15 16 ; 21 0 0 0 0 26 ;  31 0 33 34 35 36 ;
41 42 43 0 0 0]
% % Specify you conditions
% TF1 = A(:,1)==0
% TF2 = all(A(:,2:5)==0,2) & A(:,6) ~= 0
% TF6 = A(:,2) == 0 & A(:,3) A ~= 0
% % combine them
% TFall = TF1 & TF2 & TF6
% % remove
% A(TFall,:) = []


% Specify conditions
TF1 = pump_on(:,6)<=20;

% combine them
% TFall = TF1 & TF2 & TF6
% remove
pump_on(TF1,:) = [] ;

[~,sorted_inds] = sort(pump_on(:,17) );

% reorder the rows based on the sorted indices
sort_pump_on = pump_on(sorted_inds,:);

% Sort Data
time_daq_on             = sort_pump_on (:,1);          %time Stamp
V_panel_1_on            = sort_pump_on (:,3);          %Voltage Panel 1
V_panel_2_on            = sort_pump_on (:,4);          %Voltage Panel 2
V_battery_on            = sort_pump_on (:,5);          %Voltage Battery
V_pump_on               = sort_pump_on (:,6);          %Voltage Pump
C_panel_1_on            = sort_pump_on (:,7);          %Current Panel 1
```

```
C_panel_2_on           = sort_pump_on (:,8);         %Current Panel 2
C_battery_on           = sort_pump_on (:,9);         %Current Battery
C_pump_on              = sort_pump_on (:,10);        %Current Pump
T_panel_1_on           = sort_pump_on (:,11);        %Temperature Panel 1
T_panel_2_on           = sort_pump_on (:,12);        %Temperature Panel 2
T_battery_on           = sort_pump_on (:,13);        %Temperature Battery
T_ambient_on           = sort_pump_on (:,14);        %Ambient Temperature
P_panel_1_on           = sort_pump_on (:,20);        %Power Panel 1
P_panel_2_on           = sort_pump_on (:,21);        %Power Panel 2
P_battery_on           = sort_pump_on (:,22);        %Power Battery
P_pump_on              = sort_pump_on (:,23);        %Power Pump
solar_insolation_on    = sort_pump_on (:,17);        %Solar Insolation
flow_rate_on           = sort_pump_on (:,19);        %flow rate
Pressure_inlet_on      = sort_pump_on (:,15);        %Inlet Pressure
Pressure_outlet_on     = sort_pump_on (:,16);        %Outlet Pressure
C_array_on             = C_panel_1_on+C_panel_2_on;
P_array_on             = V_panel_2_on.*C_array_on;

% MPPT Parametes
MPPT_array_voltage_on        = sort_pump_on (:,24);
MPPT_array_current_on        = sort_pump_on (:,25);
MPPT_input_array_power_on    = sort_pump_on (:,26);
MPPT_output_array_power_on   = sort_pump_on (:,27);
MPPT_battery_voltage_on      = sort_pump_on (:,28);
MPPT_battery_current_on      = sort_pump_on (:,29);

solar_insolation_on(solar_insolation_on<0) = 1;
insolation_PV_array_on = solar_insolation_on.*PV_array_area;
P_array_on(P_array_on<0) =0;
PV_effeciency_on = (P_array_on./insolation_PV_array_on)*100;

%% Sort Data WRT Solar Insolation; pump is on (Average)
pump_on = average_data;

ntime_daq_avg            = pump_on (:,1);          %time Stamp
nV_panel_1_avg           = pump_on (:,3);          %Voltage Panel 1
nV_panel_2_avg           = pump_on (:,4);          %Voltage Panel 2
nV_battery_avg           = pump_on (:,5);          %Voltage Battery
nV_pump_avg              = pump_on (:,6);          %Voltage Pump
nC_panel_1_avg           = pump_on (:,7);          %Current Panel 1
nC_panel_2_avg           = pump_on (:,8);          %Current Panel 2
nC_battery_avg           = pump_on (:,9);          %Current Battery
nC_pump_avg              = pump_on (:,10);         %Current Pump
nT_panel_1_avg           = pump_on (:,11);         %Temperature Panel 1
nT_panel_2_avg           = pump_on (:,12);         %Temperature Panel 2
nT_battery_avg           = pump_on (:,13);         %Temperature Battery
nT_ambient_avg           = pump_on (:,14);         %Ambient Temperature
nP_panel_1_avg           = pump_on (:,20);         %Power Panel 1
nP_panel_2_avg           = pump_on (:,21);         %Power Panel 2
nP_battery_avg           = pump_on (:,22);         %Power Battery
nP_pump_avg              = pump_on (:,23);         %Power Pump
nsolar_insolation_avg    = pump_on (:,17);         %Solar Insolation
nflow_rate_avg           = pump_on (:,19);         %flow rate
nPressure_inlet_avg      = pump_on (:,15);         %Inlet Pressure
nPressure_outlet_avg     = pump_on (:,16);         %Outlet Pressure
nC_array_avg             = nC_panel_1_avg+nC_panel_2_avg;
```

```
nP_array_avg             = nV_panel_2_avg.*nC_array_avg;

% MPPT Parametes
nMPPT_array_voltage_avg        = pump_on (:,24);
nMPPT_array_current_avg        = pump_on (:,25);
nMPPT_input_array_power_avg    = pump_on (:,26);
nMPPT_output_array_power_avg   = pump_on (:,27);
nMPPT_battery_voltage_avg      = pump_on (:,28);
nMPPT_battery_current_avg      = pump_on (:,29);

% PV Effeciency
nsolar_insolation_avg(nsolar_insolation_avg<0) = 0;
ninsolation_PV_array_avg = nsolar_insolation_avg.*PV_array_area;
nP_array_avg(nP_array_avg<0) = 0;
nPV_effeciency_avg = (nP_array_avg./ninsolation_PV_array_avg)*100;

% A = [0 2 3 4 5 6 ; 11 0 0 0 15 16 ; 21 0 0 0 0 26 ;  31 0 33 34 35 36 ;
41 42 43 0 0 0]
% % Specify you conditions
% TF1 = A(:,1)==0
% TF2 = all(A(:,2:5)==0,2) & A(:,6) ~= 0
% TF6 = A(:,2) == 0 & A(:,3) A ~= 0
% % combine them
% TFall = TF1 & TF2 & TF6
% % remove
% A(TFall,:) = []


% Specify conditions
TF1 = pump_on(:,6)<=20;

% combine them
% TFall = TF1 & TF2 & TF6
% remove
pump_on(TF1,:) = [] ;

[~,sorted_inds] = sort(pump_on(:,17) );

% reorder the rows based on the sorted indices
sort_pump_on = pump_on(sorted_inds,:);

% Sort Data
time_daq_on_avg           = sort_pump_on (:,1);          %time Stamp
V_panel_1_on_avg          = sort_pump_on (:,3);          %Voltage Panel 1
V_panel_2_on_avg          = sort_pump_on (:,4);          %Voltage Panel 2
V_battery_on_avg          = sort_pump_on (:,5);          %Voltage Battery
V_pump_on_avg             = sort_pump_on (:,6);          %Voltage Pump
C_panel_1_on_avg          = sort_pump_on (:,7);          %Current Panel 1
C_panel_2_on_avg          = sort_pump_on (:,8);          %Current Panel 2
C_battery_on_avg          = sort_pump_on (:,9);          %Current Battery
C_pump_on_avg             = sort_pump_on (:,10);         %Current Pump
T_panel_1_on_avg          = sort_pump_on (:,11);         %Temperature
Panel 1
T_panel_2_on_avg          = sort_pump_on (:,12);         %Temperature
Panel 2
```

```
T_battery_on_avg            = sort_pump_on (:,13);         %Temperature
Battery
T_ambient_on_avg            = sort_pump_on (:,14);         %Ambient
Temperature
P_panel_1_on_avg            = sort_pump_on (:,20);         %Power Panel 1
P_panel_2_on_avg            = sort_pump_on (:,21);         %Power Panel 2
P_battery_on_avg            = sort_pump_on (:,22);         %Power Battery
P_pump_on_avg               = sort_pump_on (:,23);         %Power Pump
solar_insolation_on_avg     = sort_pump_on (:,17);         %Solar
Insolation
flow_rate_on_avg            = sort_pump_on (:,19);         %flow rate
Pressure_inlet_on_avg       = sort_pump_on (:,15);         %Inlet Pressure
Pressure_outlet_on_avg      = sort_pump_on (:,16);         %Outlet Pressure
C_array_on_avg              = C_panel_1_on_avg+C_panel_2_on_avg;
P_array_on_avg              = V_panel_2_on_avg.*C_array_on_avg;

% MPPT Parametes
MPPT_array_voltage_on_avg         = sort_pump_on (:,24);
MPPT_array_current_on_avg         = sort_pump_on (:,25);
MPPT_input_array_power_on_avg     = sort_pump_on (:,26);
MPPT_output_array_power_on_avg    = sort_pump_on (:,27);
MPPT_battery_voltage_on_avg       = sort_pump_on (:,28);
MPPT_battery_current_on_avg       = sort_pump_on (:,29);


solar_insolation_on_avg(solar_insolation_on_avg<0) = 0;
insolation_PV_array_on_avg = solar_insolation_on_avg.*PV_array_area;
P_array_on_avg(P_array_on_avg<0.0001) = 0;
PV_effeciency_on_avg = (P_array_on_avg./insolation_PV_array_on_avg)*100;
%% Sort Data WRT Solar Insolation; pump is off (Seconds)
pump_off = solar_roof;

ftime_daq              = pump_off (:,1);          %time Stamp
fV_panel_1             = pump_off (:,3);          %Voltage Panel 1
fV_panel_2             = pump_off (:,4);          %Voltage Panel 2
fV_battery             = pump_off (:,5);          %Voltage Battery
fV_pump                = pump_off (:,6);          %Voltage Pump
fC_panel_1             = pump_off (:,7);          %Current Panel 1
fC_panel_2             = pump_off (:,8);          %Current Panel 2
fC_battery             = pump_off (:,9);          %Current Battery
fC_pump                = pump_off (:,10);         %Current Pump
fT_panel_1             = pump_off (:,11);         %Temperature Panel 1
fT_panel_2             = pump_off (:,12);         %Temperature Panel 2
fT_battery             = pump_off (:,13);         %Temperature Battery
fT_ambient             = pump_off (:,14);         %Ambient Temperature
fP_panel_1             = pump_off (:,20);         %Power Panel 1
fP_panel_2             = pump_off (:,21);         %Power Panel 2
fP_battery             = pump_off (:,22);         %Power Battery
fP_pump                = pump_off (:,23);         %Power Pump
fsolar_insolation      = pump_off (:,17);         %Solar Insolation
fflow_rate             = pump_off (:,19);         %flow rate
fPressure_inlet        = pump_off (:,15);         %Inlet Pressure
fPressure_outlet       = pump_off (:,16);         %Outlet Pressure
fC_array               = fC_panel_1+fC_panel_2;
fP_array               = fV_panel_2.*fC_array;
```

```
% MPPT Parametes
fMPPT_array_voltage         = pump_off (:,24);
fMPPT_array_current         = pump_off (:,25);
fMPPT_input_array_power     = pump_off (:,26);
fMPPT_output_array_power    = pump_off (:,27);
fMPPT_battery_voltage       = pump_off (:,28);
fMPPT_battery_current       = pump_off (:,29);

% PV Effeciency
fsolar_insolation(fsolar_insolation<0) = 0;
finsolation_PV_array = fsolar_insolation.*PV_array_area;
fP_array(fP_array<0) = 0;
fPV_effeciency = (fP_array./finsolation_PV_array)*100;

% A = []
% % Specify you conditions
% TF1 = A(:,1)==0
% TF2 = all(A(:,2:5)==0,2) & A(:,6) ~= 0
% TF6 = A(:,2) == 0 & A(:,3) A ~= 0
% % combine them
% TFall = TF1 & TF2 & TF6
% % remove
% A(TFall,:) = []


% Specify conditions
TF2 = pump_off(:,6)>=10;
pump_off(TF2,:) = [] ;
[~,sorted_inds] = sort(pump_off(:,17) );
% reorder the rows based on the sorted indices
sort_pump_off = pump_off(sorted_inds,:);

% Sort Data When Pump is off
time_daq_off             = sort_pump_off (:,1);          %time Stamp
V_panel_1_off            = sort_pump_off (:,3);          %Voltage Panel 1
V_panel_2_off            = sort_pump_off (:,4);          %Voltage Panel 2
V_battery_off            = sort_pump_off (:,5);          %Voltage Battery
V_pump_off               = sort_pump_off (:,6);          %Voltage Pump
C_panel_1_off            = sort_pump_off (:,7);          %Current Panel 1
C_panel_2_off            = sort_pump_off (:,8);          %Current Panel 2
C_battery_off            = sort_pump_off (:,9);          %Current Battery
C_pump_off               = sort_pump_off (:,10);         %Current Pump
T_panel_1_off            = sort_pump_off (:,11);         %Temperature Panel
1
T_panel_2_off            = sort_pump_off (:,12);         %Temperature Panel
2
T_battery_off            = sort_pump_off (:,13);         %Temperature
Battery
T_ambient_off            = sort_pump_off (:,14);         %Ambient
Temperature
P_panel_1_off            = sort_pump_off (:,20);         %Power Panel 1
P_panel_2_off            = sort_pump_off (:,21);         %Power Panel 2
P_battery_off            = sort_pump_off (:,22);         %Power Battery
P_pump_off               = sort_pump_off (:,23);         %Power Pump
solar_insolation_off     = sort_pump_off (:,17);         %Solar Insolation
flow_rate_off            = sort_pump_off (:,19);         %flow rate
```

```
Pressure_inlet_off       = sort_pump_off (:,15);         %Inlet Pressure
Pressure_outlet_off      = sort_pump_off (:,16);         %Outlet Pressure
C_array_off              = C_panel_1_off+C_panel_2_off;
P_array_off              = V_panel_2_off.*C_array_off;

% MPPT Parametes
MPPT_array_voltage_off         = sort_pump_off (:,24);
MPPT_array_current_off         = sort_pump_off (:,25);
MPPT_input_array_power_off     = sort_pump_off (:,26);
MPPT_output_array_power_off    = sort_pump_off (:,27);
MPPT_battery_voltage_off       = sort_pump_off (:,28);
MPPT_battery_current_off       = sort_pump_off (:,29);

%% Sort Data WRT Solar Insolation; pump is off (Average)
pump_off = average_data;

ftime_daq_avg             = pump_off (:,1);          %time Stamp
fV_panel_1_avg             = pump_off (:,3);          %Voltage Panel 1
fV_panel_2_avg             = pump_off (:,4);          %Voltage Panel 2
fV_battery_avg             = pump_off (:,5);          %Voltage Battery
fV_pump_avg                = pump_off (:,6);          %Voltage Pump
fC_panel_1_avg             = pump_off (:,7);          %Current Panel 1
fC_panel_2_avg             = pump_off (:,8);          %Current Panel 2
fC_battery_avg             = pump_off (:,9);          %Current Battery
fC_pump_avg                = pump_off (:,10);         %Current Pump
fT_panel_1_avg             = pump_off (:,11);         %Temperature Panel 1
fT_panel_2_avg             = pump_off (:,12);         %Temperature Panel 2
fT_battery_avg             = pump_off (:,13);         %Temperature Battery
fT_ambient_avg             = pump_off (:,14);         %Ambient Temperature
fP_panel_1_avg             = pump_off (:,20);         %Power Panel 1
fP_panel_2_avg             = pump_off (:,21);         %Power Panel 2
fP_battery_avg             = pump_off (:,22);         %Power Battery
fP_pump_avg                = pump_off (:,23);         %Power Pump
fsolar_insolation_avg      = pump_off (:,17);         %Solar Insolation
fflow_rate_avg             = pump_off (:,19);         %flow rate
fPressure_inlet_avg        = pump_off (:,15);         %Inlet Pressure
fPressure_outlet_avg       = pump_off (:,16);         %Outlet Pressure
fC_array_avg               = fC_panel_1_avg+fC_panel_2_avg;
fP_array_avg               = fV_panel_2_avg.*fC_array_avg;

% MPPT Parametes
fMPPT_array_voltage_avg         = pump_off (:,24);
fMPPT_array_current_avg         = pump_off (:,25);
fMPPT_input_array_power_avg     = pump_off (:,26);
fMPPT_output_array_power_avg    = pump_off (:,27);
fMPPT_battery_voltage_avg       = pump_off (:,28);
fMPPT_battery_current_avg       = pump_off (:,29);

% PV Effeciency
fsolar_insolation_avg (fsolar_insolation_avg <0) = 0;
finsolation_PV_array_avg  = fsolar_insolation_avg .*PV_array_area ;
fP_array_avg (fP_array_avg <0) = 0;
fPV_effeciency_avg  = (fP_array_avg ./finsolation_PV_array_avg )*100;

% A = []
% % Specify you conditions
```

```
% TF1 = A(:,1)==0
% TF2 = all(A(:,2:5)==0,2) & A(:,6) ~= 0
% TF6 = A(:,2) == 0 & A(:,3) A ~= 0
% % combine them
% TFall = TF1 & TF2 & TF6
% % remove
% A(TFall,:) = []


% Specify conditions
TF2 = pump_off(:,6)>=10;
pump_off(TF2,:) = [] ;
[~,sorted_inds] = sort(pump_off(:,17) );
% Reorder the rows based on the sorted indices
sort_pump_off = pump_off(sorted_inds,:);

% Sort Data When Pump is off
time_daq_off_avg              = sort_pump_off (:,1);          %time Stamp
V_panel_1_off_avg             = sort_pump_off (:,3);          %Voltage
Panel 1
V_panel_2_off_avg             = sort_pump_off (:,4);          %Voltage
Panel 2
V_battery_off_avg             = sort_pump_off (:,5);          %Voltage
Battery
V_pump_off_avg                = sort_pump_off (:,6);          %Voltage Pump
C_panel_1_off_avg             = sort_pump_off (:,7);          %Current
Panel 1
C_panel_2_off_avg             = sort_pump_off (:,8);          %Current
Panel 2
C_battery_off_avg             = sort_pump_off (:,9);          %Current
Battery
C_pump_off_avg                = sort_pump_off (:,10);         %Current Pump
T_panel_1_off_avg             = sort_pump_off (:,11);         %Temperature
Panel 1
T_panel_2_off_avg             = sort_pump_off (:,12);         %Temperature
Panel 2
T_battery_off_avg             = sort_pump_off (:,13);         %Temperature
Battery
T_ambient_off_avg             = sort_pump_off (:,14);         %Ambient
Temperature
P_panel_1_off_avg             = sort_pump_off (:,20);         %Power Panel
1
P_panel_2_off_avg             = sort_pump_off (:,21);         %Power Panel
2
P_battery_off_avg             = sort_pump_off (:,22);         %Power
Battery
P_pump_off_avg                = sort_pump_off (:,23);         %Power Pump
solar_insolation_off_avg      = sort_pump_off (:,17);         %Solar
Insolation
flow_rate_off_avg             = sort_pump_off (:,19);         %flow rate
Pressure_inlet_off_avg        = sort_pump_off (:,15);         %Inlet
Pressure
Pressure_outlet_off_avg       = sort_pump_off (:,16);         %Outlet
Pressure
C_array_off_avg               = C_panel_1_off_avg+C_panel_2_off_avg;
P_array_off_avg               = V_panel_2_off_avg.*C_array_off_avg;
```

```matlab
% MPPT Parametes
MPPT_array_voltage_off_avg          = sort_pump_off (:,24);
MPPT_array_current_off_avg          = sort_pump_off (:,25);
MPPT_input_array_power_off_avg      = sort_pump_off (:,26);
MPPT_output_array_power_off_avg     = sort_pump_off (:,27);
MPPT_battery_voltage_off_avg        = sort_pump_off (:,28);
MPPT_battery_current_off_avg        = sort_pump_off (:,29);

%% Sort overall data WRT Solar Insolation (Seconds)

% Sort Data with respect to Solar Insolation
[~,sorted_inds] = sort(solar_roof(:,17) );
% Reorder the rows based on the sorted indices
x = solar_roof(sorted_inds,:);

stime_daq               = x (:,1);          %time Stamp
sV_panel_1              = x (:,3);          %Voltage Panel 1
sV_panel_2              = x (:,4);          %Voltage Panel 2
sV_battery              = x (:,5);          %Voltage Battery
sV_pump                 = x (:,6);          %Voltage Pump
sC_panel_1              = x (:,7);          %Current Panel 1
sC_panel_2              = x (:,8);          %Current Panel 2
sC_battery              = x (:,9);          %Current Battery
sC_pump                 = x (:,10);         %Current Pump
sT_panel_1              = x (:,11);         %Temperature Panel 1
sT_panel_2              = x (:,12);         %Temperature Panel 2
sT_battery              = x (:,13);         %Temperature Battery
sT_ambient              = x (:,14);         %Ambient Temperature
sP_panel_1              = x (:,20);         %Power Panel 1
sP_panel_2              = x (:,21);         %Power Panel 2
sP_battery              = x (:,22);         %Power Battery
sP_pump                 = x (:,23);         %Power Pump
ssolar_insolation       = x (:,17);         %Solar Insolation
sflow_rate              = x (:,19);         %flow rate
sPressure_inlet         = x (:,15);         %Inlet Pressure
sPressure_outlet        = x (:,16);         %Outlet Pressure
sC_array                = sC_panel_1+sC_panel_2;
sP_array                = sV_panel_2.*sC_array;
ssolar_insolation(ssolar_insolation<0) = 0;

% MPPT Parametes
sMPPT_array_voltage         = x (:,24);
sMPPT_array_current         = x (:,25);
sMPPT_input_array_power     = x (:,26);
sMPPT_output_array_power    = x (:,27);
sMPPT_battery_voltage       = x (:,28);
sMPPT_battery_current       = x (:,29);
%% Sort overall data WRT Solar Insolation (Average)

% Sort Data with respect to Solar Insolation
[~,sorted_inds] = sort(average_data(:,17) );
% Reorder the rows based on the sorted indices
y = average_data(sorted_inds,:);
```

```
stime_daq_avg            = y (:,1);          %time Stamp
sV_panel_1_avg           = y (:,3);          %Voltage Panel 1
sV_panel_2_avg           = y (:,4);          %Voltage Panel 2
sV_battery_avg           = y (:,5);          %Voltage Battery
sV_pump_avg              = y (:,6);          %Voltage Pump
sC_panel_1_avg           = y (:,7);          %Current Panel 1
sC_panel_2_avg           = y (:,8);          %Current Panel 2
sC_battery_avg           = y (:,9);          %Current Battery
sC_pump_avg              = y (:,10);         %Current Pump
sT_panel_1_avg           = y (:,11);         %Temperature Panel 1
sT_panel_2_avg           = y (:,12);         %Temperature Panel 2
sT_battery_avg           = y (:,13);         %Temperature Battery
sT_ambient_avg           = y (:,14);         %Ambient Temperature
sP_panel_1_avg           = y (:,20);         %Power Panel 1
sP_panel_2_avg           = y (:,21);         %Power Panel 2
sP_battery_avg           = y (:,22);         %Power Battery
sP_pump_avg              = y (:,23);         %Power Pump
ssolar_insolation_avg    = y (:,17);         %Solar Insolation
sflow_rate_avg           = y (:,19);         %flow rate
sPressure_inlet_avg      = y (:,15);         %Inlet Pressure
sPressure_outlet_avg     = y (:,16);         %Outlet Pressure
sC_array_avg             = sC_panel_1_avg+sC_panel_2_avg;
sP_array_avg             = sV_panel_2_avg.*sC_array_avg;
ssolar_insolation_avg(ssolar_insolation_avg<0) = 0;

% MPPT Parametes
sMPPT_array_voltage_avg        = y (:,24);
sMPPT_array_current_avg        = y (:,25);
sMPPT_input_array_power_avg    = y (:,26);
sMPPT_output_array_power_avg   = y (:,27);
sMPPT_battery_voltage_avg      = y (:,28);
sMPPT_battery_current_avg      = y (:,29);
%% Get timestamps
%Get Time Every Second
g(:,1) = [1:size(solar_roof,1)]' * 1;
mtime = (g./3600);
%Get Time Average Minutes
avg(:,1) = [1:size(average_data,1)]' * 1;
atime_avg = (avg./60)*average_minute;


%% Plot Data vs Time

%Plot Voltage Every Second
figure
plot(mtime,V_panel_1,'r',mtime,V_panel_2,'b',mtime,V_battery,'m',mtime,V_p
ump,'y', mtime,MPPT_battery_voltage ,'g',mtime,MPPT_array_voltage, 'c');
set(findall(gcf,'type','axes'),'fontsize',24 )
set(findall(gcf,'type','text'),'fontsize',24)
set(gcf,'color','w');
addaxis(mtime,solar_insolation,'k');
legend ('V panel 1','V panel 2','V battery', 'V pump+resistors','V MPPT
Battery', 'V MPPT Array','Solar Insolation');
xlabel('Time (hours)'), ylabel('Voltage (Volts)'), grid
% title(['Voltage Vs Time:']);
addaxislabel (2,'Solar Insolation (W/m^2)');
```

```
hold off
axis([0,300,-10,40])
set(findall(gcf,'type','axes'),'fontsize',24 )
set(findall(gcf,'type','text'),'fontsize',24)
set(gcf,'color','w');

% Plot Voltage (Average)
figure
plot(atime_avg,aV_panel_1,'r',atime_avg,aV_panel_2,'b',atime_avg,aV_batter
y,'m',atime_avg,aV_pump,'y', atime_avg,aMPPT_battery_voltage
,'g',atime_avg,aMPPT_array_voltage, 'c');
set(findall(gcf,'type','axes'),'fontsize',24 )
set(findall(gcf,'type','text'),'fontsize',24)
set(gcf,'color','w');
addaxis(atime_avg,asolar_insolation,'k');
legend ('V panel 1','V panel 2','V battery', 'V pump+resistors', 'V MPPT
Battery', 'V MPPT Array','Solar Insolation');
xlabel('Time (hours)'), ylabel('Voltage (Volts)'), grid
addaxislabel (2,'Solar Insolation (W/m^2)');
% title(['Voltage Vs Time:']);
axis([0,300,-12,40])
set(findall(gcf,'type','axes'),'fontsize',24 )
set(findall(gcf,'type','text'),'fontsize',24)
set(gcf,'color','w');

% % Plot Current Every Second
% figure
% plot(mtime,C_panel_1,'r',mtime,C_panel_2,'c',mtime,C_array,'m',
mtime,C_battery,'k',mtime,C_pump,'y', mtime,MPPT_array_current,'b',
mtime,MPPT_battery_current, 'g');
% set(findall(gcf,'type','axes'),'fontsize',24 )
% set(findall(gcf,'type','text'),'fontsize',24)
% set(gcf,'color','w');
% legend ('C panel 1','C panel 2','C Array','C Battery','C Pump' ,'MPPT
Array Current', 'MPPT Battery Current');
% xlabel('Time (Hours)' ), ylabel('Current (A)' ), grid
% % title(['Current Vs Time: ']);
% axis([0,24,0,22])
%
% % Plot Current (Average)
% figure
%
plot(atime_avg,aC_panel_1,'r',atime_avg,aC_panel_2,'c',atime_avg,aC_array,
'm',atime_avg,aC_battery,'k',atime_avg,aC_pump,'y',
atime_avg,aMPPT_array_current,'b', atime_avg, aMPPT_battery_current,'g');
% set(findall(gcf,'type','axes'),'fontsize',24 )
% set(findall(gcf,'type','text'),'fontsize',24)
% set(gcf,'color','w');
% legend ('C panel 1','C panel 2','C Array','C Battery','C Pump' ,'MPPT
Array Current', 'MPPT Battery Current');
% xlabel('Time (Hours)' ), ylabel('Current (A)' ), grid
% % title(['Current Vs Time: ']);
% axis([0,24,0,22])


% Plot Temperature Every Second
```

```
figure
plot(mtime,T_panel_1,'r',mtime,T_panel_2,'b',mtime,T_battery,'m',mtime,T_a
mbient,'g');
set(findall(gcf,'type','axes'),'fontsize',24 )
set(findall(gcf,'type','text'),'fontsize',24)
set(gcf,'color','w');
addaxis(mtime,solar_insolation,'k');
legend ('T panel 1','T panel 2','T battery','T Ambient','Solar
Insolation');
xlabel('Time (Hours)' ), ylabel('Temperature (C)' ), grid
% title(['Temperature & Solar Insolation Vs Time:']);
addaxislabel (2,'Solar Insolation (W/m^2)');
hold off
xlim([0 300]);
set(findall(gcf,'type','axes'),'fontsize',24 )
set(findall(gcf,'type','text'),'fontsize',24 )
set(gcf,'color','w');

% Plot Temperature (Average)
figure
plot(atime_avg,aT_panel_1,'r',atime_avg,aT_panel_2,'b',atime_avg,aT_batter
y,'m',atime_avg,aT_ambient,'g');
set(findall(gcf,'type','axes'),'fontsize',24 )
set(findall(gcf,'type','text'),'fontsize',24)
set(gcf,'color','w');
addaxis(atime_avg,asolar_insolation,'k');
legend ('T panel 1','T panel 2','T battery','T Ambient');
xlabel('Time (Hours)'), ylabel('Temperature (C)'), grid
% title(['Temperature & solar insolation Vs time:']);
addaxislabel (2,'Solar Insolation (W/m^2)');
hold off
xlim([0 300]);
set(findall(gcf,'type','axes'),'fontsize',24 )
set(findall(gcf,'type','text'),'fontsize',24 )
set(gcf,'color','w');


% Plot Power Every Second
figure
plot(mtime,P_panel_1,'r',mtime,P_panel_2,'b',mtime,P_array,'c',mtime,P_pum
p,'m', mtime,MPPT_input_array_power,'g');
set(findall(gcf,'type','axes'),'fontsize',24 )
set(findall(gcf,'type','text'),'fontsize',24 )
set(gcf,'color','w');
addaxis(mtime,solar_insolation,'k');
legend ('P panel 1','P panel 2', 'P Array','P pump+resistors','MPPT Array
Power','Solar Insolation');
xlabel('Time (Hours)' ), ylabel('Power (Watts)' ), grid
% title(['PV array power & solar insolation Vs time:']);
addaxislabel (2,'Solar Insolation (W/m^2)');
hold off
xlim([0 300]);
% ylim([-200 550]);
set(findall(gcf,'type','axes'),'fontsize',24 )
set(findall(gcf,'type','text'),'fontsize',24 )
set(gcf,'color','w');
```

```
% Plot Power (Average)
figure
plot(atime_avg,aP_panel_1,'r',atime_avg,aP_panel_2,'b',atime_avg,aP_array,
'c',atime_avg,aP_pump,'m', atime_avg,aMPPT_input_array_power,'g');
set(findall(gcf,'type','axes'),'fontsize',24 )
set(findall(gcf,'type','text'),'fontsize',24 )
set(gcf,'color','w');
addaxis(atime_avg,asolar_insolation,'k');
legend ('P panel 1','P panel 2', 'P Array','P pump+resistors','MPPT Array
Power','Solar Insolation');
xlabel('Time (Hours)','fontsize',16 ), ylabel('Power
(Watts)','fontsize',16 ), grid
addaxislabel (2,'Solar Insolation (W/m^2)','fontsize',16);
hold off
% title(['PV Array power & solar insolation Vs time:']);
set(gca,'fontsize',16)
xlim([0 300]);
set(findall(gcf,'type','axes'),'fontsize',24 )
set(findall(gcf,'type','text'),'fontsize',24 )
set(gcf,'color','w');

% Plot Solar Insolation Every Second
figure
plot(mtime,solar_insolation);
set(findall(gcf,'type','axes'),'fontsize',24 )
set(findall(gcf,'type','text'),'fontsize',24 )
set(gcf,'color','w');
legend ('Solar Insolation');
xlabel('Time (Hours)' ), ylabel ('Solar Insolation (W/m^2)' ), grid
% title(['Solar Insolation Vs Time:']);
xlim([0 160]);
ylim([0 1300]);

% Plot Solar Insolation (Average)
figure
plot(atime_avg,asolar_insolation);
set(findall(gcf,'type','axes'),'fontsize',24 )
set(findall(gcf,'type','text'),'fontsize',24 )
set(gcf,'color','w');
legend ('Solar Insolation');
xlabel('Time (Hours)' ), ylabel ('Solar Insolation (W/m^2)' ), grid
% title(['Solar Insolation Vs Time:']);
xlim([0 300]);
ylim([0 1250]);

% Plot Flowrate Every Second
figure
plot(mtime,flow_rate);
set(findall(gcf,'type','axes'),'fontsize',24 )
set(findall(gcf,'type','text'),'fontsize',24 )
set(gcf,'color','w');
legend ('Flow Rate');
xlabel('Time (Hours)' ), ylabel('Flowrate, (GPM)' ), grid
% title(['Flowrate Vs Time:']);
ylim([0 3.8]);
```

```
xlim([0 300])


% Plot Flowrate (Average)
figure
plot(atime_avg,aflow_rate);
set(findall(gcf,'type','axes'),'fontsize',24 )
set(findall(gcf,'type','text'),'fontsize',24 )
set(gcf,'color','w');
legend ('Flow Rate');
xlabel('Time (Hours)' ), ylabel('Flowrate, (GPM)' ), grid
title(['Flowrate Vs Time:']);
ylim([0 3.8]);

% % Plot Pressure Every Second
% figure
% plot(mtime,Pressure_inlet,'r',mtime,Pressure_outlet,'b');
% legend ('Inlet Pressure','Outlet Pressure');
% xlabel('Time (Hours)'), ylabel('Pressure (psi)'), grid
% title(['Pressure Vs Time:']);
% set(gca,'fontsize',12)
%
% % Plot Pressure (Average)
% figure
% plot(atime_avg,aPressure_inlet,'r',atime_avg,aPressure_outlet,'b');
% legend ('Inlet Pressure','Outlet Pressure');
% xlabel('Time (Hours)'), ylabel('Pressure (psi)'), grid
% title(['Pressure Vs Time:']);
% set(gca,'fontsize',12)

% Plot Current and Insolation Vs time Every Second
figure
hold on
plot(mtime,C_panel_1,'-
.r',mtime,C_panel_2,'c',mtime,C_array,'m',mtime,C_battery, 'r',
mtime,C_pump,'y', mtime,MPPT_array_current,'b',
mtime,MPPT_battery_current, 'g');
set(findall(gcf,'type','axes'),'fontsize',24 )
set(findall(gcf,'type','text'),'fontsize',24 )
set(gcf,'color','w');
addaxis(mtime,solar_insolation,'k');
legend ('C panel 1','C panel 2','C Array','C Battery', 'C
pump+resistors','C MPPT Array','C MPPT Battery', 'Solar Insolation');
xlabel('Time (Hours)' ), ylabel('Current (Amps)' ), grid
addaxislabel (2,'Solar Insolation (W/m^2)' );
hold off
% title(['Current and Insolation Vs Time: ']);
xlim([0 300]);
% ylim([-10 25]);
set(findall(gcf,'type','axes'),'fontsize',24 )
set(findall(gcf,'type','text'),'fontsize',24 )
set(gcf,'color','w');

% Plot Current and Insolation Vs time (Average)
figure
hold on
```

```
plot(atime_avg,aC_panel_1,'-
.r',atime_avg,aC_panel_2,'c',atime_avg,aC_array,'m',
atime_avg,aC_battery,'r',atime_avg,aC_pump,'y',
atime_avg,aMPPT_array_current,'b',atime_avg,aMPPT_battery_current,'g');
set(findall(gcf,'type','axes'),'fontsize',24 )
set(findall(gcf,'type','text'),'fontsize',24 )
set(gcf,'color','w');
addaxis(atime_avg,asolar_insolation,'k');
legend ('C panel 1','C panel 2','C Array','C Battery','C
pump+resistors','C MPPT Array','C MPPT Battery','Solar Insolation');
xlabel('Time (Hours)' ), ylabel('Current (A)' ), grid
addaxislabel (2,'Solar Insolation (W/m^2)' );
hold off
% title(['Current and Insolation Vs Time: ']);
set(findall(gcf,'type','axes'),'fontsize',24 )
set(findall(gcf,'type','text'),'fontsize',24 )
set(gcf,'color','w');
xlim([0 300]);

% Plot Effeciency
figure
plot(mtime,PV_effeciency);
set(findall(gcf,'type','axes'),'fontsize',24 )
set(findall(gcf,'type','text'),'fontsize',24 )
set(gcf,'color','w');
legend ('PV Panel Effeciency');
xlabel('Time (Hours)' ), ylabel('Effeciency %' ), grid
% title(['Effeciency Vs Time:']);
xlim([0 300])

% Plot Effeciency; Pump is ON
figure
plot(solar_insolation_on,PV_effeciency_on);
set(findall(gcf,'type','axes'),'fontsize',24 )
set(findall(gcf,'type','text'),'fontsize',24 )
set(gcf,'color','w');
addaxis(solar_insolation_on,T_panel_2_on,'r');
% axis([0,240,0,20])
legend ('PV Effeciency');
axis([0,240,0,20])
xlabel('Solar Insolation (watt/m^2)' ), ylabel('Effeciency (%)' ), grid
addaxislabel (2,'PV Array Temperature (C)','fontsize',12);
hold off
% title(['PV Effeciency:']);
set(findall(gcf,'type','axes'),'fontsize',24 )
set(findall(gcf,'type','text'),'fontsize',24 )
set(gcf,'color','w');

% PV effeciency
figure
plot(solar_insolation_on_avg,PV_effeciency_on_avg);
set(findall(gcf,'type','axes'),'fontsize',24 )
set(findall(gcf,'type','text'),'fontsize',24 )
set(gcf,'color','w');
addaxis(solar_insolation_on_avg,T_panel_2_on_avg,'r');
legend ('PV Effeciency (%)','PV Array Temperature(C)');
```

```
axis([0,1300,0,20])
xlabel('Solar Insolation (W/m^2)' ), ylabel('Effeciency (%)' ), grid
addaxislabel (2,'Temperature (C)');
hold off
% title(['PV Effeciency and Temperature vs Solar Insolation']);
set(findall(gcf,'type','axes'),'fontsize',24 )
set(findall(gcf,'type','text'),'fontsize',24 )
set(gcf,'color','w');

%% Plot Data Vs Solar Insolation; pump is on
figure
plot(solar_insolation_on,C_array_on);
axis([0,1500,0,20])
xlabel('Solar Insolation (W/m^2)' ), ylabel('PV Array Current (Amps)' ),
grid
title(['Solar Insolation vs PV Array Current']);
a = polyfit(solar_insolation_on,C_array_on,polyfit_variable);
aa = polyval(a,solar_insolation_on);
hold on
plot (solar_insolation_on,aa, '-g','LineWidth',2);
legend ('PV Array Current','Cubic Fit');

figure
plot(solar_insolation_on_avg,C_array_on_avg);
set(findall(gcf,'type','axes'),'fontsize',24 )
set(findall(gcf,'type','text'),'fontsize',24 )
set(gcf,'color','w');
xlabel('Solar Insolation (W/m^2)' ), ylabel('PV Array Current (Amps)' ),
grid
% title(['Solar Insolation vs PV Array Current']);
% b = polyfit(solar_insolation_on_avg,C_array_on_avg,polyfit_variable);
% bb = polyval(b,solar_insolation_on_avg);
% hold on
% plot (solar_insolation_on_avg,bb, '-r','LineWidth',2);
legend ('PV Array Current');
xlim ([0 1300]);
ylim ([0 18]);

figure
plot(solar_insolation_on,P_array_on);
set(findall(gcf,'type','axes'),'fontsize',24 )
set(findall(gcf,'type','text'),'fontsize',24 )
set(gcf,'color','w');
xlabel('Solar Insolation (W/m^2)'), ylabel('PV Array Power (Watts)'), grid
% title(['Solar Insolation vs PV Array Power']);
% c = polyfit(solar_insolation_on,P_array_on,polyfit_variable);
% cc = polyval(c,solar_insolation_on);
% hold on
% plot (solar_insolation_on,cc, '-r','LineWidth',2);
legend ('PV Array Power');

figure
plot(solar_insolation_on_avg,P_array_on_avg);
set(findall(gcf,'type','axes'),'fontsize',24 )
set(findall(gcf,'type','text'),'fontsize',24 )
set(gcf,'color','w');
```

```
xlabel('Solar Insolation (W/m^2)' ), ylabel('PV Array Power (Watts)' ),
grid
% % title(['Solar Insolation vs PV Array Power']);
% d = polyfit(solar_insolation_on_avg,P_array_on_avg,polyfit_variable);
% dd = polyval(d,solar_insolation_on_avg);
% hold on
% plot (solar_insolation_on_avg,dd, '-r','LineWidth',2);
legend ('PV Array Power');
xlim ([0 1300]);
ylim ([0 500]);


% %% Plot Data Vs Solar Insolation; pump is Off
% figure
% plot(solar_insolation_off,C_array_off);
% legend ('Array Current');
% xlabel('Solar Insolation (W/m^2)'), ylabel('Array Current (A)'), grid
% title(['Solar Insolation vs Array Current - Pump off:']);
% e = polyfit(solar_insolation_off,C_array_off,polyfit_variable);
% ee = polyval(e,solar_insolation_off);
% hold on
% plot (solar_insolation_off,ee, '-r*');
%
% figure
% plot(solar_insolation_off_avg,C_array_off_avg);
% legend ('Array Current');
% xlabel('Solar Insolation (W/m^2)'), ylabel('Array Current (A)'), grid
% title(['Solar Insolation vs Array Current - Pump off:']);
% f = polyfit(solar_insolation_off_avg,C_array_off_avg,polyfit_variable);
% ff = polyval(f,solar_insolation_off_avg);
% hold on
% plot (solar_insolation_off_avg,ff,'-r*');
%
% figure
% plot(solar_insolation_off,P_array_off);
% legend ('Array Power');
% xlabel('Solar Insolation (W/m^2)'), ylabel('Power (Watts)'), grid
% title(['Solar Insolation vs Power - Pump off:']);
% m = polyfit(solar_insolation_off,P_array_off,polyfit_variable);
% mm = polyval(m,solar_insolation_off);
% hold on
% plot (solar_insolation_off,mm, '-r*');
%
% figure
% plot(solar_insolation_off_avg,P_array_off_avg);
% legend ('Array Power');
% xlabel('Solar Insolation (W/m^2)'), ylabel('Power (Watts)'), grid
% title(['Solar Insolation vs Array Power - Pump off:']);
% h = polyfit(solar_insolation_off_avg,P_array_off_avg,polyfit_variable);
% hh = polyval(h,solar_insolation_off_avg);
% hold on
% plot (solar_insolation_off_avg,hh, '-r*');
% %% Plot Overall Data vs Solar Insolation; Pump is ON/OFF
%
% figure
% plot(ssolar_insolation,sC_array);
```

```
% legend ('Array Current');
% xlabel('Solar Insolation (W/m^2)'), ylabel('Array Current (A)'), grid
% title(['Solar Insolation vs Array Current']);
% i = polyfit(ssolar_insolation,sC_array,polyfit_variable);
% ii = polyval(i,ssolar_insolation);
% hold on
% plot (ssolar_insolation,ii, '-r*');
%
% figure
% plot(ssolar_insolation_avg,sC_array_avg);
% legend ('Array Current');
% xlabel('Solar Insolation (W/m^2)'), ylabel('Array Current (A)'), grid
% title(['Solar Insolation vs Array Current']);
% j = polyfit(ssolar_insolation_avg,sC_array_avg,polyfit_variable);
% jj = polyval(j,ssolar_insolation_avg);
% hold on
% plot (ssolar_insolation_avg,jj, '-r*');
%
% figure
% plot(ssolar_insolation,sP_array);
% legend ('Array Power');
% xlabel('Solar Insolation (W/m^2)'), ylabel('Power (Watts)'), grid
% title(['Solar Insolation vs Power ']);
% k = polyfit(ssolar_insolation,sP_array,polyfit_variable);
% kk = polyval(k,ssolar_insolation);
% hold on
% plot (ssolar_insolation,kk, '-r*');

% figure
% plot(ssolar_insolation_avg,sP_array_avg);
% legend (' Array Power');
% xlabel('Solar Insolation (W/m^2)','FontSize', 12), ylabel('Power
(Watts)','FontSize', 12), grid
% title(['Solar Insolation vs Array Power']);
% l = polyfit(ssolar_insolation_avg,sP_array_avg,polyfit_variable);
% ll = polyval(l,ssolar_insolation_avg);
% hold on
% plot (ssolar_insolation_avg,ll,'-r*');
% set(gca,'fontsize',12)




% figure
% [hAxes,hBar,hLine] =
plotyy(ptime,solar_insolation_kWh_day,ptime,solar_energy_incident,'bar','p
lot');
% set(hLine,'LineWidth',2,'Color','g','Marker','o');
% title('Solar Energy')
% xlabel({'Days';'July 28th, 2014 to August 3rd, 2014'},'fontsize',12)
% ylabel(hAxes(1),'Solar Energy (kWh/day/m^2)','FontSize', 12)
% ylabel(hAxes(2),'Solar Energy Incident on Panels (kWh)','FontSize', 12)
% legend('Solar insolation','Insolation Incident on PV Array');
% set(gca,'fontsize',12)
% ylim([0 10])
%
%
```

```
% figure
% [hAxes,hBar,hLine] =
plotyy(ptime,PV_energy_kWh_day,ptime,solar_energy_incident,'bar','bar');
% set(hLine,'LineWidth',2,'Color','g','Marker','o');
% title('PV Energy Production'),grid
% xlabel({'Days';'July 28th, 2014 to August 3rd, 2014'},'FontSize', 12)
% set(gca,'XTickLabel',{},'fontsize',12);
% ylabel(hAxes(1),'PV Energy Production (kWh)','FontSize', 12)
% ylabel(hAxes(2),'Solar Energy Incident on Panels (kWh)','FontSize', 12)
% legend('PV Energy Production','Solar Radiation Incident on PV
Array','FontSize', 12);
% set(gca,'XTickLabel',{})
% ylim([0 4])
% set(gca,'XTickLabel','String')

% Solar Energy Impinging on Panels
figure;
[ax, h1, h2] = plotyy(ptime, solar_insolation_kWh_day, ptime,
solar_energy_incident, 'bar', 'plot');
set(findall(gcf,'type','axes'),'fontsize',24 )
set(findall(gcf,'type','text'),'fontsize',24 )
set(gcf,'color','w');
set(h1, 'FaceColor', [0.4, 0.4, 0.4]);
set(h2, 'LineWidth', 4,'Marker','o');
% title('Solar Energy'),grid
legend('Solar Radiation per Unit Area','Solar Radiation Incident on PV
Array')
xlabel({'Days';'August 23rd, 2014 to August 27th, 2014'} );
set(get(ax(1), 'Ylabel'), 'String', 'Solar Radiation per Unit Area
(kWh/day/m^2)' );
set(get(ax(2), 'Ylabel'), 'String', 'Solar Radiation Impinging on PV Array
(kWh/day)' )
set(findall(gcf,'type','axes'),'fontsize',24 )
set(findall(gcf,'type','text'),'fontsize',24 )
set(gcf,'color','w');
ylim ([0 10]);
grid;

% PV Energy Production
figure;
[ax, h1, h2] = plotyy( ptime,PV_energy_kWh_day, ptime,
solar_energy_incident, 'bar', 'plot');
set(findall(gcf,'type','axes'),'fontsize',24 )
set(findall(gcf,'type','text'),'fontsize',24 )
set(h1, 'FaceColor', [0.4, 0.4, 0.4]);
set(h2, 'LineWidth', 4,'Marker','o');
% title('PV Energy Production'),grid
legend('PV Energy Production','Solar Radiation Incident on PV Array' )
xlabel({'Days';'August 23rd, 2014 to August 27th, 2014'} );
set(get(ax(1), 'Ylabel'), 'String', 'PV Energy Production (kWh)' );
set(get(ax(2), 'Ylabel'), 'String', 'Solar Radiation Incident on PV Array
(kWh)','FontSize',  13 )
% ylim ([0 4]);
set(findall(gcf,'type','axes'),'fontsize',24 )
set(findall(gcf,'type','text'),'fontsize',24 )
set(gcf,'color','w');
```

```
grid;

figure;
[ax, h1, h2] = plotyy( ptime,PV_energy_kWh_day, ptime,
solar_insolation_kWh_day, 'bar', 'plot');
set(findall(gcf,'type','axes'),'fontsize',24 )
set(findall(gcf,'type','text'),'fontsize',24 )
set(h1, 'FaceColor', [0.4, 0.4, 0.4]);
set(h2, 'LineWidth', 4,'Marker','o');
% title('PV Energy Production'),grid
legend('PV Energy Production','Solar Radiation Incident per Unit Area' )
xlabel({'Days';'August 23rd, 2014 to August 27th, 2014'} );
set(get(ax(1), 'Ylabel'), 'String', 'PV Energy Production (kWh)' );
set(get(ax(2), 'Ylabel'), 'String', 'Daily Solar Radiation Incident per
Unit Area (kWh/day/m^2) ','FontSize',  13 )
set(findall(gcf,'type','axes'),'fontsize',24 )
set(findall(gcf,'type','text'),'fontsize',24 )
set(gcf,'color','w');
grid;


% July 28th. 2014 to August 3, 2014
% August 4th, 2014 to August 8th, 2014
% August 9th, 2014 to August 15th, 2014
% July 28th', 'July 29th', 'July 30','July 31','Aug 1st','Aug 2nd','Aug
3rd'
```

Appendix – C: Graphical Results

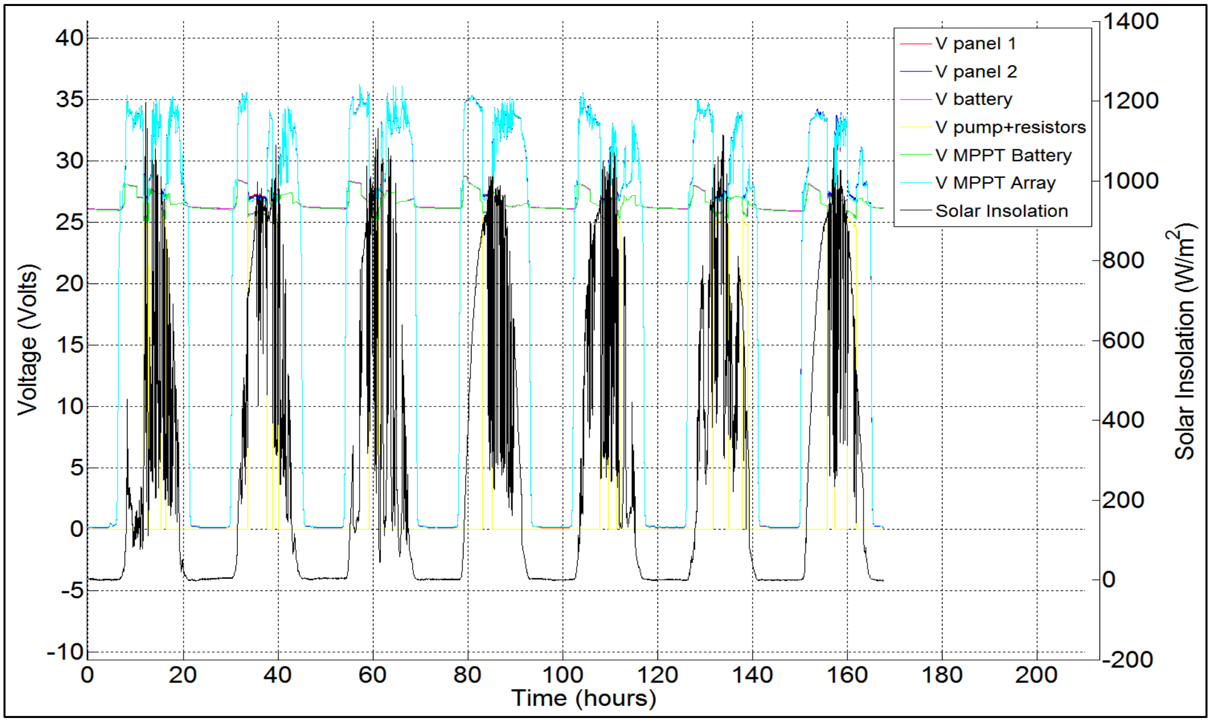

Figure C.1: Voltage and solar insolation versus time for PV array inclination at 40° and sun tracking for seven days of operation from July 28 to August 3, 2014.

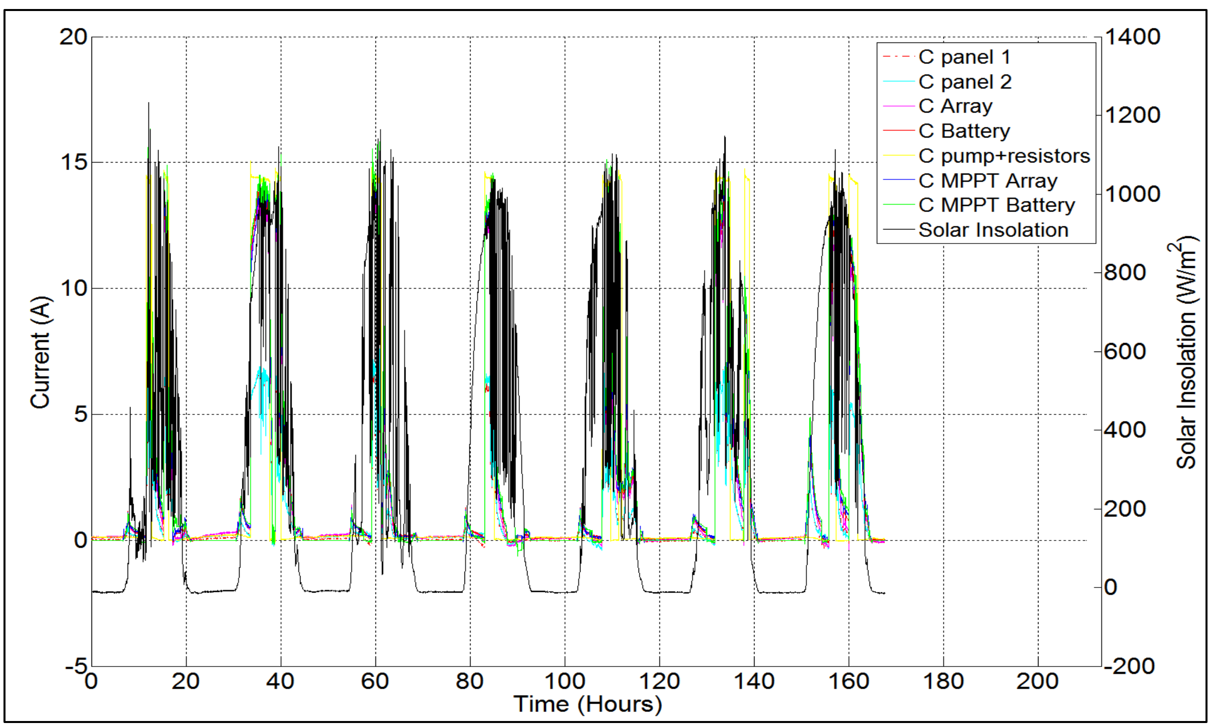

Figure C.2: Current and solar insolation versus time for PV array inclination at 40° and sun tracking for seven days of operation from July 28 to August 3, 2014.

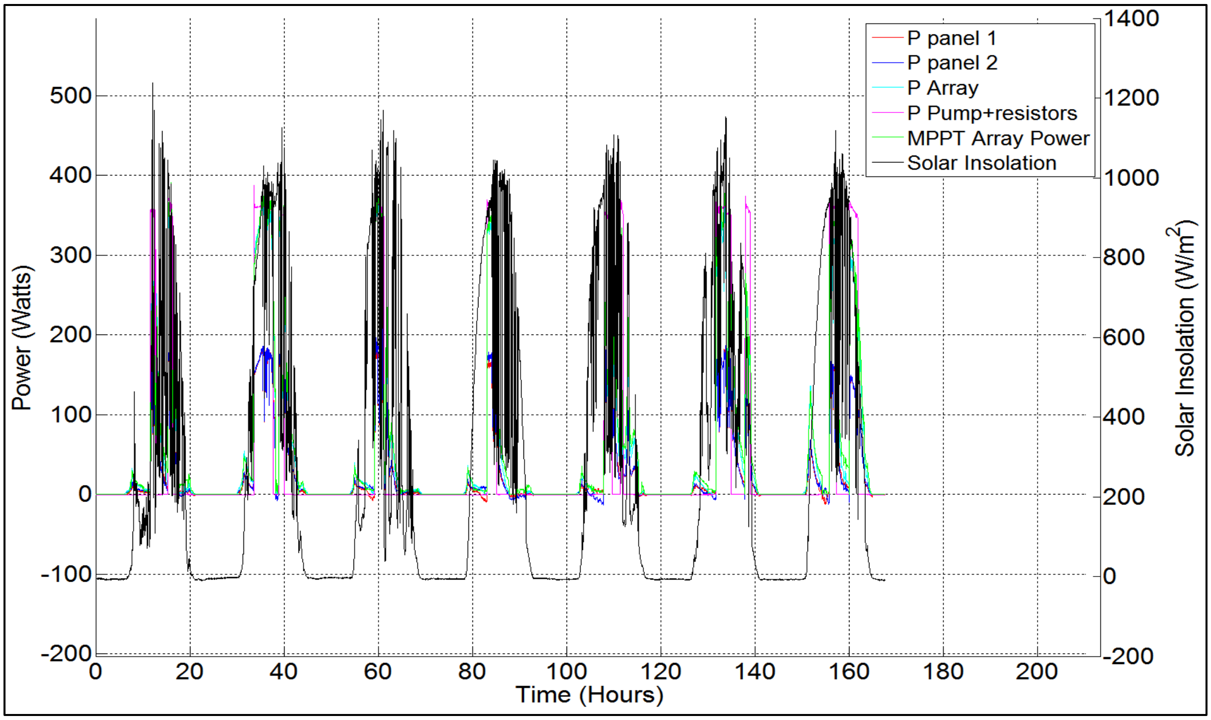

Figure C.3: Power and solar insolation versus time for PV array inclination at 40° and sun tracking for seven days of operation from July 28 to August 3, 2014.

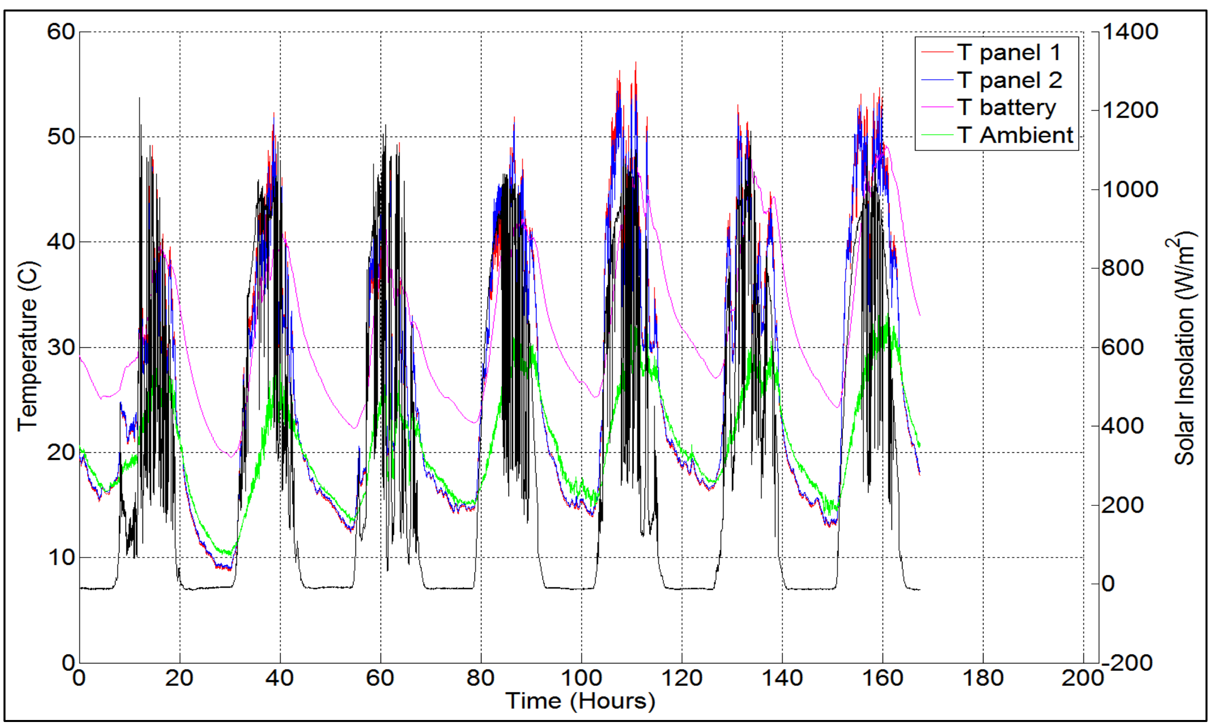

Figure C.4: Temperature and solar insolation versus time for PV array inclination at 40° and sun tracking for seven days of operation from July 28 to August 3, 2014.

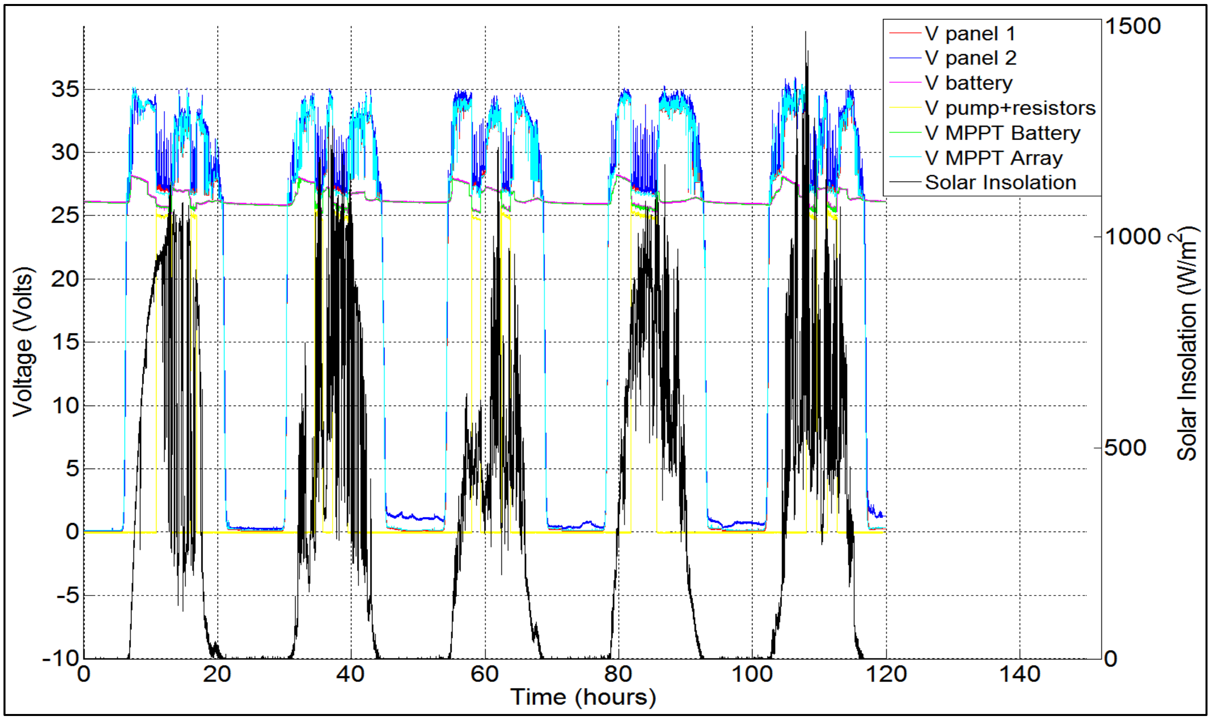

Figure C.5: Voltage and solar insolation versus time for PV array inclination at 40° and sun tracking for five days of operation from August 4th to August 8th, 2014.

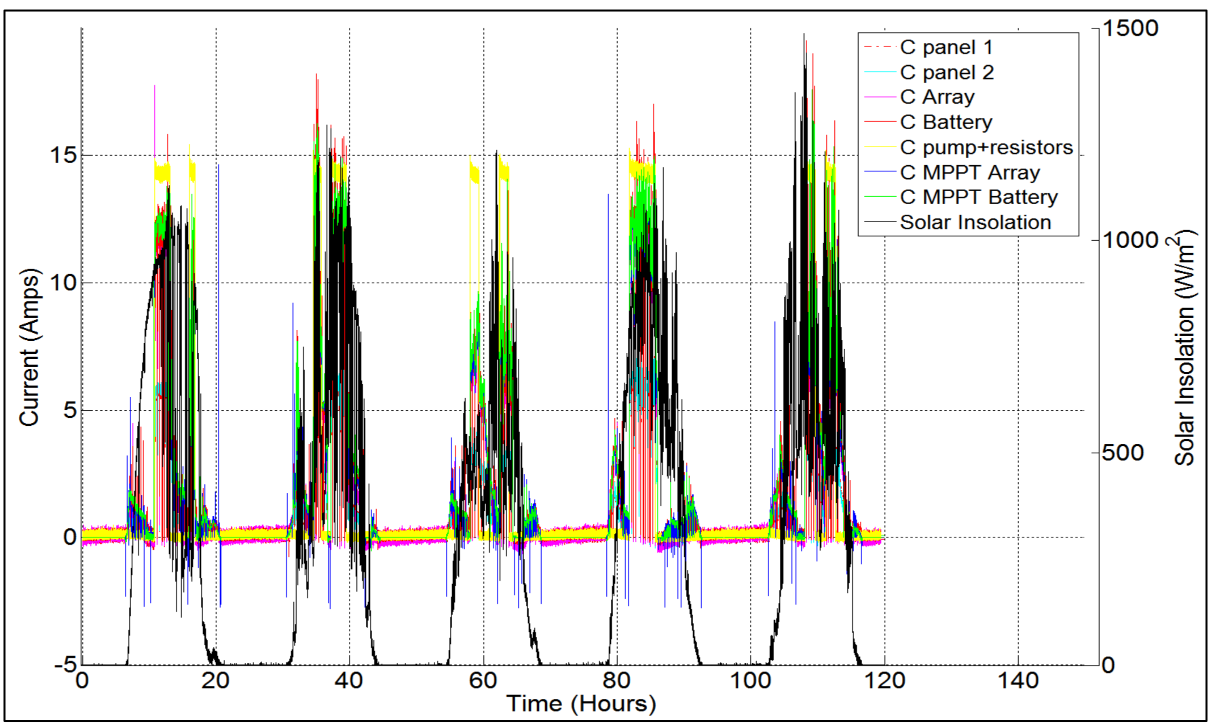

Figure C.6: Current and solar insolation versus time for PV array inclination at 40° and sun tracking for five days of operation from August 4th to August 8th , 2014.

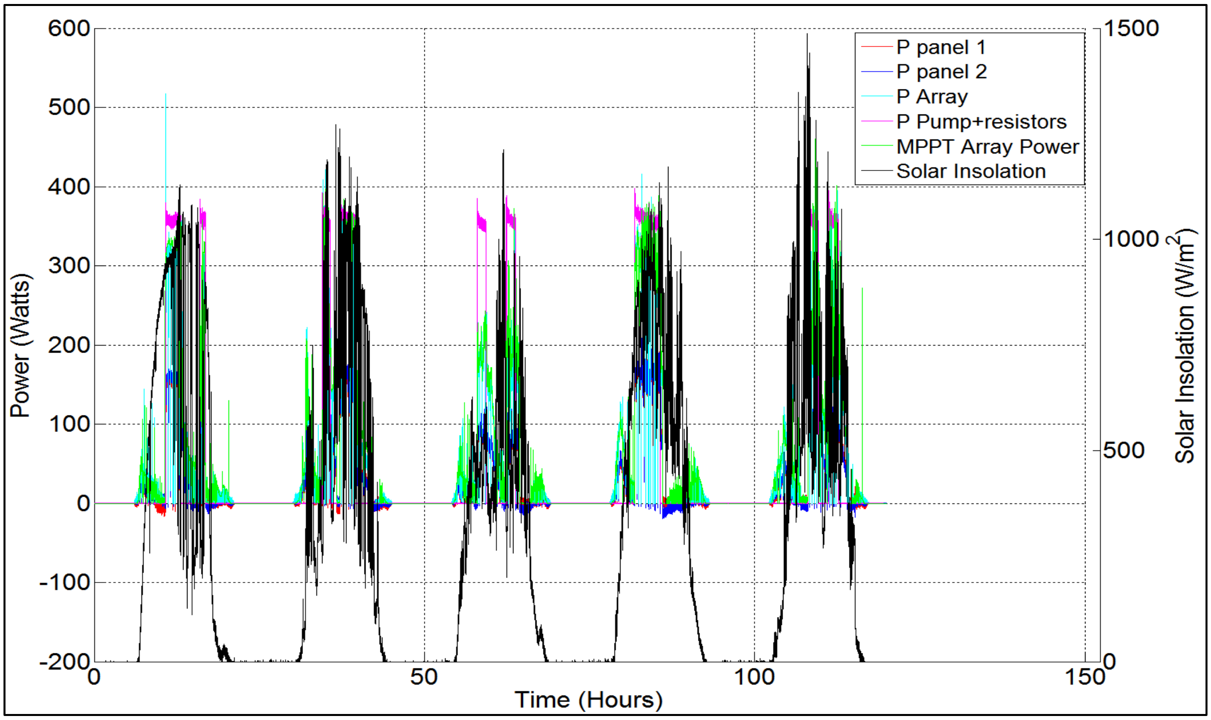

Figure C.7: Power and solar insolation versus time for PV array inclination at 40° and sun tracking for five days of operation from August 4th to August 8th , 2014.

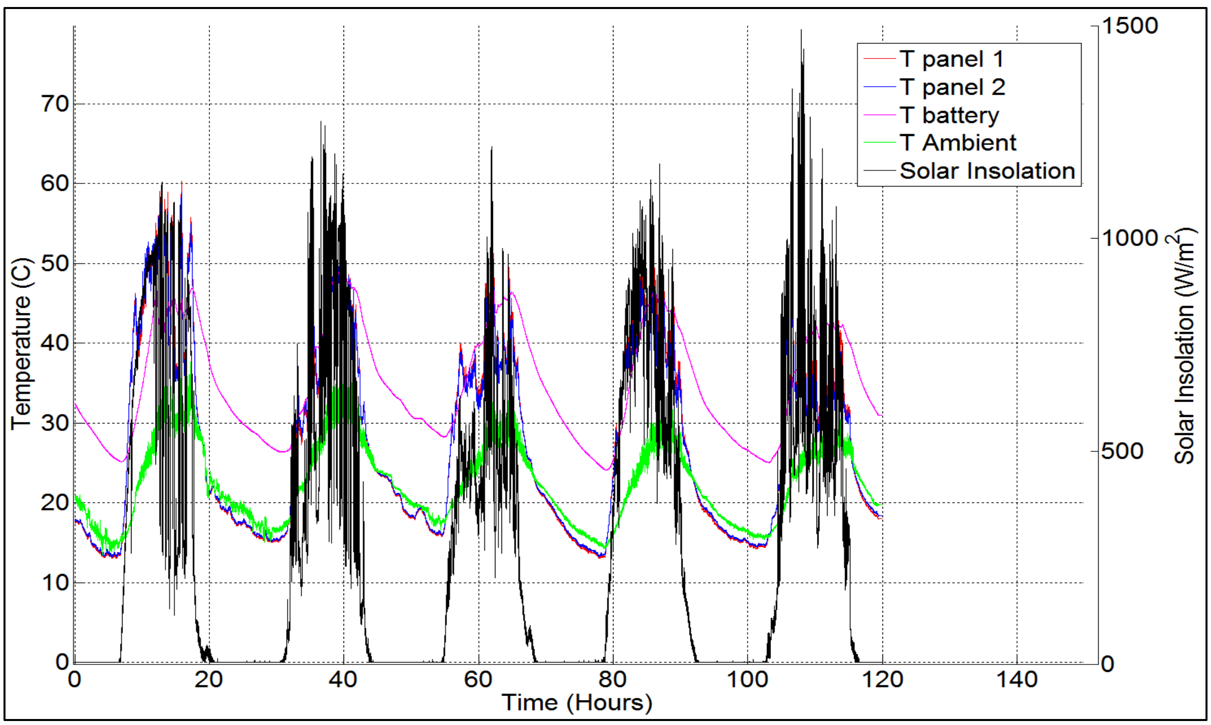

Figure C.8: Temperature and solar insolation versus time for PV array inclination at 40° and sun tracking for five days of operation from August 4th to August 8th, 2014.

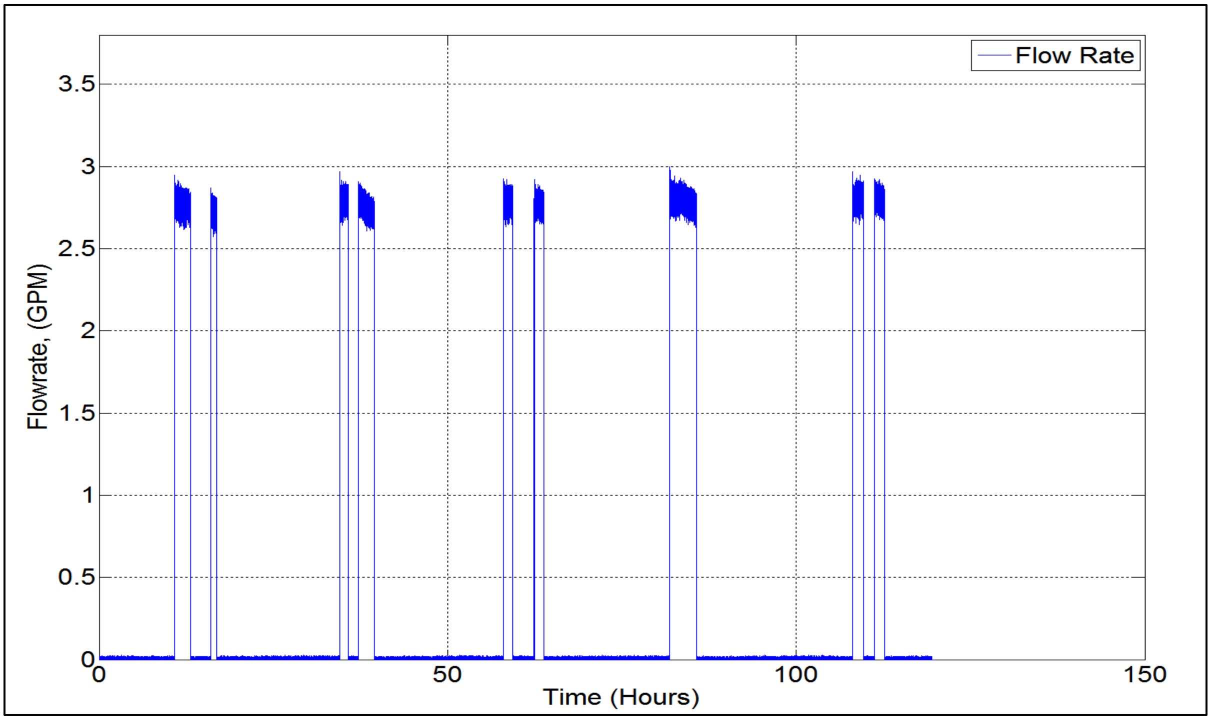

Figure C.9: Flowrate versus time for PV array inclination at 40° and sun tracking for five days of operation from August 4th to August 8th, 2014.

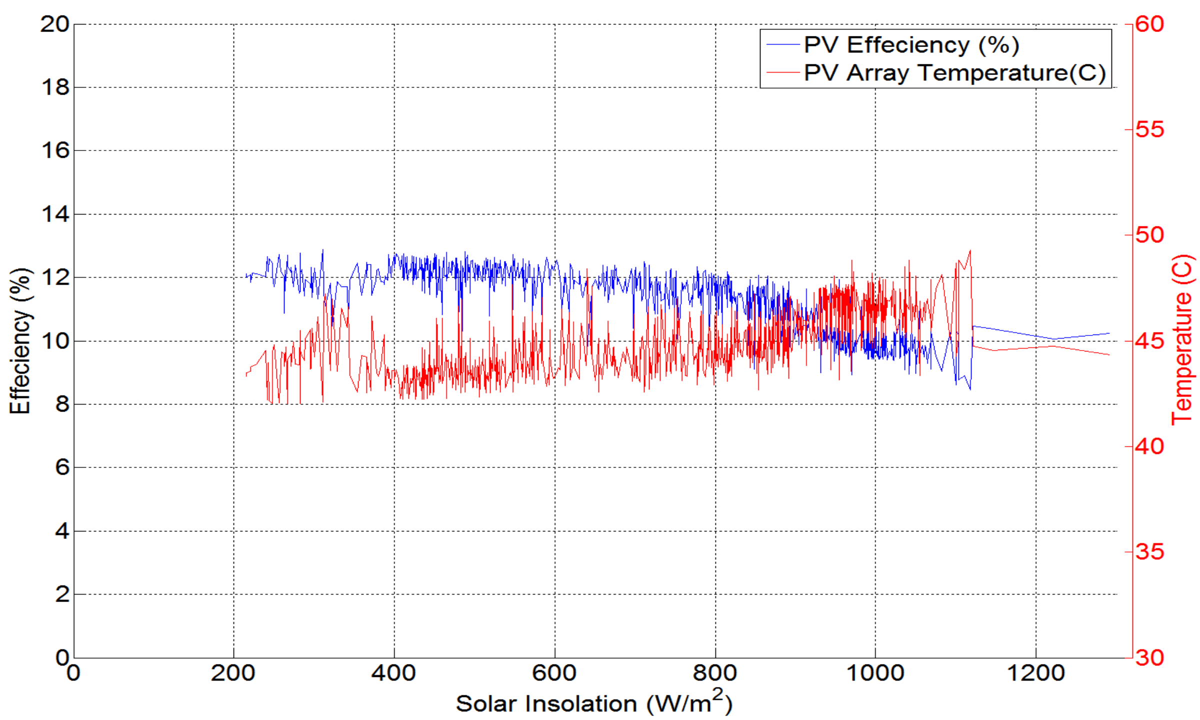

Figure C.10: PV array efficiency and temperature for PV array inclination at 40° and sun tracking for five days of operation from August 4th to August 8th, 2014.

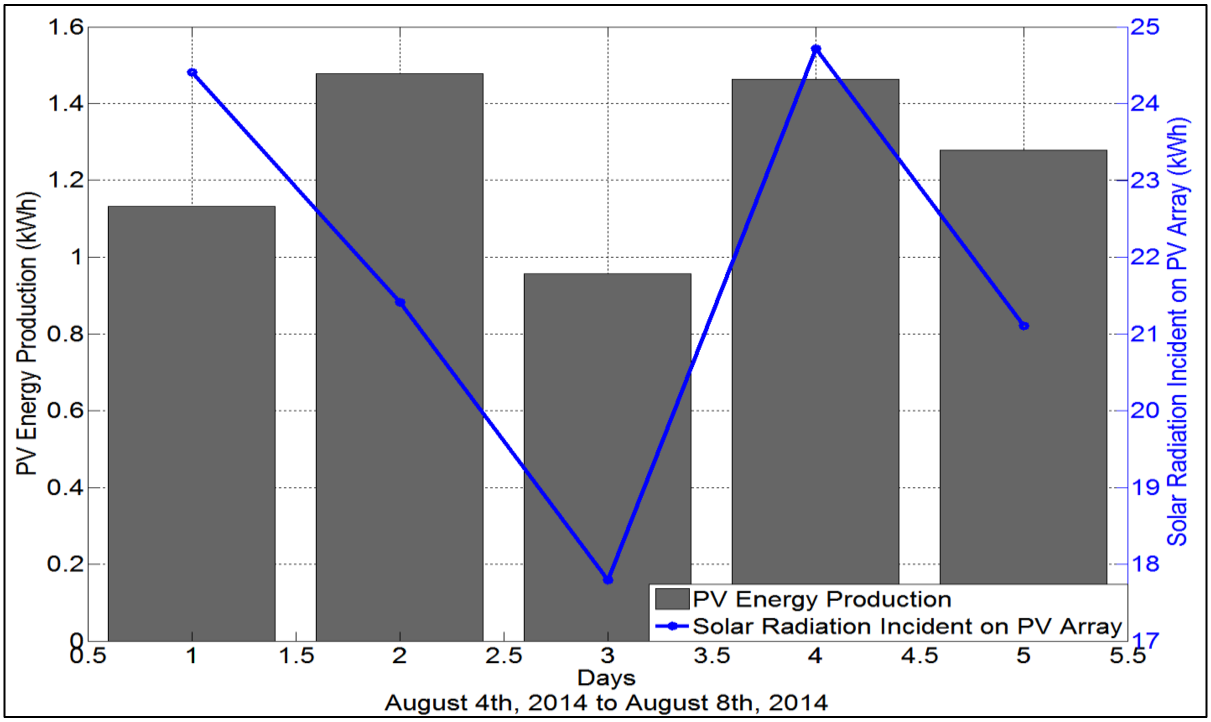

Figure C.11: PV energy production for PV array inclination at 40° and sun tracking for seven days of operation from August 4th to August 8th, 2014.

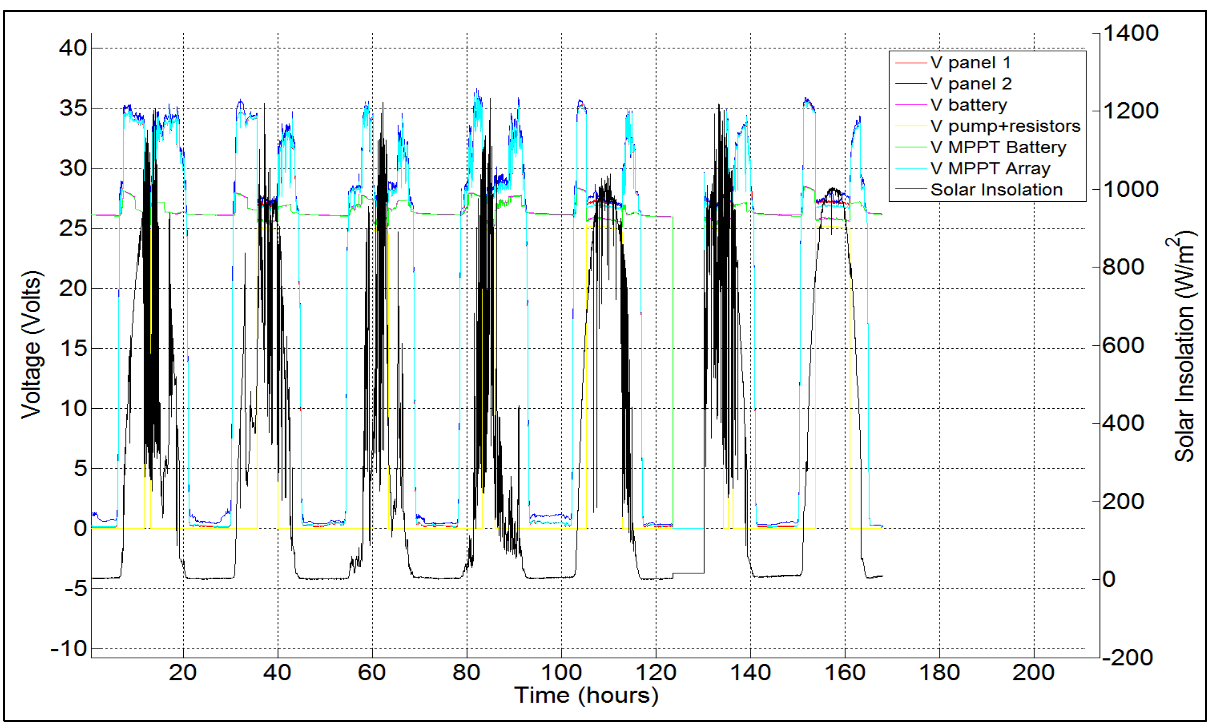

Figure C.12: Voltage and solar insolation versus time for PV array inclination at 30° and sun tracking for seven days of operation from August 9th to August 15th, 2014.

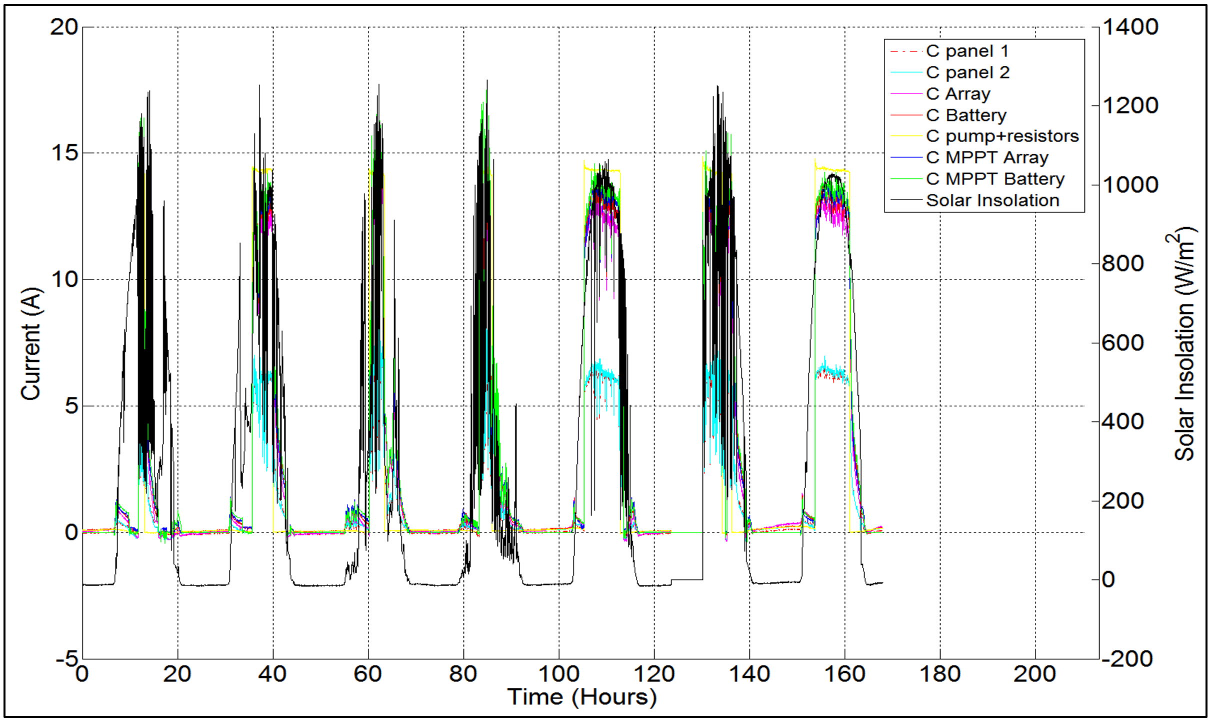

Figure C.13: Current and solar insolation versus time for PV array inclination at 30° and sun tracking for seven days of operation from August 9th to August 15th, 2014.

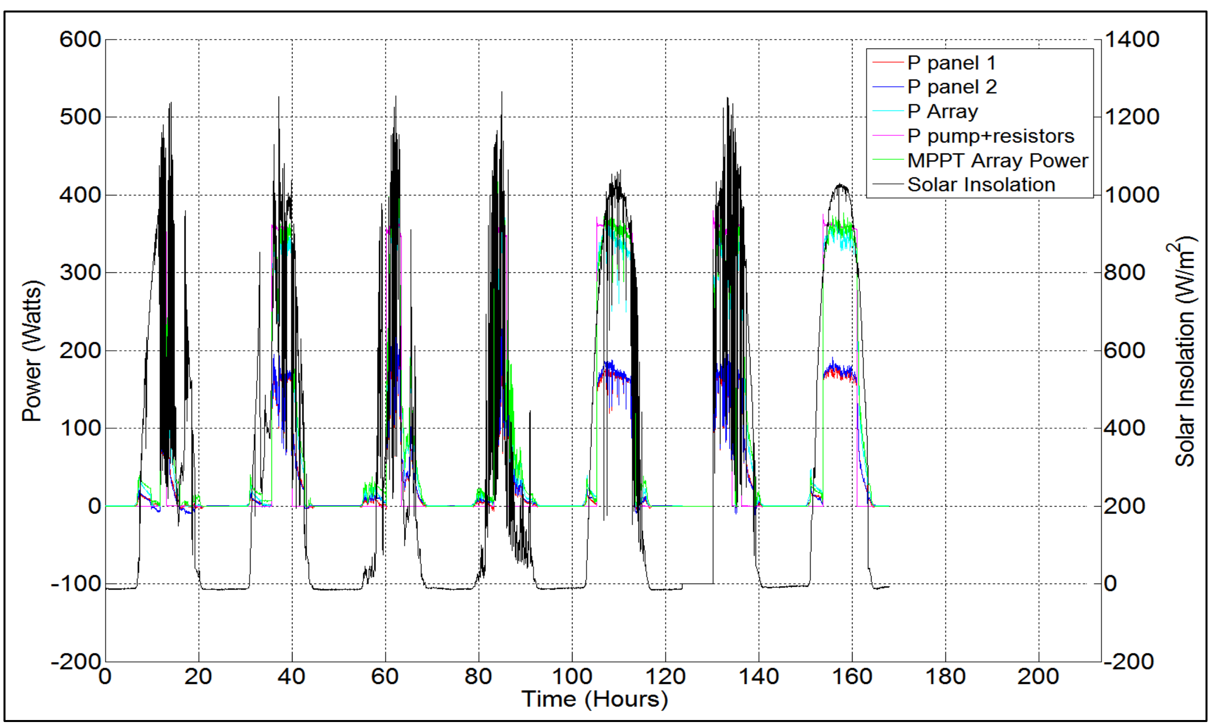

Figure C.14: Power and solar insolation versus time for PV array inclination at 30° and sun tracking for seven days of operation from August 9th to August 15th, 2014.

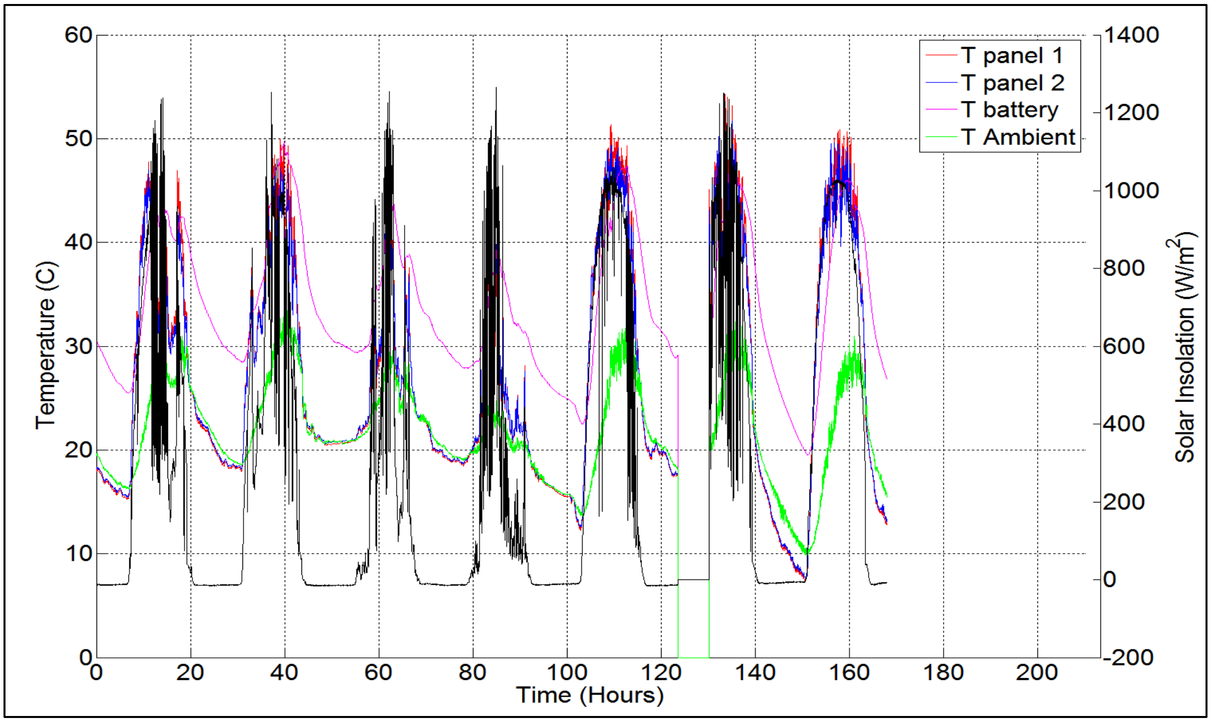

Figure C.15: Temperature and solar insolation versus time for PV array inclination at 30° and sun tracking for seven days of operation from August 9th to August 15th, 2014.

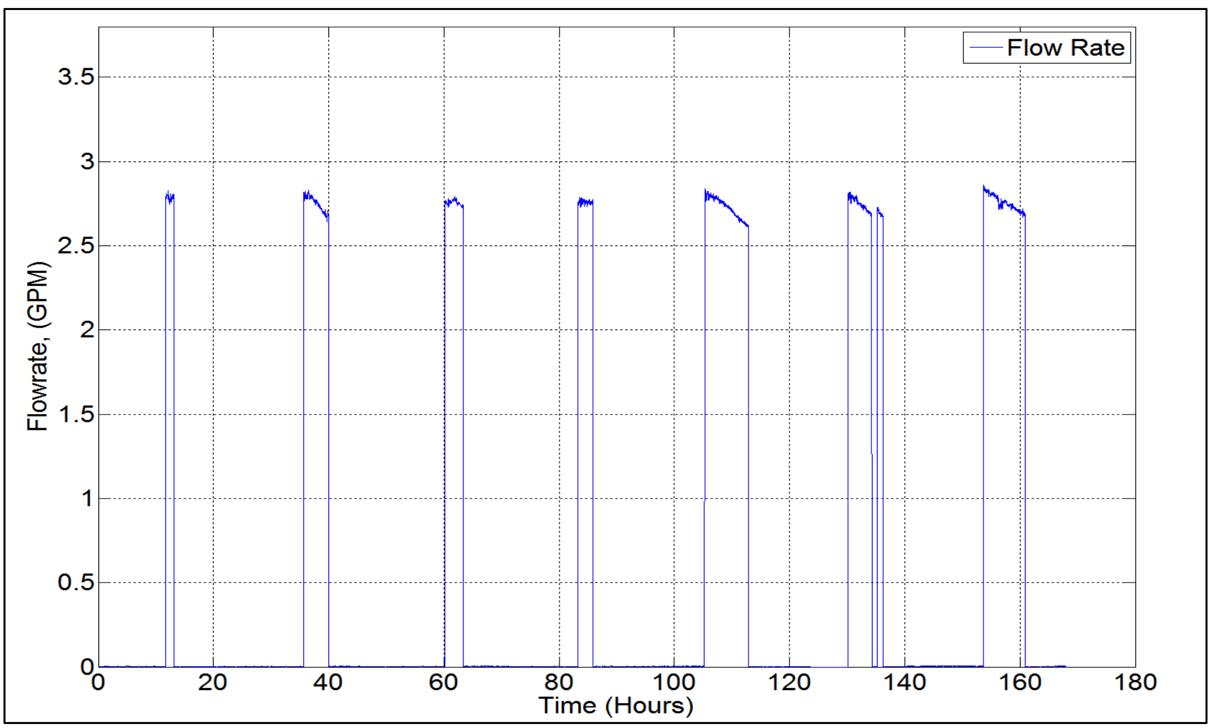

Figure C.16: Flowrate versus time for PV array inclination at 30° and sun tracking for seven days of operation from August 9th to August 15th, 2014.

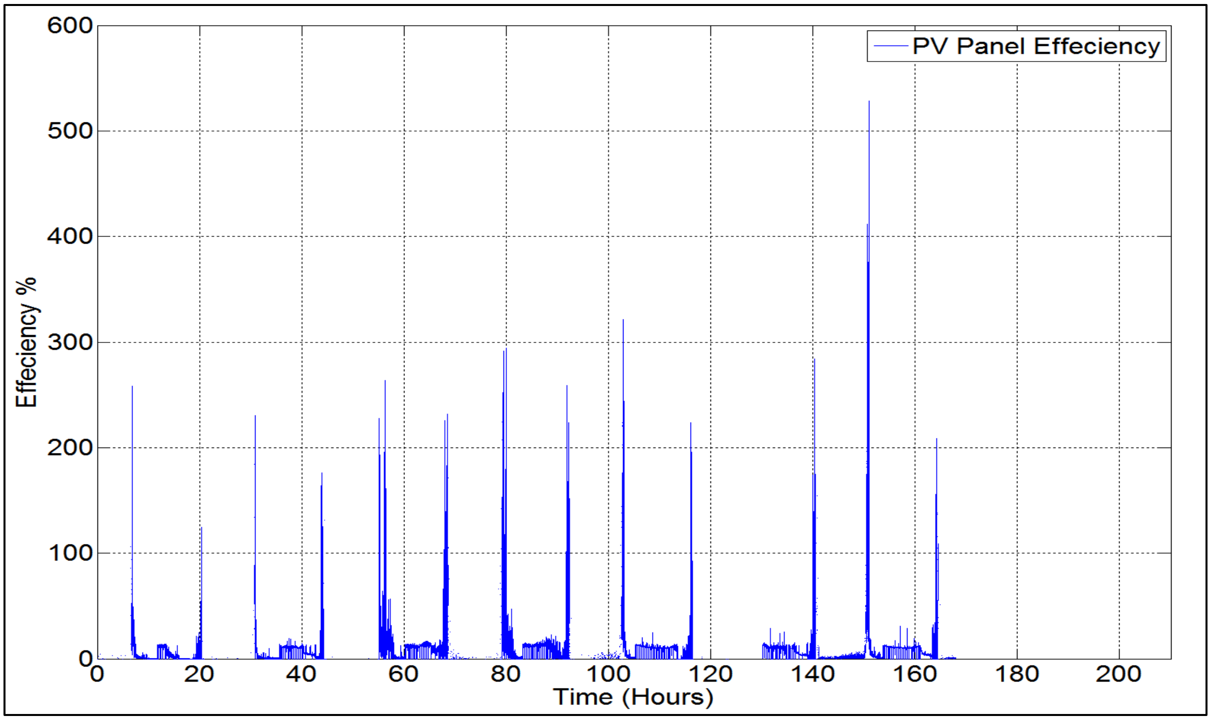

Figure C.17: Efficiency versus time for PV array inclination at 30° and sun tracking for seven days of operation from August 9th to August 15th, 2014.

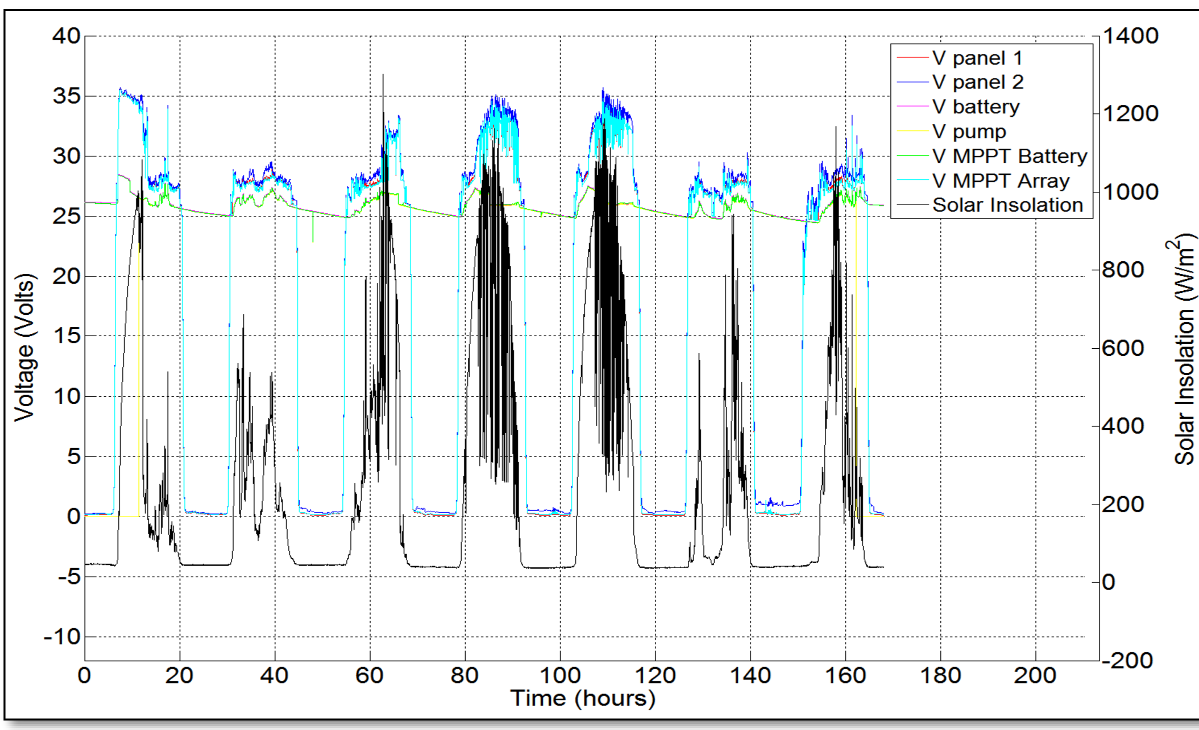

Figure C.18: Voltage and solar insolation versus time with continuous pumping with no power dissipating resistors for PV array inclination at 40° and sun tracking and sun tracking for seven days of operation from August to August 22, 2014.

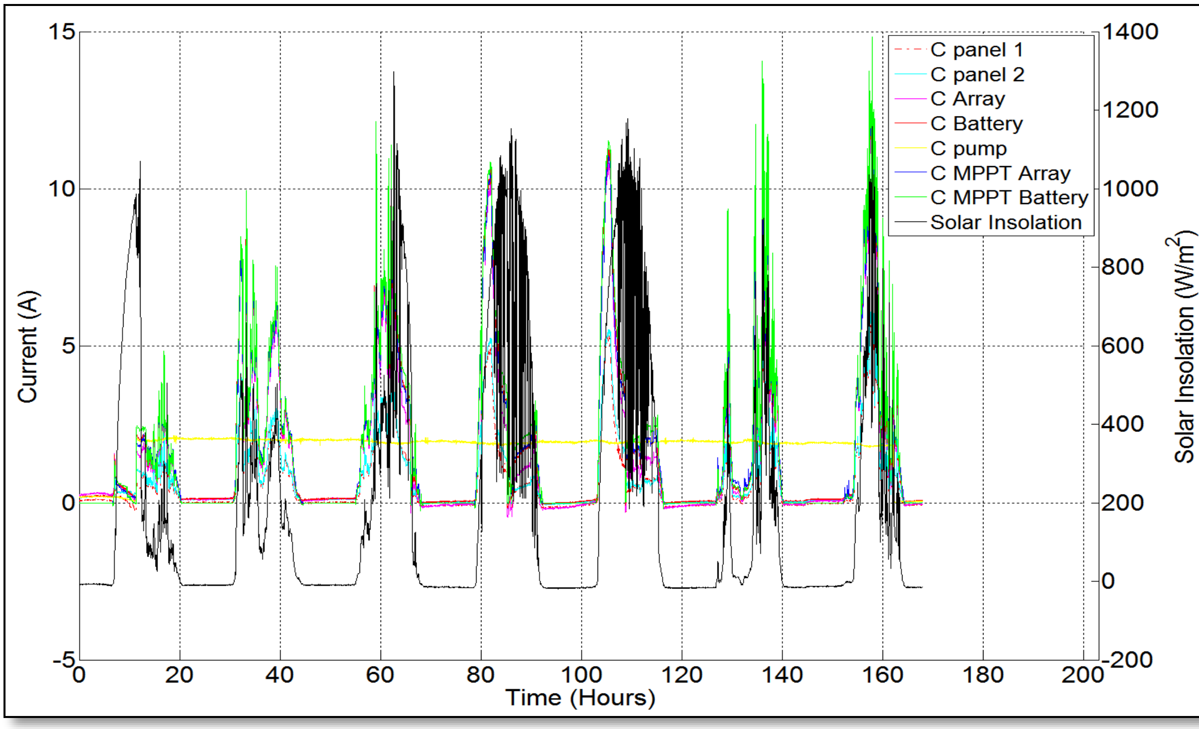

Figure C.19: Current and solar insolation versus time with continuous pumping with no power dissipating resistors for PV array inclination at 40° and sun tracking and sun tracking for seven days of operation from August to August 22, 2014.

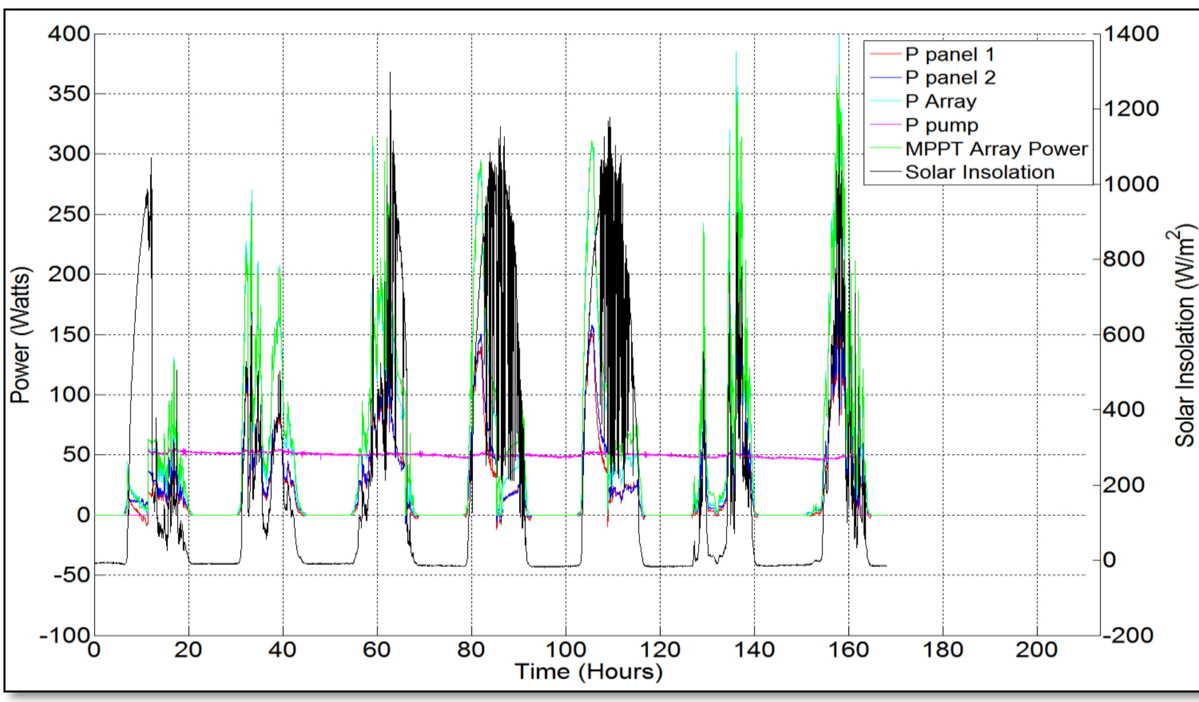

Figure C.20: Power and solar insolation versus time with continuous pumping with no power dissipating resistors for PV array inclination at 40° and sun tracking and sun tracking for seven days of operation from August to August 22, 2014.

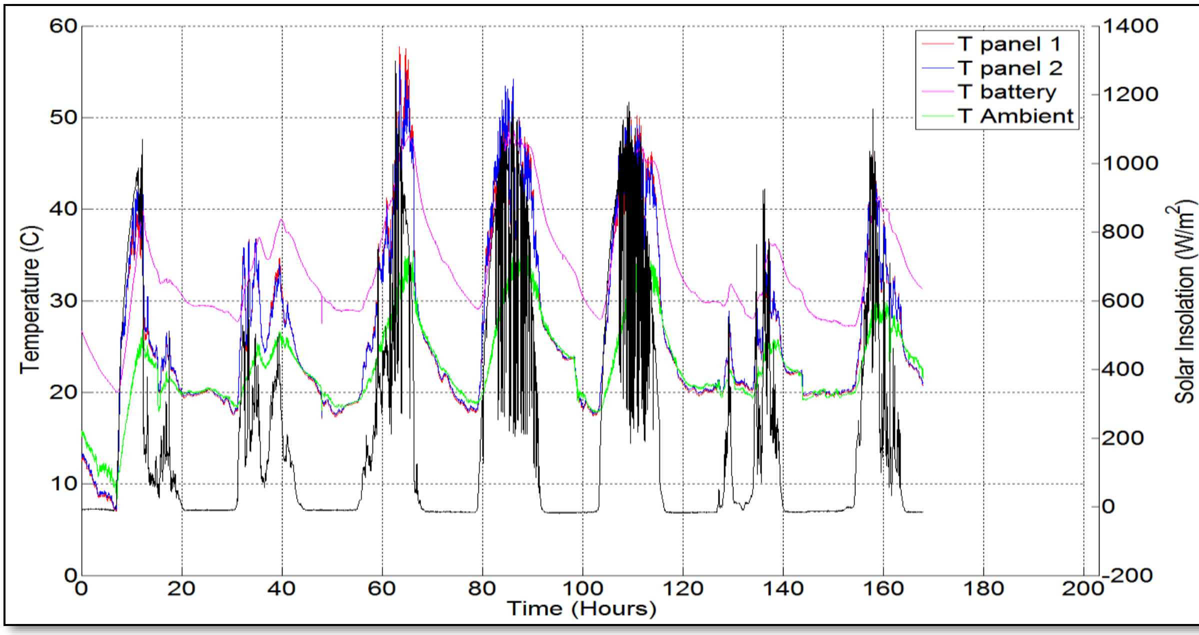

Figure C.21: Temperature and solar insolation versus time with continuous pumping with no power dissipating resistors for PV array inclination at 40° and sun tracking and sun tracking for seven days of operation from August to August 22, 2014.

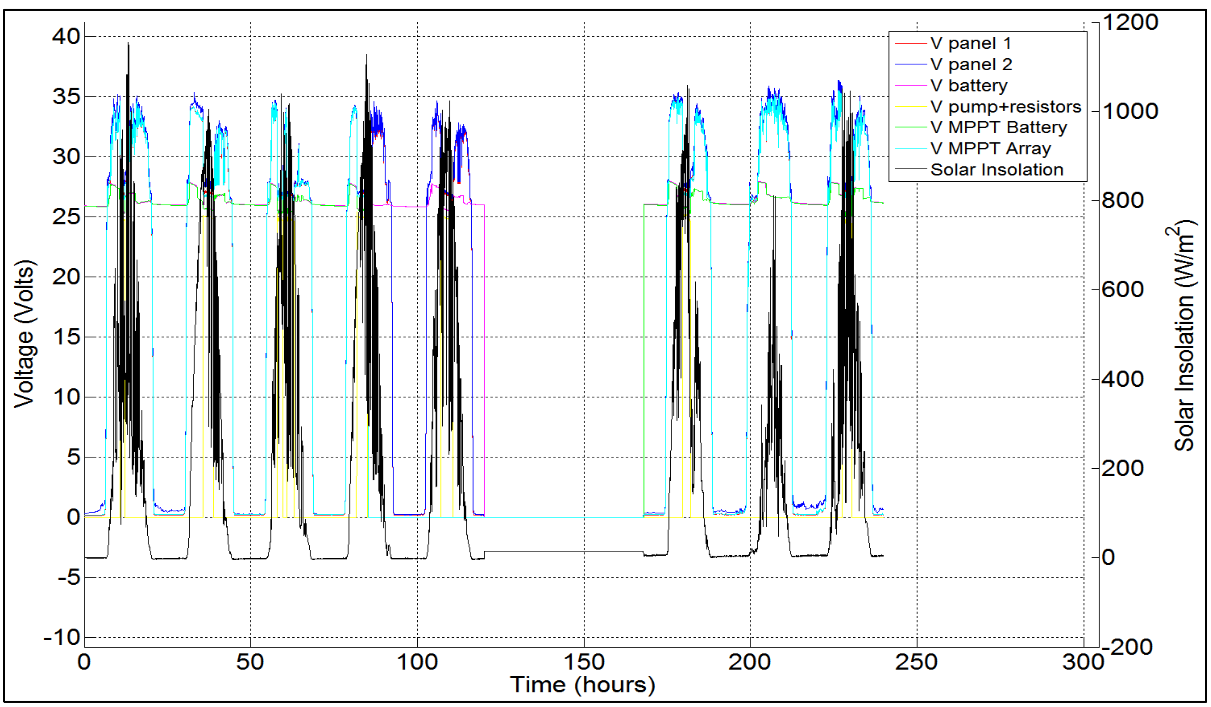

Figure C.22: Voltage and solar insolation versus time for PV array with azimuthal orientation fixed due south and inclination fixed at 40°for ten days of operation from August 23 to September 1st, 2014.

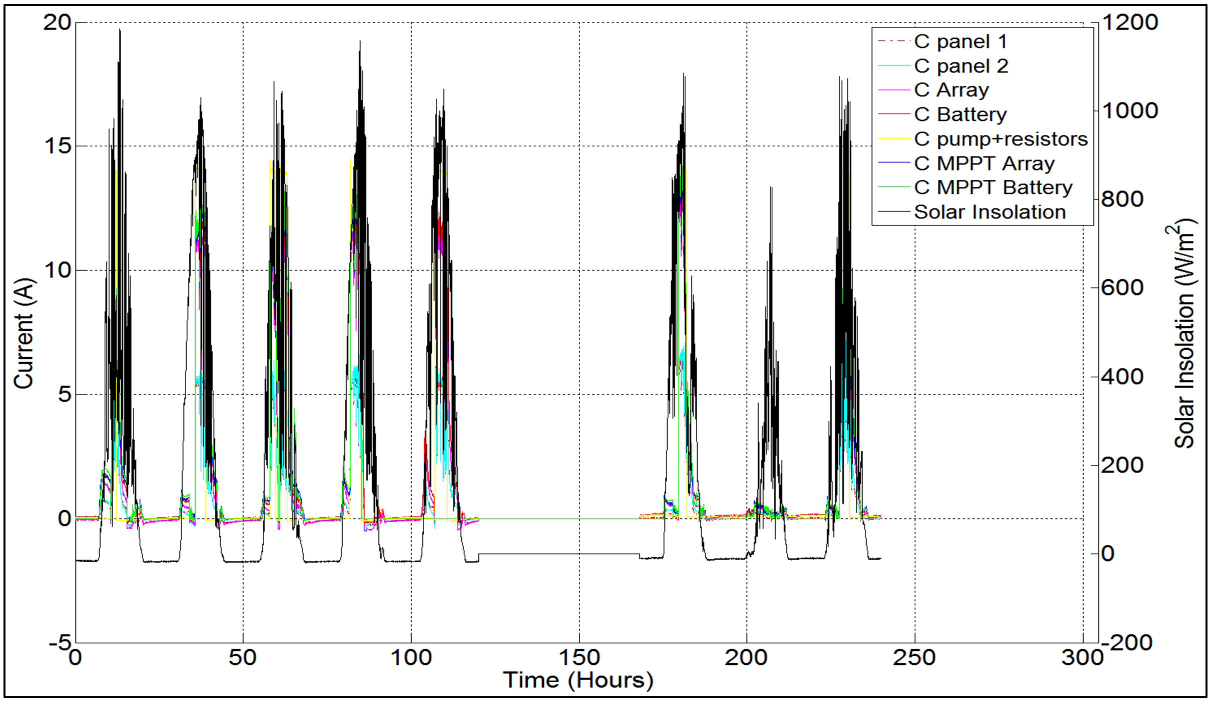

Figure C.23: Current and solar insolation versus time for PV array with azimuthal orientation fixed due south and inclination fixed at 40°for ten days of operation from August 23 to September 1st, 2014.

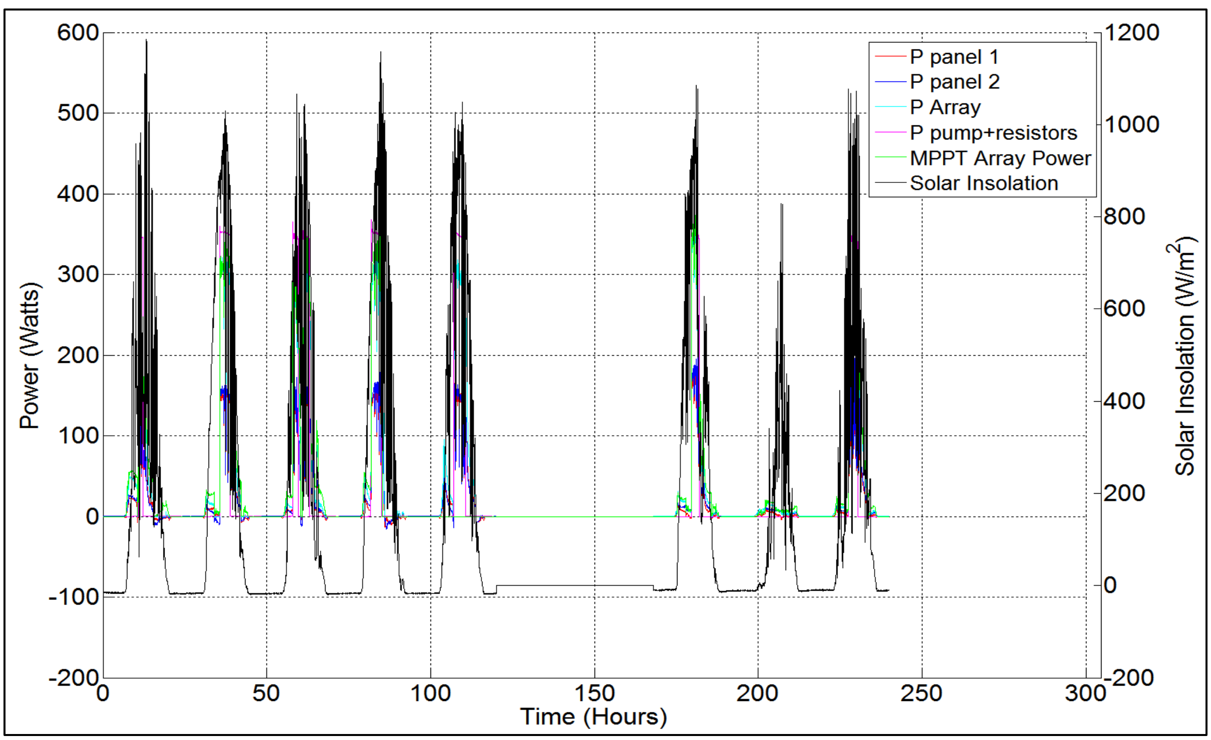

Figure C.23: Power and solar insolation versus time for PV array with azimuthal orientation fixed due south and inclination fixed at 40°for ten days of operation from August 23 to September 1st, 2014.

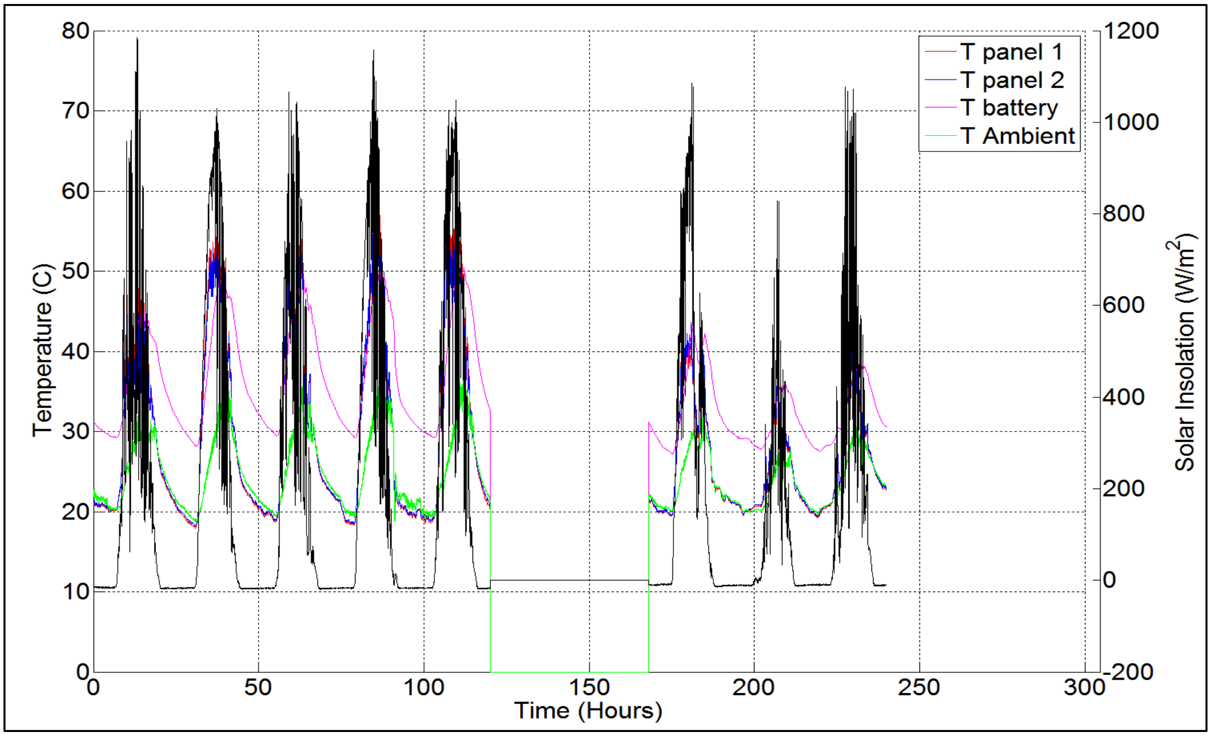

Figure C.24: Temperature and solar insolation versus time for PV array with azimuthal orientation fixed due south and inclination fixed at 40°for ten days of operation from August 23 to September 1st, 2014.